

Transport Theory in Low Dimensional Systems

from Thermoelectric Effects in Luttinger Liquids
to Hydrodynamic Expansion of Cold Atoms

Inaugural-Dissertation

zur

Erlangung des Doktorgrades

der Mathematisch-Naturwissenschaftlichen Fakultät

der Universität zu Köln

vorgelegt von

David Rasch

aus

Viernheim



Köln 2010

Berichterstatter: Prof. Dr. Achim Rosch
Prof. Dr. Matthias Vojta

Tag der mündlichen Prüfung: 09.07.2010

Abstract

The impact of lattice vibrations on the electric conductivity has been considered a settled issue since the proof of the Migdal theorem. The precondition for its validity is a higher velocity of electronic than phononic excitation modes. In some new materials, e. g. weakly coupled spin chains and heavy fermion systems, this precondition is not fulfilled. The heat conductivity of such systems is calculated by means of perturbation theory in this work.

Another subject is the interplay of Umklapp scattering and weak disorder in spin chains and one-dimensional correlated metals. Hidden conservation laws lead to a strong coupling between heat current and charge or spin current, respectively. The transport properties are calculated perturbatively within the hydrodynamic memory matrix formalism, which gives a lower bound to the conductivities. To calculate the Lorenz number of one-dimensional metals, we model within this formalism also the influence of phonons, which in physical systems contribute substantially to the heat current.

The introduction of ultracold quantum gases in optical lattices in the recent years provides a powerful tool for the modeling of many systems to solid state physics, in particular systems out of equilibrium. The relatively slow dynamics of the cold atoms allows for time resolved imaging of the atoms and thus opens up new perspectives.

In the last part of this thesis, a recent experiment, which measures the expansion of a correlated atom cloud in an optical lattice, is compared to a lattice Boltzmann simulation. Depending on the local density, the problem is shown to be described by the crossover from diffusive to ballistic transport.

Kurzzusammenfassung

Der Einfluss von Gitterschwingungen auf die elektrische Leitfähigkeit wurde bisher innerhalb des Migdaltheorems als abschließend behandelt betrachtet. Die Voraussetzung für dessen Gültigkeit ist eine, im Vergleich zu den elektronischen Anregungen, langsame Geschwindigkeit der Vibrationsmoden. Für einige neue Materialien, wie Spinketten mit schwacher Kopplung und Schwer-Fermionen-Systemen, ist diese Voraussetzung nicht erfüllt. Die Wärmeleitfähigkeit solcher Systeme wird in dieser Arbeit mittels Störungstheorie berechnet.

Ein weiteres Thema ist das Wechselspiel von Umklapp-Streuung und schwacher Unordnung in Spinketten und eindimensionalen Metallen. Versteckte Erhaltungssätze führen zu starken Kopplungen zwischen Ladungs- oder Spinstrom und Wärmestrom. Anhand des hydrodynamischen Memory-Matrix-Formalismus werden die Transporteigenschaften perturbativ berechnet. Die erzielten Leitfähigkeiten sind eine exakte untere Schranke der tatsächlichen Leitfähigkeiten. Für die Berechnung der Lorenzzahl eindimensionaler Metalle wird innerhalb dieses Formalismus auch der Einfluss von Phonon modelliert, die im physikalischen System wesentlich zum Wärmestrom beitragen.

Mit der Möglichkeit mittels ultrakalter Quantengasen in optischen Gittern wechselwirkende Systeme zu simulieren, hat die Festkörperphysik in den letzten Jahren ein wertvolles Instrument zur Untersuchung von vielen Modellen, insbesondere von Systemen außerhalb des Gleichgewichts, gewonnen.

Die vergleichsweise langsame Dynamik der kalten Atome erlaubt eine zeitaufgelöste Abbildung der Atome und eröffnet so neue Fragestellungen.

Im letzten Teil dieser Dissertation wird die experimentelle Messung der Expansion einer wechselwirkenden Atomwolke in einem optischen Gitter mit einer Gitter-Boltzmann Simulation des Problems verglichen. Die Expansion wird, abhängig von der lokalen Teilchendichte, durch diffusiven oder ballistischen Transport beschrieben.

Contents

| | | |
|----------|---|-----------|
| 1 | General Transport Theory | 5 |
| 1.1 | Boltzmann Equation | 5 |
| 1.2 | Connection to Macroscopic Transport Coefficients | 7 |
| 1.3 | The Variational Principle of Transport Theory | 9 |
| 1.4 | Theory of Linear Response | 11 |
| 1.5 | Conservation Laws: Hydrodynamic Approach | 13 |
| 2 | Scattering of Fast Phonons | 17 |
| 2.1 | Electron-Phonon Scattering | 18 |
| 2.2 | First Order Contribution: Conservation Laws | 20 |
| 2.3 | Second Order Processes | 21 |
| 2.4 | Connection to Heat Conductivity | 23 |
| 2.5 | Mean Free Path and Boundary Scattering | 24 |
| 3 | Thermoelectric Effects in One-Dimensional Systems | 29 |
| 3.1 | Basics of the Bosonization technique | 34 |
| 3.2 | Magnetothermal effects in Heisenberg chains | 38 |
| 3.2.1 | Model Hamiltonian | 38 |
| 3.2.2 | Memory Matrix | 39 |
| 3.2.3 | Results | 42 |
| 3.2.4 | Comparison with Experiments | 44 |
| 3.3 | Violation of Wiedemann-Franz Law in Luttinger Liquids | 45 |
| 3.3.1 | Model System | 46 |
| 3.3.2 | Memory Matrix for the One-Dimensional Metal | 49 |
| 3.3.3 | Results | 63 |
| 4 | Expansion of Interacting Atoms in Optical Lattices | 79 |
| 4.1 | Experimental Setup | 81 |
| 4.2 | Boltzmann Equation Description | 82 |
| 4.3 | Relaxation-Time from Memory Matrix | 86 |
| 4.4 | Results | 89 |
| A | Calculation of Phonon Lifetime | 95 |
| A.1 | Calculating the Imaginary Part with Branch Cuts | 95 |
| A.2 | Low Energy Limit of Effective Vertex | 97 |
| A.3 | Momentum Summation for Three-Dimensional Fermions | 97 |
| A.4 | Momentum Summation for One-Dimensional Fermions | 98 |

CONTENTS

| | | |
|----------|--|------------|
| B | Bosonization Calculations | 101 |
| B.1 | Time-Derivatives of Currents for Spin Chain | 101 |
| B.2 | $4k_F$ Correlation Function | 102 |
| B.3 | Local Correlation Functions for Disorder Memory Matrix | 103 |
| B.4 | Susceptibility of Heat Current | 104 |
| B.5 | Elementary Correlation Functions for Luttinger Liquids | 104 |
| B.6 | Band Curvature Corrections to Susceptibilities | 105 |
| B.7 | Correlation Functions of Umklapp Time-Derivatives | 106 |
| B.8 | Calculation of Phonon Propagator | 108 |
| B.9 | Calculation of Band-Curvature Memory Matrix | 109 |
| C | Appendices for Expanding Cloud | 111 |
| C.1 | Experimental Parameters | 111 |
| C.2 | Error Estimate for Low-Density Limit | 111 |
| C.3 | Symmetries of the System | 112 |
| C.4 | Scattering Rate | 112 |
| C.4.1 | Time-Derivative of Currents | 112 |
| C.4.2 | Real Time Correlation Function | 113 |
| C.4.3 | Susceptibilities | 114 |
| | Bibliography | 115 |
| | Acknowledgment | 121 |

Introduction

The technological importance of transport in solids can hardly be overestimated. Electrical, but also thermal conduction plays a huge role in any modern electronic device. Macroscopically, these phenomena are governed by relatively simple equations which relate the charge and thermal currents to an external voltage and temperature gradient, respectively. The involved proportionality constants are material properties.

However, the microscopic derivation of these material constants is incredibly complex. Since charge and thermal transport often are mediated by the same excitations, they are intrinsically coupled. This gives rise to the well-known issue of thermoelectric effects, which gained their own technological relevance with the applications of thermoelectric cooling and thermoelectric power generation.

In the recent years, low dimensional system became increasingly important in technical applications of transport properties, on the one hand due to the ongoing miniaturization of circuitry, which confines conducting paths in, for example, processors already on nano-scales, on the other hand some materials with embedded quasi-one-dimensional conductors provide high-end efficiencies for thermoelectrics.

Heat can be transmitted by any propagating excitations of a system, in metals e. g. electronic excitations and lattice vibrations. The interaction between different heat current carrying modes is dispersing the heat current within one subsystem, but that does not necessarily mean dissipation. Momentum that is transferred from one subsystem to the other typically in the next scattering process is transferred back into the original system, an effect called *backflow*. Due to this effect, scattering processes between different modes must be investigated carefully, in particular with respect to conserved quantities.

Furthermore, interaction effects become central, since systems of free carriers, which are often starting points for the calculation of equilibrium properties of solids, show a diverging response to an external force or temperature gradient. The reason is the lack of a scattering mechanism, which could disperse the respective current, or more generally speaking, conservation laws of the system.

Consequently, the common scheme of interaction as a weak perturbation to the free system can not be applied to transport quantities in a straight-forward way. This reveals the dilemma of transport theory, since in solid state physics, exact calculations usually are only possible for simplified models, which are supposed to still contain the relevant physics. In the special case of transport properties, exactly the simplifications that usually make a problem feasible cause diverging transport coefficients. On the other hand, numerical simulations of microscopic transport are also very difficult, since a time-dependent inhomogeneous system must be modeled. In particular, extracting the transport coefficient from data for the time-dependence of the current can be very difficult.

Already in the sixties of the past century, with the hydrodynamic memory matrix formalism, a theory has been established, which allows to compute lower bounds of conductivities

in systems close to integrability, i. e. integrable systems plus a weak perturbation that breaks the integrability. The currents are supposed to be carried dominantly by that modes of the system, which are scattered the weakest, referred to as *slow modes*. Usually, they can be identified as conserved quantities of the integrable system, that are scattered by the perturbations. Within this approach, the leading order conductivities are obtained from certain correlation functions calculated with the integrable system only.

In low-dimensional systems, this achieves a particular importance, since many interacting one-dimensional systems, like the Heisenberg model with nearest neighbor coupling, are integrable, and correlation functions can be calculated exactly, for instance within the bosonization formalism.

This allows to treat the effect of a wide range of interactions to transport properties of one-dimensional systems which exhibit the Luttinger liquid fixed point as a low energy theory.

In this work, a couple of problems of transport theory in low dimensions are investigated, with special focus on the impact of conservation laws.

The thesis is organized as follows: In the first chapter, the foundations of transport theory are introduced, and the basic methods, starting from the Boltzmann equation, relaxation time approximation, and the variational principle of transport theory, over linear response theory and the Green-Kubo relations for thermal conductivities, and finally the hydrodynamic memory matrix formalism.

The second chapter deals with the problem of phonons scattered off slow fermions, which can be either the excitations of weakly coupled spin chains in Jordan-Wigner representation, i. e. one-dimensional fermions, or three-dimensional slow fermions, as occur in the recently discovered heavy-fermion materials. The lifetime of the phonons due to fermion-phonon interaction is calculated by perturbation theory, which must go beyond the Migdal theorem because the lowest order scattering is forbidden by energy and momentum conservation. From the lifetime, the heat conductivity is deduced within the relaxation time approximation to the Boltzmann equation.

In the next chapter, thermoelectric effects in one-dimensional systems are investigated. The heat conductivity of the antiferromagnetic Heisenberg spin chain model with Umklapp scattering and weak Gaussian disorder is calculated by means of the memory matrix formalism. The interplay of disorder and Umklapp scattering leads to a suppression of the magnetic heat conductivity at finite magnetic fields, due to a hidden conservation law of the Umklapp scattering Hamiltonian. The used method accounts for the conservation law and gives an exact lower bound to the heat conductivity. A comparison to recent experiments on the magnetic heat conductivity of the spin chain compound copperpyrazinedinitrate shows qualitative agreement.

In one-dimensional metals, the Umklapp scattering has a similar conservation law, which acts different on charge and heat currents. Again by means of the memory matrix formalism, the charge and heat conductivity are calculated for a system of a weakly disordered correlated metal with Umklapp scattering. We derive a huge enhancement of the Lorenz number at commensurate filling and a strong suppression at finite doping. The large thermoelectric effects make one-dimensional conductors with Umklapp scattering interesting systems for thermoelectric cooling, as can be seen from the thermoelectric figure of merit, which is also calculated. To model a physical system, additionally coupling to lattice vibrations is included and the influence of the phonons to the Lorenz number investigated.

The last chapter describes a recent experiment with ultracold atoms, that expand in an optical lattice after the release from a trap. The setting is a realization of the Hubbard model with inhomogeneous starting condition. We set up a lattice Boltzmann simulation

with transport coefficients obtained from a microscopic calculation. In agreement to the experiment, we find a crossover from diffusive to ballistic expansion.

1 General Transport Theory

Thinking about transport, the first thing coming into our minds might be electrical conductivity, which, on a macroscopical level, is usually given by Ohm's Law. The next candidate would be heat transport which obeys Fourier's Law. The deciding common feature of these phenomena is that both are constituted by currents of conserved quantities, electric charge in the former case, energy in the latter. Generally, for any locally conserved quantity with a density $\rho(x)$ a continuity equation

$$\partial_t \rho(x) + \nabla j(x) = 0 \quad (1.1)$$

holds, where $j(x)$ is the corresponding current. Crudely speaking, this means that the only way the density in a region can be altered is via a current through its boundary.

Clearly in thermal equilibrium there can not be any currents¹. Currents can, for instance, be induced by an symmetry breaking external field or by preparing the system in a non-equilibrium state. Both possibilities are considered in this thesis.

The purpose of transport theory is to deduce the principles for the behavior of currents from the microscopic properties of a system. Addressing correlated systems as they are common in condensed matter physics within their full complexity, this surely is a demanding task. The theory of *Linear Response* reduces this in some cases to a solveable problem. By stating that, for small perturbations, *out of equilibrium* properties are determined by correlation functions *in equilibrium*.

A very general Ansatz with less restrictions is provided by *Boltzmann Theory*, which on the other hand leaves the (generally not solvable) problem of calculating the scattering term, and hence needs more approximations there. Both methods are used in this work and are introduced in the present chapter.

1.1 Boltzmann Equation

The introduction to Boltzmann theory follows [1] and can be found in more details there. Consider a quantum system with some kind of carriers, which can be e. g. electrons, phonons or quasiparticles, whose eigensystem has quantum numbers \mathbf{k} . Out of equilibrium, the eigenstates are populated according to a *distribution function* $f(\mathbf{k}, \mathbf{r}, t)$. The Boltzmann equation describes the evolution in time of this distribution function by the means of a semi-classical equation of motion.

Without collisions, the time evolution is determined by

$$\frac{d}{dt} f(\mathbf{k}, \mathbf{r}) = \frac{\partial f}{\partial t} + \frac{\partial f}{\partial \mathbf{k}} \frac{\partial \mathbf{k}}{\partial t} + \frac{\partial f}{\partial \mathbf{r}} \frac{\partial \mathbf{r}}{\partial t}, \quad (1.2)$$

¹the occurrence of persistent currents and equilibrium is subtle and shall not be addressed here

1.1. BOLTZMANN EQUATION

where $\frac{\partial \mathbf{k}}{\partial t} = \mathbf{F}$ is an external force and $\frac{\partial \mathbf{r}}{\partial t} = \mathbf{v}_k = \frac{\partial \varepsilon_k}{\partial \mathbf{k}}$ is the group velocity of a quantum mechanical (quasi) particle with dispersion ε_k . The last two terms on the right hand side of equation (1.2) describe the motion of a particle due to external fields and diffusion. Together they are called the *drift-term* $d/(dt)f_k|_{\text{drift}}$ of the Boltzmann equation.

Scattering processes modify the distribution function. Assuming elastic scattering only, starting from an occupied state $|\mathbf{k}\rangle$, the probability, that the particle is scattered out of this state, is the probability density $\mathcal{P}_{k k'}$ of the transition into another state $|\mathbf{k}'\rangle$ integrated over all possible $|\mathbf{k}'\rangle$.

The scattering probability $\mathcal{P}_{k k'} d\mathbf{k}'$ depends on the occupation f_k of the state $|\mathbf{k}\rangle$ scattered from, and for fermions of the free phase space $(1 - f_{k'})$ of the states $|\mathbf{k}'\rangle$ scattered into, and the bare transition amplitude $\mathcal{Z}_{k k'}$, i. e. the overlap of the states, as

$$\mathcal{P}_{k k'} d\mathbf{k}' = f_k (1 - f_{k'}) \mathcal{Z}_{k k'} d\mathbf{k}'. \quad (1.3)$$

For the total change of f_k one has to account for all particles scattered out of and into the state $|\mathbf{k}\rangle$, leading to

$$\left. \frac{df_k}{dt} \right|_{\text{sc}} = \int d\mathbf{k}' (f_{k'} (1 - f_k) - f_k (1 - f_{k'})) \mathcal{Z}_{k k'} \quad (1.4)$$

Combining the two equations gives a nonlinear integrodifferential equation for the distribution function,

$$\frac{\partial f_k}{\partial t} + \mathbf{F} \frac{\partial f_k}{\partial \mathbf{k}} + \mathbf{v} \frac{\partial f_k}{\partial \mathbf{r}} = \int d\mathbf{k}' (f_{k'} (1 - f_k) - f_k (1 - f_{k'})) \mathcal{Z}_{k k'}, \quad (1.5)$$

referred to as the Boltzmann equation, in its version for fermionic carriers. It is totally clear that finding a solution of this equation in almost all cases must be beyond feasibility. Hence, approximations must be made. A very common simplification is the linearization for small deviations from equilibrium, i. e. $f_k = f_k^0 + \delta f_k$. Here f_k^0 is the equilibrium distribution function, which in case of fermionic particles is the Fermi-Dirac function $f_k^{FD} = 1/(\exp(\beta(\varepsilon_k - \mu)) + 1)$, with $\beta = 1/(k_B T)$ the inverse temperature and μ the chemical potential.

For the linearized Boltzmann equation, only terms to leading order in δf_k are retained. In the force term, the leading order contribution already comes from f_k^0 , which depends on \mathbf{k} only through the dispersion ε_k . The second term contains the spatial variations of the distribution function, which for f_k^0 requires the notion of local equilibrium with local temperature and chemical potential. Here again the leading contribution comes from the equilibrium part of the distribution function. Together one obtains

$$\left. \frac{\partial f_k}{\partial t} \right|_{\text{drift}} \approx \mathbf{v} \mathbf{F} \frac{\partial f_k^0}{\partial \varepsilon_k} + \mathbf{v} \left(\frac{\partial f_k^0}{\partial T} \nabla T + \frac{\partial f_k^0}{\partial \mu} \nabla \mu \right) \quad (1.6)$$

for the drift part.

Apparently, an electric force on charged particles can equivalently be included as either an external force or a gradient of chemical potential, so only one of the two possibilities has to be taken into account.

The scattering integral readily simplifies to

$$\left. \frac{\partial f_k}{\partial t} \right|_{\text{sc}} \approx \int d\mathbf{k}' (\delta f_k - \delta f_{k'}) \mathcal{Z}_{k k'}, \quad (1.7)$$

by using that for elastic scattering processes $f_k^0 = f_{k'}^0$, since the equilibrium distribution function depends only on the energy ε_k , which in such processes is conserved. Inserting the

linearized expressions for drift and scattering into (1.5), one obtains the *linearized Boltzmann equation*:

$$\frac{\partial f_k}{\partial t} + \mathbf{v} \mathbf{F} \frac{\partial f_k^0}{\partial \varepsilon_k} + \mathbf{v} \left(\frac{\partial f_k^0}{\partial T} \nabla T + \frac{\partial f_k^0}{\partial \mu} \nabla \mu \right) = - \int d\mathbf{k}' (\delta f_k - \delta f_{k'}) \mathcal{Z}_{kk'}, \quad (1.8)$$

which is a linear integrodifferential equation for the deviation δf_k from the equilibrium distribution function. While above only elastic scattering is discussed, for inelastic scattering a similar equation is obtained, with modified transition rates $\mathcal{Z}_{kk'}$. However, there is still the task of calculating the transition probabilities $\mathcal{Z}_{kk'}$. An obvious idea would be to use Fermi's golden rule for the transition rate but, already for systems with moderate number of dimensions, the momentum integrations became unfeasible.

One frequently used method to treat this problem is the *relaxation time approximation*, which states the form

$$\left. \frac{df_k}{dt} \right|_{sc} = \frac{\delta f_k}{\tau_k} \quad (1.9)$$

for the scattering term, where τ_k is called the scattering rate. The latter usually comes from a microscopic calculation or heuristic argumentation.

Another common way to find out an approximate solution is given by the *variational principle* for the Boltzmann equation, which will be explained after the introduction of transport coefficients in the next section.

1.2 Connection to Macroscopic Transport Coefficients

The Boltzmann equation and its derivatives introduced here are about distribution functions and their dependence on external perturbations. In typical experiments currents and fields can be measured directly. Naturally, one wants to deduce predictions from transport theories which can be tested by such an experiment. Thus, ultimately one has to calculate *transport coefficients*, which connect the experimentally accessible currents and fields, so the connection between the latter and distribution functions has to be made.

For this purpose, we need a theoretical definition of particle and heat current, which roots on the continuity equations, equation (1.1). With the *polarization operator*

$$\mathbf{P} = \int d\mathbf{r} \mathbf{r} \rho(\mathbf{r}), \quad (1.10)$$

where ρ is the particle density, and its analogue for the heat current,

$$\mathbf{R}_\varepsilon = \frac{1}{2} \int d\mathbf{r} (\mathbf{r} \mathcal{H}(\mathbf{r}) + \mathcal{H}(\mathbf{r}) \mathbf{r}), \quad (1.11)$$

where $\mathcal{H}(\mathbf{r})$ is the local Hamiltonian density of the studied system, one can deduce by integrating by parts and using the continuity equation, that the particle current is

$$\mathbf{J} = \partial_t \mathbf{P} = i[\mathbf{H}, \mathbf{P}] \quad (1.12)$$

and the heat current

$$\mathbf{J}_\varepsilon = \partial_t \mathbf{R}_\varepsilon = i[\mathbf{R}_\varepsilon, \mathbf{H}], \quad (1.13)$$

1.2. CONNECTION TO MACROSCOPIC TRANSPORT COEFFICIENTS

see [2]. In many cases, for the particle current only the kinetic part of the Hamiltonian contributes, since the polarization operator commutes with the density operator, which appears in most interactions. In momentum space representation, the particle current thus reads

$$\mathbf{J} = \sum_{\mathbf{k}} \mathbf{v}_{\mathbf{k}} \rho(\mathbf{k}), \quad (1.14)$$

where the velocity $\mathbf{v}_{\mathbf{k}} = \partial_{\mathbf{k}} \varepsilon(\mathbf{k})$ is the momentum derivative of the dispersion.

The operator \mathbf{R}_{ε} generically does not commute with any parts of the Hamiltonian, and contributions to the heat current arise from every interaction. For a lattice model, one writes \mathbf{R}_{ε} in terms of the site Hamiltonian h_i and the positions \mathbf{R}_i ,

$$\mathbf{R}_{\varepsilon} = \sum_i \mathbf{R}_i h_i, \quad (1.15)$$

where the sum over all h_i gives the Hamiltonian. The heat current then is

$$\mathbf{J}_{\varepsilon} = i \sum_{l,m} \mathbf{R}_l [h_m, h_l] \quad (1.16)$$

For a free particle system, this evaluates to

$$\mathbf{J}_{\varepsilon} = \sum_{\mathbf{k}} \mathbf{v}_{\mathbf{k}} \varepsilon_{\mathbf{k}} c_{\mathbf{k}}^{\dagger} c_{\mathbf{k}}, \quad (1.17)$$

modulo potential spin sums. Contributions to the heat current from interactions are typically very specific and will not be discussed here. In many applications, the interaction contributions are neglected, in particular for perturbative calculations in the interactions.

From the expressions (1.14) and (1.17), the connection to the Boltzmann formalism is quite obvious. The current of the respective carriers can be obtained from the distribution function with

$$\mathbf{J} = \int d\mathbf{k} \mathbf{v}_{\mathbf{k}} f_{\mathbf{k}} = \int d\mathbf{k} \mathbf{v}_{\mathbf{k}} \delta f_{\mathbf{k}} \quad (1.18)$$

and the related flux of energy is given by

$$\mathbf{J}_{\varepsilon} = \int d\mathbf{k} \varepsilon_{\mathbf{k}} \mathbf{v}_{\mathbf{k}} f_{\mathbf{k}} = \int d\mathbf{k} \varepsilon_{\mathbf{k}} \mathbf{v}_{\mathbf{k}} \delta f_{\mathbf{k}}. \quad (1.19)$$

The second equalities hold because in an equilibrated system there are neither particle nor energy currents.

From the structure of the linearized Boltzmann equation one can deduce that particle and thermal currents must be linear functions of the external fields \mathbf{F} and ∇T , i. e.

$$\begin{pmatrix} \mathbf{J} \\ \mathbf{J}_{\varepsilon} \end{pmatrix} = \begin{pmatrix} L_{FF} & L_{FT} \\ L_{TF} & L_{TT} \end{pmatrix} \begin{pmatrix} \mathbf{F} \\ \frac{1}{T} \nabla T \end{pmatrix} \quad (1.20)$$

By definition, the particle current $\mathbf{J} = \sigma \mathbf{F}$ must be measured at constant uniform temperature in a finite field. So the conductivity σ is identical to the coefficient L_{FF} . The latter is obtained within the relaxation time approximation by inserting equation (1.8) with $\nabla T = 0$ into the definition of the current, yielding

$$\mathbf{J} = \int d\mathbf{k} \mathbf{v}_{\mathbf{k}}^2 \frac{\partial f_{\mathbf{k}}^0}{\partial \varepsilon_{\mathbf{k}}} \tau_{\mathbf{k}} \mathbf{F} \quad (1.21)$$

from which one can directly read of the conductivity.

For the heat current $\mathbf{J}_\varepsilon = -\kappa \nabla T$ the situation is more complicated since a heat current is always accompanied by a particle current. This gives rise to thermoelectric effects. Experimentally a heat conductivity measurement is defined for a system which is insulated against particle current. Setting $\mathbf{J} = 0$ in equation (1.20) creates automatically a counterforce $\mathbf{F} = -L_{FT}/(TL_{FF})\nabla T$ to the temperature gradient. So the heat conductivity κ is not simply $-L_{TT}/T$ but

$$\kappa = -\frac{1}{T} \left(L_{TT} - \frac{L_{TF}L_{FT}}{L_{FF}} \right). \quad (1.22)$$

Inserting equation (1.8) into the definition of the thermal current, one obtains, again within relaxation time approximation

$$\mathbf{J}_\varepsilon = \int d\mathbf{k} v_k^2 \varepsilon_k \frac{\partial f_k^0}{\partial \varepsilon_k} \tau_k \mathbf{F} - \int d\mathbf{k} v_k^2 \varepsilon_k \frac{\partial f_k^0}{\partial T} \tau_k \nabla T. \quad (1.23)$$

Comparison of the coefficients allows us to identify the first integral with L_{TF} and the second one with $\kappa = -L_{TT}/T$. Yet one coefficient, namely L_{FT} , remains undetermined. Fortunately there are general relations for this kind of problem called Onsager relations that relate the off-diagonal elements of the matrix. For the used choice of *generalized force*² $1/T \nabla T$ associated with the *generalized current* \mathbf{J}_ε , the matrix of transport coefficients is symmetric,

$$L_{FT} = L_{TF}. \quad (1.24)$$

This relation shall not be proven here, the proof can be found, e. g. in [3].

In conclusion, the relaxation time approximation provides a straightforward recipe to calculate conductivities, once the relaxation time τ_k is known.

1.3 The Variational Principle of Transport Theory

The task of finding the solution of a linear inhomogeneous integral equation with a positive definite kernel such as the linearized Boltzmann equation is a typical problem of applied mathematics. Such equations are related to the variation of a certain integral. It is well known that the solution can be formally constructed by applying a variational principle to a general trial function. For this approach it is convenient to rewrite the Boltzmann equation in a canonical form in terms of a new function ϕ_k , defined by

$$f_k = f_k^0 - \phi_k \frac{\partial f_k^0}{\partial \varepsilon_k}, \quad (1.25)$$

which is a measure of the deviation from equilibrium, namely the average extra energy that the particles carry due to transport processes. By defining the scattering operator $\hat{\mathcal{P}}$ as a momentum integration over the transition probability kernel,

$$\hat{\mathcal{P}}(\dots) = \int d\mathbf{k}'(\dots) \mathcal{P}_{\mathbf{k}\mathbf{k}'}, \quad (1.26)$$

the right hand side of the Boltzmann equation (1.8) can be written as $\hat{\mathcal{P}}\phi_k/k_B T$. Similarly, X is defined such that $X/(k_B T)$ matches the left hand side, giving an alternative formulation of the Boltzmann equation

$$X = \hat{\mathcal{P}}\phi_k \quad (1.27)$$

²the choice of the generalized force corresponding to a current is not unique, see [2]

1.3. THE VARIATIONAL PRINCIPLE OF TRANSPORT THEORY

in terms of the newly introduced operators.

Taking the *inner product*, defined by

$$\langle \phi, \psi \rangle = \int d\mathbf{k} \phi_{\mathbf{k}} \psi_{\mathbf{k}}, \quad (1.28)$$

of equation (1.27) and the trial function $\phi_{\mathbf{k}}$, the canonical form of the integral equation,

$$\langle \phi, X \rangle = \langle \phi, \hat{\mathcal{P}}\phi \rangle \quad (1.29)$$

is obtained. It can be proven by elementary algebra that the solution $\phi_{\mathbf{k}}$ of this integral equation gives the minimal value to the functional

$$\frac{\langle \phi, \hat{\mathcal{P}}\phi \rangle}{\langle \phi, X \rangle^2}, \quad (1.30)$$

as shown e. g. in [1]. However, the mathematical formulation of the problem does not give much insight into the underlying physics, which becomes clearer from a thermodynamic formulation of this variational principle.

The relevant physical quantity one has to look at is the entropy, which is generalized to non-equilibrium with the *Shannon-entropy*, defined as

$$S = -k_B \int d\mathbf{k} (f_{\mathbf{k}} \ln f_{\mathbf{k}} + (1 - f_{\mathbf{k}}) \ln(1 - f_{\mathbf{k}})). \quad (1.31)$$

Differentiating this expression with respect to time one obtains, to leading order in $\phi_{\mathbf{k}}$, the rate of entropy production

$$\dot{S} \approx -\frac{1}{T} \int d\mathbf{k} \phi_{\mathbf{k}} \dot{f}_{\mathbf{k}} + \frac{1}{T} \int d\mathbf{k} E_{\mathbf{k}} \dot{f}_{\mathbf{k}}. \quad (1.32)$$

The second term vanishes for systems with conserved energy. The remaining term can be transformed to a function of the integrals $\langle \phi, X \rangle$ and $\langle \phi, \hat{\mathcal{P}}\phi \rangle$, which constitute the mathematical form of the variational principle, equation (1.30), by inserting the Boltzmann equation (1.5) expressed in terms of the new functions $\phi_{\mathbf{k}}$, namely

$$\dot{f}_{\mathbf{k}}^{\text{sc}} = \frac{1}{k_B T} \int d\mathbf{k}' (\phi_{\mathbf{k}} - \phi_{\mathbf{k}'}) \mathcal{P}_{\mathbf{k}\mathbf{k}'} = \frac{1}{k_B T} \hat{\mathcal{P}}\phi. \quad (1.33)$$

One obtains for the scattering part of the entropy production the positive definite expression

$$\dot{S}_{\text{sc}} = \frac{1}{2k_B T} \iint d\mathbf{k} d\mathbf{k}' (\phi_{\mathbf{k}} - \phi_{\mathbf{k}'})^2 \mathcal{P}_{\mathbf{k}\mathbf{k}'} = -\frac{1}{T} \langle \phi, \hat{\mathcal{P}}\phi \rangle, \quad (1.34)$$

which implicitly proves Boltzmann's *H-theorem*³ for an assembly of fermions. On the other hand, the drift part of the entropy production rate can be deduced from equation (1.32) by applying the canonical form, equation (1.29), of the Boltzmann equation, giving

$$\dot{S}_{\text{drift}} = \frac{1}{T} \langle \phi, X \rangle, \quad (1.35)$$

³which states that the entropy of an assembly increases irreversibly, despite reversible microscopic dynamics, originally proven by Boltzmann for the ideal gas, [4].

which can be evaluated to be minus the *macroscopic* rate of entropy production,

$$\dot{S}_{\text{drift}} = -\nabla \left(\frac{1}{T} \mathbf{J}_\epsilon \right) - \frac{1}{T} \mathbf{J} \mathbf{F} = -\dot{S}_{\text{macro}}. \quad (1.36)$$

In total, the rate of entropy production is a function of the variational integrals $\langle \phi, \hat{\mathcal{P}} \phi \rangle$ and $\langle \phi, x \rangle$, and thus must become extremal.

In summary, the variational principle states that in the steady state the currents are such that the production of entropy takes the maximal value. This of course is totally equivalent to the mathematical formulation in equation (1.30).

Practically, conductivities can be calculated from this principle. For example in a system with a finite force and no thermal gradient, the macroscopic entropy production is $\dot{S}_{\text{macro}} = \mathbf{F} \mathbf{J} / T = \mathbf{J}^2 / \sigma T$. In the steady state, \dot{S}_{macro} must be equal to the entropy production due to scattering \dot{S}_{sc} , thus the equation can be solved for the conductivity, giving

$$\sigma = \frac{\mathbf{J}^2}{T \dot{S}_{\text{sc}}} = - \frac{\left(\int d\mathbf{k} \mathbf{v}_\mathbf{k} \phi_\mathbf{k} \frac{\partial f_\mathbf{k}^0}{\partial \epsilon_\mathbf{k}} \right)^2}{\langle \phi, \hat{\mathcal{P}} \phi \rangle}, \quad (1.37)$$

where the current has been expressed in $\phi_\mathbf{k}$. According to the variational principle, the conductivity thus must be extremal for the solution. Therefor, the minimization of the entropy production rate \dot{S}_{sc} for a fixed current \mathbf{J} is equivalent to solving the Boltzmann equation.

Inserting any trial function gives a lower bound to the physical conductivity. As an approximation one typically chooses a linear combination of standard functions weighted by variational parameters and performs the optimization numerically or, in simple cases, algebraically.

If the trial functions are well-chosen, the result will be close to the real solution, but a good choice requires some insight into the underlying mechanisms, since there is no general rule of which functions the variational trial function should be composed.

1.4 Theory of Linear Response

The idea of linear response theory is to split the Hamiltonian into two parts, where for the first one the eigensystem is known and the second one acts as a small perturbation to it such that one can use time-dependent perturbation theory⁴.

For the expectation value of any current operator $\hat{\mathbf{j}}(\mathbf{r}, t)$ the *Kubo formula*

$$\delta \langle \hat{j}_\alpha(\mathbf{r}, t) \rangle = -i \int_{-\infty}^t dt' \langle [\hat{j}_\alpha(\mathbf{r}, t), H'(t')] \rangle \quad (1.38)$$

gives the response to the external perturbation $H'(t')$ where the brackets stand for thermal average in the Matsubara formalism. In the case of electrical current in a solid responding to an external electric field, expressed by the vector potential \mathbf{A} , the perturbation can be written as

$$H'(t) = -\frac{1}{c} \sum_\alpha \int d\mathbf{r} \hat{j}_\alpha(\mathbf{r}) A_\alpha(\mathbf{r}, t), \quad (1.39)$$

⁴the framework of manybody perturbation theory is reviewed for example in [2]

1.4. THEORY OF LINEAR RESPONSE

where the electrical field $\mathbf{E} = c\partial_t\mathbf{A}$ is expressed in terms of the vector potential \mathbf{A} . This leads to a separable form of equation (1.38)

$$\delta \langle \hat{j}_\alpha(\mathbf{r}, t) \rangle = \frac{1}{cV} \sum_{\beta} \int_{-\infty}^t dt' \int d\mathbf{r}' \langle [\hat{j}_\alpha(\mathbf{r}, t), \hat{j}_\beta(\mathbf{r}', t')] \rangle A_\beta(\mathbf{r}', t'). \quad (1.40)$$

The time integral depends only on the difference $t - t'$. This result can be simplified further by using translational invariance to give the relation as function of the momentum. From that, the matrix which connects the current \hat{j} with the external field \mathbf{E} is obtained as

$$\sigma_{\alpha\beta}(\mathbf{q}, \omega) = \frac{1}{\omega V} \int_0^\infty dt e^{i\omega t} \langle [\hat{j}_\alpha(-\mathbf{q}, t), \hat{j}_\beta(\mathbf{q}, 0)] \rangle + i \frac{n_0 e^2}{m\omega} \delta_{\alpha\beta}, \quad (1.41)$$

which gives the conductivity in terms of correlation functions. The latter depend only on properties of the system and not on the perturbation. The second term in equation (1.41) is called the *diamagnetic* or *static* conductivity. The derived expression for $\sigma_{\alpha\beta}$ contains the Fourier transform of the retarded *current-current correlation function*, defined as

$$\Pi_{\alpha\beta}(\mathbf{q}, t - t') = -\frac{i}{V} \theta(t - t') \langle [\hat{j}_\alpha(-\mathbf{q}, t), \hat{j}_\beta(\mathbf{q}, 0)] \rangle \quad (1.42)$$

The thermal average can be carried out by doing an integral over Matsubara frequencies in complex time plane. The equivalent Matsubara current-current correlation function is

$$\Pi_{\alpha\beta}(\mathbf{q}, i\omega_n) = -\frac{1}{V} \int_0^\beta d\tau e^{i\omega_n \tau} \langle T_\tau \hat{j}_\alpha(-\mathbf{q}, \tau) \hat{j}_\beta(\mathbf{q}, 0) \rangle, \quad (1.43)$$

where T_τ denotes time-ordering and β inverse temperature. Using analytic continuation, from equations (1.41) and (1.42) it can be easily seen that

$$\sigma_{\alpha\beta}(\mathbf{q}, \omega) = \frac{i}{\omega} \left(\lim_{\delta \rightarrow 0} \Pi_{\alpha\beta}(\mathbf{q}, \omega + i\delta) + \frac{n_0 e^2}{m} \delta_{\alpha\beta} \right). \quad (1.44)$$

To obtain the dc conductivity one has to take the limits $\mathbf{q} \rightarrow 0$ and *subsequently* $\omega \rightarrow 0$. Since for a static electric field there is no absorption, the conductivity must be real, which implies that the diamagnetic term does not contribute. One concludes

$$\sigma_{dc} = \text{Re} \left[\lim_{\omega \rightarrow 0} \sigma_{\alpha\beta}(0, \omega) \right] = \lim_{\omega \rightarrow 0} \left(\frac{1}{\omega} \lim_{\delta \rightarrow 0} \text{Im} [\Pi_{\alpha\beta}(0, \omega + i\delta)] \right), \quad (1.45)$$

which gives a straightforward recipe to calculate conductivities from microscopic correlation functions. Alternatively, one can write this result as

$$\text{Re} [\sigma_{\alpha\beta}] = \frac{1}{V} \lim_{\delta \rightarrow 0} \int_0^\infty dt e^{-\delta t} \int_0^\beta d\lambda \langle \hat{j}_\beta(-t - i\lambda) \hat{j}_\alpha(0) \rangle, \quad (1.46)$$

which is completely equivalent, and it will be useful in the subsequent introduction of an hydrodynamic approach.

In the same fashion the linear transport coefficient L between any *thermodynamical flux* \mathcal{J}_I and its *conjugate thermodynamic force* \mathcal{F}_I can be obtained from the auto-correlation function of the current by

$$L_{II} = -\frac{1}{\beta} \lim_{\delta \rightarrow 0} \int_0^\infty dt e^{-\delta t} \int_0^\beta d\lambda \langle \mathcal{J}_\alpha^I(-t - i\lambda) \mathcal{J}_\beta^I \rangle, \quad (1.47)$$

which is called the *Green-Kubo relation* [5, 6].

The limitations of this approach are obvious because one still has to calculate correlation functions, which, in most cases, can only be done by means of perturbative approximations.

1.5 Conservation Laws: Hydrodynamic Approach

The calculation of the needed correlation functions for conductivities in linear response for a correlated system is again a non-trivial problem. Particularly, there is one major complication, which lies in the principles of perturbation theory. The standard method to calculate correlation functions in correlated systems is to split the Hamilton operator into two parts, the *free* part \hat{H}^0 , for which the eigensystem is known, and the *interacting* part \hat{H}^{int} , which is regarded as a weak perturbation to \hat{H}^0 .

In the case of the needed current-current correlation function, often the current J happens to be a *conserved quantity* of the free Hamiltonian \hat{H}^0 , which implies a vanishing scattering rate τ_k^{-1} and infinite conductivity σ . Naturally, for the interacting part, which contains the scattering mechanism, the relaxation time becomes finite and so does the conductivity. Apparently, a perturbative expansion in powers of the scattering operator must be highly singular. This means that the perturbation theory must be set up in a cleverer way, i. e. to do perturbation theory in the inverse coupling constant $1/g$ of the scattering process. This leads to the *Memory Matrix* formalism introduced by Mori [7] and Zwanzig [8], and introduced to solid state applications in [9].

In this section, the derivation of Memory Matrix formalism shall be reviewed, following the textbook of Forster⁵ [10]. The basic idea is that in a system with conservation laws which are weakly violated by a perturbation, the main contribution to the current comes from the *hydrodynamic* modes with the slowest decay rate. By means of the projection operator technique the relevant part of the problem is separated. For this, the current must be reformulated as series of modes, which form a Hilbert space with the scalar product

$$(A|B) = \frac{1}{V} \int_0^\beta d\tau \langle A^\dagger(0) B(i\tau) \rangle - \beta \langle A^\dagger \rangle \langle B \rangle. \quad (1.48)$$

The second term can always be absorbed by a redefinition of A as $A - \langle A \rangle$. The operators A, B are regarded as vectors of the Hilbert space and their time dependence is generated by the *Liouville operator* $\mathcal{L} \cdot = [H, \cdot]$ with

$$|A(t)\rangle = |e^{iHt} A e^{-iHt}\rangle = e^{i\mathcal{L}} |A\rangle \quad (1.49)$$

⁵Note that for convenience all definitions of correlation functions deviate slightly from [10] by a factor of β

1.5. CONSERVATION LAWS: HYDRODYNAMIC APPROACH

In this language, the Kubo-expression for the conductivity reads

$$\sigma = \int_0^{\infty} dt e^{i\omega t} (j(t)|j), \quad (1.50)$$

where the Laplace transform can be carried out to give

$$\sigma = \left(j \left| \frac{i}{\omega - \mathcal{L}} \right| j \right). \quad (1.51)$$

Note that this expression is totally equivalent to the linear response Kubo formula, equation (1.38), including the diamagnetic term, which can be seen by changing to the Lehmann representation.

The Hilbert space spanned by all modes of the system can be decomposed into one subspace which is spanned by modes with short scattering times and one subspace which contains modes that would be protected by conservation laws in the unperturbed system. Without the perturbation, the latter would have infinite scattering times, which are rendered finite, but still large by the perturbation. In the hydrodynamic regime, these slowly decaying, or shorter, *slow modes* of the system carry most of the current. To proceed, one defines projection operators \mathcal{P} and \mathcal{Q} onto the subspace spanned by slow modes respectively by all other modes. For a set $\{J_1, \dots, J_N\}$ of slow modes the projection operator \mathcal{P} can be written as

$$\mathcal{P} = \sum_{i,j=1}^N |J_i\rangle \frac{1}{(J_i|J_j)} (J_j|, \quad (1.52)$$

where the denominator is the i, j element of the matrix of *static susceptibilities*

$$\chi_{i,j} = (J_i|J_j), \quad (1.53)$$

related to the according equal time correlation function.

In such a system with N slow modes, the physical current can be written as a series of modes

$$|j\rangle = \sum_i \frac{1}{(J_i|J_i)} (J_i|j) |J_i\rangle, \quad (1.54)$$

with the index i running over all modes. The physical conductivity σ then mainly depends on all J_i - J_j correlation functions, but as it will be seen later on, only the slow mode conductivities must be retained. They are organized as the *matrix of conductivities*

$$\sigma_{i,j} = \left(J_i \left| \frac{i}{\omega - \mathcal{L}} \right| J_j \right). \quad (1.55)$$

Applying the truncation in *slow* and *fast* subspaces on the Liouville operator $\mathcal{L} = \mathcal{L}\mathcal{P} + \mathcal{L}\mathcal{Q}$, one can evaluate the current-current correlation function further, as

$$\left(j \left| \frac{i}{\omega - \mathcal{L}} \right| j \right) = \left(j \left| \frac{i}{\omega - \mathcal{L}\mathcal{Q}} \right| j \right) + \left(j \left| \frac{1}{\omega + \mathcal{L}\mathcal{Q}} \mathcal{L}\mathcal{P} \frac{i}{\omega - \mathcal{L}} \right| j \right), \quad (1.56)$$

where the algebraic operator identity

$$\frac{1}{X+Y} = \frac{1}{X} - \frac{1}{X} Y \frac{1}{X+Y} \quad (1.57)$$

has been applied. In the first term of equation (1.56) the $i/(\omega - \mathcal{L}\mathcal{Q})$ can be expanded in a Taylor series in \mathcal{L} . It can be easily seen that only the zero-order term of this series can contribute, since every higher order term contains a projector \mathcal{Q} onto the fast decaying modes on the right side, which kills its contribution.

Inserting the definition of \mathcal{P} into the second term, one obtains after some simple algebra

$$\left(j \left| \frac{1}{\omega + \mathcal{L}\mathcal{Q}} \mathcal{L}\mathcal{P} \frac{i}{\omega - \mathcal{L}} \right| j\right) = \left(j \left| \frac{1}{\omega + \mathcal{L}\mathcal{Q}} \mathcal{L} \right| j\right) \left(j \left| \frac{i}{\omega - \mathcal{L}} \right| j\right) \chi^{-1}. \quad (1.58)$$

Resinserting this into equation (1.56), the equation can be solved for $(j(t)|j)$, giving the matrix expression

$$\sigma_{i,j} = \chi_{i,j} (-i(\omega\chi + L) + M)_{i,j}^{-1} \chi_{i,j} \quad (1.59)$$

for the conductivity, where the matrix $L = (j|\mathcal{L}|j)$ is independent of frequency and will be neglected later on, and

$$M_{i,j} = \left(J_i \left| \mathcal{L}\mathcal{Q} \frac{i}{\omega - \mathcal{L}\mathcal{Q}} \mathcal{Q}\mathcal{L} \right| J_j\right) = \left(\partial_t J_i \left| \mathcal{Q} \frac{i}{\omega - \mathcal{L}\mathcal{Q}} \mathcal{Q} \right| \partial_t J_j\right) \quad (1.60)$$

are the elements of the *memory matrix*. The physical conductivity σ can be obtained from equation (1.59) with

$$\sigma = \sum_{i,j=1}^N \frac{(j|J_i)(J_j|j)}{\chi_{i,i}\chi_{j,j}} \sigma_{i,j}. \quad (1.61)$$

This expression for the conductivity is exact for the perfect choice of the slow modes. However, it has been shown [11] that the conductivity obtained with *any* set of modes gives a lower bound to the real conductivity. This means that the better the choice of the slow modes and the more modes are included, the better the result for the conductivity.

The dependence of the quality of the result of the choice of slow modes makes the memory matrix formalism resemble the variational principle of transport theory, where also an improved test function gives an increase in the accuracy of the obtained lower bound for the conductivity. Actually the two approaches are completely equivalent in cases where the Boltzmann equation applies, as Belitz has proven in 1984, [12]. The advantage of using the memory matrix formalism lies in an inherent possibility of finding suitable slow modes and, of course, the matrix structure of the scattering which accounts for conservation laws. In addition, the memory matrix formalism can even be used in cases where no Boltzmann equation description is possible as, for instance, in Luttinger liquids.

By construction, the conserved quantities of the unperturbed system are a good choice for the slow modes. Using them reveals the biggest advantage of the formalism: the memory matrix, equation (1.60), is a matrix of correlation functions of *time derivatives* of currents. If these currents are conserved quantities of the pure system, their time derivatives are already linear in the perturbations. Due to this, the memory matrix in lowest order in the perturbations is equal to the memory matrix calculated within the Liouville operator of the *unperturbed system*. This is a great simplification and accounts for the practical significance of the formalism.

For the actual calculation of the memory matrix, it is convenient to drop the scalar product introduced for the derivation and switch back to the language of correlation functions. Then the definition, equation (1.60), reads

$$M_{i,j} = \frac{i}{\omega} \left(\int_0^\infty dt e^{i\omega t} \langle [J_i(t), J_j] \rangle^{\text{low}} + \beta \langle J_i^\dagger \rangle \langle J_j \rangle \right) = \frac{i}{\omega} \left(\langle J_i; J_j \rangle_\omega^{\text{low}} - \langle J_i; J_j \rangle_{\omega=0}^{\text{low}} \right), \quad (1.62)$$

1.5. CONSERVATION LAWS: HYDRODYNAMIC APPROACH

where $\langle .; . \rangle^{\text{low}}$ denotes the Fourier transform of the Matsubara correlation function, calculated with the low energy Hamiltonian. As already pointed out, in equation (1.45), the dc-conductivity is obtained by taking the limit $\omega \rightarrow 0$ of the real part of the conductivity σ at $\mathbf{q} = 0$. Since the matrix χ is purely real, one sees from equation (1.59) that one needs the real part of the memory matrix,

$$\text{Re} [M_{i,j}] = \frac{1}{\omega} \text{Im} \left[\langle J_i; J_j \rangle_{\omega}^{\text{low}} - \langle J_i; J_j \rangle_{\omega=0}^{\text{low}} \right]. \quad (1.63)$$

This object can, not easily but routinely, be calculated for several correlated systems for which a low energy theory is known. In particular in one-dimensional systems, where many systems are known to exhibit the Luttinger Liquid behavior as low energy fixed point, this is extremely useful. Accordingly, the formalism has been applied in the past to calculate properties like Umklapp resistivity in one-dimensional fermion systems [13], conductivity of clean one-dimensional wires [14], heat conduction and Wiedemann-Franz law of disordered Luttinger liquids [15], thermal conductivity of spin-1/2 chains [16], heat transport of clean spin-ladders coupled to phonons [17], and it has been demonstrated a powerful tool for the treatment of transport properties in correlated systems.

2 Scattering of Fast Phonons

One typical application of the relaxation time approximation to the linearized Boltzmann equation is the calculation of the heat conductivity in a metal, i. e. a system where electrons and phonons can carry heat currents. In the "conventional" case where the velocity of the phonons is much higher than the electron velocity, the theory is well established. The scattering rates for all kinds of interactions have been calculated a long time ago ¹ from the respective self-energies in first order perturbation theory.

Especially for the electron-phonon interaction the perturbation theory treatment works very well, giving accurate predictions for conductivities. The deeper reason for the good convergence is found with the *Migdal theorem* ([18]), which states that vertex corrections to the electron-phonon interaction only play a minor role in systems where the electrons are much faster than the phonons. More precisely the exact interaction vertex, i. e. the sum over all vertex corrections, is

$$\Gamma = \gamma \left(1 + \mathcal{O} \left[\left(\frac{m}{M} \right)^{\frac{1}{2}} \right] \right) \quad (2.1)$$

where γ is the bare interaction vertex and m , M are the masses of the electrons and phonons, respectively.

This theorem seemed to cover all the practically relevant regimes. However, with the discovery of heavy fermion compounds ([19], see [20] for a review), the question of electron phonon scattering must be revisited. Also spinchain compounds with small coupling constants provide a realization of a fast-phonon-slow-fermion setup, when one uses the Jordan-Wigner mapping of the spinons to spinless fermions [21].

Despite the large research interest that heavy fermion materials attracted in the recent years, the question of such systems interacting with phonons hardly appears in the literature. Only very recently, a group of theorists from Würzburg, Göttingen and Baton Rouge, [22], studied the impact of phonons to the coherence scale of models of heavy fermions. They investigated a periodic Anderson model with coupling of the conduction electrons to Holstein phonons by means of a combination of the slave boson method and Migdal-Eliashberg approximation, as well as the dynamical mean-field theory. From the obtained phonon corrections to the electronic selfenergy they conclude the breakdown of the Migdal theorem and a large reduction of the coherence temperature already at weak electron phonon coupling. Also, an enhancement of magnetic instabilities driven by Ruderman-Kittel-Kasuya-Yosida interactions between local moments is predicted. As a goal to future studies, they want to investigate the interplay of these instabilities within the framework of cluster methods.

Concerning magnetic systems, only a two-dimensional example could be found in the literature. Motivated by an experimental study on the isotope effect on the Néel temperature in antiferromagnetic cuprates, [23], R. Hlubina and G. K. Sadiek investigated an effective

¹for a review of the theory of electron and phonon heat conduction see [1]

2.1. ELECTRON-PHONON SCATTERING

spin model for strongly interacting electrons at half filling, coupled to phonons, [24]. The phonon energy was assumed to be larger than the antiferromagnetic coupling, and the authors concluded the existence of an isotope effect to the Néel temperature in this limit, which matches the order of magnitude of the observations in the experiment.

In the context of superconductivity of fullerene compounds, which have a very low Fermi energy of the order of the Debye frequency, C. Grimaldi, L. Pietronero, and S. Strässler formulated a generalization to the Eliashberg equation for interaction with phonons which includes vertex corrections, [25, 26, 27], from which they derived the occurrence of non-adiabatic effects. In particular, they predict a strong dependence of the critical temperature of superconductivity on the ratio of the Debye frequency and the Fermi energy.

However, so far nobody seems to have investigated the transport properties of systems with slow fermionic excitations coupled to fast phonons. In this chapter, the heat conductivity of phonons scattered from fast fermions, both, one- and three-dimensional, will be discussed.

2.1 Electron-Phonon Scattering

On the most general level the Hamiltonian of a solid contains interaction terms between all possible degrees of freedom, in particular kinetic terms for electrons and ions plus interactions between them. This is simplified using the Born approximation, which assumes that electrons move around easily, but ions stay fixed at their positions and form the crystal lattice.

By relaxing the constraint for the ions slightly, allowing for small vibrations around the mean position one introduces collective modes of lattice vibrations. These so-called *phonons* are bosonic quasi-particles with linear dispersion at low energies, which is captured within the *harmonic approximation*. The derivation is straight-forward by using canonical quantization of the displacement fields (see e. g. [2]).

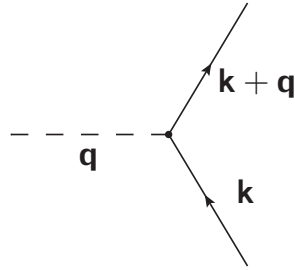


Figure 2.1: Elementary vertex for interaction between electrons and phonons. Dashed lines represent phonon Green's function and continuous lines fermionic ones. While the fermion propagator has a direction dependence, the phonon propagator is the superposition of two counterpropagating modes.

A solid with a simple cubic lattice has three acoustic phonon modes with different polarizations. For simplicity, here only one transverse mode is taken into account. The Hamiltonian for this simplified system then reads

$$H^{\text{ph}} = \sum_{\mathbf{q}} \omega_{\mathbf{q}} a_{\mathbf{q}}^{\dagger} a_{\mathbf{q}}, \quad (2.2)$$

where $a_{\mathbf{q}}^{(\dagger)}$ annihilates (creates) a phonon with (crystal-) momentum \mathbf{q} and the phonon

frequency

$$\omega_{\mathbf{q}} \approx \sqrt{\frac{K}{M}} a |\mathbf{q}| \quad (2.3)$$

is linear for small momenta. The latter depends on the ion mass M , the lattice spacing a (which is set to be 1 in the following), and the force constant K .

The lattice vibrations have direct impact on the electronic system, which can be described in the *tight-binding* approximation². Within this, the electronic wave-functions in real-space are written in a series of *Wannier-functions*, which are localized at the lattice sites. Their dynamics then are dominated by the overlap of Wannier-functions at neighboring sites, which allows to write the Hamiltonian in second quantization as

$$H^{\text{el}} = \sum_{i,j,\sigma} t_{ij} c_{i\sigma}^{\dagger} c_{j\sigma}, \quad (2.4)$$

where t_{ij} denotes the hopping amplitude from a Wannier state at site i to a Wannier state at site j and $c_{i\sigma}^{\dagger}$ annihilates (creates) an electron with spin σ at site i . For simplicity here only one Wannier state per site is assumed, which corresponds to taking into account only the lowest electronic band. For fixed ion positions, this Hamiltonian is easily diagonalized by Fourier transformation, which yields

$$H^{\text{el}} = \sum_{\mathbf{k},\sigma} \varepsilon_{\mathbf{k}} c_{\mathbf{k}\sigma}^{\dagger} c_{\mathbf{k}\sigma} \quad (2.5)$$

with the electronic dispersion $\varepsilon_{\mathbf{k}}$.

Allowing for weak deviations from the equilibrium positions of the ions, the hopping matrix elements t_{ij} become a function of this deviation, since the overlap of neighboring Wannier-functions changes when the ions are displaced from their position, e. g. by a vibrational mode. By expanding the t_{ij} in a power series in the displacement one obtains to linear order an electron phonon interaction part to the Hamiltonian. Generally it has the form

$$H^{\text{el-ph}} = - \sum_{\mathbf{q},\mathbf{G}} \rho(\mathbf{q} + \mathbf{G}) V_{\text{el-ph}}(\mathbf{q} + \mathbf{G}) (\mathbf{q} + \mathbf{G}) \sqrt{\frac{\hbar}{2MN\omega_{\mathbf{q}}}} (a_{\mathbf{q}} + a_{-\mathbf{q}}^{\dagger}), \quad (2.6)$$

where the sum is over all phonon momenta \mathbf{q} in the first Brillouin zone and all reciprocal lattice vectors \mathbf{G} . The sum over the reciprocal lattice vectors reflects the lower symmetry of a solid in comparison to free space, which reduces the conservation of momentum to the conservation of *crystal momentum*, which means momentum modulo reciprocal lattice vectors. The main effect in this context is the possible scattering of electrons and phonons with high momenta, which sum up to a reciprocal lattice vector, which is called an *Umklapp*-, or *U*-process, in contrast to a *Normal*- or *N*-process. At low temperatures only small momenta are thermally populated, hence the summation can be restricted to *N*-processes. ρ is the Fourier transform of the electron density

$$\rho(\mathbf{q}) = \sum_{\mathbf{k},\sigma} c_{\mathbf{k}+\mathbf{q}\sigma}^{\dagger} c_{\mathbf{k}\sigma}. \quad (2.7)$$

The electron electron interaction is neglected here, since it must be subleading in the phonon scattering process. For three dimensional fermions this approximation is also legitimated by Landau Fermi-Liquid theory [29, 30, 31], which assures that interaction between electrons at low temperatures only renormalizes the effective mass, i. e. the dispersion.

²see any textbook on solidstate physics, e. g. [28]

2.2 First Order Contribution: Conservation Laws

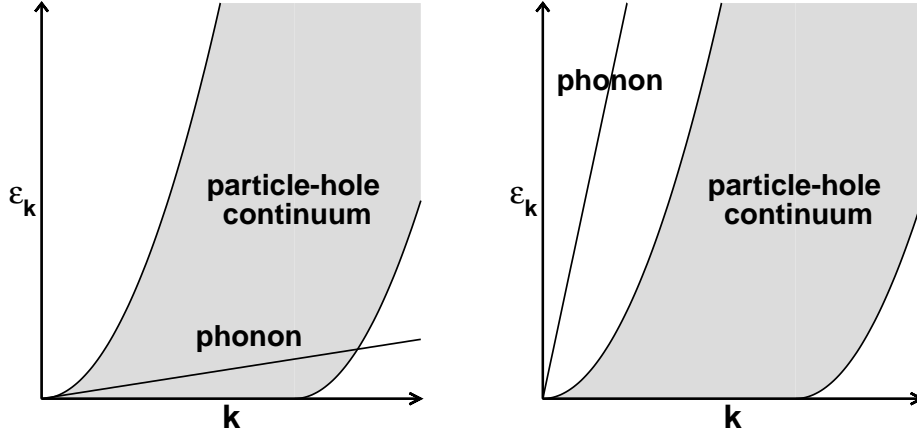


Figure 2.2: Excitation spectra of three-dimensional phonons and three-dimensional fermions. As in the latter case, for ratio of velocities $v_P/v_F \ll 1$ (left) there is damping, for $v_P/v_F \gg 1$ (right) there is none.

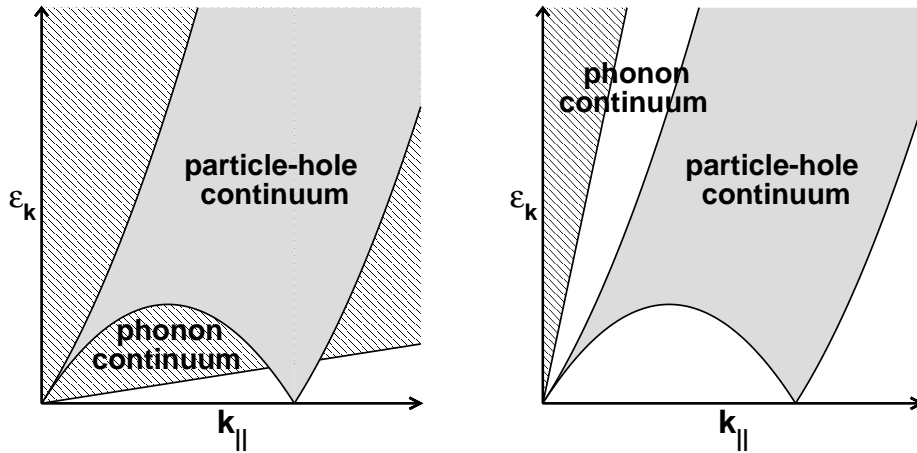


Figure 2.3: Excitation spectra of three-dimensional phonons and one-dimensional fermions. As function of the parallel component of the momentum $k_{||}$, the phonon spectrum becomes a continuum. For ratio of velocities $v_P/v_F \ll 1$ (left) the spectra overlap, thus phonons can decay into particle-hole excitations. For $v_P/v_F \gg 1$ (right) there is no damping and the lifetime of the phonons is infinite to first order.

While for the scattering of slow phonons the first order self-energy of the phonons already gives a good approximation to the lifetime, for fast phonons this can be excluded by simple physical arguments. Concerning three-dimensional fermions, the one-particle excitation spectrum for small momenta is the well-known particle hole continuum with quadratic boundary, see figure 2.2. An acoustic phonon with dispersion $\omega_{\mathbf{q}} = v_P |\mathbf{q}|$ will intersect this continuum for $v_P \ll v_F$, but there is no intersection at small momenta for large phonon velocities v_P . At large momenta the spectra might intersect at some point, since higher bands or multi-particle excitations start to play a role, but at low temperatures the corresponding high energy phonon states just will not be populated. Thus the first order scattering process can

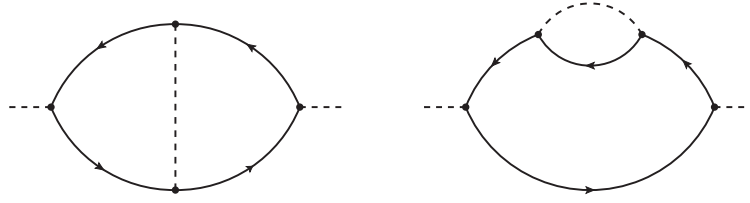


Figure 2.4: All allowed diagrams to the phonon self-energy to second order.

not conserve energy and momentum in any accessible part of the phase space, implying the phonon self-energy being zero to first order in electron-phonon interaction.

In the case of one-dimensional fermions, depicted in figure 2.2, the situation is only slightly different. The scattering process between three-dimensional phonons and one-dimensional fermions doesn't conserve (crystal-) momentum, but only its parallel component. So the relevant spectrum of the phonons is no longer linear, but a continuum with $\omega_q \geq v_P |q_{||}|$. On the other hand, in one dimension the particle hole continuum of the fermions narrows to a small wedge at small momenta. In total, just like for three-dimensional fermions, there is no intersection of the phonon and fermion excitation spectra and thus no phonon decay in first order perturbation theory.

2.3 Second Order Processes

In second order perturbation theory, it is possible to construct two distinct diagrams from the elementary vertex (figure 2.1). They are shown in figure 2.4. It turns out during the calculation that these diagrams would cancel exactly for a purely linear electron dispersion. Thus, the backscattering of a phonon must be a band-curvature effect.

For the calculation of the phonon lifetime, from which the heat conductivity can be obtained in relaxation time approximation, only the imaginary parts of these diagrams are needed. This can be achieved in a convenient way by exploiting the *branch cuts* of the Green's functions (see Appendix A). By directly applying the imaginary part to the diagrams, one generates a sum of products of real and imaginary parts of the contained free propagators. Only those contributions which contain "propagating" Green's functions from one external leg to the other are of interest, since local bubbles cannot transport momentum.

It can easily be seen that this is the case only for such diagrams where each two interaction vertices are connected by a real part of a fermion Green's function. By combining them into the *effective vertex* (figure 2.5) the imaginary part of the phonon self-energy can be expressed as a single diagram

Unlike the elementary vertex, which depends only on one phonon momentum and no

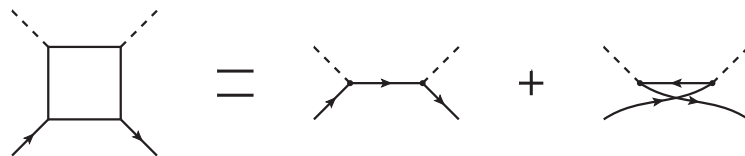


Figure 2.5: Effective vertex for scattering of a phonon and a fermion. The inner fermionic Green's function contributes only with its real part, which renormalizes the vertex.

2.3. SECOND ORDER PROCESSES

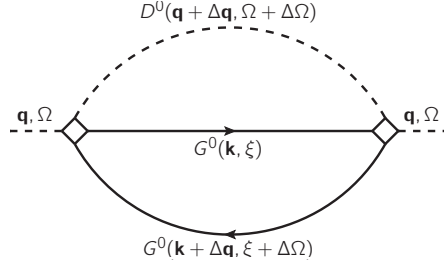


Figure 2.6: Phonon-selfenergy to second order expressed in effective scattering vertices

energy

$$M_q^{\text{elem}} = -V_{\text{el-ph}}(\mathbf{q}) \mathbf{q} \sqrt{\frac{\hbar}{2MN\omega_q}}, \quad (2.8)$$

the effective vertex depends on the momenta of both involved phonons plus momentum and energy of the inner virtual fermion. Consider the phonon and fermion coming in from the left with momentum \mathbf{q} and $\mathbf{k} + \Delta\mathbf{q}$ and energy Ω and $\xi + \Delta\Omega$ respectively. After the scattering the momentum $\Delta\mathbf{q}$ and the energy $\Delta\Omega$ has been transferred. The effective vertex for this process expressed in formulas is

$$M_{\mathbf{q}, \mathbf{q}+\Delta\mathbf{q}, \mathbf{k}}^{\text{eff}} = M_q^{\text{elem}} \left(\text{Re} [G^0(\mathbf{k} - \mathbf{q}, \xi - \Omega)] + \text{Re} [G^0(\mathbf{k} + \mathbf{q} + \Delta\mathbf{q}, \xi + \Omega + \Delta\Omega)] \right) M_{\mathbf{q}+\Delta\mathbf{q}}^{\text{elem}}. \quad (2.9)$$

In this particular case, for the diagram shown in figure 2.6, it can be seen that the external energy Ω dominates the scattering amplitude. The imaginary part of the phonon self-energy is, as demonstrated in appendix A.1,

$$\begin{aligned} \text{Im} [\Pi^{\text{el-ph}}(\mathbf{q}, \Omega)] &= \sum_{\Delta\mathbf{q}, \mathbf{k}} \int \frac{d\xi d\Delta\Omega}{\pi^2} (n_F(\xi + \Delta\Omega) - n_F(\xi)) (n_B(\Delta\Omega) - n_B(\Delta\Omega + \Omega)) \\ &\times (M_{\mathbf{q}, \mathbf{q}+\Delta\mathbf{q}, \mathbf{k}}^{\text{eff}})^2 (\delta(\Omega + \Delta\Omega - \omega_{\mathbf{q}+\Delta\mathbf{q}}) - \delta(\Omega + \Delta\Omega + \omega_{\mathbf{q}+\Delta\mathbf{q}})) \delta(\xi + \Delta\Omega - \varepsilon_{\mathbf{k}+\Delta\mathbf{q}}) \delta(\xi - \varepsilon_{\mathbf{k}}), \end{aligned} \quad (2.10)$$

where the imaginary parts of the bare Green's functions have been inserted. Performing the frequency integration over the latter delta functions yields for the effective vertices

$$M_{\mathbf{q}, \mathbf{q}+\Delta\mathbf{q}, \mathbf{k}}^{\text{eff}} = M_q^{\text{elem}} \left(\frac{1}{\Omega - (\varepsilon_{\mathbf{k}+\mathbf{q}+\Delta\mathbf{q}} - \varepsilon_{\mathbf{k}+\Delta\mathbf{q}})} - \frac{1}{\Omega - (\varepsilon_{\mathbf{k}} - \varepsilon_{\mathbf{k}-\mathbf{q}})} \right) M_{\mathbf{q}+\Delta\mathbf{q}}^{\text{elem}}. \quad (2.11)$$

By expanding the fermionic energies up to quadratic order, this simplifies to

$$M_{\mathbf{q}, \mathbf{q}+\Delta\mathbf{q}, \mathbf{k}}^{\text{eff}} = M_q^{\text{elem}} \left(\frac{\frac{\hbar^2}{m}(\mathbf{q} + \Delta\mathbf{q})\mathbf{q}}{(\Omega - \Delta_1)(\Omega - \Delta_2)} \right) M_{\mathbf{q}+\Delta\mathbf{q}}^{\text{elem}} \approx M_q^{\text{elem}} \frac{\hbar^2(\mathbf{q} + \Delta\mathbf{q})\mathbf{q}}{m\Omega^2} M_{\mathbf{q}+\Delta\mathbf{q}}^{\text{elem}}, \quad (2.12)$$

where $\Delta_1 = \varepsilon_{\mathbf{k}+\mathbf{q}+\Delta\mathbf{q}} - \varepsilon_{\mathbf{k}+\Delta\mathbf{q}}$ and $\Delta_2 = \varepsilon_{\mathbf{k}} - \varepsilon_{\mathbf{k}-\mathbf{q}}$ are of order $v_F|\mathbf{q}|$ and thus negligible compared to Ω , since $v_F \ll v_P$. In the case of one-dimensional fermions, only the parallel components of the phonon momenta enters the effective vertex, since the components orthogonal to the chains is not conserved in the intermediate scattering processes. From the latter equation it can be seen easily that for a perfectly linear fermionic dispersion, the effective vertex vanishes.

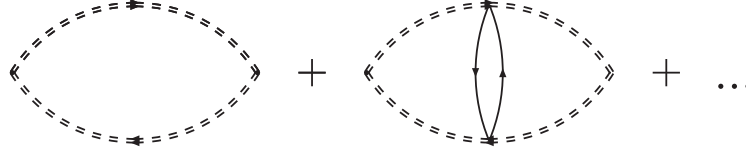


Figure 2.7: Diagrammatic calculation of the heat current-heat current correlation function with the full phonon propagator (dashed double line) and vertex corrections from effective electron phonon interaction.

The above integrals are evaluated in appendix A in the limit of small external momentum and temperature for both settings. The result for the scattering from three-dimensional fermions is

$$\text{Im} [\Pi^{\text{el-ph}}(\mathbf{q}, v_P \mathbf{q})]^{3D} \propto \frac{a^6}{m^2 M^2} \left(\frac{V_{\text{el-ph}}}{v_F v_P} \right)^4 q^4 T^3. \quad (2.13)$$

In the case of scattering from one-dimensional fermions, the setting has a lower symmetry, which is reflected in the phonon lifetime

$$\text{Im} [\Pi^{\text{el-ph}}(\mathbf{q}, v_P \mathbf{q})]^{1D} \propto \frac{a^4 V_{\text{el-ph}}^4}{m^2 M^2 v_F^2 v_P^4} q^4 \cos^2(\phi) T, \quad (2.14)$$

it obtains an angle dependency. Only phonons which carry momentum parallel to the fermion chains are damped, those perpendicular are not scattered at all.

2.4 Connection to Heat Conductivity

Up to now, only imaginary parts of phonons were discussed, which are some kind of lifetime of the quasi-particle. However, it is important to distinguish *relaxation times*, as appear in the Boltzmann equation, and *lifetimes*. The difference is crucial, since the scattering of a quasi-particle does not disperse all carried energy-current in all cases. Depending on the kind of scattering, currents can persist although the carriers have been scattered, e.g. if the scattering process alters the direction only weakly. This is known as *forward scattering* and has evident consequences, for example in the electrical conductivity of normal metals. There the scattering is almost elastic, leading to an extra T^2 contribution to the scattering rate $\tau_{\text{el}}^{-1} = T^3$, resulting in the *Bloch T^5 law* of electrical resistivity ([32]).

Formally, the heat conductivity κ in linear response is, in analogy to (1.45)

$$\kappa = \lim_{\Omega \rightarrow 0} \frac{1}{\Omega T} \text{Im} [\langle \mathbf{J}_\epsilon \mathbf{J}_\epsilon \rangle (\Omega)], \quad (2.15)$$

where the heat current \mathbf{J}_ϵ in this context denotes only the phonon contribution. The heat current-heat current correlation function can be calculated from the phonon Green's function diagrammatically, see figure 2.7. It can be written as a bubble of the selfenergy corrected phonon propagator, with vertex corrections from the effective electron phonon scattering process.

In general, the effect of the conservation laws, e. g. forward scattering, is contained in this series only if one takes all vertex corrections into account. However, the effective electron phonon scattering for fast phonons favors backward scattering, since the energy of a fast phonon can not be absorbed by a slow fermion otherwise. Thus, there is no cancellation

2.5. MEAN FREE PATH AND BOUNDARY SCATTERING

between selfenergy and vertex corrections, and the corrections from vertex corrections are of order one. To describe the physics of the scattering, it suffices therefore to take into account the selfenergy corrections in D and neglect the vertex corrections.

With this simplification, the heat current heat current correlation function can be obtained from the phonon Green's function D by

$$\langle J_\epsilon J_\epsilon \rangle (i\Omega) \approx \frac{1}{4} \sum_{\mathbf{q}, \omega_n} v_q^2 \omega_q^2 D(\mathbf{q}, i\omega_n + i\Omega) D(\mathbf{q}, i\omega_n). \quad (2.16)$$

The factor $1/4$ in front comes from the definition of the phonon propagator, which is chosen symmetrically as

$$D(\mathbf{q}, i\omega) = \left\langle (a_q^\dagger + a_{-q}) (a_q + a_{-q}^\dagger) \right\rangle (i\omega). \quad (2.17)$$

It is an easy task to evaluate the imaginary part of expression (2.16) with the technique described in appendix A. Doing so, $\text{Im} [\langle J_\epsilon J_\epsilon \rangle (i\Omega)]$ is expressed as function of the imaginary part of the phonon propagator. The latter can be obtained easily from Dyson equation, which gives the connection between self-energy and full Green's function. Assuming the self-energy broadens the two peaks of the free phonon Green's function only slightly, such that they remain clearly separated, one obtains

$$\begin{aligned} \text{Im} [D(\mathbf{q}, \omega)] &= \text{Im} \left[\frac{1}{\omega - \omega_q - i\Pi(\mathbf{q}, \omega)} + \frac{1}{\omega + \omega_q - i\Pi(\mathbf{q}, \omega)} \right] \\ &= \frac{\Pi(\mathbf{q}, \omega)}{(\omega - \omega_q)^2 + \Pi(\mathbf{q}, \omega)^2} + \frac{\Pi(\mathbf{q}, \omega)}{(\omega + \omega_q)^2 + \Pi(\mathbf{q}, \omega)^2}. \end{aligned} \quad (2.18)$$

Inserting this into the heat conductivity,

$$\kappa = \lim_{\Omega \rightarrow 0} \frac{1}{\Omega V T} \frac{1}{4\pi} \sum_{\mathbf{q}} \int d\omega v_q^2 \omega_q^2 (n_B(\omega) - n_B(\omega + \Omega)) \text{Im} [D(\mathbf{q}, \omega)] \text{Im} [D(\mathbf{q}, \omega + \Omega)], \quad (2.19)$$

it becomes apparent that there are two contributions for small Ω , each from the vicinity of one common pole of the two Green's functions. The Bose functions are approximately constant around the pole, so the integrals both are simply over the square of a Lorentzian, and hence yield the same result, namely

$$\kappa = -\frac{1}{VT} \sum_{\mathbf{q}} v_q^2 \omega_q^2 \frac{\partial n_B(\omega_q)}{\partial \omega_q} \frac{1}{2\Pi(\mathbf{q}, \omega_q)}. \quad (2.20)$$

By applying the identity $\partial_\omega n_B(\omega) = -T/\omega \partial_T n_B(\omega)$, one can conclude from comparison to equation (1.23) that the relaxation time in the Boltzmann equation is $\tau_q = 1/(2\Pi)$, which is identical to the definition of the phonon lifetime.

2.5 Mean Free Path and Boundary Scattering

In the last section, an expression for the heat conductivity depending on the phonon lifetime has been derived. In principle, this could directly be evaluated and one would be done. However, the prerequisite is of course, that the momentum sum converges, which might fail if the scattering mechanism is too weak. In this case, other scattering mechanisms must be taken into account to describe the physical situation, where the heat conductivity usually

is finite. Within the relaxation time approximation, various scatterings can be treated by the *Matthiessen's rule* [33], which states that, if for each scattering process on its own a relaxation time can be defined, the total relaxation rate, i.e. the inverse relaxation time, is the sum of the separate relaxation rates. This rule is only phenomenological, its validity is discussed e. g. in [1].

According to Matthiessen's rule, in each scattering process each mode is scattered with the same relaxation time. Here a slightly different approach is used, where the relaxation times are allowed to be momentum dependent. That way, an interplay of different scattering mechanisms can be described, where each mode is scattered predominantly by the process with the smallest mean free path for its momentum. The effective momentum dependent scattering time is defined by

$$\frac{1}{\tau_{\mathbf{k}}} = \sum_i \frac{1}{\tau_{\mathbf{k}}^i}, \quad (2.21)$$

where $\tau_{\mathbf{k}}^i$ is the momentum dependent scattering time of the i th scattering mechanism.

The lifetimes obtained in the previous section diverge for small values of the phonon momentum \mathbf{q} , which means that the phonon can propagate a huge distance, namely the mean free path $l = v_P \tau_{\mathbf{q}}$, without being scattered. In practice, the real mean free path is limited, in the absence of other scatterers, at the latest by the diameter of the system. Within the current approach, a relaxation time for the surface scattering of phonons thus can be achieved from the mean free path as $\tau_{\text{surf}} = \Lambda/v_P$, with the system diameter Λ . According to equation (2.21), the total relaxation time is then

$$\tau_{\text{tot}} = \frac{\tau_{\text{surf}}}{1 + \frac{\tau_{\text{surf}}}{\tau_{\text{el-ph}}}}. \quad (2.22)$$

Using this combined relaxation time, the momentum sum can not be calculated in a closed form, instead numerical computation must be applied. Expressed as a momentum integral, in the case of scattering from three-dimensional fermions, the heat-conductivity is

$$\kappa^{3D}(T, \Lambda) = -\frac{4\pi}{T} \int_0^\infty d\mathbf{q} q^4 v_P^2 \frac{\partial n_B(\frac{v_P \mathbf{q}}{T})}{\partial \mathbf{q}} \frac{\Lambda}{1 + \frac{\Lambda}{v_P} C q^4 T^3}, \quad (2.23)$$

with the constant $C = a^6 (V_{\text{el-ph}}/v_F v_P)^4 / m^2 M^2$, which is, together with its asymptotics, depicted in figure 2.5.

For small temperatures, the heat conductivity $\kappa_{\text{low}}^{3D} \approx 16\pi^5/(15v_P^2)\Lambda T^3$ reflects clearly the signature of surface scattering, with the T^3 power law of the Debye heat capacity. Above the crossover to higher temperatures, where fermion scattering dominates, the heat capacity behaves asymptotically like $\kappa_{\text{high}}^{3D} \approx 4\pi C^{1/4} v_P^{7/4} \Lambda^{1/4} T^{-9/4}$.

In the case of scattering from one-dimensional fermions it is possible to investigate the heat conductivity *in* chain direction and *perpendicular* to the chain direction. This can be achieved by replacing the factor $v_{\mathbf{q}}^2$ in equation (2.20) by either the square of the velocity in chain direction $v_{\mathbf{q}} \sin \phi$ in the former or perpendicular to with $v_{\mathbf{q}} \cos \phi$ in the latter case. With this, one obtains for the direction dependent heat conductivity

$$\begin{aligned} \kappa_{\parallel}^{1D}(T, \Lambda) &= -\frac{2\pi}{T} \int_0^\infty d\mathbf{q} \int_0^\pi d\phi \sin(\phi) q^4 v_P^2 \sin^2(\phi) \frac{\partial n_B(\frac{v_P \mathbf{q}}{T})}{\partial \mathbf{q}} \frac{\Lambda}{1 + \frac{\Lambda}{v_P} \tilde{C} q^4 \cos^2(\phi) T}, \\ \kappa_{\perp}^{1D}(T, \Lambda) &= -\frac{2\pi}{T} \int_0^\infty d\mathbf{q} \int_0^\pi d\phi \sin(\phi) q^4 v_P^2 \cos^2(\phi) \frac{\partial n_B(\frac{v_P \mathbf{q}}{T})}{\partial \mathbf{q}} \frac{\Lambda}{1 + \frac{\Lambda}{v_P} \tilde{C} q^4 \cos^2(\phi) T}, \end{aligned} \quad (2.24)$$

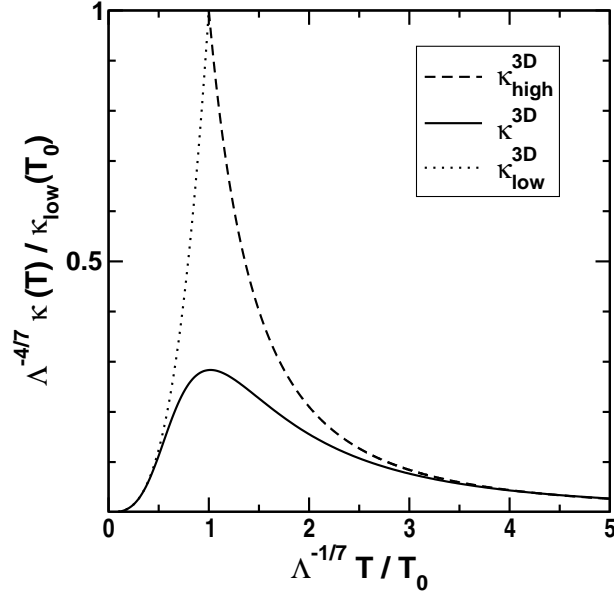


Figure 2.8: Heat conductivity of fast phonons scattering from slow three-dimensional fermions. At low temperature, boundary scattering provides the dominant scattering mechanism, at high temperatures, the low frequency divergence is regulated by the cutoff from finite sample diameter Λ . Here the Λ -dependence of the crossover has been scaled out by introducing $T_0 = (15/4\pi^4)^{4/21} (C/v_P)^{1/21}$.

where the constant \tilde{C} is the one-dimensional analogue to the three-dimensional case, $\tilde{C} = C/a^2$. Since there is no directional dependence in the surface scattering part of the relaxation time, the low T behavior is identical to the case of three-dimensional fermions, weighted with a factor $1/3$ in parallel direction and $2/3$ perpendicular. The high T behavior is in direction perpendicular to the chains $\kappa_{\text{high},\perp}^{\text{1D}} \approx 8\pi^3/3(v_P\Lambda T/\tilde{C})^{1/2}$, on the other hand the parallel conductivity $\kappa_{\text{high},\parallel}^{\text{1D}} \approx 8\pi/3v^{7/4}\Lambda^{1/4}\tilde{C}^{-3/4}T^{-3/4}$ drops with increasing temperature.

In case of the perpendicular component of the heat conductivity with one-dimensional fermions, the high temperature limit seems not to match the numerical integration. In fact, the crossover is very slow, such that the two curves converge only at very high temperatures, beyond the scale of the figure.

For a more accurate treatment, some more peculiarities must be considered. In the first instance, phonon heat transport is not the only contribution to the heat transport, one should take into account the fermion system. However, since the phonon velocity is in the studied systems much larger than the fermion velocity, the main contribution comes from the former.

In principle, the fermion heat conductivity could be described in a similar way by calculating the fermion lifetime, and then using the relaxation time approximation. Summing up the two contributions would give the total heat conductivity of the combined system. Unfortunately, this approach is incorrect, the reason is again related to conservation laws. If a phonon is damped by the scattering off a fermion, or vice versa, the energy and momentum that are dissipated from the phonon system don't vanish, but are carried by the fermion system, causing heat flux there, to be eventually transferred back to the phonon system in the next scattering event. This effect, called *drag*, is quite typical for Boltzmann equation problems. It can be treated for example by using so-called *conserving approximations* for the self-energies, or the hydrodynamic memory matrix approach, which accounts for the role of conservation

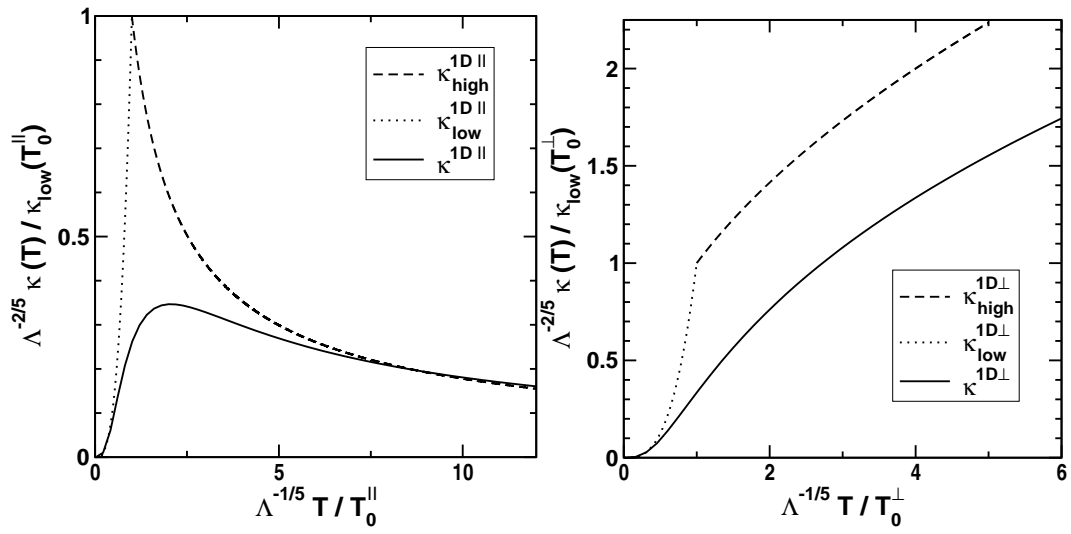


Figure 2.9: Heat conductivity from fast phonons scattered from one-dimensional slow fermions, *left* contribution from phonons in chain direction, *right* from those perpendicular. The low temperature asymptotics are, as in the case of three-dimensional fermions, dominated by surface scattering with the characteristic T^3 law, where the parallel contribution is $1/3$ of the three-dimensional result and the perpendicular $2/3$. In the figure this behavior is hidden in the different crossover scales $T_0^{\parallel} = (2\pi^4/15)^{-4/15} v_P (\tilde{C}\Lambda)^{-1/5}$ and $T_0^{\perp} = (15/4\pi^2)^{-4/15} v_P (\tilde{C}\Lambda)^{-1/5}$. In the high temperature regime the phonon-fermion scattering becomes dominant, giving the depicted $T^{-3/4}$ and $T^{1/2}$ dependencies. The additional Λ dependencies from the long wavelength cutoff are scaled out.

2.5. MEAN FREE PATH AND BOUNDARY SCATTERING

laws for the scattering between different modes, i.e. the matrix structure of the scattering rates.

The latter will be applied in this thesis for a few model systems in one dimension. Also other shortcomings of this section, like thermoelectric effects, are included into the discussion.

3 Thermoelectric Effects in One-Dimensional Systems

One-dimensional systems are, in many senses, special since widely used concepts of solid state theory are invalid. There is, for instance, the absence of long-range order due to the Mermin-Wagner theorem [34, 35], which prohibits the use of mean-field-like methods. Also the concept of the Fermi liquid breaks down, crudely speaking a consequence of the special Fermi surface topology in one dimension. Instead, the notion of the *Luttinger liquid* (named after Luttinger, who introduced the underlying model for one-dimensional interacting fermions [36]) arises, which is the low-energy fixed point of many one-dimensional microscopic models. Some major consequences are algebraic power laws for correlation functions, and the fact that all possible excitations must be collective ones, or, in more detail, *spin-charge-separation*.

Properties like these can be derived by use of the bosonization technique, which utilizes the possibility to linearize the spectrum of many (originally fermionic) Hamiltonians around the Fermi points. The eigenspace of such a Hamiltonian with a linear spectrum corresponds to a bosonic Hilbert space by means of an exact operator identity [37, 38, 39]¹. In the language of those bosonic fields, the Hamiltonian can be diagonalized, yielding the celebrated Luttinger Hamiltonian. The latter happens to describe a Lorentz-invariant system, implying the conservation of the energy current. Furthermore, the system is integrable and thus contains an infinite number of conservation laws. The effect of integrability to transport properties, in particular in the context of spin chain materials, has been discussed controversially in the recent years

The theoretical interest was boosted by experiments which found evidence for large magnetic thermal conductivities in low-dimensional quantum magnets, e. g. experiments by Sologubenko et al. [42, 43, 44, 45], Hess et al. [46], Kudo et al. [47], in a range of materials with different coupling constants.

A review of experimental results on heat transport in low dimensional quantum system was published in 2007 by C. Hess, [48].

On the theoretical side, the interest mainly concentrated on the question, under which conditions transport in a quantum spin chain becomes anomalous, which means that the respective conductivity has a delta peak in the zero frequency limit, which is referred to as *Drude peak*. This concept applies for thermal as well for spin or charge transport. Anomalous transport is often measured by the prefactor of this peak, called *Drude weight* or, in case of spin transport, equivalently *spin stiffness*.

Zotos and collaborators claimed in 1997, [49], that conservation laws in integrable quantum systems lead to dissipationless thermal transport at finite temperatures. In the following, several studies on both, integrable and nonintegrable quantum spin chains, have been investigated with focus on this problem. In 1998, some of the authors of [49] published results of

¹For a comprehensive review see [40] or [41]

an exact diagonalization study of the heat conductivity in an anisotropic Heisenberg model (XXZ-model), [50]. They found a long-time decay of the heat current heat current correlation function to a finite value, which is the signature of anomalous (ballistic) transport for values of the anisotropy Δ between zero, which is equivalent to the XY-model, and one, the isotropic Heisenberg model.

Narozhny et al. found, also by means of exact diagonalization, ballistic thermal transport in the XXZ model, which they traced to the high number of degenerate states rather than the integrability.

The problem of the *spin* Drude weight in quantum spin chains has been discussed more controversially one year later, Zotos published the results of a Bethe-ansatz calculation of the spin Drude weight in the anisotropic Heisenberg model for $\Delta < 1$, [51]. The resulting spin Drude weight was a monotonically decreasing function of temperature for all studied values of anisotropy, and approaches the $T = 0$ value like a power law. In the isotropic limit, $\Delta = 1$, the spin Drude weight vanished at all finite temperatures.

Starting 2002, Heidrich-Meisner et al. published several studies of the heat *and* spin transport in integrable and nonintegrable systems by means of exact diagonalization and mean field theory, [52, 53, 54, 55]. In agreement to Zotos Bethe-ansatz results, they found in the XXZ model a finite spin Drude weight for all $\Delta < 1$ and vanishing Drude weight in the isotropic case. Other results were normal transport in several nonintegrable models, like frustrated Heisenberg chains, dimerized chain, and a spin ladder. For the XXZ model in finite magnetic field a strong field dependence of the spin Drude weight was derived in the gapless regime.

A numerical calculation of the transport properties of the antiferromagnetic and ferromagnetic XXZ model, in the gapless [56] as well the gapped [57] regime was given by Klümper and Sakai in 2003. By means of a lattice path integral formulation, they found a finite thermal and spin Drude weight, i. e. ballistic transport.

Also in 2003, Fujimoto and Kawakami published a study on several one-dimensional quantum liquids with the Luttinger liquid low energy fixed point, including some nonintegrable models. Their conformal perturbation theory calculation of the transport properties yielded a non-vanishing finite temperature Drude weight also for the nonintegrable systems, which is the result of the conservation of momentum in the studied systems.

Another exact treatment of the XXZ chain by thermodynamic Bethe-ansatz, [58], yielded contradicting results for two different bases. The choice of basis they considered the correct one, the spinon anti-spinon basis, lead to a spin Drude weight monotonously decreasing with temperature only for small anisotropies. At the isotropic point they found a finite spin Drude weight with an infinite positive slope at $T = 0$.

Motivated by experimental data from NMR experiments on the spin chain compound Sr_2CuO_3 , [59], which concluded spin diffusion, Sirker *et al.* obtained good agreement to the experimental data in a field theoretical approach to the XXZ model with the assumption that the spin Drude weight vanishes for finite temperatures, [60]. Earlier numerical results which predicted a finite Drude weight were reinvestigated with a direct calculation of the current current correlation function with a DMRG algorithm. The resulting correlation function were nonmonotonic in time and did not converge to an asymptotic value up to large times. In combination, they concluded in contradiction to older results that the low temperature spin Drude weight of the XXZ chain must be either zero or very small.

Very recently, the question of anomalous transport in integrable and nonintegrable one-dimensional quantum systems was addressed with an approach new in this field, the adaptive time-dependent density matrix renormalization group, [61]. The authors studied frustrated

and integrable spin chains, and obtained once more diffusive transport for nonintegrable and ballistic transport for integrable systems.

However, the problem whether anomalous transport can occur in nonintegrable systems is hard to solve, since the interpretation of numerical studies always is complicated by finite size effects and numerical errors, and on the other hand analytical transport calculations for nonintegrable systems are very difficult.

In 2007 Jung and Rosch established a formalism to calculate lower bounds to the heat conductivity of *almost* integrable systems, i. e. an integrable system plus a weak perturbation which breaks the integrability, [62]. The authors applied the scheme to a XXZ chain with weak next-nearest neighbor coupling in [63] and discussed the question how *nonlocal* conservation laws can affect transport properties.

Apart from the question of integrability and anomalous transport, also some research on normal transport in one-dimensional systems has been done.

For example, Giamarchi et al. studied an antiferromagnetic spin chain in the presence of Umklapp scattering by means of a memory function approach, and concluded wrongly normal thermal transport in this system, [13]. The correct solution of this problem was given by Shimshoni et al. , [16], where they stressed the matrix structure of the scattering rates due to conservation laws in the Umklapp processes, which yields normal transport only from the interplay of at least two Umklapp processes.

The effect of phonon coupling and impurity scattering to the spinon heat transport has been investigated within a Boltzmann equation calculation by Chernyshev and Rozhkov, [64]. They claimed, that in the regime of exchange coupling of the spins bigger than the Debye energy the main relaxation mechanism of the magnetic heat current was the coupling to phonons, where the heat current was dissipated quickly to the phonon bath. However, they did not take into account the backflow of momentum from the phonon bath to the spin system, which is a very important effect for transport.

Similar assumptions have been used by Louis et al. , who investigated the isotropic antiferromagnetic Heisenberg model and the antiferromagnetic XY model coupled to phonons within a memory function approach, [65], which thus has the same problems.

An approach which takes into account the conservation of the total momentum of phonon and spin system is given with the memory matrix formalism, used by Boulat et al. to calculate the heat conductivity of spin ladder systems with Umklapp scattering, coupled to phonons, [17]. Depending on the ratio of spin gap and Debye energy, the obtained magnetic contribution to the heat conductivity are positive or negative.

In general, transport properties of Luttinger liquid like models must be dominated by additional symmetry-breaking effects, that are not contained in the free bosonic description. Typical symmetry-breaking candidates are the so-called *Umklapp* processes, band-curvature effects or disorder scattering. As shown by Haldane [66], these additional effects to the “free” Luttinger model can also be treated within the bosonization formalism.

Coming from a lattice model, Umklapp processes can be generated in a natural way by keeping those terms in the bosonized Hamiltonian, that oscillate with a frequency corresponding to a reciprocal lattice vector. For any commensurate filling the suitable Umklapp can be found, which physically can be viewed as the scattering of the matching number of fermions from one Fermi-point to the other.

As pointed out in [14], at least *two* Umklapp processes are needed to dissipate momentum effectively. The reason is a class of conservation laws contained in the Umklapp Hamiltonians, protecting the respective *pseudo momenta* of each process. Components of currents *parallel*, in the Hilbert space spanned by the used slow modes, to a pseudomomentum decay

exponentially slowly. Since pseudo momenta of two different Umklapp processes are orthogonal two processes are sufficient to destroy the persistence of the complete current. The disadvantage of relying on two Umklapp processes as an unique scattering mechanism is their strong thermal suppression away from the respective commensurate filling. In particular since the suppression gets stronger for higher Umklapps, while the commensurate points of lower order scatterings are separated further.

For experiments, the situation described above thus is not very relevant, since, in the first place, very low temperatures would be necessary. Achieving such low temperatures in a transport measurement is complicated by intrinsic heating. Second, in physical realizations of one-dimensional systems, the manufacture of very clean systems is a non-trivial issue. Presently, the interplay of Umklapp scattering at one commensurate point with disorder scattering is of greater experimental interest, due to better accessibility, than that of two Umklapp processes.

In this chapter, thermoelectric and thermomagnetic effects, that result from the interplay of Umklapp scattering and disorder scattering in two one-dimensional model systems are discussed. The first example is an antiferromagnetic spin-1/2 Heisenberg chain in finite magnetic field,

$$H_{\text{Heisenberg}} = -J \sum_i \mathbf{S}_i \cdot \mathbf{S}_{i+1} - g_L \mu_B \sum_i B S_i^z, \quad (3.1)$$

with nearest-neighbor coupling $J < 0$, \mathbf{S}_i spin operators at site i , the Landé g -factor, the Bohr magneton μ_B , and B the modulus of the magnetic field, which is assumed to point into z -direction. The elementary excitations of this Hamiltonian are spin-waves, or *spinons*. The spinon heat conductivity and its dependency on an external magnetic field is studied. Heisenberg chains are interesting systems for transport calculations, given the striking properties of the pure model: being soluble via Bethe-ansatz [67], its thermodynamic properties are basically known [56]. Consequently, it has been tackled with many approaches, bringing already considerable knowledge about their characteristics

By use of Jordan-Wigner transformation, the low energy part of the Heisenberg model can be mapped into spinless fermions with repulsive nearest-neighbor interaction, and the external magnetic field acting as a chemical potential. The resulting fermionic model,

$$H_{\text{JW}} = - \sum_i \left(J \left(c_{i+1}^\dagger c_i + h.c. \right) + J \left(c_{i+1}^\dagger c_{i+1} - \frac{1}{2} \right) \left(c_i^\dagger c_i - \frac{1}{2} \right) + g_L \mu_B B \left(c_i^\dagger c_i - \frac{1}{2} \right) \right) \quad (3.2)$$

can be treated by bosonization, showing that indeed the Luttinger liquid is the low energy fixed point of the Heisenberg chain. In the case of disordered chains, it is known [68] that interactions strongly renormalize the disorder strength. Additionally, for Umklapp processes, it is possible to extract the exact coupling constants from the Bethe-ansatz solution, which allows predictions with few free parameters.

As already pointed out, the Heisenberg chain is an integrable system, which theoretically would have an infinite spinon heat conductivity. In physical systems this is obstructed, for instance, by disorder, or coupling to phonons. Experimental studies of this setting have attracted lot of interest in the recent years [42, 43, 44, 46, 47]. In particular, measurements on the spin chain compound copper pyrazine dinitrate $\text{Cu}(\text{C}_4\text{H}_4\text{N}_2)(\text{NO}_3)_2(\text{CuPzN})$ [69] have motivated our studies. This compound has a relatively small exchange coupling $J/k_B \approx 10.3K$, which makes the regime of completely polarized system accessible, and thus it allows us to separate the spinon part of the heat conductivity from the phonon part by assuming that the latter is not affected by a magnetic field. In the magnetic part, a pronounced dip

is observed, whose position scales linearly with the magnetic field, thus indicating a simple underlying mechanism.

Here, a quantitative description by an antiferromagnetic Heisenberg model with weak Gaussian disorder is attempted. For the commensurate filling corresponding to zero magnetic field, the $4k_F$ Umklapp process is retained in the Hamiltonian. This process transfers two spinons from one Fermi-point to the other, while the excess momentum of $4k_F$ can be absorbed by the lattice. The treatment is made comparable to real measurements by including the physical coupling constants, obtained from Bethe-Ansatz calculations. The results of this project have been published in [70].

In a second example, the interplay of thermal and electric conductivity in a metallic system is studied. The model of interest is the well-established paradigm for interacting electrons, the Hubbard model [71], which reads in one dimension

$$H_{\text{Hubbard}} = \sum_{i,\sigma} \left(-t \left(c_{i+1,\sigma}^\dagger c_{i,\sigma} + h.c. \right) + U c_{i,\uparrow}^\dagger c_{i,\uparrow} c_{i,\downarrow}^\dagger c_{i,\downarrow} \right). \quad (3.3)$$

The first term describes the kinetics of the electrons with t the amplitude of an electron hopping to a neighboring site, and the second the interaction with U the overlap integral between the wavefunctions of two electrons of opposite spin, located at the same site.

Just like for the Jordan-Wigner spinless fermions, the spinful case of interacting electrons in one dimension has a bosonization description, with the difference that the latter needs separate bosonic fields for charge *and* spin degrees of freedom.

One hallmark result of one-dimensional physics is the separation of spin and charge excitations, which is reflected in the effective bosonic Hamiltonian for the Hubbard model, which contains no mixing of charge and spin fields, but is quadratic in both with different velocities and interaction parameters. This behavior has recently been confirmed experimentally in ARPES studies of SrCuO_2 [72].

The inclusion of Umklapp scattering terms in the Hamiltonian must break this symmetry, since in processes which transfer an odd number of electrons from one Fermi-point to the other, along with the respective number of charge fields also an odd number² of spin fields must be transferred.

In normal (three-dimensional) metals, the Wiedemann-Franz law, which states that the ratio of thermal conductivity and electric conductivity times temperature, called the Lorenz number L , is a constant [73],

$$L = \frac{\kappa}{\sigma T} = \frac{\pi^2}{3} \left(\frac{k_B}{e} \right)^2 \equiv L_0, \quad (3.4)$$

where e is the charge of the electron, is valid for a wide range of materials. To be precise, the more important *elastic* scattering is in a system, the better the Wiedemann-Franz law is fulfilled, because only *inelastic* scattering can degrade a thermal current without degrading a charge current [28]. For Fermi liquids at zero temperature with impurity scattering it is valid exactly. This ratio is of particular interest due to its technical relevance for thermoelectrical power generation. Materials with a large Wiedemann-Franz ratio are likely to make up efficient thermoelectric elements [74], which reflects in a high thermoelectric figure of merit [75], a quantity also studied later on in this thesis.

For Luttinger liquids it has been shown by means of a memory function approach [15] that weak disorder leads only to violations of the Wiedemann-Franz ratio of the order of one.

²one to leading order in temperature

3.1. BASICS OF THE BOSONIZATION TECHNIQUE

Deviations of larger order usually happen when the excitation spectrum changes drastically, e. g. when Umklapp scattering opens a gap³. In a Mott insulating state the electric conductivity is suppressed to zero, while heat can still be transported by excitations of the spin sector.

Adding Umklapp scattering should cause large effects in the Wiedemann-Franz ratio even in a situation where no gap is opened, since electrical and thermal conductivities are affected in very different ways. These deviations from L_0 are expected to be strongest at the commensurate point with the lowest number of electrons transferred, i. e. half filling, because for this process the thermal suppression is the weakest. However, the transfer of two or any other even number of electrons does not affect the spinons in the system. Thus, at half filling, the impact of Umklapp scattering on the Wiedemann-Franz ratio is limited due to the spinon part of the heat conductivity, which is not altered. Strong deviations at half filling are expected anyway in systems with an additional mechanism that breaks the spin-charge separation. As example for this kind of system, the Wiedemann-Franz ratio of an one-dimensional metal with band curvature is studied in this thesis.

Another regime with large violations of the Wiedemann-Franz law can be found in one-dimensional metals without band curvature effects, but at commensurate points where odd numbers of electrons are scattered, most prominently the $6k_F$ process at one third filling, which is also discussed in this work. In contrast to the spin chain, in the one-dimensional metal it is not possible to separate the phonon contribution by a simple experimental trick. In particular the contribution to the heat conductivity in general is large and has to be accounted for. Coupling between electronic system and lattice vibrations is mediated via the hopping matrix elements. Basically, the coupling must be expanded in the displacement, which leads to additional terms in any part of the Hamiltonian that contains the lattice spacing a . In particular, besides a coupling to the charge density, new Umklapp processes with involved phonons arise. The results for the violation of the Wiedemann-Franz law in weakly disordered correlated metals without coupling to phonons have been published in [78], the calculations including phonons are hitherto unpublished.

3.1 Basics of the Bosonization technique

The Bosonization technique is a mapping from one-dimensional fermionic field operators to bosonic fields. It relies on the linearization of the original dispersion relation around the two Fermi-points, thus yielding effective low energy theories of the studied models. In the special (academic) case of a perfect linear fermionic spectrum, the mapping is exact given that the two branches of left- and right-moving fermions are separately extended to minus infinity⁴.

This kind of spectrum is unbounded, as can be seen in figure 3.1, which raises the problem of how to calculate expectation values. Doing it naively yields infinities for many operators, e. g. the particle number which counts all occupied states down to minus infinity, which have been added artificially. To avoid this problem, one has to apply *normal ordering* of the operators before taking the expectation value, which means that all contained destruction operators must be put right of all construction operators. Equivalently, the quasiparticle

³In higher dimensions, the Mott metal-insulator transition is a well-known effect [76]. It has been shown that in Luttinger liquids at commensurate fillings Umklapp scattering leads to an insulating state in the charge sector, while spin properties are unaffected [77]

⁴This model is referred to as *Tomonaga-Luttinger model*

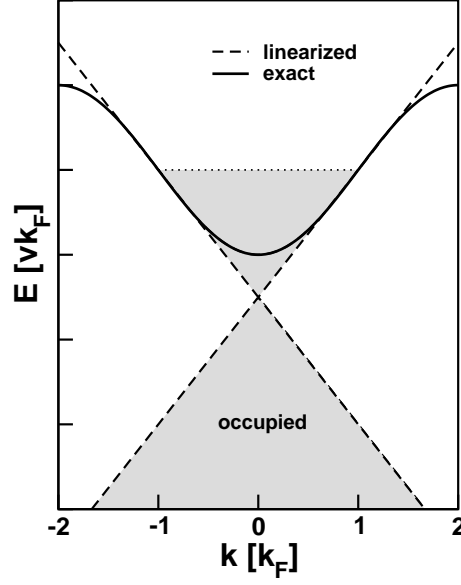


Figure 3.1: The linearization of the spectrum results in two separate branches for left- and right-moving particles, which are occupied with infinitely many particles at negative energies.

vacuum average of the respective operator can be subtracted to get the meaningful operator

$$: \hat{A} : = \hat{A} - \langle 0 | \hat{A} | 0 \rangle. \quad (3.5)$$

In such a system, particle-hole excitations become independent of the momenta of the involved particles, forming well-defined quasi-particles of bosonic nature. Thus, interaction operators that are quartic in the fermionic formulation become quadratic when expressed in the basis of creators and annihilators of those basic excitations⁵. Remarkably, the kinetic part of the model remains quadratic, yielding in total an easy to diagonalize Hamiltonian.

To achieve this important simplification⁶, one makes use of the exact operator identity

$$\psi_{R/L}(x) = F_{R/L} \lim_{a \rightarrow 0} \frac{1}{\sqrt{2\pi a}} e^{i(\pm(k_F - \frac{\pi}{L})x)} e^{-i(\pm\phi(x) - \theta(x))} \quad (3.6)$$

between the right- or left-moving fermion field and the bosonic fields $\phi(x)$, $\theta(x)$. The so-called Klein-factors $F_{R/L}$ decrease the total number of fermions by one, ensuring the identity of the bosonic and fermionic operator. For most applications, namely those where fermion fields only appear pairwise, Klein-factors can safely be dropped. In the limit $L \rightarrow \infty$ and $a \rightarrow 0$ the model becomes continuous. In practice the thermodynamic limit can be taken from the beginning, while a is kept finite until the very end of the calculation as it regularizes certain correlation functions.

The bosonic fields can be interpreted physically in terms of the densities $\rho_{R/L}$ of right- and left-moving fermions as

$$\begin{aligned} \partial_x \phi(x) &= -\pi (\rho_R(x) + \rho_L(x)) \\ \partial_x \theta(x) &= \pi (\rho_R(x) - \rho_L(x)). \end{aligned} \quad (3.7)$$

⁵Note that this implies all excitations of the system being collective ones

⁶for a detailed derivation of the analysis see e.g. [40, 41]

3.1. BASICS OF THE BOSONIZATION TECHNIQUE

As can be verified by an elementary calculation, $\phi(x)$ and $1/(\pi)\partial\theta(x)$ are conjugate fields with the canonical commutation relation

$$[\phi(x), \partial_{x'}\theta(x')] = i\pi\delta(x' - x). \quad (3.8)$$

In the more general case of spinful fermions, separate fields $\phi_{\uparrow/\downarrow}$, $\theta_{\uparrow/\downarrow}$ for both spin species generically appear. In a typical Hamiltonian fields with different spins are coupled in the interaction part. By introducing total charge and spin degrees of freedom as

$$\begin{aligned} \rho(x) &= \frac{1}{\sqrt{2}} (\rho_{\uparrow}(x) + \rho_{\downarrow}(x)) \\ \sigma(x) &= \frac{1}{\sqrt{2}} (\rho_{\uparrow}(x) - \rho_{\downarrow}(x)), \end{aligned} \quad (3.9)$$

a unitary transformation is defined, which diagonalizes the Hamiltonian with the corresponding relation for the bosonic fields

$$\begin{aligned} \phi_c(x) &= \frac{1}{\sqrt{2}} (\phi_{\uparrow}(x) + \phi_{\downarrow}(x)) \\ \phi_s(x) &= \frac{1}{\sqrt{2}} (\phi_{\uparrow}(x) - \phi_{\downarrow}(x)) \end{aligned} \quad (3.10)$$

and similarly for the θ . This transformation retains the commutation relations between ϕ and θ of the same kind unchanged, while fields of different sectors always commute. Hence, the identity between fermionic and bosonic fields in the spinful case reads

$$\psi_{R/L,\sigma}(x) = \frac{1}{\sqrt{2\pi a}} e^{\pm i k_F x} e^{-\frac{i}{\sqrt{2}}(\pm\phi_c(x) - \theta_c(x) + \sigma(\pm\phi_s(x) - \theta_s(x))}, \quad (3.11)$$

where $\sigma = \pm 1$ for spin up or down, and after taking the thermodynamic limit⁷.

Inserting the mapping into the spinless model with nearest-neighbor density-density interaction we obtained from the Jordan-Wigner transformation of the Heisenberg model, equation (3.2), it is argued that all oscillatory terms average out to zero, leaving

$$H_{\text{spinless}} = v \int \frac{dx}{2\pi} \left(K(\partial_x \theta(x))^2 + \frac{1}{K}(\partial_x \phi(x))^2 \right), \quad (3.12)$$

where v is the renormalized velocity and K the Luttinger interaction parameter. This Hamiltonian is the low energy fixed point of a whole class of one-dimensional models, apart from the antiferromagnetic Heisenberg model from which we derived it.

For spinful fermions, we to start from the Hubbard-model, equation (3.3), which leads to a very similar result, namely

$$H_{\text{spinful}} = \int \frac{dx}{2\pi} \sum_{i=c,s} v_i \left(K_i(\partial_x \theta_i(x))^2 + \frac{1}{K_i}(\partial_x \phi_i(x))^2 \right) \quad (3.13)$$

with separate v and K for spin and charge degrees of freedom. This Hamiltonian decomposes into an independent sum of a spin part and a charge part, which is known as spin-charge separation. This is again true for the exactly linear spectrum. Allowing for small quadratic deviations actually couples the degrees of freedom.

⁷Klein-factors are dropped from now on

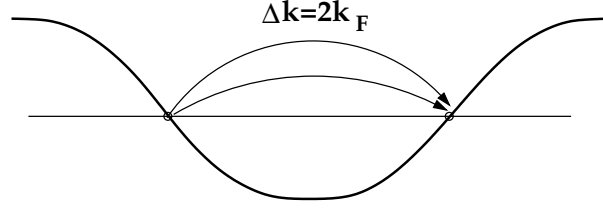


Figure 3.2: Typical Umklapp process at half filling: two electrons can be transferred from one Fermi-point to the other when their momentum matches a reciprocal lattice vector

These two models are obviously translationally invariant, implying momentum is a constant of motion. The original models were defined on a lattice where momentum is conserved only modulo a reciprocal lattice vector. This information is lost by going to the continuum limit, but by some effort important lattice effects can be reintroduced.

Clearly processes that are allowed by the symmetries of the original model must not vanish if the spatial average is done correctly. In particular, all processes that are allowed by the operators for a discrete translation by a multiple of a lattice constant, \mathcal{T}_a , inversion \mathcal{P} , or time reversal \mathcal{T} will contribute in the end. Of special interest for transport calculations are those of these processes which alter the scattering rates, i.e. do not commute with the respective currents. It can be shown⁸ that only those processes degrade the currents, that change the total number of right- and left-moving particles.

In the case of the spin chain, they are to leading order of the form⁹

$$\begin{aligned} H_{nm}^U &= g_{nm}^U \int dx \left[e^{i\Delta k_{nm}x} \prod_{j=0}^n \psi_R^\dagger(x+ja) \psi_L(x+ja) + h.c. \right] \\ &= \frac{g_{nm}^U}{(2\pi a)^n} \int dx \left(e^{i\Delta k_{nm}x} e^{i2n\phi(x)} + h.c. \right) \end{aligned} \quad (3.14)$$

which means that n spinons are transferred from one Fermi-point to the other, matching m units of lattice momentum G . Each process depends on the magnetization through

$$\Delta k_{nm} = n2k_F - mG \quad (3.15)$$

and is exponentially suppressed when moving away from the respective commensurate filling.

For the spinful system, the argumentation works analogously, but it must be considered that the transferred particles carry charge and spin. Thus one obtains

$$H_{mn_c n_s}^U = \frac{g_{mn_c n_s}^U}{(2\pi a)^{n_c}} \int dx \left(e^{i\Delta k_{mn_c n_s}x} e^{i\sqrt{2}(n_c\phi_c(x) + n_s\phi_s(x))} + h.c. \right), \quad (3.16)$$

for the process where n_c particles are transferred matching m units of lattice momentum, and n_s is the number of spin fields that are transferred thereby, typically one for odd numbers of electrons and zero for even numbers. The momentum mismatch is now controlled by the Fermi-momentum, since real electrons are described.

These so-called *Umklapp*-processes contain the relevant physics of the lattice symmetries that are needed for a bosonization description of transport theory. It will be shown in the subsequent sections that these processes and their hidden conservation laws have a strong impact on transport coefficient and give rise to interesting phenomena.

⁸see [16]

⁹here finite magnetic field is assumed. For odd n , time-reversal symmetry forbids terms like that and one has to go to the next higher order

3.2 Magnetothermal effects in Heisenberg chains

In this section the antiferromagnetic spin-1/2 Heisenberg chain is modeled by an effective low-energy description in terms of a bosonic Hamiltonian, including effects of weak disorder and Umklapp scattering close to half filling (which corresponds to zero magnetic field). From this, the thermal conductivity is derived with the memory matrix formalism and the effects of the hidden conservation law are studied. By using exact coupling constants from Bethe-Ansatz calculations, the theory is formulated in physical units, allowing for direct comparison with experimental data from CuPzN.

3.2.1 Model Hamiltonian

As a model Hamiltonian for the spin chain compound, the antiferromagnetic Heisenberg model in the presence of a magnetic field and with weakly disordered exchange couplings $\delta J_i \ll J$ shall be used. The original Hamiltonian,

$$H = - \sum_i (J + \delta J_i) \mathbf{S}_i \cdot \mathbf{S}_{i+1} + g_L \mu_B B \sum_i S_i^z, \quad (3.17)$$

which is similar to equation (3.1) plus weak deviations δJ_i of the spin-couplings, where g_L is the Landé g -factor and μ_B the Bohr magneton, is mapped to Jordan-Wigner fermions and then translated to a bosonic Hamiltonian.

It is useful to split the effective low-energy Hamiltonian of the system into three parts

$$H = H_{LL} + H_U + H_{dis}, \quad (3.18)$$

namely the Luttinger liquid part H_{LL} , the Umklapp part H_U , and the disorder part H_{dis} . Explicitly, the first one reads

$$H_{LL} = v \int \frac{dx}{2\pi} \left(K (\partial_x \theta(x))^2 + \frac{1}{K} (\partial_x \phi(x))^2 \right), \quad (3.19)$$

where $\partial_x \phi(x)$ denotes fluctuations of the magnetization in x -direction and $\partial_x \theta(x)$ is the conjugate variable, with the commutation relation

$$[\phi(x), \partial_{x'} \theta(x')] = i\pi \delta(x - x'). \quad (3.20)$$

The generic Luttinger liquid parameters K and v for the low energy fixed point of the spin-rotationally invariant Heisenberg model are known to be $K = 1/2$ and $v = \pi/(2)Ja$.

For the Umklapp Hamiltonian, only the dominant process is kept, which close to half filling is the $4k_F$ term

$$H_U = \frac{g}{(2\pi a)^2} \int dx \left(e^{i\Delta k x} e^{i4\phi(x)} + h.c. \right). \quad (3.21)$$

For later use, the first part will be called $H_{U,1}$ and its hermitian conjugate $H_{U,2}$. Notice that such a term transfers two spinons from one Fermi point to the other while the lattice absorbs the excess momentum $4k_F = 2\pi/a$. Away from half filling, this contribution to the Hamiltonian oscillates with $\Delta k = 4k_F - 2\pi/a = 4\pi \langle S_z \rangle / a$, causing it to be suppressed exponentially for $v\Delta k \gg k_B T$. Exactly at half filling, which corresponds to $\Delta k = 0$, the Umklapp scattering is a marginally irrelevant operator whose strength decreases logarithmically with temperature.

The form of the disorder part of the Hamiltonian,

$$H_{\text{dis}} = \frac{1}{2\pi a} \int dx \eta(x) \left(i e^{i2\phi(x)} + h.c. \right), \quad (3.22)$$

has been derived in [68], it describes the scattering from one Fermi point to the other with $\eta(x) \sim \delta_J$. Here, the disorder is assumed to be uncorrelated with $\langle \eta(x) \eta(x') \rangle = D_{\text{dis}} \delta(x-x')$, where D_{dis} is the disorder strength. In the same paper the authors showed that the interaction leads to a strong renormalization of disorder. To avoid this effect, temperature is assumed to be sufficiently high, such that the renormalized disorder remains weak, $\delta J_i \ll \sqrt{JT}$.

3.2.2 Memory Matrix

The first step for the calculation of the heat conductivity with the memory matrix formalism is the identification of the slow modes of the system. This is easily achieved by seeing that the so-called *pseudomomentum* related to the $4k_F$ -scattering, $Q = J_H + v\Delta k/(4K)J_s$, where the heat current is defined as

$$J_H = v^2 \int dx \partial_x \theta(x) \partial_x \phi(x) \quad (3.23)$$

while the spin-current

$$J_s = \frac{vK}{\pi} \int dx \partial_x \theta(x), \quad (3.24)$$

is a conserved quantity of the clean system $H_{\text{LL}} + H_{\text{U}}$. These definitions correspond directly to the lattice conductivities for free particles, equations (1.14) and (1.17). Interaction contributions to the heat current are not taken into account, because they do not contribute to the conductivities to leading order in the interactions.

The conservation of Q can be seen by calculating the commutator of the pseudomomentum with the Hamiltonian, $[Q, H_{\text{LL}} + H_{\text{U}}]$, which vanishes. Both constituents of Q are constants of motion in the Luttinger liquid, since it is Galilei invariant, so only the effect of H_{U} must be considered.

Acting on the heat current, which is the momentum operator P times v^2 , the commutator gives $v^2 \Delta k$, since in the process a momentum of Δk is generated,

$$[J_H, H_{\text{U},1}] = v^2 [P, H_{\text{U},1}] = v^2 \Delta k P. \quad (3.25)$$

The spin-current on the other hand is changed by $-4v$ as two spinons with velocity v are scattered into states with velocity $-v$,

$$[J_s, H_{\text{U},1}] = -4v J_s \quad (3.26)$$

Thus, in the commutator of the pseudomomentum Q with H_{U} the contributions from heat- and spin-current cancel exactly. This conservation law is broken when weak disorder is added, making both currents slowly decaying modes and therefore suitable candidates to set up the operator space for the memory matrix. In the following, J_H is chosen to be the first mode and J_s the second. For more transparency, matrix elements are labeled with H and s , which stands for the respective number of the mode.

The heat conductivity can be obtained by applying the scheme described in section 1.5 in a straightforward way. This will give the magnetic part of the heat conductivity of one spin

3.2. MAGNETOTHERMAL EFFECTS IN HEISENBERG CHAINS

chain to leading order in the Umklapp coupling constant g , which is the small parameter of the perturbation theory.

As explained in [40], in the presence of *marginal operators* the coupling constant is renormalized in a *renormalization group* flow. Correlation functions can be calculated with the fixed point Hamiltonian and the renormalized coupling constants, but logarithmic corrections must be added to capture the influence of the marginal operators on the correlation functions at high temperatures. Therefore, calculating the correlation functions to leading order in g , i. e. without logarithmic corrections, is equivalent to calculating them in leading order in $1/\ln(T/J)$ and $1/\ln(B/J)$. Provided that the used slow modes are the relevant ones, the resulting heat conductivity should be accurate, and additionally it is a lower bound to the real value in any case [16].

Since the memory matrix approach is perturbative, it is legitimate to separate the contributions from disorder and Umklapp scattering, because cross contributions are always subleading. In practice, for this reason, the heat conductivity can be written as

$$\kappa_{\text{mag}} \approx \frac{1}{T} \left(\chi (\hat{M}^{\text{U}} + \hat{M}^{\text{dis}})^{-1} \chi \right)_{1,1}, \quad (3.27)$$

with the memory matrix \hat{M} as an independent sum of the contributions from disorder and Umklapp scattering, and the matrix of susceptibilities as defined in equation (1.53).

Since in this context the $\hat{\chi}$ -matrix is diagonal, only the 1,1-component is needed to calculate the heat conductivity from equation (3.27). As shown in [16], one obtains easily

$$\chi_{1,1} = \frac{\pi v T^2}{3}. \quad (3.28)$$

The memory matrix is constituted, as already pointed out, by the zero energy limit of the imaginary parts of the correlation functions of the *time-derivatives* of the respective currents, see equation (1.60). These derivatives are obtained in the usual manner from the commutator with the Hamiltonian, where for the Umklapp part H_{U} is used and for the disorder part H_{dis} . To distinguish these, the short notation $\partial_t^{\text{U}}, \partial_t^{\text{dis}}$ is used for the respective parts of the total time derivative. One obtains after a short calculation, which can be found in appendix B.1 in equations (B.5) and (B.4), for the Umklapp parts

$$\partial_t^{\text{U}} J_H = \frac{v\Delta k}{4K} \partial_t^{\text{U}} J_S = \frac{v\Delta k}{4K} i \frac{4vKg}{(2\pi a)^2} \int dx \left(e^{i\Delta kx} e^{i4\phi(x)} - h.c. \right) \quad (3.29)$$

and, see equations (B.6) and (B.7), for the disorder parts

$$\begin{aligned} \partial_t^{\text{dis}} J_S &= -\frac{vK}{\pi a} \int dx \eta(x) \left(e^{i2\phi(x)} + h.c. \right) \\ \partial_t^{\text{dis}} J_H &= \frac{v^2}{2a} \int dx \eta(x) \left(\partial_x e^{i2\phi(x)} - h.c. \right). \end{aligned} \quad (3.30)$$

With these expressions the correlation functions between the respective time-derivatives of currents must be calculated. Due to equation (3.29) for the Umklapp part of the memory matrix only one correlation function is involved:

$$\hat{M}^{\text{U}} = \begin{pmatrix} \left(\frac{v\Delta k}{4K} \right)^2 & -\frac{v\Delta k}{4K} \\ -\frac{v\Delta k}{4K} & 1 \end{pmatrix} \lim_{\omega \rightarrow 0} \frac{1}{i\omega} \text{Im} \underbrace{\int dt (e^{-i\omega t} - 1) \langle \partial_t^{\text{U}} J_S; \partial_t^{\text{U}} J_S \rangle}_{\Gamma(B,T)}, \quad (3.31)$$

and the latter integral shall be called $\Gamma(B, T)$.

Since the correlation functions put into the integrand are *time-ordered* Green's functions, in principle the obtained correlation function $\langle \partial_t^U J_s \partial_t^U J_s \rangle(\omega)$ is also a time-ordered one. What actually is needed to calculate the conductivity is the corresponding *retarded* correlation function, which is obtained by doing the Wick rotation $\tau = it + \text{sign}(t)$, [79]. For the correlation functions used here, this is equivalent to

$$\chi^R(t, x) = -2\theta(t) \text{Im}(\chi^T(x, t)), \quad (3.32)$$

where χ^R denotes the retarded and χ^T the time-ordered correlation function¹⁰.

The existence of a hidden conservation law is reflected in the fact that the matrix in equation (3.31) has a zero eigenvalue. Inserting the above expression for the spin current, one obtains

$$\begin{aligned} \Gamma(B, T) &= \\ &= -\frac{16v^2 K^2 g^2}{(2\pi a)^4} \int dt (e^{-i\omega t} - 1) \int dx \int dx' \left\langle \left(e^{i\Delta k x} e^{i4\phi(x)} - h.c. \right) \left(e^{i\Delta k x'} e^{i4\phi(x')} - h.c. \right) \right\rangle \\ &= \frac{16v^2 K^2 g^2}{(2\pi a)^4} \int dt (e^{-i\omega t} - 1) \int dx \int dx' e^{i\Delta k(x-x')} \left\langle e^{i4\phi(x)} e^{-i4\phi(x')} \right\rangle. \end{aligned} \quad (3.33)$$

It can be shown by symmetry arguments¹¹ that the integral in the last line for $\omega \ll 1$ is approximately equal to

$$-\omega \int dt \int dx \int dx' t e^{-i\Delta k(x-x')} \text{Im} \left(\left\langle e^{i4\phi(x)} e^{-i4\phi(x')} \right\rangle \right). \quad (3.34)$$

The $4k_F$ correlation function in the latter line can be transformed by use of the standard identity¹²

$$\left\langle e^{\sum_j A_j \phi(r_j) + B_j \theta(r_j)} \right\rangle = e^{-\frac{1}{2} \langle (\sum_j A_j \phi(r_j) + B_j \theta(r_j))^2 \rangle} \quad (3.35)$$

to a function of the elementary ϕ - ϕ correlation function, which is known, namely

$$\left\langle e^{i4\phi(x)} e^{-i4\phi(x')} \right\rangle = e^{16\langle \phi(x)\phi(x') \rangle}. \quad (3.36)$$

Inserting this into equation (3.33), the integral can be done by contour integration, as explicitly shown in appendix B.2). The resulting Umklapp memory matrix then is

$$\hat{M}^U = \begin{pmatrix} \left(\frac{v\Delta k}{4K}\right)^2 & -\frac{v\Delta k}{4K} \\ -\frac{v\Delta k}{4K} & 1 \end{pmatrix} \frac{-g^2 v \Delta k^2}{8\pi^2} n'_B \left(\frac{v\Delta k}{2} \right) \quad (3.37)$$

with n'_B the derivative of the Bose function. Calculating the disorder part of the memory matrix is a bit less cumbersome: In the first place, it must be diagonal since the time-derivatives of the heat- and spin current contain different numbers of fields. Secondly, the uncorrelated disorder makes the correlation function purely local. The same arguments apply

¹⁰for more detail see [40].

¹¹see B.2

¹²for a proof see e.g. [40]

3.2. MAGNETOTHERMAL EFFECTS IN HEISENBERG CHAINS

as for the Umklapp memory matrix, and one obtains

$$\begin{aligned} M_{ss}^{\text{dis}} &= \lim_{\omega \rightarrow 0} \frac{1}{i\omega} \frac{v^2 K^2}{\pi^2 a^2} \text{Im} \int dt (e^{-i\omega t} - 1) \int dx \int dx' \langle \eta(x) \eta(x') \rangle \\ &\quad \times \left\langle \left(e^{i2\phi(x)} + h.c. \right) \left(e^{i2\phi(x')} + h.c. \right) \right\rangle \\ &\approx \lim_{\omega \rightarrow 0} \frac{1}{i\omega} \frac{v^2 K^2}{\pi^2 a^2} \text{Im} \int dt (-i\omega t) \int dx \int dx' D_{\text{dis}} \delta(x - x') e^{4\langle \phi(x) \phi(x') \rangle} \end{aligned} \quad (3.38)$$

for the disorder spin current relaxation rate and

$$M_{HH}^{\text{dis}} \approx \lim_{\omega \rightarrow 0} \frac{1}{i\omega} \frac{v^4}{4\pi^2 a^2} \text{Im} \int dt (-i\omega t) \int dx \int dx' D_{\text{dis}} \delta(x - x') \partial_x \partial_{x'} e^{4\langle \phi(x) \phi(x') \rangle} \quad (3.39)$$

for the disorder heat current relaxation rate. These integrals can again be evaluated elementary, which is done in B.3. The resulting disorder memory matrix is

$$\hat{M}^{\text{dis}} = \begin{pmatrix} T & 0 \\ 0 & \frac{2}{\pi^2 T} \end{pmatrix} \frac{v\pi D_{\text{dis}}}{8a}. \quad (3.40)$$

Like \hat{M}^{dis} , the matrix of susceptibilities χ must be diagonal, thus the heat conductivity is governed by the 1, 1-component of the inverse memory matrix solely. Being only 2×2 , the inverse can be calculated directly, giving

$$M_{HH}^{-1} = \frac{M_{ss}^U + M_{ss}^{\text{dis}}}{(M_{HH}^U + M_{HH}^{\text{dis}})(M_{ss}^U + M_{ss}^{\text{dis}}) - M_{sH}^U{}^2} \quad (3.41)$$

Together with the susceptibility of the heat current¹³ $\chi_{HH} = \pi v T^2 / 3$, a closed expression for the heat conductivity can be derived.

3.2.3 Results

The magnetic heat conductivity turns out to be only a function of the scaling variable $h = \mu_B g B / k_B T$ and the dimensionless parameter

$$\alpha(T) = \frac{D_{\text{dis}} v^2}{(k_B T)^2 g(T)^2 a} \quad (3.42)$$

which measures the relative strength of the (renormalized) disorder and Umklapp scatterings. The latter contains the coupling constant $g(T)$ for the $4k_F$ -Umklapp process, which is an unknown parameter within this theory. However, the problem of Umklapp scattering in the XXZ-chain, which contains the isotropic Heisenberg chain as a limiting case, can be treated by Bethe-Ansatz, giving an analytic formula for the coupling constant. Lukyanov did such a study on a XXZ-chain, using a slightly different notation [80], with the result that his coupling constant¹⁴ \tilde{g} , which is related to g by

$$g(T) = \frac{\pi^2 J a}{2} \tilde{g}(T). \quad (3.43)$$

¹³see B.4

¹⁴in his notation

fulfills the transcendental equation

$$\frac{1}{\tilde{g}} + \frac{\ln(\tilde{g})}{2} = \ln\left(\frac{e^{\frac{1}{4}+\gamma}\sqrt{\frac{\pi}{2}}J}{T}\right) \quad (3.44)$$

where $\gamma = 0.5772\dots$ is the Euler constant. Within the precision of this calculation $\tilde{g}(T)$ turns out to be $\approx 1/\ln(J/T)$, but to include subleading corrections the solution of equation (3.44) shall be used to obtain $g(T)$.

Using the variables introduced above, the normalized heat conductivity reads

$$\frac{\kappa_{\text{mag}}(B, T)}{\kappa_{\text{mag}}(0, T)} = \frac{\pi^3\alpha(T) - 2\pi^2h^2n'_B(h)}{\pi^3\alpha(T) - (2\pi^2 + 4h^2)h^2n'_B(h)} \quad (3.45)$$

with $n_B(h) = 1/(e^h - 1)$. This result is valid in the scaling limit of weak disorder and $1/\ln(B/J), 1/\ln(T/J) \ll 1$. It gives a lower bound to the exact heat conductivity of the model system and should provide, for the sensible choice of slow modes, an accurate approximation to the former. As can be seen in figure 3.3, a dip is predicted to evolve in the field dependence of the heat conductivity at $B \sim T$.

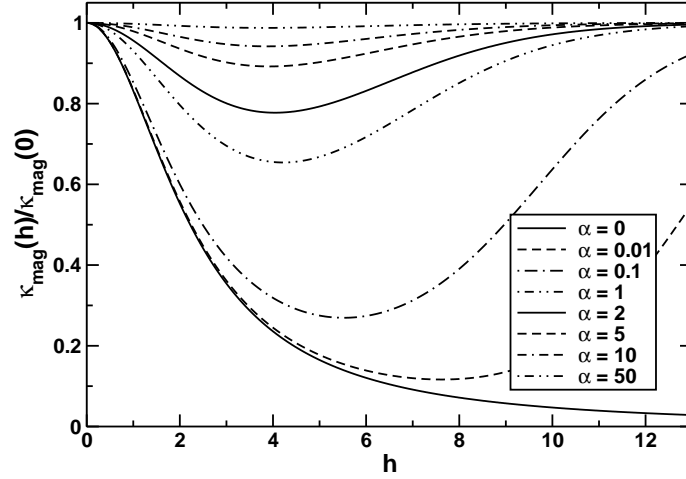


Figure 3.3: Field dependence of the normalized heat conductivity as a function of rescaled field $h = g\mu_B B / k_B T$ for various α . With decreasing α the dip gets broader and deeper

The limiting behavior of the field dependence of the thermal conductivity can be easily extracted from (3.45). For α small compared to $h^2 n'_B(h)$, i.e. weak disorder and not too strong fields¹⁵, one finds

$$\frac{\kappa_{\text{mag}}(B, T)}{\kappa_{\text{mag}}(0, T)} \approx \frac{1}{1 + \frac{2h^2}{\pi^2}}. \quad (3.46)$$

This implies a strong reduction of κ_{mag} of order 1 for $\mu_B B \sim k_B T$ as long as the renormalized disorder is sufficiently weak, $\alpha(T) \ll 1$. In the opposite limit, where $\alpha(T)$ is the dominant contribution in the denominator, one obtains by a Taylor series for small h a small suppression of κ_{mag} as

$$\frac{\kappa_{\text{mag}}(B, T)}{\kappa_{\text{mag}}(0, T)} \approx 1 + \frac{4n'_B(h)h^4}{\pi^3\alpha(T)}, \quad (3.47)$$

¹⁵of course for $h \rightarrow \infty$ the normalized heat conductivity goes to 1 for any fixed α since Umklapp scattering is exponentially suppressed

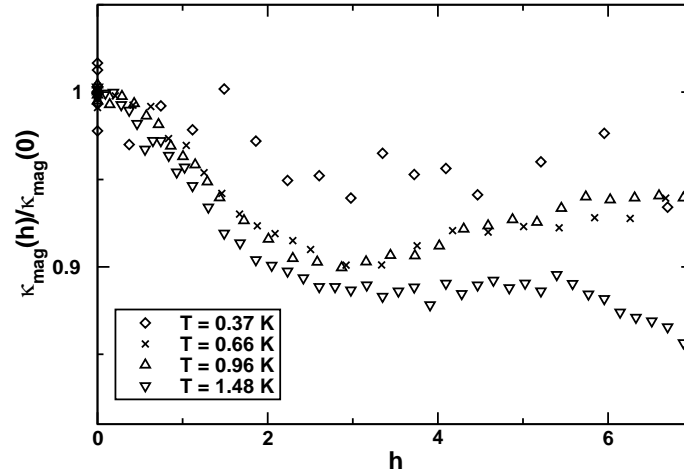


Figure 3.4: Experimental thermal conductivity of CuPzN by A. Sologubenko et. al. ([69]), expressed as function of rescaled field $h = g\mu_B B / k_B T$ for some temperatures

which gives rise to a minimum at $h \approx 3.83$, independently of α , where $\kappa_{\text{mag}}/\kappa_{\text{mag}}^0$ approximately takes the value $1 - 0.63/\alpha(T)$.

The deeper reason for this structure in the suppression of the heat conductivity is the conservation of the pseudomomentum $Q = J_H + v\Delta k/(4K)J_s$ in the Umklapp Hamiltonian. Exactly at the commensurate point the pseudo-momentum is equal to the heat current, which therefore can be altered solely by disorder scattering. Then, moving away from the commensurate filling, J_H is no longer identical to the pseudo-momentum, and thus less protected from decay due to Umklapp processes. Finally, at large fields, the Umklapp process is thermally suppressed, leading again to disorder dominated behavior.

3.2.4 Comparison with Experiments

The obtained theoretical results contain only one free parameter, namely $\kappa_{\text{mag}}(0, T)$. In a suitable experimental realization of a Heisenberg chain, this parameter could be fixed by a zero-field measurement.

One such realization is given by the spin chain compound copper pyrazine dinitrate $\text{Cu}(\text{C}_4\text{H}_4\text{N}_2)(\text{NO}_3)_2$, abbreviated by CuPzN, whose structural and magnetic properties are well-studied. Its relatively small exchange coupling of only $J/k_B \approx 10.3$ K [81, 82] allows to polarize the system with moderate magnetic fields of $B_c = 15$ T, which is easily accessible experimentally. CuPzN has an orthorhombic structure with lattice constants $a = 6.712$ Å, $b = 5.142$ Å, and $c = 11.73$ Å at room temperature [83]. The chains of Cu^{2+} spins $S = 1/2$ run along the a axis. Inelastic neutron scattering, magnetization, and specific heat measurements have confirmed that CuPzN is very well described by the antiferromagnetic Heisenberg model with nearest-neighbor couplings, equation (3.1) [81, 82, 84]. The one-dimensional nature of the spin interaction is reflected by a very low ordering temperature, $T_N = 0.107$ K, and therefore the ratio of interchain J' to intrachain J couplings is estimated to be tiny, $|J'/J| \approx 4.4 \times 10^{-3}$ [85].

The experimentally accessible heat conductivity is constituted by contributions from phonons and spinons, but the purely phononic contribution $\kappa_{\text{ph}}(T)$ is assumed to be independent of the magnetic field, whilst the spinon part $\kappa_{\text{mag}}(B, T)$ strongly depends on it. This was verified in [69] by measuring the field dependence of the heat conductivity parallel and

perpendicular to the chains. Thus, as argued there, the spinon part of the heat conductivity can be extracted by subtracting the zero-field value, giving the field dependend part of the magnetic heat conductivity

$$\Delta\kappa_{\text{mag}}(T, B) = \kappa(T, B) - \kappa(T, B = 0) = \kappa_{\text{mag}}(T, B) - \kappa_{\text{mag}}(T, B = 0). \quad (3.48)$$

Unfortunately the measurement of $\kappa_{\text{mag}}(T, 0)$ is obscured by a large phonon background, but as a crude estimate¹⁶, $\kappa_{\text{mag}} \approx 3.5T^2 \text{ WmK}^{-3}$, can be obtained from the behavior at large fields, which corresponds to a heat conductivity per spin chain of $\kappa_{\text{mag}} \approx 2.110T^2 \text{ WmK}^{-3}$. For the four lowest studied temperatures, $T = 0.37, 0.66, 0.96, 1.48 \text{ K}$, this yields for the dimensionless parameter $\alpha(T) \approx 0.52, 0.12, 0.049, 0.016$, respectively. These estimates allow a quantitative comparison between theory and experiment.

Qualitatively, there is an overall agreement between the theoretical curves shown in figure 3.3 and the experimentally obtained data depicted in figure 3.4 in the same units. However, looking at the details two main discrepancies are observed. The experimentally measured $\kappa_{\text{mag}}(B, T)/\kappa_{\text{mag}}(0, T)$ shows a pronounced dip at $h = g\mu_B B/(k_B T) \approx 3$, whereas the dip in the theoretical curve is rather located around $h \approx 4$ for large α and at even higher values of h for the α corresponding to the studied temperatures. Secondly, the magnitude of the suppression is strongly overestimated by the theoretical prediction of more then 50% reduction, compared with only 10% in the experiment.

As an explanation for such differences, one should note that for the temperatures and magnetic fields shown in figure 3.4 both subleading effects of order $\ln(B/T)/\ln(J/T)$ or $\ln(\ln(J/T))/\ln(J/T)$ and band-curvature effects¹⁷, that have been neglected in the calculation, can become important. For example, \tilde{g}^2 calculated to leading order is for $J/T = 30$ a factor 2.5 larger than the value obtained from equation (3.44).

More importantly, the model Hamiltonian (3.18) apparently does not correctly capture all aspects of the physics of CuPzN samples. Especially, modeling the disorder by equation (3.22) might not be appropriate. This was also the conclusion of [69] from an analysis of the heat conductivity at large fields $B \sim 15 \text{ T}$ in the quantum critical regime where the magnetization is close to saturation. Indeed, for other types of disorder rather than Gaussian, the matrix (3.40) will have a different structure which will affect the quantitative predictions, while the qualitative picture will remain unmodified. For example, it might be necessary to take the interplay between forward scattering and interactions into account. Forward scattering affects transport at $B = 0$ only weakly but it can reduce the Umklapp dip in κ_{mag} considerably as the suppression of κ_{mag} at larger fields relies on momentum conservation.

A more realistic modeling of disorder should also account for the possibility that defects might cut the one-dimensional chains in long pieces, [45, 69]. In such a situation, one has also to model how phonons or weak inter-chain interactions couple heat into and out off such long chain segments.

3.3 Violation of Wiedemann-Franz Law in Luttinger Liquids

The second example of transport properties discussed here are thermoelectric-electric effects in one-dimensional correlated metals. For several reasons this setting is much more complex than the preceding example of heat transport in spin chains: the bosonization description of a metal involves four bosonic fields instead of two for the spin chain. This already increases

¹⁶see [69] for details

¹⁷the overall downturn of κ_{mag} in large fields

3.3. VIOLATION OF WIEDEMANN-FRANZ LAW IN LUTTINGER LIQUIDS

the number of slow modes that must be taken into account, since in the pure model without Umklapp scattering and disorder the spin momentum as well as the charge momentum is a conserved quantity. Equivalently the reason is that the heat current of the Luttinger liquid is not parallel to the total momentum because spin and charge excitations have different velocities.

Secondly, as explained before, the strongest effects can not be found with the simplest Umklapp process which does not alter the spinon momentum. Instead, the more complicated third-filling commensurate point must be used, or an additional effect which mixes spinon and charge momentum also at half filling has to be added to the description. The prerequisites for the latter are given by band curvature, which breaks the Galilei-invariance of the system and degrades also the spin part of the heat current. This further complications arise due to the change in total particle number in a non-linear spectrum at finite temperatures, which must be balanced by an additional chemical potential shift.

The final point lies in the different question asked in the two problems: For the spin chain it is experimentally possible to extract the spinon part of the heat conductivity from the phonon background by arguing that the phonon system doesn't change with the magnetic field. For the one-dimensional correlated metal it is impossible to separate the phonon heat conductivity from the electronic one, since the Fermi momentum, which determines the Umklapp scattering here is tuned by the electronic band filling, which experimentally is harder to control. The phonon heat conductivity must be included because it is a relevant part of the physical effect that shall be described: in metals typically the main contribution to the heat conductivity comes from the phonon system, which hence dominates this part of the Wiedemann-Franz ratio as well as the thermoelectric-electric figure of merit. For this reason, phonons are also included into the calculation, making the memory matrix a four by four matrix with correspondingly many independent elements, from which not only the bare heat-conductivity, but also the Seebeck coefficient and the electrical conductivity must be derived.

3.3.1 Model System

The model system shall describe the low energy theory of a one-dimensional metal, which is described by the Luttinger liquid Hamiltonian, embedded into a three-dimensional solid with its lattice vibrations. For this system, interactions between electrons and phonons as well as Umklapp and disorder scattering are added as perturbations. Band curvature effects might also be included.

The total Hamiltonian of the system,

$$H = H_{LL} + H_{ph} + H_U + H_{dis} + H_{c-ph} + H_{BC} \quad (3.49)$$

is the sum of all these effects, where the first two terms,

$$H_{LL} = \sum_{i=c,s} \int \frac{dx}{2\pi} \left(K_i (\partial_x \theta_i(x))^2 + \frac{1}{K_i} (\partial_x \phi_i(x))^2 \right), \quad (3.50)$$

with the parameters for spin and charge part introduced earlier, and

$$H_{ph} = \int \frac{dx}{2\pi} \left((\pi P(x))^2 + v_p^2 (\nabla q(x))^2 \right) \quad (3.51)$$

constitute the low energy part for the spinon, charge and the displacement fields of the lattice ions. The phonon displacement field $q(x)$ obeys, as well as the Luttinger liquid fields,

equation (3.8), bosonic commutation relations with its conjugate momentum P ,

$$[P_\alpha(\mathbf{r}), q_\beta(\mathbf{r}')] = i\delta_{\alpha,\beta}\delta(\mathbf{r} - \mathbf{r}'). \quad (3.52)$$

The interaction between the lattice vibrations and the Luttinger liquid is, in analogy with the three-dimensional metal explained in chapter 2, mediated by the change in hopping amplitudes. From this, a direct coupling term between the charge field $\phi_c(x)$ and the displacement field $q(x)$ with the form

$$H_{c-ph} = g_N \int dx (\partial_x \phi_c(x)) (\partial_x q(x)) \quad (3.53)$$

emerges, where g_N is the coupling constant for *normal processes*. The linear coupling of the phonons to the spin fields at vanishing magnetic field is forbidden by spin inversion symmetry. In principle, a higher order coupling between the spin field and phonon fields exists, but it is less important for the transport problems studied here and therefore neglected.

Besides the normal processes, also the coupling constant of Umklapp scattering as introduced in section 3.1 is affected by distortions of the lattice from phonons. For small displacement of the ions, the coupling constants with phonons $\tilde{g}_{mn_c n_s}^U$ can be expanded in a Taylor series around the rigid-ions value $g_{mn_c n_s}^U$, giving

$$\tilde{g}_{mn_c n_s}^U = g_{mn_c n_s}^U (1 + \alpha \partial_x q(x)), \quad (3.54)$$

where α is the series coefficient.

Inserting the new coupling constant, the Umklapp Hamiltonian for Luttinger liquids in the absence of phonons, equation (3.16), to leading order in the displacement field changes to¹⁸

$$H_{mn_c n_s}^U = \frac{g_{mn_c n_s}^U}{(2\pi a)^{n_c}} \int dx \left((1 + \alpha \partial_x q(x)) e^{i\Delta k_{mn_c n_s} x} e^{i\sqrt{2}(n_c \phi_c(x) + n_s \phi_s(x))} + h.c. \right). \quad (3.55)$$

Notice that such a term allows Umklapp processes combined with phonon scattering. The Umklapp processes with involved phonon at first glance seem to be subleading to the conventional ones. However, since the phonons in typical one-dimensional models are the slowest relevant modes, and the Umklapp processes away from commensurate filling are exponentially suppressed $\sim v\Delta k/T$, the range of momentum-mismatches where phonon-assisted Umklapp-scattering affects the conductivities is bigger than for pure Umklapp-processes, making the latter subleading to the former for some possible fillings. In addition, taking into account processes to the same order in the whole matrix provides the valuable cross-check of the eigenvalues, of which one must vanish due to the conservation law and the rest must be positive for each order separately

The coupling constants $g_{mn_c n_s}^U$ and momentum mismatch $\Delta k_{mn_c n_s}$ from the respective commensurate point are, of course, different for each combination of transferred fields n_c and n_s , and the latter a function of the band filling.

As in the case of Umklapp scattering in Heisenberg chains, the Hamiltonian for Umklapp scattering for any commensurate point has a hidden conservation law, which leads to a singular memory matrix for any choice of slow modes. This conservation law in a physical system is violated by impurities, which here again are modeled by Gaussian disorder. The

¹⁸see [16]

3.3. VIOLATION OF WIEDEMANN-FRANZ LAW IN LUTTINGER LIQUIDS

effect of Gaussian disorder on thermal transport in Luttinger liquids has been studied before by Li and Orignac [15], who modeled the weak backscattering due to disorder as

$$H_{\text{dis}} = \frac{1}{\pi a} \int dx \eta(x) \left(e^{i\sqrt{2}\phi_c(x)} \cos\left(\sqrt{2}\phi_s(x)\right) + h.c. \right), \quad (3.56)$$

where the Gaussian correlated impurity potential $\eta(x)$ fulfills

$$\langle \eta(x)\eta(x') \rangle = D_{\text{dis}} \delta(x - x'), \quad (3.57)$$

and D_{dis} is the disorder strength. In principle, the phonons are also affected by the impurity potential.

However, a phonon with small momentum has a very long wavelength, which locally is a weak distortion of the lattice. If the impurity is a part of this lattice, and hence moves together with the other ions in a vibrational mode, the coupling between phonon and impurity vanishes for small phonon momenta, and the phonons mean free path diverges like $L_q \sim q^{-4}$ in the limit $q \rightarrow 0$, see [1]. Thus, phonon disorder scattering is ineffective to degrade a thermal current, and the heat conductivity diverges in a phonon system with no other scattering mechanism.

Here, only the disorder scattering of charge and spin fields is taken into account, and the phonon heat current is degraded indirectly via the normal processes and the disorder scattering of the Luttinger liquid fields.

Indeed, this treatment of the phonon impurity scattering is not completely correct, since it describes the scattering of the Luttinger liquid fields from *fixed* impurities, while in a real system the impurities are shifted together with their surrounding by lattice vibrations. If implemented correctly, the same situation as for phonons scattering directly from point defects is restored, and the mean free path of the low frequency phonons diverges again.

To describe the dissipation of the phonon momentum completely, one must go beyond the effects discussed here, which can become quite complicated. In this context, the scattering from fixed impurities is used anyway, as an easy approximation to the dissipation of the phonon heat current. However, one has to keep in mind that this doesn't reflect the physical scattering mechanism.

At even commensurate fillings, the Umklapp Hamiltonian has another conservation law since only charge fields are transferred. Thus, the spinon contribution to the heat current can not be degraded by these Umklapp processes. This symmetry results in a much weaker suppression of the heat conductivity than at odd commensurabilities, which is the signature of the perfect spin-charge separation in the Luttinger liquid model. In a real one-dimensional model, the dispersion is not exactly linear, such effect can be modeled within the bosonization language as a perturbation which mixes the spin and charge sector, as shown by Haldane [39]. Exactly at half filling, using the typical tight-binding cosine dispersion, the spectrum is truly linear, and thus there would be no mixing of charge and spin fields. However, this particle-hole symmetry of the band is also not realized in the physical system, since next-nearest neighbor hoppings violate it and generate a small curvature even at half filling.

Translated into the notation used here, the Haldane band-curvature Hamiltonian reads

$$H_{\text{BC}} = -\frac{1}{6\sqrt{2}m} \int dx \left((\partial_x \phi_c(x))^3 + 3(\partial_x \phi_c(x)) ((\partial_x \phi_s(x))^2 + (\partial_x \theta_s(x))^2 + (\partial_x \theta_c(x))^2) \right. \\ \left. + 6(\partial_x \phi_s(x))(\partial_x \theta_s(x))(\partial_x \theta_c(x)) \right) - \delta\mu \int dx \partial_x \phi_c(x), \quad (3.58)$$

where m is the band curvature parameter. Here an extra correction term with a temperature dependent chemical potential $\delta\mu$ has been included to rebalance the particle number, which is independent of temperature only for an exactly linear spectrum. It is calculated from the change of particle number due to band curvature to leading order in $1/m$,

$$\begin{aligned}\langle\delta N\rangle^{\text{BC}} &= \frac{1}{\pi} \int dx \langle\partial_x \phi_c(x)\rangle^{\text{BC}} \approx \frac{1}{\pi} \left\langle \int dx \partial_x \phi_c(x) \left(- \int dx' d\tau h^{\text{BC}} \right) \right\rangle \\ &= \frac{1}{\pi} \left(- \int dx dx' d\tau \langle\partial_x \phi_c(x) \partial_{x'} \phi_c(x', \tau)\rangle \delta\mu \right. \\ &\quad \left. - \frac{1}{2\sqrt{2}m} \int dx dx' d\tau \langle\partial_x \phi_c(x) \partial_{x'} \phi_c(x', \tau)\rangle \right. \\ &\quad \left. \times \sum_{i=c,s} (\langle\partial_{x'} \phi_i(x') \partial_{x'} \phi_i(x')\rangle + \langle\partial_{x'} \theta_i(x') \partial_{x'} \theta_i(x')\rangle) \right),\end{aligned}\quad (3.59)$$

with h^{BC} the density corresponding to the band curvature Hamiltonian. From this one can read of the $\delta\mu$ that enforces $\delta N = 0$ directly, namely

$$\delta\mu = \frac{1}{6\sqrt{2}m} \int dx' d\tau \sum_{i=c,s} (\langle\partial_{x'} \phi_i(x') \partial_{x'} \phi_i(x')\rangle + \langle\partial_{x'} \theta_i(x') \partial_{x'} \theta_i(x')\rangle), \quad (3.60)$$

where the integrals over the local correlation functions can easily be done,

$$\delta\mu = \frac{\pi^2 T^2}{12m} \left(\frac{1}{v_c^2} \left(K_c + \frac{1}{K_c} \right) + \frac{1}{v_s^2} \left(K_s + \frac{1}{K_s} \right) \right). \quad (3.61)$$

Including such contribution to the band curvature Hamiltonian, the particle number becomes, at least to leading order, again independent of temperature, as in the physical system.

3.3.2 Memory Matrix for the One-Dimensional Metal

The first step setting up the memory matrix for this system is again the choice of the slow modes. It is guided by the effects that shall be described and the correlation functions one wants to obtain from it.

For the calculation of the Wiedemann-Franz ratio the charge conductivity σ_c and the heat conductivity κ are needed. Clearly, the charge current

$$J_c = v_c K_c (N_R - N_L) = \sqrt{2} v_c K_c \int dx \partial_x \theta(x), \quad (3.62)$$

must be included to calculate the charge conductivity. For the calculation of the heat conductivity, the total heat current is needed, but to make the effect of Umklapp scattering more transparent it is splitted into several modes here.

Without the phonon contribution, the Umklapp Hamiltonian conserves the pseudomomentum

$$Q_{mn_c n_s} = \frac{\Delta k_{mn_c n_s}}{2n_c v_c K_c} J_c + P_{LL}, \quad (3.63)$$

whose constituents are the charge current J_c and Luttinger liquid momentum

$$P_{LL} = - \sum_{i=c,s} (\partial_x \phi_i(x)) (\partial_x \theta_i(x)). \quad (3.64)$$

3.3. VIOLATION OF WIEDEMANN-FRANZ LAW IN LUTTINGER LIQUIDS

Thus, the momentum of the Luttinger liquid P_{LL} is chosen as the second slow mode. Different from the case of Heisenberg chains, the Luttinger liquid contribution to the heat current,

$$J_H = - \sum_{i=c,s} v_i^2 \int dx (\partial_x \phi_i(x)) (\partial_x \theta_i(x)), \quad (3.65)$$

is not parallel to the momentum any more, since charge and spin excitations have different velocities. Thus, the Luttinger liquid heat conductivity can not be obtained from the momentum alone, but J_H must be included as another slow mode. Equivalently, it would be possible to choose the spinon and charge momenta as slow modes instead of J_H and P_{LL} , and obtain all correlation functions by collecting the contributions. The connection between the is a simple linear transformation, there is no physical difference.

To make the heat conductivity complete, the part of momentum of the phonon system which is parallel to the chain direction, given by

$$P_{ph} = - \int d\mathbf{r} \pi P(x) \partial_x q(x), \quad (3.66)$$

is added.

As in the precedent section, matrix elements are labeled by the corresponding mode. In matrix notation the order is, from one to four, charge current J_c , Luttinger liquid momentum P_{LL} , Luttinger liquid heat current J_H , and phonon momentum P_{ph} .

The charge conductivity σ_c is, for the strictly linear system, simply the (1, 1)-component of the resulting conductivity matrix $\hat{\sigma}$, since the charge current obtained from the continuity equation is equal to the first slow mode. If band curvature is added, the physical charge current is modified to

$$J_c^{\text{phys}} = J_c + \frac{1}{m} P_{LL}, \quad (3.67)$$

again to leading order in $1/m$. In this case an interaction contribution to the charge current arises, since the band curvature Hamiltonian does not commute with the polarization operator, see equation (1.17). This correction must be taken into account, because it couples different slow modes and thus generates corrections to leading order in the perturbations.

After this change, more components of the matrix of conductivities enter the physical charge conductivity, namely

$$\sigma_c^{\text{BC}} = \hat{\sigma}_{J_c, J_c} + \frac{2}{m} \hat{\sigma}_{J_c, P_{LL}} + \frac{1}{m^2} \hat{\sigma}_{P_{LL}, P_{LL}}. \quad (3.68)$$

For the heat current the corrections due to band curvature are subleading, and we can use the free part of the heat current again. However, several elements of $\hat{\sigma}$ contribute from the beginning. The heat conductivity can be constructed by using the free part of the physical heat current,

$$J_H^{\text{phys}} \approx J_H + v_P^2 P_{ph}, \quad (3.69)$$

yielding the heat conductivity for the electrically insulated system,

$$\kappa_0 = \frac{1}{T} L_{TT} = \frac{1}{T} (v_P^4 \hat{\sigma}_{P_{ph}, P_{ph}} + N_{\text{chain}} \hat{\sigma}_{J_H, J_H}), \quad (3.70)$$

which is related to the macroscopic transport coefficient L_{TT} . Note that the phonon heat current is obtained from the phonon momentum in chain direction, summed over three-dimensional momenta, thus giving a heat conductivity per area. In contrast, the obtained

conductivities for the Luttinger liquid are calculated for one chain. To combine the two, one needs an extra factor of chain density N_{chain} in all Luttinger liquid conductivities to match the units. However, this factor is trivial and does not introduce any new effect, that can not be absorbed into coupling constants. Therefore it can be safely set to one in the following.

As explained in section 1.2, the total heat conductivity κ contains additional thermoelectric corrections, because a temperature gradient in an electrically insulated system generates automatically a particle countercurrent, namely

$$\kappa = \frac{1}{T} \left(L_{TT} - \frac{L_{TE}^2}{L_{EE}} \right) = \kappa_0 - TS^2 \sigma_c, \quad (3.71)$$

with the Seebeck coefficient, defined by

$$S = \frac{1}{T} \frac{L_{TE}}{L_{EE}} = \frac{1}{T} \frac{\hat{\sigma}_{J_c, J_H} + \frac{v_p^2}{\sqrt{N_{\text{chain}}}} \hat{\sigma}_{J_c, P_{ph}}}{\hat{\sigma}_{J_c, J_c}}. \quad (3.72)$$

In case of curved band, the charge conductivity in κ and S of course must be replaced by σ_c^{BC} , leading to

$$S^{\text{BC}} = \frac{1}{T} \frac{\hat{\sigma}_{J_H, J_c} + \frac{1}{m} \hat{\sigma}_{J_H, P_{LL}} + \frac{v_p^2}{\sqrt{N_{\text{chain}}}} \hat{\sigma}_{P_{ph}, J_c} + \frac{v_p^2}{m N_{\text{chain}}} \hat{\sigma}_{P_{ph}, P_{LL}}}{\sigma_c^{\text{BC}}}, \quad (3.73)$$

and

$$\kappa^{\text{BC}} = \kappa_0 + T (S^{\text{BC}})^2 \sigma_c^{\text{BC}}. \quad (3.74)$$

Also the generalized susceptibilities are different. Without band curvature, for the first three modes, J_c , P_{LL} , and J_H , the generalized susceptibilities χ_{ij} are easily calculated similar to equation (B.22). The susceptibility of the phonon momentum has been calculated in [86] and can be readily used. All cross susceptibilities between Luttinger liquid fields and phonon momentum vanish, since only local contractions appear. The complete matrix of susceptibilities thus reads

$$\hat{\chi} = \frac{\pi T^2}{3} \begin{pmatrix} \frac{6v_c K_c}{\pi^2 T^2} & 0 & 0 & 0 \\ 0 & \frac{1}{v_c^3} + \frac{1}{v_s^3} & \frac{1}{v_c} + \frac{1}{v_s} & 0 \\ 0 & \frac{1}{v_c} + \frac{1}{v_s} & v_c + v_s & 0 \\ 0 & 0 & 0 & \frac{2}{5} \frac{T^2}{v_p^5} \end{pmatrix}. \quad (3.75)$$

With band curvature and for fixed particle number, the susceptibilities with leading order band curvature correction can be calculated by

$$\chi_{ij}^{\text{BC}} = \left\langle \int dx d\tau j_i(x, 0) j_j(x, \tau) \left(1 - \int dx' d\tau' h^{\text{BC}}(x' \tau') \right) \right\rangle, \quad (3.76)$$

where the part including the integral is the correction and rest the hitherto susceptibility. The calculation is carried out explicitly in appendix B.6, yielding corrections to leading order only for two elements of the $\hat{\chi}$ -matrix, namely for $\chi_{J_c, P_{LL}}$ and χ_{J_c, J_H} . One finds

$$\chi_{J_c, P_{LL}} = \frac{\pi T^2}{3m} \left(\frac{1}{v_c^3} + \frac{1}{v_s^3} \right), \quad (3.77)$$

and

$$\chi_{J_c, J_H} = \frac{\pi T^2}{3m} \left(\frac{1}{v_c} + \frac{1}{v_s} \right), \quad (3.78)$$

3.3. VIOLATION OF WIEDEMANN-FRANZ LAW IN LUTTINGER LIQUIDS

respectively. The former result can be easily understood, remembering that the change in particle number δN must be equal to $\langle J_c^{\text{phys}} P_{LL} \rangle$. Since the band curvature Hamiltonian has been corrected to rebalance the particle number by a chemical potential, one can deduce from this one component of $\hat{\chi}$ to leading order in $1/m$,

$$0 = \langle J_c^{\text{phys}} P_{LL} \rangle = \chi_{J_c, P_{LL}} + \frac{1}{m} \chi_{P_{LL}, P_{LL}}, \quad (3.79)$$

and thus reproducing the same expression for $\chi_{J_c, P_{LL}}$.

3.3.2.1 Time-Derivatives of Slow Modes

In the next step the time-derivatives of the slow modes with respect to each perturbation, or *generalized forces* as they are also called, have to be calculated in order to set up the memory matrix.

Starting with the disorder Hamiltonian, one obtains

$$\partial_t^{\text{dis}} J_c = i \frac{2v_c K_c}{a} \int dx \eta(x) \left(e^{i\sqrt{2}\phi_c(x)} - h.c. \right) \cos(\sqrt{2}\phi_s(x)) \quad (3.80)$$

for the time-derivative of the Luttinger liquid part of the charge current,

$$\partial_t^{\text{dis}} P_{LL} = \frac{1}{\pi a} \int dx \eta(x) \partial_x \left(\cos(\sqrt{2}\phi_s(x)) \left(e^{i\sqrt{2}\phi_c(x)} + h.c. \right) \right) \quad (3.81)$$

for the Luttinger liquid momentum, and

$$\begin{aligned} \partial_t^{\text{dis}} J_H = \frac{1}{\pi a} \int dx \eta(x) & \left(v_s^2 \left(\partial_x \cos(\sqrt{2}\phi_s(x)) \right) \left(e^{i\sqrt{2}\phi_c(x)} + h.c. \right) \right. \\ & \left. + v_c^2 \cos(\sqrt{2}\phi_s(x)) \partial_x \left(e^{i\sqrt{2}\phi_c(x)} + h.c. \right) \right) \end{aligned} \quad (3.82)$$

for the heat current. It is not necessary to take into account the phonon momentum in the disorder scattering, since it is known that the heat current of three-dimensional phonons can not be degraded by scattering from point defects, [1].

The time-derivatives from Umklapp scattering are

$$\begin{aligned} \partial_t^U J_c &= -i \frac{2\pi n_c v_c K_c g_{mn_c n_s}^U}{(2\pi a)^{n_c}} \int dx (1 + \alpha \partial_x q(x)) \left(e^{i\Delta k x} e^{i\sqrt{2}(n_c \phi_c(x) + n_s \phi_s(x))} - h.c. \right), \\ \partial_t^U P_{LL} &= \frac{g_{mn_c n_s}^U}{(2\pi a)^{n_c}} \int dx (1 + \alpha \partial_x q(x)) \sum_{i=c,s} (-\pi) \left(e^{i\Delta k x} \left(\partial_x e^{i\sqrt{2}n_i \phi_i(x)} \right) e^{i\sqrt{2}n_i \phi_i(x)} + h.c. \right), \\ \partial_t^U J_H &= \frac{g_{mn_c n_s}^U}{(2\pi a)^{n_c}} \int dx (1 + \alpha \partial_x q(x)) \sum_{i=c,s} (-\pi v_i^2) \left(e^{i\Delta k x} \left(\partial_x e^{i\sqrt{2}n_i \phi_i(x)} \right) e^{i\sqrt{2}n_i \phi_i(x)} + h.c. \right) \\ \partial_t^U P_{ph} &= \frac{g_{mn_c n_s}^U}{(2\pi)^{n_c}} \int dx \partial_x \left(e^{i\Delta k x} e^{i\sqrt{2}(n_c \phi_c(x) + n_s \phi_s(x))} + h.c. \right) \alpha \partial_x q(x). \end{aligned} \quad (3.83)$$

From these, the conserved currents of the Umklapp Hamiltonian can be derived. In the case of no involved phonon, we already know that the pseudomomentum $Q_{mn_c n_s}$, equation (3.63) is conserved, but with phonons it is less obvious. Consider one unit of Luttinger liquid momentum scattered by an one-phonon Umklapp process. The change in momentum $\partial_t^U P_{LL}$ can be compensated by adding π units of phonon momentum, as can be seen by

evaluating the derivative of the product in the last line of equation (3.83). However, this generates a second term from the derivative of $e^{i\Delta k x}$, which again can be canceled by adding $\Delta k/(2n_c v_c K_c)$ units of charge current. In total, one obtains the conserved pseudomomentum for the one-phonon Umklapp process,

$$Q_{mn_c n_s}^1 = \frac{\Delta k}{2n_c v_c K_c} J_c + P_{LL} + P_{ph}. \quad (3.84)$$

Additional terms coupling the two subsystems of the Luttinger liquid and the vibrational modes arise from the normal processes, with the respective time derivatives

$$\begin{aligned} \partial_t^{\text{c-ph}} J_c &= \sqrt{2} v_c K_c \pi g_N \int dx \partial_x^2 q(x) \\ \partial_t^{\text{c-ph}} P_{LL} &= -\pi g_N \int dx (\partial_x^2 q(x)) (\partial_x \phi_c(x)) \\ \partial_t^{\text{c-ph}} J_H &= -\pi v_c^2 g_N \int dx (\partial_x^2 q(x)) (\partial_x \phi_c(x)) \\ \partial_t^{\text{c-ph}} P_{ph} &= -g_N \int dx (\partial_x^2 \phi_c(x)) (\partial_x q(x)) \end{aligned} \quad (3.85)$$

What is not included so far is the effect of band curvature. Here symmetry reduces the number of finite generalized forces: The charge current J_c and the Luttinger liquid momentum P_{LL} commute with the band curvature Hamiltonian, as it is still Galilei-invariant. Since no corrections from lattice distortion are taken into account in this term, also the phonon momentum P_{ph} commutes with H_{BC} , so the only finite contribution comes from the Luttinger liquid heat current J_H .

The corresponding time-derivative can be obtained by making use of the way the momentum operators of each sector act on operators, namely

$$[\hat{P}_\alpha, H] = -i \partial_x^\alpha H, \quad (3.86)$$

where the partial derivative ∂_x^α acts only on fields of the respective sector, charge or spin. Since the heat current is composed of momentum operators of the two sectors, it follows

$$\partial_t^{\text{BC}} J_H = i [J_H, H_{BC}] = -v_c^2 \partial_x^c H_{BC} - v_s^2 \partial_x^s H_{BC}. \quad (3.87)$$

In practice, only mixed terms can contribute, since unmixed ones are surface terms and all fields are assumed to vanish at the infinite. Therefore, one obtains

$$\begin{aligned} \partial_t^{\text{BC}} J_H &= \frac{v_c^2 - v_s^2}{2\sqrt{2}m} \int dx \left((\partial_x^2 \phi_c(x)) \left((\partial_x \phi_s(x))^2 + (\partial_x \theta_s(x))^2 \right) \right. \\ &\quad \left. + 2K_c^{-\frac{1}{2}} (\partial_x^2 \theta_c(x)) \partial_x \phi_s(x) \partial_x \theta_s(x) \right). \end{aligned} \quad (3.88)$$

The result can be cross-checked with the symmetry between charge and spin sector, which causes the two contributions to cancel exactly when the velocities v_c and v_s become equal. This cancellation also reflects the Galilei-invariance of the total momentum, which becomes a multiple of the heat current for equal velocities.

3.3.2.2 Disorder Contribution

The contribution to the memory matrix from disorder affects only the Luttinger liquid fields, since three-dimensional phonons cannot be scattered by point defects in the limit $q \rightarrow 0$. The exact form of the correlation functions can be taken from [15], where exactly the same Hamiltonian has been used to calculate the transport properties of the heat and charge currents of a Luttinger liquid by means of a memory *function* approach¹⁹. Also the correlation functions involving the Luttinger liquid momentum P_{LL} can be derived from this, because the time-derivative of the latter has a very similar structure as the one of the heat current. The matrix can be written, using some shorthand notations, as

$$\hat{M}^{\text{dis}} = c_{\text{dis}} \Gamma_{\text{dis}} \begin{pmatrix} \left(\frac{4K_c v_c}{2\pi T}\right)^2 & 0 & 0 & 0 \\ 0 & \frac{\left(\frac{K_c}{v_c^2} + \frac{K_s}{v_s^2}\right) K_t}{1+K_t} & \frac{K_t^2}{1+K_t} & 0 \\ 0 & \frac{K_t^2}{1+K_t} & v_c v_s \tilde{K} & 0 \\ 0 & 0 & 0 & 0 \end{pmatrix} \quad (3.89)$$

where K_t and \tilde{K} are functions of the Luttinger liquid parameters, namely

$$\begin{aligned} K_t &= K_c + K_s, \\ \tilde{K} &= \frac{(K_c v_c^2 + K_s v_s^2) K_t}{v_c v_s (1 + K_t)}, \end{aligned} \quad (3.90)$$

c_{dis} is a common prefactor of the matrix elements, also depending on these parameters through the Gamma function $\Gamma(x)$,

$$c_{\text{dis}} = \frac{(2\pi)^{K_t-1}}{2} \left(\frac{v_c}{v_s}\right)^{K_t} \frac{\Gamma^2\left(\frac{K_t}{2}\right)}{\Gamma(K_t)} \quad (3.91)$$

and the scattering rate Γ_{dis} contains the complete temperature-dependence, which is equal for each element, i. e.,

$$\Gamma_{\text{dis}} = \frac{D_{\text{dis}}}{a^2} \left(\frac{aT}{v_c}\right)^{K_t}. \quad (3.92)$$

3.3.2.3 Luttinger Liquid part of Umklapp Contribution

To obtain the memory matrix for Umklapp scattering, more work has to be done. Since the structure of the matrix is quite complicated, for more transparency two sectors are explained separately. In the pure Luttinger liquid one has to calculate a three by three submatrix which to leading order does not involve any phonon fields. This submatrix is simply embedded into the full four by four matrix with phonons, thus for transparency it is introduced first.

All Umklapp derivatives of slow modes have a typical common structure, namely they are composed of exponential functions of the momentum mismatch Δk , and the charge and the spin fields with different derivatives of single factors with respect to the space variable. By pulling out these derivatives, the needed correlation functions can be obtained by using again the identity equation (3.36), which is, of course, equally valid for spin and charge fields.

¹⁹which didn't take Umklapp scattering into account and thus misses the striking effect of hidden conservation laws.

One obtains for example for the auto correlation function of the Umklapp time-derivative of the charge current the integral

$$\langle \partial_t^U J_c \partial_t^U J_c \rangle(\omega) = \frac{(g_{mn_c n_s}^U)^2}{(2\pi a)^{2n_c}} 8v_c^2 K_c^2 n_c^2 \pi^2 \int_{-\infty}^{\infty} dt i\omega t \int_{-\infty}^{\infty} dx e^{i\Delta k x} e^{2n_c^2 \langle \phi_c(x) \phi_c(0) \rangle} e^{2n_s^2 \langle \phi_s(x) \phi_s(0) \rangle}. \quad (3.93)$$

Again, the retarded correlation function is obtained from the time-ordered by

$$\chi^R(t, x) = -2\theta(t) \text{Im}(\chi^T(x, t)). \quad (3.94)$$

Apart from the different prefactors, the correlation functions from other modes differ in the spatial derivatives, see B.7. As described there, for the Luttinger liquid momentum P_{LL} this additional derivative can be absorbed into the prefactor by partial integration, as done for the spin chain. The reason why this works for the momentum and not for the heat current J_H is that the sum over the contributions from derivatives of the charge and spin sector can be combined into a derivative of the product of the two. Thus the derivative can be shifted to the exponential of momentum mismatch, giving for the auto correlation function of the time-derivative of the Luttinger liquid momentum and the cross correlation function with the time-derivative of the charge current the same result as for $\langle \partial_t^U J_c \partial_t^U J_c \rangle(\omega)$ times a function of the momentum mismatch, namely

$$\langle \partial_t^U P_{LL} \partial_t^U P_{LL} \rangle(\omega) = \frac{\Delta k^2}{4v_c^2 K_c^2 n_c^2} \langle \partial_t^U J_c \partial_t^U J_c \rangle(\omega) \quad (3.95)$$

for the former, and

$$\langle \partial_t^U J_c \partial_t^U P_{LL} \rangle(\omega) = \frac{-\Delta k}{2v_c K_c n_c} \langle \partial_t^U J_c \partial_t^U J_c \rangle(\omega) \quad (3.96)$$

for the latter.

For the heat current, the different velocities of the contributions from charge and spin part prohibit to combine the sum into a total derivative, and hence generate more complicated and very lengthy expressions, which are best expressed with the abbreviation for the typical integrals

$$F_{mn} = \int dt i\omega t \int dx e^{i\Delta k x} \left(\partial_x^m e^{2n_c^2 \langle \phi_c(x) \phi_c(0) \rangle} \right) \left(\partial_x^n e^{2n_s^2 \langle \phi_s(x) \phi_s(0) \rangle} \right). \quad (3.97)$$

With this, one obtains the correlation functions

$$\langle \partial_t^U J_H \partial_t^U J_H \rangle(\omega) = -\frac{2(\pi g_{mn_c n_s}^U)^2}{(2\pi a)^{2n_c}} (v_c^4 F_{20} + 2v_c^2 v_s^2 F_{11} + v_s^4 F_{02}) \quad (3.98)$$

$$\langle \partial_t^U P_{LL} \partial_t^U J_H \rangle(\omega) = -\frac{2(\pi g_{mn_c n_s}^U)^2}{(2\pi a)^{2n_c}} (v_c^2 F_{20} + (v_c^2 + v_s^2) F_{11} + v_s^2 F_{02}) \quad (3.99)$$

$$\langle \partial_t^U J_c \partial_t^U J_H \rangle(\omega) = i \frac{4(\pi g_{mn_c n_s}^U)^2 v_c K_c n_c}{(2\pi a)^{2n_c}} (v_c^2 F_{10} + v_s^2 F_{01}). \quad (3.100)$$

In general, one has to compute the integrals F_{20} , F_{10} , F_{11} , F_{00} , F_{01} , and F_{20} as function of the momentum mismatch and temperature. The number of integrals can be reduced by realizing that some of the integrals can be related to each other by further use of partial integration. One finds

$$F_{02} = -(i\Delta k F_{01} + F_{11}) \quad (3.101)$$

3.3. VIOLATION OF WIEDEMANN-FRANZ LAW IN LUTTINGER LIQUIDS

and

$$F_{20} = -(i\Delta k F_{10} + F_{11}), \quad (3.102)$$

which allows to eliminate F_{10} and F_{01} from the matrix.

Further simplifications can be achieved for even Umklapp processes, where in the leading process only charge fields are transferred, implying $n_s = 0$. In this case all integrals F_{mn} with a finite n vanish automatically, and the rest can be transformed into F_{00} , giving

$$\langle \partial_t^U J_H \partial_t^U J_H \rangle(\omega) \stackrel{n_s=0}{=} \frac{2 (\pi g_{mn_c n_s}^U)^2}{(2\pi a)^{2n_c}} v_c^4 \Delta k^2 F_{00}, \quad (3.103)$$

$$\langle \partial_t^U P_{LL} \partial_t^U J_H \rangle(\omega) \stackrel{n_s=0}{=} \frac{2 (\pi g_{mn_c n_s}^U)^2}{(2\pi a)^{2n_c}} v_c^2 \Delta k^2 F_{00}, \quad (3.104)$$

$$\langle \partial_t^U J_c \partial_t^U J_H \rangle(\omega) \stackrel{n_s=0}{=} -\frac{4 (\pi g_{mn_c n_s}^U)^2 v_c^3 K_c n_c}{(2\pi a)^{2n_c}} \Delta k F_{00}. \quad (3.105)$$

Thus, the whole (sub-)matrix of Umklapp scattering rates can be expressed by one integral, F_{00} , which for $n_s = 0$ can be evaluated analytically, as shown by Giamarchi [13, 87]. Here the form as in [14] is used, which reads²⁰

$$F_{00} \stackrel{n_s=0}{\approx} 4n_c^2 \frac{2 \sin\left(\frac{\pi K_c n_c^2}{2}\right)}{\pi^4 a^{2n_c-2} v_c} \left(\frac{2\pi a T}{v_c}\right)^{n_c K_c-2} \left(-\frac{\left| \Gamma\left(\frac{n_c^2 K_c}{4} - i\frac{v_c \Delta k}{4\pi T}\right) \right|^2 \Gamma\left(1 - \frac{n_c^2 K_c}{2}\right)^2}{\left| \Gamma\left(1 - \frac{n_c^2 K_c}{4} - i\frac{v_c \Delta k}{4\pi T}\right) \right|^2} \right. \\ \left. + \frac{\Gamma\left(\frac{n_c^2 K_c}{4} - i\frac{\omega+v_c \Delta k}{4\pi T}\right) \Gamma\left(\frac{n_c^2 K_c}{4} - i\frac{\omega-v_c \Delta k}{4\pi T}\right) \Gamma\left(1 - \frac{n_c^2 K_c}{2}\right)^2}{\Gamma\left(1 - \frac{n_c^2 K_c}{4} - i\frac{\omega+v_c \Delta k}{4\pi T}\right) \Gamma\left(1 - \frac{n_c^2 K_c}{4} - i\frac{\omega-v_c \Delta k}{4\pi T}\right)} \right). \quad (3.106)$$

By using Euler's reflection formula $\Gamma(1-z)\Gamma(z) = \pi/\sin(\pi z)$, the leading term in frequency, which enters into the memory matrix, can be extracted as

$$F_{00} \stackrel{n_s=0}{=} i\omega \frac{2n_c^2}{\pi^4 a^{2n_c-2} T} \left(\frac{2\pi a T}{v_c}\right)^{n_c K_c-2} \frac{\left| \Gamma\left(\frac{K_c n_c^2}{4} + i\frac{v_c \Delta k}{4\pi T}\right) \right|^4}{\Gamma\left(\frac{K_c n_c^2}{2}\right)^2}, \quad (3.107)$$

from which the scattering rates for all modes can be easily obtained.

As already said, this is only valid for even commensurabilities. When spin fields are transferred in an Umklapp process the integration must be done numerically for each parameter. For this purpose as many parameters as possible must be scaled out by the right choice of integration variables. Inserting the elementary Green's functions B.23 into the integral F_{mn} and substituting $\tilde{t} = \pi T t$ and $\tilde{x} = \pi T x / v_c$ yields

$$F_{mn} = i\omega \frac{(\pi a T)^{K_c n_c^2 + K_s n_s^2 + m + n - 3}}{v_c^{K_c n_c^2 + m + n - 1} v_s^{K_s n_s^2} a^{m + n - 3}} \tilde{F}_{mn}, \quad (3.108)$$

²⁰note that in [14] the Fourier transform of time in the definition of the memory matrix has not been approximated by the low energy linear behavior. Thus the formula holds only approximately where the expression on the right is exact and the one on the left is not.

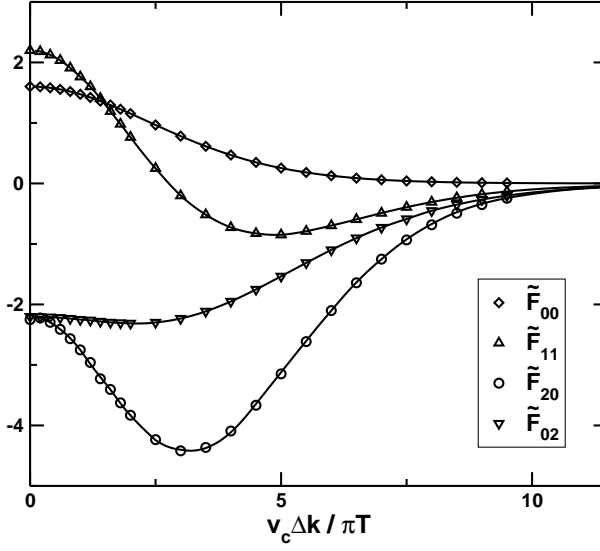


Figure 3.5: Numerical values for the dimensionless parametric integrals \tilde{F}_{mn} of the one third filling Umklapp process with $n_c = 3$ and $n_s = 1$ for some values of $v_c \Delta k / \pi T$ and interpolations. The used Luttinger liquid parameters are $K_c = 0.6$, $K_s = 0.8$, $v_s/v_c = 2$

with the dimensionless integrals

$$\begin{aligned} \tilde{F}_{mn} = 2\text{Im} \left(\int_0^\infty d\tilde{t} \int_{-\infty}^\infty d\tilde{x} e^{i\delta\tilde{x}} \left(\partial_{\tilde{x}}^m \left(\sinh(\tilde{x} + \tilde{t} - i\epsilon) \sinh(\tilde{x} - \tilde{t} + i\epsilon) \right)^{-\frac{K_c n_c^2}{2}} \right) \right. \\ \left. \times \left(\partial_{\tilde{x}}^n \left(\sinh \left(\tilde{x} \frac{v_s}{v_c} + \tilde{t} - i\epsilon \right) \sinh \left(\tilde{x} \frac{v_s}{v_c} - \tilde{t} + i\epsilon \right) \right)^{-\frac{K_s n_s^2}{2}} \right) \right). \quad (3.109) \end{aligned}$$

The exact value would be obtained in the limit $\epsilon \rightarrow 0$, practically the cutoff-dependency of the integrals is weak, so with the result for several finite ϵ the limit can be taken by linear extrapolation to zero.

For a fixed set of Luttinger liquid parameters K_c , K_s and ratio of velocities v_s/v_c , for each commensurability these integral depend only on the effective momentum mismatch $\delta = v_c \Delta k / \pi T$. Figure 3.5 shows the numerical values of the integrals \tilde{F}_{00} , \tilde{F}_{11} , \tilde{F}_{20} , and \tilde{F}_{02} for a set of momentum mismatches δ and the parameters $K_c = 0.6$, $K_s = 0.8$, $v_s/v_c = 2$ for the one third filled band, where three charge fields and one spin field are transferred in the Umklapp process. Between the computed points the integrals are interpolated by a cubic spline.

With the integrals introduced up to now, the Umklapp contribution to the memory matrix for the Luttinger liquid subsystem can be written down explicitly,

$$\begin{aligned} \hat{M}_{LL}^U = \lim_{\omega \rightarrow 0} \frac{1}{\omega} \text{Im} \frac{(\pi g_{mn n_s}^U)^2}{(2\pi a)^{2n_c}} \\ \times \begin{pmatrix} 8v_c^2 K_c^2 n_c^2 F_{00} & -4v_c K_c n_c \Delta k F_{00} & -\frac{4v_c K_c n_c}{\Delta k} (v_c^2 (F_{20} + F_{11}) + v_s^2 (F_{11} + F_{02})) \\ " & 2\Delta k^2 F_{00} & 2(v_c^2 F_{20} + (v_c^2 + v_s^2) F_{11} + v_s^2 F_{02}) \\ " & " & 2(v_c^4 F_{20} + 2v_c^2 v_s^2 F_{11} + v_s^4 F_{02}) \end{pmatrix} \quad (3.110) \end{aligned}$$

3.3. VIOLATION OF WIEDEMANN-FRANZ LAW IN LUTTINGER LIQUIDS

In the limit $\omega \rightarrow 0$ the only ω dependence is the factor $i\omega$ in the definition of the F_{mn} , equation (3.108), which cancels with the $1/\omega$ from the definition of the memory matrix. Taking the imaginary part only acts on the i from the same expression, since everything else is real.

Inserting the Umklapp integrals F_{mn} , the main part of the temperature dependence can be pulled out of the matrix by defining the scattering rate

$$\Gamma_U = \frac{(g_{mn}^U n_s)^2}{a^{2n_c-1}} \left(\frac{aT}{v_c} \right)^{K_c n_c^2 + K_s n_s^2 - 1}, \quad (3.111)$$

and the common dimensionless prefactor of the memory matrix elements

$$C_U = \frac{\pi^{K_c n_c^2 + K_s n_s^2 + 1}}{(2\pi)^{2n_c-1}} \left(\frac{v_c}{v_s} \right)^{K_s n_s^2}. \quad (3.112)$$

One obtains for the memory matrix

$$\hat{M}_U = \Gamma_U C_U \begin{pmatrix} \frac{4v_c^2 K_c^2 n_c^2}{T^2} \tilde{F}_{00} & -\frac{2v_c K_c n_c}{T^2} \Delta k \tilde{F}_{00} & -\frac{2v_c K_c n_c}{\Delta k} \left(\tilde{F}_{20} + \tilde{F}_{11} + \frac{v_s^2}{v_c^2} (\tilde{F}_{02} + \tilde{F}_{11}) \right) \\ " & \frac{\Delta k^2}{T^2} \tilde{F}_{00} & \tilde{F}_{20} + \tilde{F}_{11} + \frac{v_s^2}{v_c^2} (\tilde{F}_{02} + \tilde{F}_{11}) \\ " & " & v_c^2 \tilde{F}_{20} + 2v_s^2 \tilde{F}_{11} + \frac{v_s^4}{v_c^2} \tilde{F}_{02} \end{pmatrix}, \quad (3.113)$$

where $"$ denotes that a value is equal to its transposed element. In this form of the Umklapp memory matrix, for each element the dimensionality can be read of, which is useful for later analysis.

3.3.2.4 Phonon Part of the Umklapp Contribution

Taking also phonons into account, this block matrix remains unchanged to leading order, while additional elements with higher order in the phonon coupling appear for cross correlations with the phonon momentum. The resulting correlation functions are integrals similar to the F_{mn} , but with additional phonon propagators $\langle \partial_x q(x) \partial_{x'} q(x') \rangle$ in the integrand.

Here it is important to be aware that the right phonon propagator to be used is the Green's function of the displacement field *along the chain*, which is calculated in appendix B.8

$$\langle q(x, t) q(0, 0) \rangle = \frac{\pi T}{v_P x} \left(\coth \left(\pi T \left(\frac{x}{v_P} + t - i\epsilon \right) \right) - \coth \left(\pi T \left(-\frac{x}{v_P} + t - i\epsilon \right) \right) \right). \quad (3.114)$$

Making use of the above equation, the needed correlation functions can be expressed in terms of the integrals

$$K_{lmn} = \int dt i \omega t \int dx e^{i \Delta k x} \left(\partial_x^l \langle q(x) q(0) \rangle \right) \left(\partial_x^m e^{2n_c^2 \langle \phi_c(x) \phi_c(0) \rangle} \right) \left(\partial_x^n e^{2n_s^2 \langle \phi_s(x) \phi_s(0) \rangle} \right), \quad (3.115)$$

which again are brought to a dimensionless form and computed numerically for a discrete set of momentum mismatches. With the substitutions $\tilde{x} = v_c x / \pi T$ and $\tilde{t} = t / \pi T$ one obtains

$$K_{lmn} = i \omega \left(\frac{\pi a T}{v_c} \right)^{l+m+n-1} \left(\frac{\pi a T}{v_c} \right)^{K_c n_c^2} \left(\frac{\pi a T}{v_s} \right)^{K_s n_s^2} \frac{v_c}{v_P} \tilde{K}_{lmn}. \quad (3.116)$$

Here the dimensionless integrals \tilde{K}_{lmn} are given by

$$\begin{aligned} \tilde{K}_{lmn} = 2\text{Im} \left(\int_0^\infty d\tilde{t} \int_{-\infty}^\infty d\tilde{x} e^{i\delta\tilde{x}} \left(\partial_{\tilde{x}}^l \frac{1}{\tilde{x}} \left(\coth \left(\frac{v_c}{v_P} \tilde{x} + \tilde{t} - i\epsilon \right) - \coth \left(-\frac{v_c}{v_P} \tilde{x} + \tilde{t} - i\epsilon \right) \right) \right) \right. \\ \times \left(\partial_{\tilde{x}}^m (\sinh(\tilde{x} + \tilde{t} - i\epsilon) \sinh(\tilde{x} - \tilde{t} + i\epsilon))^{-\frac{K_c n_c^2}{2}} \right) \\ \left. \times \left(\partial_{\tilde{x}}^n \left(\sinh \left(\tilde{x} \frac{v_c}{v_s} + \tilde{t} - i\epsilon \right) \sinh \left(\tilde{x} \frac{v_c}{v_s} - \tilde{t} + i\epsilon \right) \right)^{-\frac{K_s n_s^2}{2}} \right) \right), \end{aligned} \quad (3.117)$$

where δ is the effective momentum mismatch defined before, and the limit $\epsilon \rightarrow 0$ must be taken by extrapolation. The numerical integration has been done for the same set of parameters as for the pure Luttinger liquid, the results are depicted in figure 3.6.

Some of the obtained curves show sign-changes as function of $v_c \Delta k / (\pi T)$, which for a scattering rate of course is forbidden. The actual physical scattering rates, i. e. the diagonal elements of the memory matrix, listed below, are linear combinations of the K_{lmn} , and thus are positive. However, since the K_{lmn} enter the memory matrix in many different linear combinations, they are depicted separately. In terms of the integrals K_{lmn} , the phonon contributions to elements of the Umklapp memory matrix read

$$M_{J_c, J_c}^{U, P} = \frac{(\alpha g_{mn_c n_s}^U)^2}{(2\pi a)^{2n_c}} 8\pi^2 n_c^2 v_c^2 K_c^2 K_{200} \quad (3.118)$$

$$M_{J_c, P_{LL}}^{U, P} = \frac{(\alpha g_{mn_c n_s}^U)^2}{(2\pi a)^{2n_c}} 4\pi^2 n_c v_c K_c (iK_{210} + iK_{201}) \quad (3.119)$$

$$M_{J_c, J_H}^{U, P} = \frac{(\alpha g_{mn_c n_s}^U)^2}{(2\pi a)^{2n_c}} 4\pi^2 n_c v_c K_c (v_c^2 iK_{210} + v_s^2 iK_{201}) \quad (3.120)$$

$$M_{J_c, P_{ph}}^{U, P} = \frac{(\alpha g_{mn_c n_s}^U)^2}{(2\pi a)^{2n_c}} 4\pi n_c v_c K_c (\Delta k K_{200} + iK_{210} + iK_{201}) \quad (3.121)$$

$$M_{P_{LL}, P_{LL}}^{U, P} = -\frac{(\alpha g_{mn_c n_s}^U)^2}{(2\pi a)^{2n_c}} 2\pi^2 (K_{220} + 2K_{211} + K_{202}) \quad (3.122)$$

$$M_{P_{LL}, J_H}^{U, P} = -\frac{(\alpha g_{mn_c n_s}^U)^2}{(2\pi a)^{2n_c}} 2\pi^2 (v_c^2 (K_{220} + K_{211}) + v_s^2 (K_{202} + K_{211})) \quad (3.123)$$

$$M_{P_{LL}, P_{ph}}^{U, P} = \frac{(\alpha g_{mn_c n_s}^U)^2}{(2\pi a)^{2n_c}} 2\pi (\Delta k (iK_{210} + iK_{201}) - K_{220} - 2K_{211} - K_{202}) \quad (3.124)$$

$$M_{J_H, J_H}^{U, P} = -\frac{(\alpha g_{mn_c n_s}^U)^2}{(2\pi a)^{2n_c}} 2\pi^2 (v_c^4 K_{220} + 2v_c^2 v_s^2 K_{211} + v_s^4 K_{202}) \quad (3.125)$$

$$M_{J_H, P_{ph}}^{U, P} = -\frac{(\alpha g_{mn_c n_s}^U)^2}{(2\pi a)^{2n_c}} 2\pi (v_c^2 (K_{220} + K_{211} - \Delta k iK_{210}) + v_s^2 (K_{202} + K_{211} - \Delta k iK_{201})) \quad (3.126)$$

$$M_{P_{ph}, P_{ph}}^{U, P} = \frac{(\alpha g_{mn_c n_s}^U)^2}{(2\pi a)^{2n_c}} (\Delta k^2 K_{200} + 2\Delta k (iK_{210} + iK_{201}) - (K_{220} + 2K_{211} + K_{202})) \quad (3.127)$$

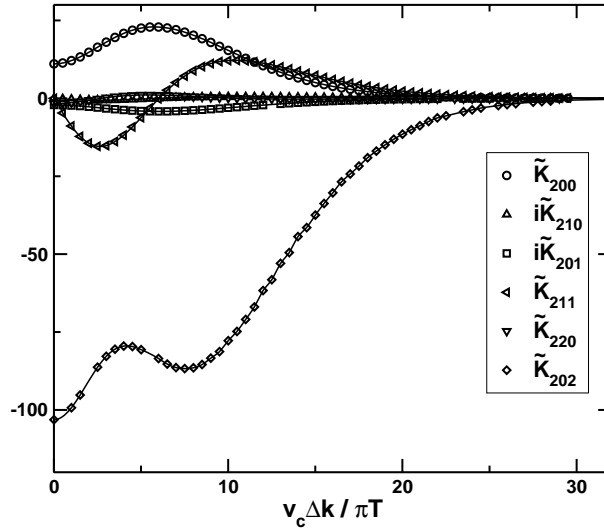


Figure 3.6: Numerical values for the dimensionless integrals \tilde{K}_{lmn} needed to calculate the scattering rates for the Umklapp process at one third filling with one phonon involved. The used parameters are $v_c = 0.5$, $v_s = 1.$, $v_P = 0.1$, $K_c = 0.6$, $K_s = 0.8$. The effective momentum mismatch becomes temperature dependent, and the values of the integrals are scaled with high powers of temperature, which suppress the scattering strongly. Integrals with K_{lmn} with even $l + m + n$ are even functions of Δk , while $i\tilde{K}_{210}$ and $i\tilde{K}_{201}$ are odd functions of Δk .

Despite the appearing i factors in some places, the obtained correlation functions are indeed real. The additional i comes from derivatives of the factor $e^{i\Delta k x}$ and thus is an *internal* part of the integrals K_{210} and K_{201} . Thus, for these two cases, one must take the real part instead of the imaginary part of the integral to get the retarded correlation function. Since real and imaginary parts of the elementary correlation functions of all three excitation modes are even functions of x , integrals over an expression involving an odd number of derivatives of them times an even function over the whole space evaluate to zero. The only finite contribution arises from the additional odd part of $e^{i\Delta k x}$, namely $i \sin(\Delta k x)$. Together with the external i , this gives a contribution to the imaginary part of the integrals around the delta-like pole of each propagator.

Similar to the Umklapp memory matrix of the Luttinger liquid without phonons, equation (3.113), a dimensionless version of the phonon Umklapp memory matrix built from the elements listed in equations (3.118) to (3.127) can be obtained with the scattering rate

$$\Gamma_U^P = \frac{(\alpha g_{mn}^U)^2}{a^{2n_c-1}} \left(\frac{aT}{v_c} \right)^{K_c n_c^2 + K_s n_s^2 + 3} \quad (3.128)$$

and the dimensionless prefactor

$$c_U^P = \frac{\pi^{K_c n_s^2 + K_s n_s^2 + 3}}{(2\pi)^{2n_c-1}} \left(\frac{v_c}{v_s} \right)^{K_s n_s^2} \frac{v_c}{v_s}. \quad (3.129)$$

The resulting memory matrix reads

$$\hat{M}^{U,P} = c_U^P \Gamma_U^P \begin{pmatrix} a_c^2 \tilde{K}_2 & a_c \tilde{K}_3 & a_c \tilde{K}_{3w} & \frac{a_c}{\pi} (\delta \tilde{K}_2 + \tilde{K}_3) \\ " & -\tilde{K}_4 & -\tilde{K}_{4w} & \frac{1}{\pi} (\delta \tilde{K}_3 - \tilde{K}_4) \\ " & " & -\tilde{K}_{4ww} & -\frac{1}{\pi} (\tilde{K}_{4w} - \delta \tilde{K}_{3w}) \\ " & " & " & \frac{1}{\pi^2} (\delta^2 \tilde{K}_2 + 2\delta \tilde{K}_3 - \tilde{K}_4) \end{pmatrix}, \quad (3.130)$$

where a_c is the prefactor of the Umklapp derivative of the charge current, equation 3.83), times an extra factor $v_c/(\pi T)$ from the T -dependence of the K_{lmn} which deviate from Γ_U^P . Similarly, factors Δk systematically combine with these extra T -dependencies to effective momentum mismatches $\delta = v_c \Delta k/(\pi T)$.

Also, a short notation for the appearing linear combinations of the integrals \tilde{K}_{lmn} has been used, where \tilde{K}_i stands for the sum over all \tilde{K}_{lmn} whose indices l, m, n add up to i

$$\tilde{K}_i = \sum_{l,m,n} \delta_{i,l+m+n} \tilde{K}_{lmn}, \quad (3.131)$$

and \tilde{K}_{iw} stands for the corresponding linear combination

$$\tilde{K}_{iw} = \sum_{l,m,n} (\mathbf{1}_{\{m>n\}} v_c^2 + \mathbf{1}_{\{m<n\}} v_s^2 + \delta_{m,n}) \tilde{K}_{lmn}, \quad (3.132)$$

in which each contribution is weighted with v_c^2 if the number of derivatives is higher in the charge sector, and with v_s^2 vice versa. This is expressed in the formula by use of the characteristic function $\mathbf{1}_{\{A\}}$, which is equal to one on the set A and zero everywhere else. For equal numbers of derivatives, $m = n$, the weight in the sum is one. The only linear combination which appears in the matrix and does not fit into this scheme,

$$\tilde{K}_{4ww} = v_c^4 \tilde{K}_{220} + 2v_c^2 v_s^2 \tilde{K}_{211} + v_s^4 \tilde{K}_{202} \quad (3.133)$$

is labeled with \tilde{K}_{4ww} .

3.3.2.5 Contribution from Normal Processes

An additional effect on the transport properties comes from the normal processes between phonons and charge modes, which generates another contribution to the memory matrix. The respective time-derivatives have been stated above. From these one gets for the charge current charge current element

$$\langle \partial_t^{c-ph} J_c \partial_t^{c-ph} J_c \rangle(\omega) = 2v_c^2 K_c^2 \pi^2 g_N^2 \int dt i\omega t \int dx \langle \partial_x^2 \phi_c(x) \partial_x^2 \phi_c(0) \rangle = 0, \quad (3.134)$$

which vanishes due to the fast decay at the infinite, since the integrand is a differential with respect to the integration variable.

All other elements containing J_c as well give no contribution, since the time-derivatives of the other modes all contain phonon fields, which thus can not pair up to a non-local correlation function with $\partial_t^{c-ph} J_c$.

The correlation functions of the remaining modes can be transformed by partial integration to expressions which contain the same single correlation function. In total, one obtains the matrix

$$\hat{M}^{c-ph} = \begin{pmatrix} 0 & 0 & 0 & 0 \\ 0 & -\pi^2 & -\pi^2 v_c^2 & \pi \\ 0 & -\pi^2 v_c^2 & -\pi^2 v_c^4 & \pi v_c^2 \\ 0 & \pi & \pi v_c^2 & -1 \end{pmatrix} g_N^2 \left(\frac{\pi a T}{v_c} \right)^5 \frac{K_c}{2v_c v_P} I^N(v_c, v_P), \quad (3.135)$$

3.3. VIOLATION OF WIEDEMANN-FRANZ LAW IN LUTTINGER LIQUIDS

with the numerical integral

$$I^N(v_c, v_p) = 2\text{Im} \left(\int_0^\infty dt \int_{-\infty}^\infty dx \left(\frac{2 \cosh(x+t-i\epsilon)^2 + 1}{\sinh(x+t-i\epsilon)^4} + \frac{2 \cosh(x-t+i\epsilon)^2 + 1}{\sinh(x-t+i\epsilon)^4} \right) \right. \\ \left. \times \partial_x^2 \left(\frac{1}{x} \left(\coth \left(\frac{v_c}{v_p} x + t - i\epsilon \right) - \coth \left(-\frac{v_c}{v_p} x + t - i\epsilon \right) \right) \right) \right). \quad (3.136)$$

A scattering rate of the normal processes is defined by

$$\Gamma_N = g_N^2 \left(\frac{\pi a T}{v_c} \right)^5 \frac{K_c}{2v_c v_p}. \quad (3.137)$$

The submatrix without the charge current mode has full rank, implying that the normal processes do not conserve any quantities. The numerical integral I^N must be calculated in the limit $\delta \rightarrow 0$ for a set of velocities one is interested in. For example, for $v_c = 0.5$, $v_p = 0.1$, the integral evaluates to $I^N(v_c = 0.5, v_p = 0.1) = -8.02$.

3.3.2.6 Band Curvature Contribution

The memory matrix from band curvature has only one finite element, the diagonal element for the Luttinger liquid heat current, which is the only mode that can be scattered in a leading order process. Inserting the respective time-derivative of the heat current J_H derived above, one obtains the auto-correlation function

$$\langle \partial_t^{\text{BC}} J_H \partial_t^{\text{BC}} J_H \rangle(\omega) = \frac{(v_c^2 - v_s^2)^2}{16m^2} \int dt i\omega t \int dx \\ \times \left(\langle \partial_x^2 \phi_c(x) \partial_x^2 \phi_c(0) \rangle \langle ((\partial_x \phi_s(x))^2 + (\partial_x \theta_s(x))^2) ((\partial_x \phi_s(0))^2 + (\partial_x \theta_s(0))^2) \rangle \right. \\ + 4 \langle \partial_x^2 \theta_c(x) \partial_x^2 \theta_c(0) \rangle \langle \partial_x \phi_s(x) \partial_x \theta_s(x) \partial_x \phi_s(0) \partial_x \theta_s(0) \rangle \\ \left. + 4 \langle \partial_x^2 \phi_c(x) \partial_x^2 \theta_c(0) \rangle \langle ((\partial_x \phi_s(x))^2 + (\partial_x \theta_s(x))^2) \partial_x \phi_s(0) \partial_x \theta_s(0) \rangle \right). \quad (3.138)$$

In appendix B.9 from this an expression with an explicit temperature dependence is derived, which gives for the finite memory matrix element

$$M_{J_H, J_H}^{\text{BC}} = \frac{(v_c^2 - v_s^2)^2}{v_c^4 v_s^4} v_c K_c \left(K_s^2 + \frac{1}{K_s^2} - 2 \right) \frac{\pi^8 T^8}{32m^2} B \left(\frac{v_s}{v_c} \right) \quad (3.139)$$

with the dimensionless integral

$$B(\lambda) = \int_0^\infty dt \int_{-\infty}^\infty dx t \text{Im} \left(\frac{2 + \cosh(x+t-i\delta)^2}{\sinh(x+t-i\delta)^4} \frac{1}{\sinh(x\lambda+t-i\delta)^2 \sinh(x\lambda-t+i\delta)^2} \right) \quad (3.140)$$

that depends only on the ratio v_s/v_c and the cutoff δ . The weak cutoff dependence is again linearly extrapolated to get the proper value for the analytically continued correlation function. In our case, $v_s/v_c = 2$, the resulting numerical value of the integral is $B(\lambda) = 0.35411$.

3.3.3 Results

After having completed all necessary preparations, now the physical results can be discussed. From the memory matrix, all transport coefficients can be obtained directly. In particular, the Lorenz number

$$L = \frac{\kappa}{\sigma_c T} \quad (3.141)$$

can be derived, which is the key to our central question, whether the Wiedemann-Franz law is violated. Given the high complexity of the studied system, this is done in several steps, subsequently completing the picture.

First, the effects in the correlated metal without phonons, i. e. with fixed ion positions is discussed. For a detailed analysis the focus is set to single commensurate point. Then the full physical picture including phonon heat transport follows.

3.3.3.1 Rigid Ion Approximation

The charge conductivity of a one-dimensional metal with finite band curvature m and disorder strength D_{dis} is calculated, taking into account the leading Umklapp processes at $1/2$, $1/3$, and $1/4$ band filling plus their multiples²¹.

As can be seen from equation (3.108), the scattering rates due to Umklapp processes have a high power of the number of transferred fields as temperature dependence, namely $T^{n_c^2 K_c + n_s^2 K_s}$. Thus, for higher commensurabilities the importance of Umklapp scattering is rapidly decreasing. For the typical values $K_c = 0.6$ and $K_s = 0.8$ for the Luttinger interaction parameters, this means that for Umklapp processes with more than four fields transferred, the scattering rate is at least, for the $10k_F$ -process at $1/5$ -filling, $(T/\epsilon_F)^{6.2}$ times smaller than the corresponding scattering rates at quarter filling. Therefore, higher Umklapp processes are not taken into account.

Using equation (3.68) and the memory matrix including the contributions from the respective Umklapp processes, equation (3.110), from disorder scattering equation (3.89) and band curvature scattering, equation (3.139), the conductivity can be calculated for any temperature and band filling.

Figure 3.7 shows the charge conductivity σ_c as function of the band filling ν for a very pure system with disorder strength $D_{\text{dis}} = 10^{-7}g^2$ in units of the Umklapp coupling constant g , which is set to 0.01 for all studied processes.

The conductivity shows sharp dips at the commensurate fillings, which become narrower and less accentuated with decreasing temperature. At the two lower temperatures, the sizes of the dips are, as expected, deepest at half filling, then less deep at $1/3$ and least deep at $\nu = 1/4$. Between the dips, the conductivity takes its value of $\nu = 0$, showing that Umklapp scattering does not play a role in this regime.

At the highest temperature $T = 0.015v_s/a$, additional dips evolve between the commensurate fillings. The reason is the very high purity of the system: Umklapp scattering can degrade currents only in combination with another scattering process, which breaks its conservation of the respective pseudomomentum. Since the disorder scattering in the considered system is so weak, for high temperatures the Umklapp scattering from the next-nearest commensurate point becomes the second strongest scattering process, which leads to a lower value of the conductivity at some regions between two commensurate points.

²¹ $\nu = 0$ and $\nu = 1$ formally are multiples of the commensurabilities taken into account, but the system is a band insulator at that point and the bosonic description must break down. So these points are explicitly excluded from the discussion

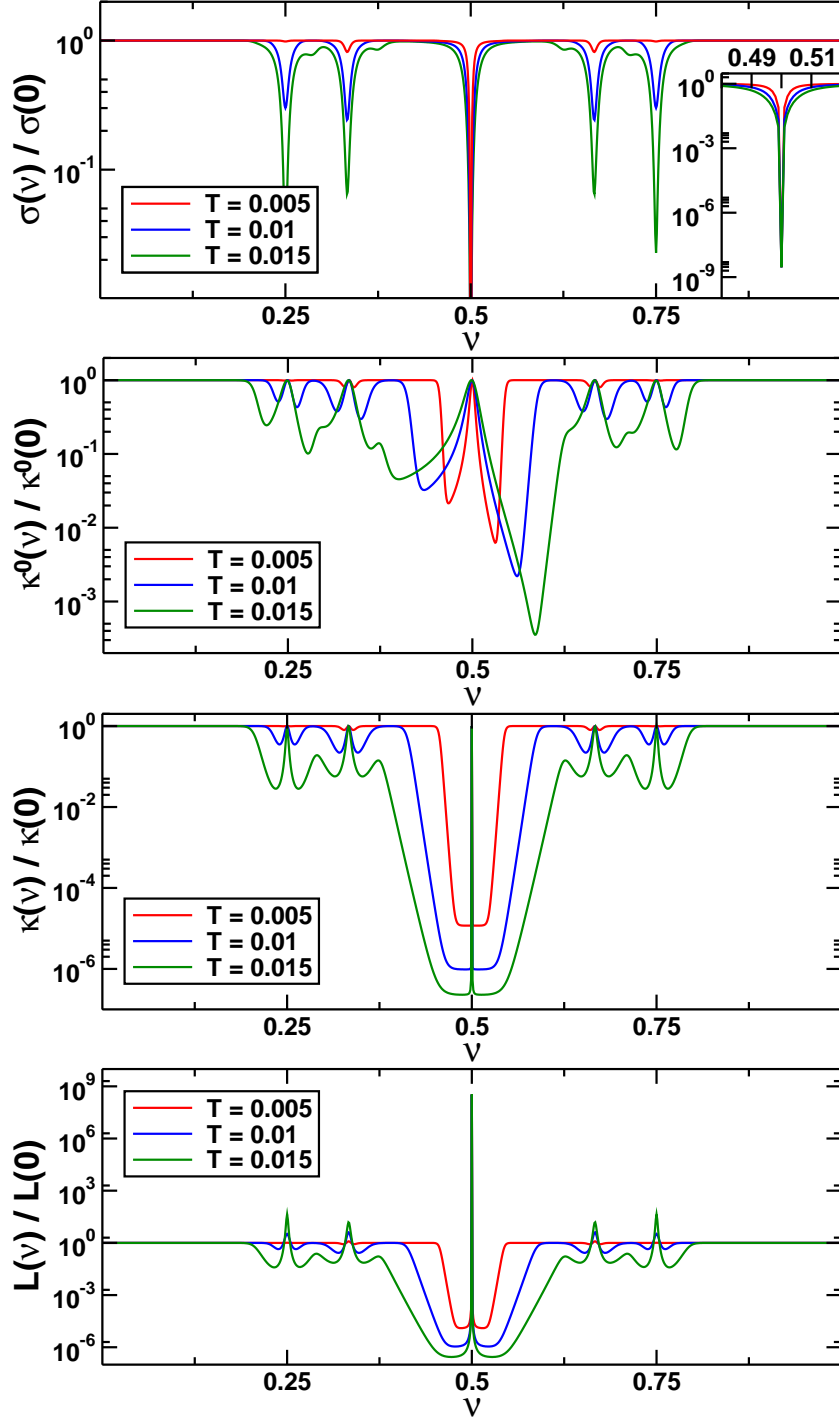


Figure 3.7: Transport properties of the correlated one-dimensional metal with weak Umklapp scattering and disorder: beginning at the top, as function of the band filling, charge conductivity σ_c , plain heat conductivity κ_0 , heat conductivity including thermoelectric corrections κ and Lorenz number L , all in units of the respective $\nu = 0$ values, where Umklapp scattering vanishes. The inset in the first figure shows the $\nu = 1/2$ dip in its full size. Parameters: $\nu_c/\nu_s = 0.5$, $K_c = 0.6$, $K_s = 0.8$, $g_{mn_c n_s}^U = 0.01$, $D_{\text{dis}} = 10^{-7} g^2$

The inset of the figure shows the full size of the central dip, where the conductivity is suppressed by a factor of 10^8 . This very high number of course is the result of a unrealistic choice of parameters to demonstrate the striking effect. In physical systems, the effective disorder typically is much stronger.

Below the electric conductivity, the heat conductivity without thermoelectric corrections κ_0 is shown for the same temperatures. As the electric conductivity, in the vicinity of commensurate fillings there is a suppression due to Umklapp scattering, which increases in width and depth with temperature. However, coming very close to the commensurability, Umklapp scattering is inefficient in decreasing the heat current, and there is no suppression of κ_0 . Like for the electric conductivity, the Umklapp features in κ_0 become wider with increasing temperature. At the highest temperature in the figure, $T = 0.015$, the minima due to different Umklapp processes already start to intersect. Going to even higher temperatures, the more dominant signature of the $4k_F$ process around half filling would hide the effects of the other Umklapp processes. The strong asymmetry of the dips left and right of the same commensurate filling is caused by the band curvature, which breaks the particle-hole symmetry.

The latter seems to be restored in the heat conductivity κ , which is shown in the third part of figure 3.7. The band curvature effects to the plain heat conductivity κ_0 and the thermoelectric correction $TS^2\sigma_c$ cancel exactly, giving in total features in the heat conductivity, which are symmetric around each commensurate point. The suppression of the heat conductivity from Umklapp scattering sets in at the same values of distance to commensurate dopings $\delta\nu$, but the total suppression is stronger and the upturn close to the commensurate filling narrower than without the thermoelectric correction.

To understand this behavior, it is necessary to have a closer look at the conservation laws of the Umklapp processes, and their overlaps with the respective currents. As shown in equation (3.63), each Umklapp process conserves a pseudomomentum, which is a linear combination of the charge current and the total momentum of the Luttinger liquid. Assuming the temperature being low enough, such that the effects of each Umklapp process are well-separated and at each filling only one Umklapp process plays a role. From the continuity equation, one can show [14] that the cross susceptibility between the conserved pseudomomentum of this process $Q_{mn_c n_s}$ and the charge current is, neglecting exponentially small corrections, proportional to the distance to the respective commensurate filling,

$$\chi_{J_c Q_{mn_c n_s}} = 2\delta\nu = \frac{\Delta k}{2n_c v_c K_c} \chi_{J_c J_c} + \chi_{J_c P_{LL}}, \quad (3.142)$$

while the cross susceptibility $\chi_{J_c Q_{mn_c n_s}}$ is positive and has a quadratic temperature dependence, $\chi_{J_c Q_{mn_c n_s}} \sim T^2$. The cross susceptibility measures, crudely speaking, the overlap between current modes.

Exactly at a commensurate filling, the overlap of the charge current with the pseudomomentum corresponding to this commensurability vanishes, which means that the charge current is orthogonal to the pseudomomentum. Thus, J_c can not profit from the conservation law and is strongly decreased by Umklapp scattering.

In contrast, the heat current does have a finite overlap with the pseudomomentum at commensurate dopings. Accordingly, the heat current is protected by the pseudomomentum conservation, and the heat conductivity is only limited by disorder and band curvature scattering.

Due to these strongly different scattering mechanisms for heat and charge current, the Lorenz number L has big peaks at each commensurate doping, as can be seen in the lowest part of figure 3.7.

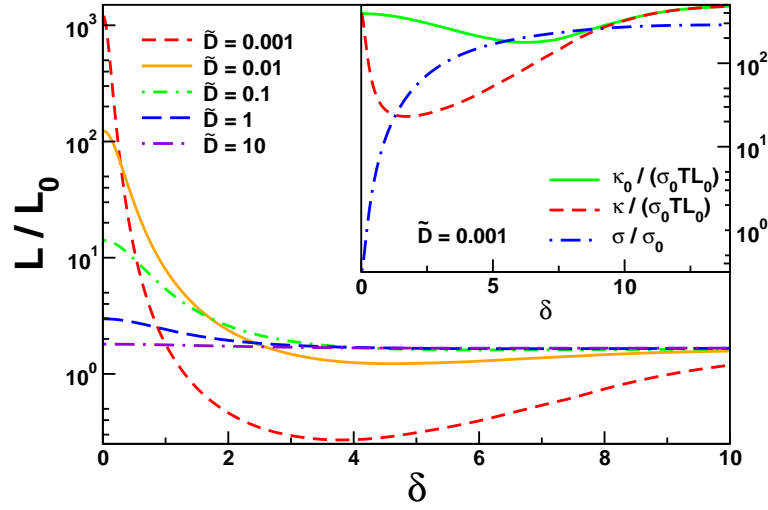


Figure 3.8: Lorenz number L divided by the Wiedemann-Franz value L_0 for the $6K_F$ Umklapp process around $\nu = 1/3$ as function of effective momentum mismatch $\delta = v_c \Delta k / (\pi T)$. The violations of the Wiedemann-Franz law depend strongly on the ratio \tilde{D} between renormalized disorder strength and Umklapp scattering. For weak disorder $\tilde{D} \ll 1$, a peak of height $1/\tilde{D}$ with width $\sqrt{\tilde{D}}$ is followed by a pronounced minimum. *Inset:* conductivity σ_c and heat conductivities κ , κ_0 in units of the respective conductivity without Umklapp scattering, as function of effective momentum mismatch δ . The suppression due to Umklapp scattering is strongest at $\delta = 0$ for σ_c , where it is ineffective for κ and κ_0 . The latter become suppressed at finite momentum mismatches, which is explained by the conservation laws.

Away from commensurate fillings, according to equation (3.142) the overlap between charge current and conserved pseudomomentum, and therefore also the charge conductivity σ_c , grows rapidly up to its value due to disorder scattering.

On the other hand, the heat conductivity at $\delta\nu \sim T$ gets strongly suppressed by the thermoelectric counter term. Physically, this suppression can be understood qualitatively in the low disorder limit. The origin lies in the boundary condition $J_c = 0$, under which the heat conductivity must be measured. Since the component of the charge current perpendicular to $Q_{mn_c n_s}$ decays rapidly due to Umklapp scattering, J_c becomes almost parallel to the pseudomomentum. Thus, the heat current measurement effectively is done under the constraint of vanishing pseudomomentum. This destroys the possibility of the heat current to profit from the conservation law. The heat conductivity hence is dominated by Umklapp scattering, which leads to strong suppression in this regime of $\delta\nu$.

For Umklapp processes which transfer an even number of electrons, the spinon part of the heat conductivity can not be scattered. Here the included band curvature effects play their crucial role: they couple the spinon and charge contributions to the heat current, which leads to an affection of both components by Umklapp scattering and thus a stronger suppression of the heat conductivity in the vicinity of commensurate dopings.

In total, the Lorenz number becomes strongly enhanced at commensurate fillings, and suppressed in the vicinity.

The influence of band curvature scattering makes a quantitative analysis of the effect more complicated, since perturbative calculations for limiting cases require knowledge, which processes are more or less important.

For the $6k_F$ -process, which is effective around $\nu = 1/3$, the band curvature is not essential

to observe the deviations of the Lorenz number from the Wiedemann-Franz value, since it affects also the spinon heat conductivity by itself. Thus, for a better understanding, we study a system which contains only the Luttinger liquid with weak impurity scattering and the Umklapp process from the $\nu = 1/3$ commensurability,

$$H = H_{\text{LL}} + H_{\text{dis}} + H_{1,3,1}^{\text{U}}, \quad (3.143)$$

with the respective Hamiltonians defined in equations (3.50), (3.56), and (3.55). For such a system with a fixed set of Luttinger liquid parameters v_c , v_s , K_c , K_s , the Lorenz number depends only on the ratio of the scattering rates Γ_{U} , defined in equation (3.111), and Γ_{dis} , equation (3.92),

$$\tilde{D} = \frac{\Gamma_{\text{dis}}}{\Gamma_{\text{U}}} = \frac{D_{\text{dis}} a^{2n_c-3}}{(g_{mn_c n_s}^{\text{U}})^2 \left(\frac{aT}{v_c}\right)^{\gamma}}, \quad (3.144)$$

with $\gamma = (n_c^2 - 1)K_c + (n_s^2 - 1)K_s - 1$, and the effective momentum mismatch

$$\delta = \frac{v_c \Delta k}{\pi T}. \quad (3.145)$$

Figure 3.8 shows the Lorenz number as function of δ divided by the value without Umklapp scattering $L_0 = \pi^2/3$ for several values of \tilde{D} with the parameters $v_c/v_s = 0.5$, $K_c = 0.6$, $K_s = 0.8$. At commensurate filling $\delta = 0$, L/L_0 exhibits a maximum of size $1/\tilde{D}$, followed by a pronounced dip around $\delta \approx 4$.

The inset shows the dependence on the effective momentum mismatch δ of the conductivities in units of the respective disorder dominated conductivity, defined by

$$\sigma_0 = \frac{v_c^2 a^{2n_c-3}}{(g_{mn_c n_s}^{\text{U}})^2} \left(\frac{v_c}{aT}\right)^{\beta}, \quad (3.146)$$

with $\beta = K_c n_c^2 + K_s n_s^2 - 3$. Since in the disorder dominated regime, the Wiedemann-Franz law is valid, κ_0^0 can be obtained from this as $\kappa_0^0 = \sigma_0 T L_0$. The charge conductivity is suppressed strongly at $\delta = 0$ and increases with increasing δ , while the heat conductivities κ and κ_0 take the same value at $\delta = 0$ as for large δ and are suppressed at intermediate values. The minimum for the heat conductivity with thermoelectric correction lies at smaller values than for κ_0 , and the total suppression is stronger.

The underlying mechanism can be understood well by looking at a simplified model with only charge modes. Of course, this is the same model as studied in section 3.2, but there thermoelectric corrections were not considered, because the spin density, in contrast to the charge density, is not a conserved quantity. For such a model, momentum operator and heat current operator are parallel and we get a two by two memory matrix for disorder and Umklapp scattering with the structure

$$\hat{M} = d(T) \begin{pmatrix} \frac{1}{T^2} & 0 \\ 0 & 1 \end{pmatrix} + u(T) f(\delta) \begin{pmatrix} \frac{1}{T^2} & -\frac{\delta}{T} \\ -\frac{\delta}{T} & \delta^2 \end{pmatrix}, \quad (3.147)$$

where the first component is the charge current and the second the momentum. The Umklapp part of the matrix reflects the typical conservation law of a linear combination of the momentum and the charge current times the effective momentum mismatch δ . In front of it stands the overall Umklapp scattering rate u , which carries the temperature dependence, and a dimensionless function $f(\delta)$, which decreases exponentially for large momentum mismatches. The disorder part of the memory matrix is diagonal and does not conserve any current. Its scattering rate is called $d(T)$.

3.3. VIOLATION OF WIEDEMANN-FRANZ LAW IN LUTTINGER LIQUIDS

The corresponding matrix of generalized susceptibilities is assumed to be diagonal with elements χ_1 for the charge current and χ_2 for the momentum.

From equation (3.147), the conductivities can be obtained easily by inverting the two by two matrix. To analyze the limit of strong Umklapp scattering, $d(T)$ is assumed to be much smaller than $u(T)$, and the conductivities are expanded in a Taylor series in δ . One obtains for the charge conductivity

$$\sigma_c = \chi_1^2 (\hat{M}^{-1})_{1,1} \stackrel{\delta^2 \ll \frac{d(T)}{u(T)}}{\approx} \chi_1^2 T^2 \left(\frac{1}{d(T) + u(T)} + \delta^2 \frac{u(T)^2}{d(T)(d(T) + u(T))} \right). \quad (3.148)$$

$$\stackrel{d(T) \ll u(T)}{\approx} \chi_1^2 T^2 \left(\frac{1}{u(T)} + \frac{\delta^2}{d(T)} \right)$$

Exactly at the commensurate point $\delta = 0$, $\sigma_c \sim 1/u(T)$ is suppressed by Umklapp scattering. Going to finite δ , in agreement to the above discussion for the more general case, the charge current starts to profit from the conservation law and the scattering is reduced rapidly as function of δ until at

$$\delta_c = \sqrt{1 - \frac{d(T)}{u(T)}} \stackrel{d(T) \ll u(T)}{\approx} 1 - \frac{d(T)}{2u(T)} \sim 1 - \frac{\tilde{D}}{2} \quad (3.149)$$

the crossover to disorder dominated scattering is reached. In the opposite limit of $\delta \rightarrow \infty$, the conductivity is dominated by disorder scattering $\sigma_c(\delta \rightarrow \infty) \sim 1/(d(T))$.

The heat conductivity without thermoelectric corrections is, to leading order in δ ,

$$\kappa_0 = \frac{v_c^4 \chi_2^2}{T} (\hat{M}^{-1})_{2,2} \stackrel{\delta^2 \ll \frac{d(T)}{u(T)}}{\approx} \frac{v_c^4 \chi_2^2}{T} \left(\frac{1}{d(T)} - \delta^2 \frac{u(T)}{d(T)(u(T) + d(T))} \right). \quad (3.150)$$

As explained above for the correlated metal, the heat conductivity at commensurate filling, which corresponds to $\delta = 0$, is protected from Umklapp scattering by the conservation law, and thus $\kappa_0(\delta = 0) \sim 1/(d(T))$. With increasing δ , the impact of Umklapp scattering increases as the overlap of the momentum with the protected current becomes smaller, and the heat conductivity starts to become suppressed.

Starting from the other side, at large δ Umklapp scattering plays no role, then in the limit of weak Umklapp scattering, the heat conductivity becomes

$$\kappa_0 \stackrel{\delta \gg 1}{\approx} \frac{v_c^4 \chi_2^2}{T} \left(\frac{1}{d(T)} - \delta^2 f(\delta) \frac{u(T)}{d(T)^2} \right), \quad (3.151)$$

where $f(\delta) \sim e^{-\delta}$ for large δ . The minimum value of κ_0 can be obtained directly by calculating the derivative of κ_0 with respect to δ . One finds the minimum at

$$\delta_{\kappa_0}^{\min} = 2 + \mathcal{W} \left(\frac{2u(T)}{e^2 d(T)} \right), \quad (3.152)$$

where \mathcal{W} denotes the Lambert W function. In the weak disorder limit $d(T) \ll u(T)$, the position of the minimum can be approximated by

$$\delta_{\kappa_0}^{\min} \approx 2 + \ln \left(\frac{2}{e^2} \frac{u(T)}{d(T)} \right). \quad (3.153)$$

Taking thermoelectric corrections into account, in the heat conductivity,

$$\kappa = \frac{v_c^4 \chi_2^2}{T} \left((\hat{M}^{-1})_{2,2} - \frac{(\hat{M}^{-1})_{1,2}^2}{(\hat{M}^{-1})_{1,1}} \right) \delta^2 \ll \frac{d(T)}{u(T)} \approx \frac{v_c^4 \chi_2^2}{T} \left(\frac{1}{d(T)} - \delta^2 \frac{u(T)}{d(T)^2} \right), \quad (3.154)$$

the leading correction in δ is $\sim u(T)/(d(T))^2$ instead of $\sim 1/(d(T))$ as for the plain heat conductivity, so the thermoelectric corrections make the peak at commensurate filling narrower. Therefore, the corrected heat conductivity is suppressed strongly close to commensurate filling, and a crossover to Umklapp dominated scattering takes place. The minimum of the heat conductivity with thermoelectric corrections can again be estimated from the derivative with respect to δ , which vanishes at

$$\delta_\kappa^{\min} \approx 2. \quad (3.155)$$

At the minimum, κ takes the value

$$\kappa(\delta_\kappa^{\min}) = \frac{v_c^4 \chi_2^2}{T} \frac{1}{d(T) + \frac{4}{e^2} u(T)}, \quad (3.156)$$

which is strongly suppressed by Umklapp scattering. In the weak disorder regime, the minimum is very broad and extends to small values of δ . Hence the crossover scale to the disorder dominated regime around commensurate filling can be obtained equating equation (3.154) and (3.156), and solve for δ . The resulting crossover scale is

$$\delta_\kappa^{\text{cross}} = \frac{1}{\sqrt{\frac{e^2}{4} + \frac{u(T)}{d(T)}}} \frac{d(T) \ll u(T)}{\approx} \sqrt{\frac{d(T)}{u(T)}} \sim \tilde{D}, \quad (3.157)$$

where the second part gives the weak disorder expansion.

For very large δ , the heat conductivity takes the form

$$\kappa \stackrel{\delta \gg 1}{\approx} \frac{v_c^4 \chi_2^2}{T} \left(\frac{1}{d(T)} - \delta^2 f(\delta) \frac{u(T)}{d(T)^2} \right), \quad (3.158)$$

which is identical to the corresponding expression for the bare heat conductivity, equation (3.151).

From the derived behavior of the charge and heat conductivity, features of the Lorenz number L in the weak disorder regime can be deduced. At the commensurate point, the conductivity $\sigma_c \sim T^2/u(T)$ is dominated by Umklapp scattering and $\kappa \sim 1/(d(T))$ by disorder scattering, so the Lorenz number

$$L(\delta = 0) \approx \frac{v_c^4 \chi_2^2}{\chi_1^2 T^4} \frac{u(T)}{d(T)} \sim \frac{1}{\tilde{D}} \quad (3.159)$$

becomes very big. The temperature dependence of the susceptibilities cancels exactly with the temperature to power four, giving a temperature independent Lorenz number. Around $\delta_\kappa^{\text{cross}} = \sqrt{d(T)/u(T)}$, the heat conductivity starts to be suppressed by Umklapp scattering, thereby spoiling the enhancement of L . Simultaneously, the suppression of the charge conductivity decreases, up to its crossover to disorder scattering at $\delta_c = \sqrt{1 - d(T)/u(T)}$. Since the minimum of the heat conductivity at $\delta_\kappa^{\min} = 2$ lies at values of δ bigger than the

3.3. VIOLATION OF WIEDEMANN-FRANZ LAW IN LUTTINGER LIQUIDS

crossover to disorder dominated scattering in the charge conductivity, the Lorenz number takes its minimal value at $\delta = \delta_\kappa^{\min}$, which in the weak disorder regime evaluates to

$$L(\delta_\kappa^{\min}) \stackrel{\delta^2 \ll \frac{d(T)}{u(T)}}{\approx} \frac{v_c^4 \chi_2^2}{\chi_1^2 T^4} \frac{5e^2}{16} \frac{d(T)}{u(T)} \sim \tilde{D}. \quad (3.160)$$

The width of the peak around commensurate filling in the weak disorder regime is limited by the crossover to Umklapp dominated scattering of the heat current $\delta_\kappa^{\text{cross}}$, equation (3.157), which is smaller than the crossover to disorder dominated scattering of the charge current δ_c , equation (3.149). This gives a peak width $\sim \sqrt{d(T)/u(T)}$.

For bigger momentum mismatches $\delta > \delta_\kappa^{\min}$, the Lorenz number increases again, until it reaches its disorder scattering value far away from the commensurate filling, where the Wiedemann-Franz law holds.

The described simplified scenario also explains the observed effects of the $6k_F$ Umklapp scattering in weakly disordered correlated metals. Indeed, the description of the latter requires two separate modes for heat current and momentum, and thus the Umklapp memory matrix can not be brought to the form as in equation (3.147) by partial integration, but the underlying conservation law for the pseudomomentum holds nonetheless. Since the two modes momentum and heat current are strongly coupled by both, Umklapp and disorder scattering, they form a “complex of complicated codependencies”, which is hard to disentangle. On the other hand, this strong entanglement allows to deduce an overall similar scattering behavior of the two modes, apart from different prefactors. Accordingly, the considerations about the dominant scattering mechanisms in different regimes remain valid.

Hence, the explanation of the scattering behavior can be generalized. The charge conductivity at commensurate filling is strongly suppressed with the Umklapp scattering rate, $\sigma_c \sim 1/\Gamma_U$. With increasing effective momentum mismatch a crossover to disorder scattering $\sigma_c \sim 1/\Gamma_{\text{dis}}$ sets in around $\delta \sim T \sim \tilde{D}^{-1/\gamma}$, which is a weak dependency on the disorder strength.

The plain heat conductivity is protected from Umklapp scattering at $\delta = 0$, and thus dominated by disorder scattering, $\kappa_0 \sim 1/\Gamma_{\text{dis}}$. The same is true for the heat conductivity with thermoelectric corrections, which for $\delta = 0$ is identical to κ_0 . For finite δ , they both become dominated by Umklapp scattering, but with different crossover scales and minima. While the minimum of the plain heat conductivity shifts $\sim \text{const} + \ln(\tilde{D})$ and the crossover is smooth, the minimum of the heat conductivity with thermoelectric corrections is at a value of δ independent of \tilde{D} , and the crossover happens sharply at $\delta \sim \sqrt{\tilde{D}}$.

This behavior is in qualitative agreement with the results of the numerical calculation for a certain set of parameters, which is shown in the inset of figure 3.8. The scaling behavior, which is not shown, is in good agreement with the predictions from the simplified model.

The crossover of the charge conductivity σ_c from disorder dominated to Umklapp dominated scattering is hard to find, since there is no distinct feature.. The deviations between prediction and exact calculation can not be explained by a total prefactor, that might be contained in one of the scattering matrices, but must lie in the structure of these matrices, and the two different velocities that are involved in the Luttinger liquid. Anyway, the studied toy model correctly predicts a strong difference in the structure of the features from Umklapp scattering in the plain and the corrected heat conductivity, which must be associated to the conservation law, even when the obtained crossover scales are not exact.

Due to the suppression of the charge conductivity at commensurate filling, the Lorenz number is enhanced to $L(\delta = 0) \sim 1/\tilde{D}$. The enhancement of L is limited by the starting

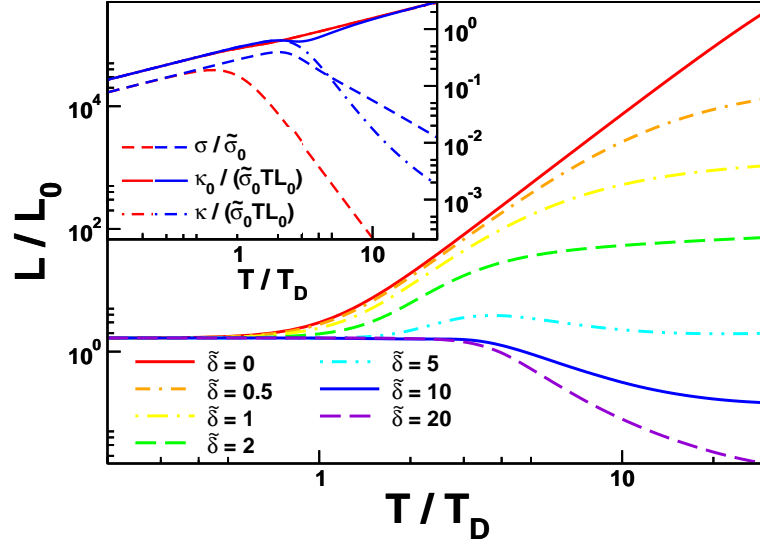


Figure 3.9: The relative Lorenz number L/L_0 close to $\nu = 1/3$ as function of the temperature, where T_D is the temperature scale at which Umklapp scattering becomes dominant, see equation (3.162). Depending on $\tilde{\delta}$ the Lorenz number can increase or decrease with temperature. *Inset:* conductivities in units of conductivities without Umklapp scattering as function of temperature for $\tilde{\delta} = 0$ (red) and $\tilde{\delta} = 10$ (blue).

suppression of the heat conductivity, which renders the width of the peak in the weak disorder limit $\sim \sqrt{\tilde{D}}$. Between the crossover of the heat conductivity κ to Umklapp dominated scattering and the crossover of the charge conductivity to disorder dominated behavior, the Lorenz number takes its minimum value, which is of the order $L(\delta \approx 1) \sim \tilde{D}$.

To study the temperature dependence of the Lorenz number, the dimensionless variables introduced in equations (3.144) and (3.145) are not appropriate, since the effective momentum mismatch δ as well as the ratio of disorder and Umklapp scattering rate \tilde{D} are temperature dependent. Instead of these, the Lorenz number as a function of temperature is expressed in the units

$$\tilde{\delta} = \frac{\delta}{\tilde{D}^{1/\gamma}} \quad (3.161)$$

and with the effective temperature scale

$$T_D = \frac{v_c}{a} \left(\frac{D_{\text{dis}} a^{2n_c-3}}{(g_{mnc}^U)^2} \right)^{\frac{1}{\gamma}}, \quad (3.162)$$

where γ is the exponent of the temperature dependence of the renormalized disorder as defined in equation (3.144). Figure 3.9 shows the Lorenz number as function of T/T_D for different values of $\tilde{\delta}$. For small temperatures, disorder scattering becomes increasingly more important due to the renormalization. Hence, the Lorenz number L approaches its value without Umklapp scattering L_0 for all values of $\tilde{\delta}$. At larger temperatures $T > T_D$, the curves for different $\tilde{\delta}$ start to split. Small values of δ lead to an increase in L/L_0 with temperature, high $\tilde{\delta}$ cause a decrease.

Exactly at $\tilde{\delta} = 0$, the effective momentum mismatch δ also must be zero and thus the maximum value of L/L_0 in figure 3.8 is taken. However, with increasing temperature

3.3. VIOLATION OF WIEDEMANN-FRANZ LAW IN LUTTINGER LIQUIDS

$\tilde{D} \sim T^{-\gamma}$ decreases²², and the maximum value of $L(\delta = 0) \sim 1/\tilde{D}$ hence becomes bigger.

Away from commensurate filling, it is difficult to relate the features of the Lorenz number as function of effective temperature to the results in units of \tilde{D} and δ . Apart from the total upturn of $L(T/T_D)$ due to the temperature dependence of \tilde{D} , the effective distance to commensurate filling changes with T . For large $\tilde{\delta}$, with increasing temperature the effective momentum mismatch δ starts moving into the minimum where κ is suppressed by Umklapp scattering. On the other hand, for smaller $\tilde{\delta}$ one starts closer to commensurate filling, such that the shift of δ with temperature moves these values of $\tilde{\delta}$ into the beginning maximum in the vicinity of $\delta = 0$. According to this, also the curves for bigger $\tilde{\delta}$ should show an upturn for even higher temperatures, which indeed can be seen for the case of $\tilde{\delta} = 10$ in the figure.

Of course, the temperature dependence of the Lorenz number can be obtained more directly from the conductivities as functions of temperature, which are shown for the two cases $\tilde{\delta} = 0$ and $\tilde{\delta} = 10$ in the inset of figure 3.9. To make the conductivities comparable, they are expressed in dimensionless units by dividing σ_c by

$$\tilde{\sigma}_0 = \left(\frac{D_{\text{dis}} a^{2n_c-3}}{(g_{mn_c n_s}^U)^2} \right)^\zeta \frac{v_c^2}{D_{\text{dis}}}, \quad (3.163)$$

with $\zeta = (2 - K_c - K_s)/\gamma$, and the two heat conductivities κ , κ_0 by $\tilde{\sigma}_0 T L_0$.

In the first case, $\tilde{\delta} = 0$, which is depicted with red lines in the figure, the charge conductivity σ_c is dominated by disorder scattering up to $T = T_D$, where the crossover to Umklapp dominated scattering takes place. At higher temperatures σ_c gets strongly suppressed, in contrast to the heat conductivity at $\tilde{\delta} = 0$, which for all temperatures is dominated by disorder scattering, since it is protected from Umklapp scattering by the conservation law. The plain heat conductivity κ_0 for $\tilde{\delta} = 0$ can not be seen in the figure, since it is identical to κ at commensurate filling, thus the two curves lie exactly on top of each other. The Lorenz number thus is increasing for $T > T_D$, due to the strong suppression of σ_c , which is not balanced by a decrease in κ/T .

In the second case, $\tilde{\delta} = 10$, depicted in blue, both, charge and heat conductivity experience a crossover to Umklapp dominated scattering at the same temperature $T/T_D > 1$. However, the heat conductivity becomes eventually smaller than the charge conductivity, resulting in a decrease of the Lorenz number L at high temperatures.

In summary, the effects of the interplay of the $6k_F$ Umklapp process with weak disorder scattering in a correlated metal result in large violations of the Wiedemann-Franz law. At commensurate filling, the Lorenz number is enhanced strongly to $L/L_0 \sim 1/\tilde{D}$, while at dopings of the order $\delta \sim 1$ it is suppressed down to $L/L_0 \sim \tilde{D}$. Thermoelectric corrections play an important role in this context, since they allow the heat conductivity to be suppressed by Umklapp scattering already at $\delta \sim \sqrt{\tilde{D}}$, which leads to a more pronounced minimum in the Lorenz number.

The occurrence of strong thermoelectric effects makes weakly disordered one-dimensional correlated metals interesting systems for thermoelectric power generation and thermoelectric cooling. The efficiency of these processes is limited by material properties, and materials with good properties are rare. In recent years, the interest of researchers with focus on applications in this field already directed towards low dimensional metals, [74]. The relevant quantity to

²²given that $\gamma = (n_c^2 - 1)K_c + (n_s^2 - 1)K_s - 1$ is positive, which for the systems under consideration is true. For possible systems with strong repulsive interactions, $K_c < n_c^2 - 1$, γ becomes negative. In such systems Umklapp scattering opens a gap in the charge sector and does not become less important in the low temperature limit.

measure the properties of a material for thermoelectric power generation is given with the *thermoelectric figure of merit* ZT , defined as

$$ZT = \frac{T\sigma_c S^2}{\kappa}, \quad (3.164)$$

see [75]. Materials with figure of merit $ZT > 1$ are already interesting for commercial use.

For the systems studied here, one can easily see from the definition of the heat conductivity with thermoelectric corrections, equation (3.71), that the figure of merit can be expressed as

$$ZT = \frac{\kappa_0}{\kappa} - 1. \quad (3.165)$$

For the weak disorder regime, we derived that $\kappa \sim 1/\Gamma_U$ at $\delta \sim \sqrt{\tilde{D}}$, while $\kappa_0 \sim 1/\Gamma_{\text{dis}}$ in this regime. Thus, the figure of merit for this system becomes of order $ZT \sim 1/\tilde{D} - 1$, which for a clean system can be a very large number.

Unfortunately, in real physical systems lattice vibrations play a major role in heat transport. For a reliable prediction of a material with good thermoelectric properties one has to include the phonon system into the analysis.

3.3.3.2 General Case

To discuss the possible violation of the Wiedemann-Franz law by Umklapp scattering in existing physical systems, the minimal model system must include phonons and their dominant relaxation mechanisms. As an example, again the $6k_F$ process around $1/3$ filling is used. The important effects of the weakly disordered correlated metal coupled to a phonon system are described with the Hamiltonian for the Luttinger liquid with disorder plus the phonon Hamiltonian and the normal processes and Umklapp contributions, which couple both,

$$H = H_{\text{LL}} + H_{\text{dis}} + H_{\text{ph}} + H_{\text{c-ph}} + H_{1,3,1}^{\text{U}}, \quad (3.166)$$

where the constituents have been introduced in equations (3.50), (3.51), (3.56), (3.53), and (3.55).

The large variety of effects in such a complex systems bring a wide range of characteristic scattering rates, namely Γ_{dis} for the disorder scattering, equation (3.92), Γ_U for the Umklapp scattering, equation (3.111), $\Gamma_{\text{U,p}}$ for phonon-assisted Umklapp scattering, equation (3.128), and Γ_{N} for phonon scattering in normal processes, equation (3.137).

Consequently, it is impossible to find universal units in which the resulting effects to the conductivities and the Lorenz number can be depicted in a simple and complete way. An approach to the full picture is tried by showing plots of the Lorenz number L as function of the deviation $\Delta\nu = \Delta ka/(2\pi n_c)$ from commensurate filling for different temperatures T , impurity concentrations D_{dis} , and phonon couplings α . In principle, the coupling constant for phonon forward scattering g_{N} is a fourth independent parameter, which is chosen here equal to the backward scattering, $g_{\text{N}} = \alpha g_{\text{U}}$ for simplicity. The Luttinger liquid parameters have the same values as before.

Figure 3.10 shows the Lorenz number as function of the filling for different disorder strengths D , given in units of $(g_{mn}^{\text{U}}/a^{2n_c})^2/a^{2n_c-3}$. The temperature is chosen as $T = 0.2v_s/a$, and the coupling to the phonons as $\alpha = 0.01$. In the inset, the contributions to the conductivities from phonons and the Luttinger liquid are shown for one impurity concentration. As in the case without phonons, the conductivities are given in dimensionless units by dividing

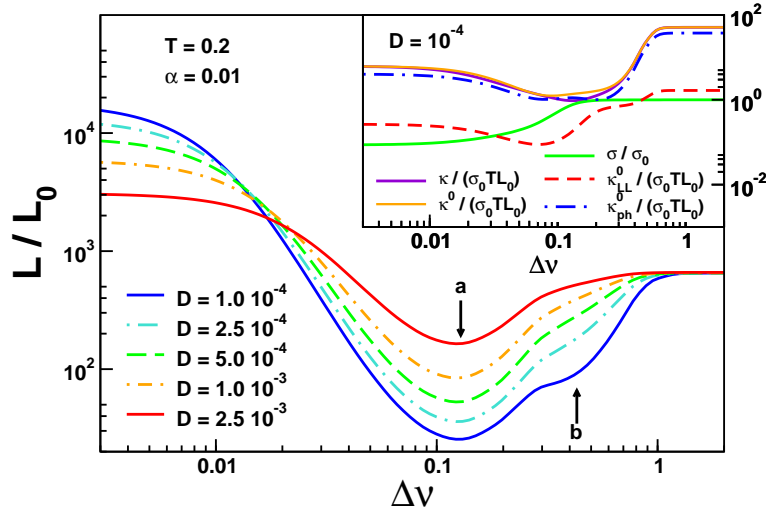


Figure 3.10: Lorenz number of the weakly disordered Luttinger liquid coupled to phonons with Umklapp scattering as function of the doping $\Delta\nu$ from the commensurate filling $\nu = 1/3$ for different disorder strengths D in units of g_0^2/a^{2n_c-3} . Luttinger liquid parameters are chosen as before, phonon coupling $\alpha = 0.01$ and the temperature $T = 0.2v_s/a$. Since phonons are coupled weakly, the high phonon heat conductivity (see inset for all conductivities as function of $\Delta\nu$ for one disorder strength in units like in figure 3.8) leads to an enhancement of the Lorenz number for large dopings. The normal and phonon assisted Umklapp processes suppress the heat conductivity, which reflect in dips in the Lorenz number at the positions a (normal Umklapp) and b (phonon assisted). Close to commensurate filling, the heat conductivity is partially, but no longer totally, protected by the two non parallel conservation laws, while the charge conductivity is suppressed strongly. This leads to an enhancement of the Lorenz number, which is, like all Umklapp features, the bigger the smaller the disorder strength D is.

them by σ_0 , which is the disorder value of the charge conductivity. The heat conductivities are divided by $\sigma_0 TL_0$, which is the corresponding Luttinger liquid disorder heat conductivity.

Far away from commensurate filling, all conductivities become independent of $\Delta\nu$. The charge conductivity σ_c and the Luttinger liquid contribution to the bare heat conductivity κ_{LL}^0 are dominated by disorder scattering, while the phonon contribution is degraded by indirect disorder scattering via N -processes. For the parameters chosen here, the contribution from the phonons to the heat conductivity is much bigger than κ_{LL}^0 at large $\Delta\nu$. Therefore, the Lorenz number in this regime is enhanced in comparison to the Wiedemann-Franz value L_0 , which is valid in the clean Luttinger liquid.

Going to smaller values of $\Delta\nu$, phonon assisted Umklapp scattering starts to decrease the heat conductivity. This affects both, the Luttinger liquid and the phonon contribution to the heat conductivity. From the discussion in the preceding section, we know that the suppression of the heat conductivity due to Umklapp scattering is maximal at $\delta \approx 1$, see equation (3.153), which translates to $\Delta\nu = T/(6v)$ with the velocity according to the involved excitation. For the parameters used here, the phonon Umklapp minimum is expected around $\Delta\nu = 1/3$, which is in good agreement with the data. The phonon contribution to the heat conductivity is also suppressed by this process, but here the discussion does not apply. We observe that the suppression sets in at slightly smaller values of $\Delta\nu$ than in the Luttinger liquid contribution.

The phonon assisted Umklapp scattering features in the total heat conductivity reflect

in a shoulder in the Lorenz number, signed in the figure with a b.

At even smaller values of $\Delta\nu \approx 0.1$, the normal Umklapp scattering starts to be effective in degrading the heat current. The minimum of the Luttinger liquid contribution should be at $\Delta\nu \approx 0.067$, which is again matched by the results, depicted in the inset. Also the phonon contribution is affected by the normal Umklapp process, but not as strongly as the Luttinger liquid contribution, since it couples to this scattering process only indirectly.

Unlike the Luttinger liquid without phonons, the heat conductivity is not completely protected by conservation laws close to commensurate filling. Since there are two scattering processes with a conservation law, each scatters the protected current of the other. Thus, the heat currents are scattered close to commensurate filling, and the heat conductivity does not recover to its value of large $\Delta\nu$ as in the case without phonons. For the same reason, thermoelectric corrections only play a minor role in the system including phonons, as can be seen in the figure at the small difference between κ and κ^0 .

The charge conductivity starts to be suppressed around $\Delta\nu \approx 0.1$. We expect normal Umklapp scattering to set in at $\Delta\nu \approx 0.067$, so probably both Umklapp processes play a role here. Due to the shape of the crossover, it is difficult to separate the influence of both. However, the interplay of the starting suppression of σ_c and the minimum of κ around $\Delta\nu \approx 0.7$ yields a strong Umklapp minimum in the Lorenz number around $\Delta\nu \approx 0.12$, which is signed in the figure with an a. The depth of both Umklapp features increases with decreasing disorder strength, since the relative strength of Umklapp scattering grows.

Close to commensurate filling $\Delta\nu = 0$, the charge conductivity is suppressed strongly, which together with the partially protected heat conductivity yields a moderate enhancement of the Lorenz number. The enhancement is the bigger the cleaner the system is, which again is explained by the increasing relative strength of the Umklapp scattering.

Figure 3.11 shows the Lorenz number as function of $\Delta\nu$ for different temperatures, while the disorder strength and the phonon coupling are kept fix at $D_{\text{dis}} = 10^{-4}$ and $\alpha = 0.1$. In the inset the temperature dependence of the conductivities is shown for fixed doping $\Delta\nu = 0.1$.

The Lorenz number again exhibits two minima around $\Delta\nu \approx T/(6v_c)$ and $\Delta\nu \approx T/(6v_p)$ due to the suppression of the heat conductivity by normal and phonon assisted Umklapp scattering. For the highest temperature $T = 0.1$, the phonon assisted Umklapp minimum at $\Delta\nu \approx 0.18$ is very pronounced, while the normal phonon dip is reduced to a diffuse shoulder around $\Delta\nu \approx 0.04$. The situation is the other way round for the lowest temperature $T = 0.05$, where the normal Umklapp dip at $\Delta\nu \approx 0.03$ becomes pronounced and the phonon Umklapp feature around $\Delta\nu \approx 0.1$ becomes a shoulder.

The reason for the inverted dominance of the processes is the different temperature exponent of Γ_U and $\Gamma_{U,p}$, see equations (3.111) and (3.128).

Note that the positions of the features agree roughly with the prediction for the position of the minimum of the heat conductivity $\Delta\nu = T/(6v_{c,p})$. Small deviations can be explained by the influence of the starting suppression of the charge conductivity, and the different position of the minimum in the phonon heat conductivity.

The temperature dependence of the Lorenz number far away from commensurate filling can be explained by the phonon contribution to the heat conductivity. As can be seen in the inset, the Luttinger liquid contribution to the heat conductivity and the charge conductivity obey the Wiedemann Franz law at low temperatures, which corresponds to large $\Delta\nu$. The phonon contribution has a strong temperature dependence in this regime, which reflects in the temperature dependent enhancement of the Lorenz number.

Since the phonon heat current couples indirectly to the disorder scattering, the corre-

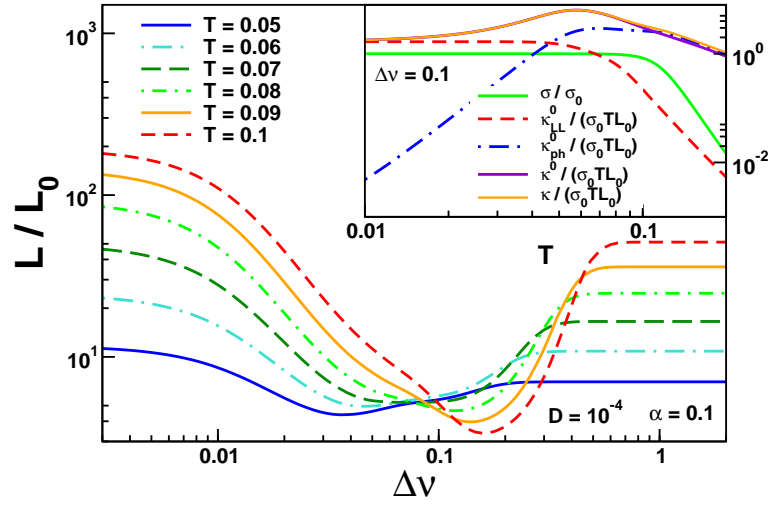


Figure 3.11: Lorenz number close to $\nu = 1/3$ as function of the doping $\Delta\nu$ for different temperatures T in units of v_s/a . The disorder strength is $D = 10^{-4}$ and the phonon coupling $\alpha = 0.1$. Higher temperatures increase the size of the Umklapp features, since the relative strength of the Umklapp scattering processes compared to the disorder increases. Far away from commensurate filling, L is enhanced by the influence of the phonon contribution to the heat conductivity, which has a strong temperature dependence, see text. The minima of the Lorenz number move slightly as function of temperature. *inset*: conductivities for $\Delta\nu = 0.1$ as function of temperature. In the low T regime, σ_c and κ_{LL}^0 are disorder dominated and obey the Wiedemann-Franz law, while the phonon contribution has a strong temperature dependence, see text. At high temperature Umklapp scattering affects all currents, leading to the rich structure of minima observed in the Lorenz number. Thermoelectric corrections are very small, as can be seen at the tiny difference between κ and κ^0 .

sponding heat conductivity is

$$\kappa_{ph}^0 \sim \frac{1}{T} v_p^4 \chi_{P_{ph}, P_{ph}}^2 \frac{\Gamma_{dis} + \Gamma_N}{\Gamma_{dis} \Gamma_N}. \quad (3.167)$$

Depending on the phonon coupling α and the disorder strength D_{dis} , and of the temperature regime, the bottleneck can either be the disorder scattering, when the phonon momentum is equilibrated with the Luttinger liquid by strong phonon coupling, or the phonon scattering when $\Gamma_{dis} \gg \Gamma_N$. The Lorenz number has a temperature dependence in both cases, since $\kappa_{ph} \sim T^2$ when the bottleneck is the phonon coupling, and $\kappa_{ph} \sim T^{5.6}$ when disorder scattering is the weaker process. Which case applies can be seen, apart from the temperature dependence, which hints towards equilibrated subsystems, from the dependence of the Lorenz number of the phonon coupling α , which will be discussed later. However, at very low temperatures, the phonon scattering rate vanishes rapidly $\Gamma_N \sim T^5$, while the disorder scattering $\Gamma_{dis} \sim T^{K_c + K_s}$ has a moderate temperature exponent. Thus, independent of the parameters, at really low temperatures the phonon scattering will always be the bottleneck.

The temperature dependence of the phonon contribution to the heat conductivity leads to an increase of the Lorenz number with increasing temperature in the disorder dominated regime.

Finally, figure 3.12 shows the dependence of the Lorenz number of the phonon coupling α . Most prominently, an increase in the phonon coupling is seen in the phonon assisted

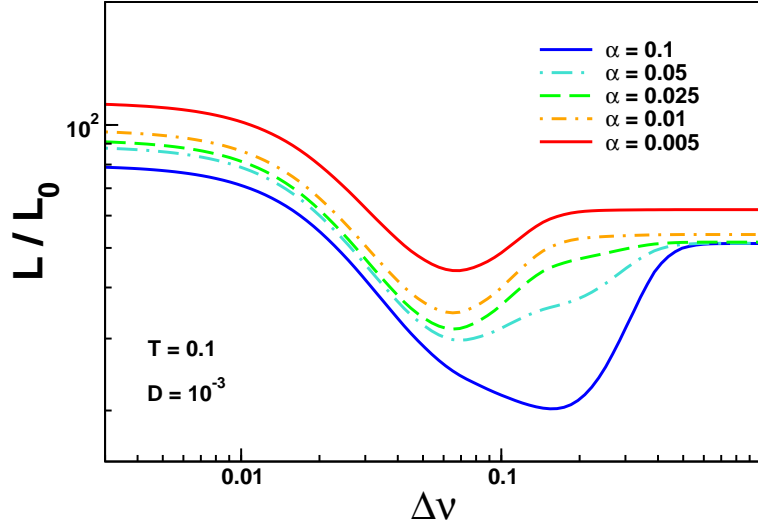


Figure 3.12: Lorenz number L/L_0 close to $\nu = 1/3$ as function of the doping $\Delta\nu$ for different values of phonon coupling α . Temperature is $T = 0.1$ and disorder strength $D = 10^{-3}$. Higher values of α increase the importance of the dip in the Lorenz number due to phonon assisted Umklapp scattering at $\Delta\nu \approx 0.2$, while the dip from normal Umklapp scattering is unaffected. Far away from commensurate filling, the phonon contribution to the heat conductivity results in an α -dependence of the Lorenz number at low phonon couplings. This change of dependence reflects the change of the bottleneck scattering process of the phonon heat current, see text. The higher heat conductivity from phonons at low coupling yields an overall enhancement of the Lorenz number.

Umklapp dip in the Lorenz number around $\Delta \approx 0.2$. It evolves from a shallow shoulder at weak coupling to a pronounced dip for the biggest coupling $\alpha = 0.1$.

Apart from that, an overall decrease of the Lorenz number with increasing α can be observed, which has its cause in the phonon contribution to the heat current. In particular, far away from commensurate filling, the crossover from disorder dominated phonon scattering to normal process dominated phonon scattering can be observed, since for the one the phonon contribution to the heat conductivity is independent of α , while in the other, the phonon heat conductivity has a $1/\alpha^2$ dependence.

In the regime, where normal processes are the dominant scattering mechanism for the phonon heat current, the heat conductivity is enhanced for all $\Delta\nu$, since the normal process is also the bottleneck for indirect Umklapp scattering, and phonon assisted Umklapp scattering is ineffective, as can be seen from the missing feature. Therefore, the Lorenz number is enhanced for all dopings in the weak phonon coupling regime.

On the other hand, strong phonon coupling leads to a lower enhancement of the Lorenz number in the vicinity of commensurate filling. This can be explained by the stronger mutual violation of the conservation laws of normal and phonon assisted Umklapp scattering, which partially protect the heat current from Umklapp scattering.

However, it must be reminded that the dissipation of the phonon heat current in our description relies strongly on the scattering of the Luttinger liquid fields of *fixed* impurities, which is an unjustified approximation. A correct treatment would have to model scattering of impurities moving with the displacement field and include further scattering mechanisms to degrade the phonon momentum. However, it must be reminded that the dissipation of the

3.3. VIOLATION OF WIEDEMANN-FRANZ LAW IN LUTTINGER LIQUIDS

phonon heat current in our description relies strongly on the scattering of the Luttinger liquid fields of *fixed* impurities, which is an unjustified approximation. A correct treatment would have to model scattering of impurities moving with the displacement field and include further scattering mechanisms to degrade the phonon momentum.

In total, also in the general case of a weakly disordered correlated metal coupled to lattice vibrations, the Wiedemann-Franz law is violated due to the interplay of Umklapp scattering and weak disorder.

The size of the violations though is much smaller than in the case without phonons, where the enhancement close to commensurate filling is caused by the protection of the heat current against Umklapp scattering by the conservation of pseudo momentum. In the presence of phonons, the second Umklapp process including a phonon spoils the conservation law and reduces the enhancement.

Furthermore, the minimum of the Lorenz number due to suppression of the heat conductivity by Umklapp scattering and the simultaneous weak scattering of the charge current at finite fillings becomes less pronounced by introducing phonons, since the suppression of the charge conductivity due to phonon-assisted Umklapp scattering is effective for higher momentum mismatches, which reduces the combined effect for the suppression of the Lorenz number.

On the other hand, enhancement of the Lorenz number due to the weak scattering of phonons can be observed, which is not surprising.

In particular, the thermoelectric figure of merit $ZT = \kappa_0/\kappa - 1$, which in the case without phonons was of the order of $1/\tilde{D}$, is strongly reduced by the influence of lattice vibrations. Due to the intersecting conservation laws, the thermoelectric corrections to the heat conductivity are decreased and the figure of merit becomes very small, at least in the regimes studied here.

4 Expansion of Interacting Atoms in Optical Lattices

Physics out of equilibrium in condensed matter systems are in general hard to tackle, both theoretically and in experiment. On the theoretical side, the difficulties lie in the great complexity that already arises in the description of rather simple model systems, when moving away from equilibrium. Experimentally, it is very hard to probe a nano-scaled system time-resolved and at the same time with high spatial resolution.

However, in the recent years with the development of optical lattices and the increased experimental control of cold quantum gases confined to them great new possibilities for the study of non-equilibrium in condensed matter opened up. Nowadays they allow to model condensed matter type systems, in particular varieties of the Hubbard model, on a bigger scale with a huge freedom of tuning parameters.

For this purpose, fermionic or bosonic atoms of alkali metals are loaded into a confining trap and an optical lattice is formed by standing waves from counterpropagating laser beams. The interaction between the electric field and the atomic polarizability acts as a simple cubic lattice to the atoms, in the case of fermions making them a copy of electrons on a lattice. The tight-binding hopping amplitude is controlled by the intensity of the laser beams, which determines the lattice depth. Additionally, interaction between the atoms can be modeled with a *Feshbach resonance*, which provides a possibility to tune the scattering length of atomic collisions by a magnetic field.

These *quantum simulators*¹ already allowed valuable contributions in the field condensed matter physics in equilibrium, for example the realization of the quantum phase transition from a superfluid to a Mott insulator in a gas of ultracold atoms [88], and in this context the collapse and revival of coherence of the matter wave field of a Bose-Einstein condensate [89] have been confirmed experimentally.

Another hallmark has been the experimental preparation of a Mott-insulator in a two-component Fermigas [90, 91], which is to a good approximation a realization of the fermionic Hubbard model. Motivated by the actual experimental activity, the same scenario had already been studied just before that by means of inhomogeneous DMFT² [92], and a direct comparison of experimental results and theoretical predictions is included in [90].

The inhomogeneous DMFT has proven a particularly useful tool to describe the relevant systems theoretically, which are typically, due to the trap, not translational invariant. Very recently, it has been used to study the spin order of a Bose system [93] and, in combination with a high temperature series expansion and in comparison to experimental data, the entropy of an repulsively interacting Fermi gas, [94]. These are only some important examples, a more complete review of the achievements made with ultracold quantum gases in optical

¹as they are called after a proposal of Richard Feynman

²Dynamical Mean Field Theory

lattices is given in [95].

Of special appeal, however, is the ability to investigate settings out of equilibrium. The high tunability in combination with the slow dynamics of cold atoms allows to investigate time-dependent processes.

Various exciting results have recently been reported, e. g. how a non-integrable one-dimensional Bose-gas out of equilibrium thermalizes [96] or the direct time-resolved observation of the correlated tunnelling of two interacting ultracold atoms through a barrier in a double-well potential [97]. Another important aspect and prerequisite of experiments is the adiabatic preparation of many-body states, that has been studied in [98].

An interesting peculiarity has been found with the discovery of repulsively bound states in bosons [99]. At strong repulsive interactions, initially prepared double occupancies, later termed *doublons*, are prohibited to decay into single-particle excitations, since the large energy of the pair can not be distributed to a small number of excitations. Thus the decay process is exponentially suppressed and the doublons form metastable quasi-particles. The investigation of a similarly prepared metastable state in the fermionic Hubbard model lead to the prediction of exotic (π, π) superconductivity, [100]. In [101] the implications for cooling have been deployed to introduce the so-called *quantum distillation*. For the fermionic Hubbard model, this exponential decay has been experimentally confirmed in [102] and explained by a diagrammatic calculation.

In the context of this thesis, which is focused on transport questions, the field of ultracold quantum gases in optical lattices also opens up new possible settings that go beyond the classical four point current measurement as response to a field gradient. Making use of the huge tunability, one can prepare an initial state narrowly confined by the trapping potential and release it suddenly. The slow dynamics of the atoms allow to image the following expansion time-resolved.

In [103] this has been done for attractively interacting fermions in an optical lattice, showing anomalous behavior in the cloud radius.

Experimental data by U. Schneider and collaborators on the expansion of repulsively interacting fermions also shows interesting features in the expansion rate. For small interactions the motion of the fermions is ballistic, which is reflected in a square-shaped atom cloud after some time. At high interactions the expansion is decelerated by collisions that restore local equilibrium, leading to a symmetric, circular cloud and diffusive transport.

This behavior has been modeled here by a lattice Boltzmann simulation in relaxation-time approximation in collaboration with Stephan Mandt, who also did some closer analysis of the diffusive regime, which will not be discussed here. The results of the project will be published together with the experimental outcome in a joint article with U. Schneider, I. Bloch, et al., [104]. The scattering rate is obtained from a memory matrix calculation, accounting for the conservation laws in the collisions. By using the Hubbard interaction as a perturbation, one produces a density-dependent scattering rate, which interpolates between the ballistic transport regime for small interactions or densities close to maximal and minimal filling and the diffusive regime for strong interactions and intermediate filling. The modeling of the expanding cloud is a neat example for the combined use of the techniques used in the preceding chapters. A quantitative comparison to the experimental data is made, and the quality of the theoretical description is discussed.

4.1 Experimental Setup

In the experiment, the lowest hyperfine states of potassium ^{40}K atoms represent the spin up and spin down states of electrons. The scattering length can be tuned by the Feshbach resonance with a magnetic field, modelling a short-range interaction with the corresponding strength. A cloud of $N = 1 - 1.5 \times 10^5$ atoms is loaded into a red detuned crossed dipole trap. By evaporative cooling down to $T = 0.13T_F$ a quantum degenerate mixture of the two species is prepared³, where T_F denotes the Fermi-temperature in the harmonic trap. Then the trapping frequencies are increased adiabatically to their final values $\omega = 100(2\pi)/s$ in horizontal, and $\omega = 400(2\pi)/s$ in vertical direction. The three-dimensional simple-cubic optical lattice with a wavelength $\lambda = 738\text{nm}$ is ramped up linearly within 56ms to a depth of $8E_r$ ⁴. During this process, the magnetic field is kept at the value corresponding to no interaction, i. e. 209.2G. This sequence results in a band-insulating state surrounded by a metallic shell.

Subsequently, the interaction strength is set to the respective value for the expansion, which must be done at locally fixed particle number, to prevent changes in the density profile. To that purpose, the lattice is ramped up to $20E_r$ within $200\mu\text{s}$, which is slow enough to avoid excitations to the second band, but faster than the atom cloud can rearrange. By this process the coherence of atoms at different lattice sites is completely destroyed. As the atoms become strictly localized, their momentum must be maximally blurred. This corresponds to a local distribution function with formally infinite temperature, where every momentum is equally probable.

After having prepared an initial state with well-known distribution functions, the expansion process is started by quickly lowering the lattice depth to the desired value between $4E_r$ and $15E_r$ and simultaneously reduce the trapping potential to a value which cancels the deconfining of the optical lattice, ensuring in total zero confining.

The following expansion is monitored by in-situ imaging along the vertical axis of the cloud. Optionally, the tunneling in one direction can be suppressed by deepening the respective component of the optical lattice. Then the expansion happens independently in each separate layer, but the resulting image is a weighted average over all layers. There seems to be no qualitative difference between expansion in three and two dimensions. The expansion rate is observed to be fastest for the zero interaction case, and to be symmetrically suppressed for higher repulsive or attractive interactions. At large interactions, the distribution remains circular, whilst in the free expansion it takes a rectangular shape.

Experimentally, both cases, expansion in a two-dimensional and in a three-dimensional optical lattice, yield similar expansion rates and cloud shapes. The reason is that the system is not entirely homogeneous, since gravitation accelerates the atoms in z-direction. In the two-dimensional case, the motion is restricted to the two directions perpendicular to the gravitation, so there is no effect. In three dimensions, the force on the atoms leads to so-called *Bloch oscillations* in z-direction. According to the semiclassical equations of motions in energy bands [28], the atoms are accelerated by the force into a higher momentum state. Due to the periodicity of the dispersion relation, the velocity of the atom, which is the derivative of the energy with respect to momentum, must also be a periodic function. Thus, averaged over a Bloch period, the particle does not gain velocity. This effect has been predicted by F. Bloch in the early days of solid state theory, [105], but could not be observed

³The preparation of the bandinsulating state works similar as described in [90]

⁴In experiments with cold quantum gases, lattice depths are typically given in recoil energies. $1E_r = \hbar^2/(2m\lambda^2)$

4.2. BOLTZMANN EQUATION DESCRIPTION

in real solids because the Bloch period is much longer than typical scattering times of conduction electrons. Only some years ago, Bloch oscillations were experimentally observed in semiconductor superlattices, where the lattice period, which determines the Bloch period, is much bigger than in usual solids, [106]. Also for a gas of ultracold bosonic atoms in an optical lattice, Bloch oscillations have been detected recently, [107].

In the experimental system for the expansion, gravitation induces oscillations with the amplitude $2J/(mg)$, where J is the hopping amplitude from one lattice site to the other. The oscillation amplitude is of the order of the lattice constant of the optical lattice, which prohibits the atom cloud to expand in vertical direction, at least as long as the scattering time is longer than the Bloch period. Effectively, the expansion experiment therefore can be described by a two-dimensional simulation.

4.2 Boltzmann Equation Description

A theoretical description of the experiment introduced in the preceding section must cover a large range of regimes of an interacting quantum system out of equilibrium. Naturally, it is very difficult to cover all these regimes exactly, a good approximation would have to match as many limiting cases as possible, e. g. the limiting cases of high and low density. Despite the fact that the setting does not meet the preconditions for the Boltzmann equation being valid, the latter turns out to fulfill this demand: In the low density regime, where the atoms expand freely, their motion is semiclassical and hence well described by the drift term. At large interactions scattering becomes dominant in the center of the trap where the density is high, driving the distribution function quickly towards local equilibrium. Such a setting exhibits diffusive transport of particles and energy which can be described by the Boltzmann equation in relaxation time approximation [108].

Thus calculating a scattering rate matching the transport coefficients of the diffusive regime and using it in the linearized Boltzmann equation yields an equation of motion for the distribution functions which is valid in the two limiting cases. For that purpose the diffusion constants, that relates the currents to the gradients of particle and energy density, n and ε , as

$$\begin{pmatrix} J \\ J_\varepsilon \end{pmatrix} = \begin{pmatrix} D_p & D_{p\varepsilon} \\ D_{\varepsilon p} & D_\varepsilon \end{pmatrix} \begin{pmatrix} \nabla n \\ \nabla \varepsilon \end{pmatrix} \quad (4.1)$$

must be identified with the standard transport coefficients for energy and particle transport, defined by

$$\begin{pmatrix} J \\ J_\varepsilon \end{pmatrix} = \begin{pmatrix} L_{EE} & L_{ET} \\ L_{TE} & L_{TT} \end{pmatrix} \begin{pmatrix} \mathbf{E} \\ \frac{1}{T} \nabla T \end{pmatrix}. \quad (4.2)$$

Writing the electric field as

$$\mathbf{E} = \nabla \mu = \frac{\partial \mu}{\partial n} \nabla n \quad (4.3)$$

and the temperature gradient as

$$\nabla T = \frac{\partial T}{\partial \varepsilon} \nabla \varepsilon, \quad (4.4)$$

the identification can be done from the equation

$$\begin{pmatrix} D_p & D_{p\varepsilon} \\ D_{\varepsilon p} & D_\varepsilon \end{pmatrix} = \begin{pmatrix} L_{EE} & L_{ET} \\ L_{TE} & L_{TT} \end{pmatrix} \begin{pmatrix} \frac{\partial \mu}{\partial n} & \frac{\partial \mu}{\partial \varepsilon} \\ \frac{\partial T}{\partial \mu} & \frac{1}{T} \frac{\partial T}{\partial \varepsilon} \end{pmatrix}. \quad (4.5)$$

Since the density of the atom cloud is varying slowly in space, the equilibrium transport coefficients can be used. As discussed in chapter 1, they are related to the current-current correlation functions by the Green-Kubo relations. As in the previous chapter, they can be calculated to leading order in the interaction with the memory matrix formalism. Since the lowest order contribution is already included in the L_{ij} , the factors $\partial\mu/\partial n$ and $\partial T/\partial \varepsilon$ to leading order can be replaced by their non-interacting values.

The calculation of the scattering rates by means of the memory matrix formalism is carried out in chapter 4.3. The resulting τ can be entered into the Boltzmann equation in relaxation-time approximation, equation (1.8). Thus, one has to solve a partial differential equation for the distribution function with given starting conditions. The Boltzmann equation to this problem reads

$$\begin{aligned} \partial_t f(\mathbf{k}, \mathbf{r}) = & -\mathbf{v} \cdot (\nabla_{\mathbf{r}} f(\mathbf{k}, \mathbf{r})) + U(\nabla_{\mathbf{r}} n(\mathbf{r})) \cdot (\nabla_{\mathbf{k}} f(\mathbf{k}, \mathbf{r})) \\ & - \frac{1}{\tau(\mu(\mathbf{r}), \beta(\mathbf{r}), U^2)} (f(\mathbf{k}, \mathbf{r}) - f^0(\varepsilon(\mathbf{k}), \mu(\mathbf{r}), \beta(\mathbf{r}))) \end{aligned} \quad (4.6)$$

where the velocity \mathbf{v} is given by the derivative of the dispersion with respect to the momentum

$$\mathbf{v} = \nabla_{\mathbf{k}} \varepsilon(\mathbf{k}) = \nabla_{\mathbf{k}} (-2J \cos(k_x) - 2J \cos(k_y)), \quad (4.7)$$

and U is the interaction strength, which controls the force term as well as the scattering. In the following, all energies will be given in units of the hopping amplitude J , which in the calculations is set to $J = 1$. The scattering term is built such that the distribution function f always alters towards the equilibrium form f^0 , and simultaneously the conservation of particle number and energy is ensured by adaption of the local inverse temperature $\beta(\mathbf{r})$ and chemical potential $\mu(\mathbf{r})$.

In this description, the distribution function is continuous in space and momentum. It can be solved using standard numerical methods⁵, but for the implementation it must be discretized, where it should be noted that the spacial lattice is *not* equivalent to the optical lattice. Derivatives must be replaced by quotients of differences, which are chosen symmetrically. In momentum coordinates, the quotient of differences are chosen as

$$\partial_{k_i} f(\mathbf{k}) = \frac{f(\mathbf{k} + \Delta k_i) - f(\mathbf{k} - \Delta k_i)}{2\Delta k_i}. \quad (4.8)$$

It is natural to choose periodic boundary conditions for the momentum coordinates, which reflects the physical content of the Bloch theorem. In real space a higher density of discretization points than in momentum space will be needed, to describe decently the inhomogeneity of the problem. Accordingly, the spatial derivatives are implemented with a higher order quotient of differences, namely

$$\partial_{r_i} f(\mathbf{r}) = \frac{-f(\mathbf{r} + 2\Delta r_i) + 8f(\mathbf{r} + \Delta r_i) - 8f(\mathbf{r} - \Delta r_i) + f(\mathbf{r} - 2\Delta r_i)}{12\Delta r_i}, \quad (4.9)$$

which gives a smoother approximation to the infinitesimal derivative.

Unlike in momentum coordinates, periodic boundary conditions are not the natural choice for the real space coordinates. There is no link between the different edges of the simulated space, and one does not expect particles to flow in at all. Nevertheless, they are used here to gain stronger control over the numerical stability, in particular the conservation of

⁵In this project, fourth order Runge-Kutta algorithm has been used

4.2. BOLTZMANN EQUATION DESCRIPTION

the particle number. With open boundary conditions the particle number is not conserved, since particles drain through the boundaries. Closed boundary conditions cause a reflection of atoms reaching the edge, which is practically equivalent to periodic ones due to the used symmetry of the system. With periodic boundary conditions, the particle number is conserved exactly, also in the discretized version, as can be seen by summing over all momenta and lattice sites of the discretized Boltzmann equation.

The disadvantage traded in for this is an unphysical inflow of particles. Fortunately, this is really tiny as long as no considerable density has moved close to the edges of the system. Since the density moves at most ballistically with the maximum velocity corresponding to the momentum $k_i = \pi/4$, it is obvious when the validity of the description breaks down. After that time, the simulation becomes unmeaningful, but even with the correct boundary conditions, it would have been impossible to extract a characteristic width from the simulated cloud with considerable density flown out of the grid from the beginning.

The discretized version is a system of coupled partial differential equations for each $\mathbf{k}(p_x, p_y)$, which are coupled through the force and the scattering term.

To model the starting conditions, the local chemical potential is calculated from the trapping potential, namely

$$\mu(n_x, n_y, n_z) = -a_0 r(n_x, n_y, n_z)^2 + b_0, \quad (4.10)$$

with the parameters chosen matching to the experiment $a_0 = 0.00970237D_0$ and b_0 varying between $15D_0$ and $20D_0$ for each run of the experiment⁶, both in units of the bandwidth $D_0 = 4J$. With the chemical potential, the local density can be obtained by summing the equilibrium Fermi-distribution function at every site over all discrete momenta $\mathbf{k}(p_x, p_y, p_z)$, which is a three-dimensional sum, since this part of the preparation happens before the layers are separated. One obtains

$$n(n_x, n_y, n_z) = \frac{1}{N_x N_y N_z} \sum_{p_x, p_y, p_z} \frac{1}{e^{\beta(\varepsilon(\mathbf{k}(p_x, p_y, p_z)) - \mu(r(n_x, n_y, n_z)))} + 1} \quad (4.11)$$

with $\varepsilon(\mathbf{k})$ the three-dimensional analogue to the dispersion introduced in equation (4.7) and the experimental temperatures vary between $\beta = 0.13D_0$ and $0.19D_0$.

Then the distribution function gets quenched in the preparation process by temporarily prohibiting tunneling between different lattice sites, which locally levels the occupation of every momentum state while keeping the particle number at every site fixed. The starting distribution function thus is obtained from

$$f(n_x, n_y, n_z, p_x, p_y) = \frac{1}{n(n_x, n_y, n_z)}, \quad (4.12)$$

where practically the z space coordinate is the same for the whole system of differential equations, which describes the time evolution within one layer, and thus can be dropped as a functional dependency. This distribution function describes the state of a system at infinite temperature, which makes the practical use of the chemical potential impossible, because the latter also would have to be infinite, but still generate the correct particle number. Instead, the fugacity $z(\mathbf{r}) = \exp(\beta(\mathbf{r})\mu(\mathbf{r}))$ is used, which remains well-defined in this limit.

The fugacity must be obtained by solving the equation

$$\left(\frac{n(f(\mathbf{r}))}{\varepsilon(f(\mathbf{r}))} \right) = \frac{1}{N_x N_y} \sum_{p_x, p_y} \left(\frac{f^0(\mathbf{k}(p_x, p_y), z(\mathbf{r}), \beta(\mathbf{r}))}{\varepsilon(\mathbf{k}(p_x, p_y)) f^0(\mathbf{k}(p_x, p_y), z(\mathbf{r}), \beta(\mathbf{r}))} \right) \quad (4.13)$$

⁶the exact parameters are given in appendix C.1

for z and β , which is done by means of the generalized Newton algorithm. In the first step, the energy density of the quenched distribution function is zero, since all momenta are equally occupied and the dispersion is symmetric in \mathbf{k} ⁷. If the equation is fulfilled, both the equilibrium distribution function and the real distribution function contain the same particle number and energy per particle. Thus, the scattering process which shifts weight in the distribution function towards the equilibrium form conserves these two quantities.

Note that the equilibrium distribution function might look different from what one would expect, since locally high energy content might enforce an inversion of the occupation probability, which corresponds to a *negative* inverse temperature. This doesn't impose a problem, the equilibrium distribution function changes continuously from positive through zero inverse temperature to negative.

During the simulation, the inverse temperature and the fugacity must be readjusted to the changing distribution function in every time step at every space point. For the used Runge-Kutta algorithm of fourth order, this means that also in the intermediate time steps the readjustment has to be performed. Since within a time step the distribution function changes only slightly, the fugacity and inverse temperature from the preceding time step is typically very close to the solution of the equation and only few iterations are needed to reach a good numerical accuracy.

The numerical effort can be reduced by taking advantage of the fact that only a minor part of the simulated space contains a noteworthy amount of particles. In the low density limit the Pauli principle becomes ineffective, such that the equilibrium values of the particle and energy density are approximated well by summing over the Maxwell-Boltzmann distribution instead of the Fermi-distribution. This gives a closed expression for the particle density

$$n(\mathbf{r}) \approx z(\mathbf{r}) \sum_{\mathbf{k}} e^{-\beta(\mathbf{r})\varepsilon(\mathbf{k})} = z(\mathbf{r}) \frac{1}{4\pi^2} \int_{-\pi}^{\pi} d\mathbf{k} e^{2\beta(\mathbf{r})(\cos(k_x)+\cos(k_y))} = z(\mathbf{r}) J_0(2\beta(\mathbf{r}))^2 \quad (4.14)$$

and the energy

$$\begin{aligned} \varepsilon(\mathbf{r}) &\approx z(\mathbf{r}) \sum_{\mathbf{k}} \varepsilon(\mathbf{k}) e^{-\beta(\mathbf{r})\varepsilon(\mathbf{k})} = -z(\mathbf{r}) \frac{4}{4\pi^2} \int_{-\pi}^{\pi} d\mathbf{k} \cos(k_x) e^{2\beta(\mathbf{r})(\cos(k_x)+\cos(k_y))} \\ &= -4z(\mathbf{r}) J_1(2\beta(\mathbf{r})) J_0(2\beta(\mathbf{r})) \end{aligned} \quad (4.15)$$

as functions of fugacity and inverse temperature in terms of Bessel functions $J_n(x)$ of the first kind. In particular, the *energy per particle* $\varepsilon(\mathbf{r})/n(\mathbf{r})$ is, as easily can be seen, only a function of β and not of z . This simplifies the task to find the right fugacity and temperature a lot, since constructing an inverse function numerically is much easier on an one-dimensional space then on a two-dimensional one.

Practically, for a large set of temperatures, the energy per particle is computed and stored as a list of tuples with first entry the energy per particle and second entry the corresponding inverse temperature β . Then a cubic spline is constructed from the set, which gives inverse temperature for any energy density within the covered range⁸. Since the spline has to be built only once for the whole simulation, this procedure is very efficient. Knowing the local

⁷due to this reason it is necessary to chose the momentum discretization as a multiple of four to ensure meaningful solutions for the inverse temperature and fugacity

⁸In the simulation 10000 equally distributed values of β from $-50D_0$ to $50D_0$ are used.

4.3. RELAXATION-TIME FROM MEMORY MATRIX

temperature $\beta(\mathbf{r})$, the fugacity can be obtained by solving equation (4.14) for z , giving

$$z(\mathbf{r}) = \frac{n(\mathbf{r})}{J_0(2\beta(\mathbf{r}))^2}, \quad (4.16)$$

which can be evaluated at small numerical costs.

This approximation scheme is applied for lattice sites with a density $n(\mathbf{r}) \leq 0.0001$. As shown in C.2, the relative error of the particle number Δn made by replacing the Fermi-Dirac distribution function with the Maxwell-Boltzmann statistics for high temperatures is equal to the fugacity, for which in this limit

$$z = \frac{n(\mathbf{r})}{1 - n(\mathbf{r})} \quad (4.17)$$

holds. Thus the relative error is $\Delta n = \mathcal{O}(10^{-4})$. The error of the energy is of the same order of magnitude.

On top of using the low density approximation, the numerical effort can further be reduced by making use of the systems symmetry. The Hubbard model on the underlying simple cubic lattice has of course the symmetries of the point group of a square plus all translations by a primitive vector, but the initial state prepared in the trapping potential doesn't have the translational symmetry. Hence all physical information is contained in a wedge of size one eighth of the total system, which reproduces in the other parts by applying the symmetry operations⁹.

4.3 Relaxation-Time from Memory Matrix

For the implementation of the lattice-Boltzmann calculation a reasonable estimate of the relaxation-time as function of filling and temperature is needed. As an approximation to this quantity the conductivity of the Hubbard model in local equilibrium is calculated and a scattering rate matching this conductivity constructed.

The integrable, unperturbed part of the Hamiltonian is the free propagation of fermions on a two-dimensional lattice with a tight-binding dispersion $\varepsilon(\mathbf{k}) = -2(\cos(k_x a) + \cos(k_y a))$, written in momentum space as

$$H^{\text{kin}} = \sum_{\mathbf{k}, \sigma} \varepsilon_{\sigma}(\mathbf{k}) c_{\mathbf{k}\sigma}^{\dagger} c_{\mathbf{k}\sigma}. \quad (4.18)$$

The remaining part of the Hubbard model, the interaction, is used as a perturbation to the integrable H^{kin} , which again breaks the integrability and renders the conductivities corresponding to the slow modes finite. Of practical interest for the simulation is, of course, the conductivity of the particle current,

$$\mathbf{J} = \sum_{\mathbf{k}, \sigma} \mathbf{v}_{\mathbf{k}} c_{\mathbf{k}\sigma}^{\dagger} c_{\mathbf{k}\sigma}, \quad (4.19)$$

and that of the heat current \mathbf{J}_{ε}

$$\mathbf{J}_{\varepsilon} = \sum_{\mathbf{k}, \sigma} \mathbf{v}_{\mathbf{k}} \varepsilon_{\mathbf{k}} c_{\mathbf{k}\sigma}^{\dagger} c_{\mathbf{k}\sigma} \quad (4.20)$$

⁹see C.3 for details of the symmetry group

but to achieve a more accurate lower bound to the real conductivity the particle momentum \mathbf{P} and the hole momentum \mathbf{P}_{hole} ,

$$\begin{aligned}\mathbf{P} &= \sum_{\mathbf{k}, \sigma} \mathbf{k} c_{\mathbf{k}\sigma}^\dagger c_{\mathbf{k}\sigma} \\ \mathbf{P}_{\text{hole}} &= \sum_{\mathbf{k}, \sigma} (1 - \mathbf{k}) c_{\mathbf{k}\sigma}^\dagger c_{\mathbf{k}\sigma}\end{aligned}\quad (4.21)$$

are included as additional slow modes. By taking into account the momenta as slow modes, the correct asymptotics for low density and temperature, which are dominated by Umklapp scattering, is achieved. As in chapter 3, the time derivative of these modes is calculated only with the perturbation to the Hamiltonian, since they are conserved quantities of the unperturbed part H^{kin} . For this purpose, the perturbation is best also written in momentum space operators,

$$H^{\text{int}} = U \sum_{\mathbf{q}, \mathbf{k}, \mathbf{k}', \sigma, \sigma'} c_{\mathbf{k}\sigma}^\dagger c_{\mathbf{k}+\mathbf{q}\sigma} c_{\mathbf{k}'+\mathbf{q}\sigma'}^\dagger c_{\mathbf{k}'\sigma'}.\quad (4.22)$$

Since all four modes have the structure sum over \mathbf{k} over a function of the momentum times the particle density in common the calculation of the time derivative must be done only once for all. It is again performed by the commutator of the current with H^{int} , leading to

$$\partial_t \mathbf{J}_i = U \sum_{\mathbf{q}, \mathbf{k}, \mathbf{k}'} (g_i(\mathbf{k} + \mathbf{q}) - g_i(\mathbf{k}) + g_i(\mathbf{k}' - \mathbf{q}) - g_i(\mathbf{k}')) c_{\mathbf{k}+\mathbf{q}\uparrow}^\dagger c_{\mathbf{k}\uparrow} c_{\mathbf{k}'-\mathbf{q}\downarrow}^\dagger c_{\mathbf{k}'\downarrow}\quad (4.23)$$

with g_i the \mathbf{k} -dependent prefactor of each current \mathbf{J}_i , see appendix C.4.1. From these, the correlation function of every pair of time derivatives of currents must be calculated, as always within the unperturbed theory. Since the latter is particularly simple, this can actually be done in real time with the definition

$$\langle \partial_t \mathbf{J}_i; \partial_t \mathbf{J}_j \rangle(\omega) = \int dt e^{i\omega t} (-i\theta(t)) \langle [\partial_t \mathbf{J}_i(t), \partial_t \mathbf{J}_j(0)] \rangle.\quad (4.24)$$

The imaginary part of the correlation function can be partially evaluated, see appendix C.4.2, giving

$$\begin{aligned}\text{Im} \langle \partial_t \mathbf{J}_i; \partial_t \mathbf{J}_j \rangle(\omega) &= \pi U^2 \sum_{\mathbf{k}_1, \mathbf{k}_2, \mathbf{k}_3, \mathbf{k}_4, \mathbf{G}} \prod_{l=i,j} (g_l(\mathbf{k}_1) + g_l(\mathbf{k}_2) - g_l(\mathbf{k}_3) - g_l(\mathbf{k}_4)) \\ &\times (\delta(\omega - (\varepsilon_{\mathbf{k}_4} + \varepsilon_{\mathbf{k}_3} - \varepsilon_{\mathbf{k}_2} - \varepsilon_{\mathbf{k}_1}) - \delta(-\omega - (\varepsilon_{\mathbf{k}_4} + \varepsilon_{\mathbf{k}_3} - \varepsilon_{\mathbf{k}_2} - \varepsilon_{\mathbf{k}_1})) \\ &\times \delta_{\mathbf{k}_1+\mathbf{k}_2, \mathbf{k}_3+\mathbf{k}_4+\mathbf{G}} f_{\mathbf{k}_1} f_{\mathbf{k}_2} (1 - f_{\mathbf{k}_3}) (1 - f_{\mathbf{k}_4})\end{aligned}\quad (4.25)$$

where a sum over four independent momenta within the first Brillouin zone and all reciprocal lattice vectors \mathbf{G} remains. The Kronecker delta ensures momentum conservation and the two delta functions energy conservation.

From equation (4.25) the conductivities for particle and heat current can be obtained from

$$\sigma_{ij} = (\hat{\chi} \hat{M}^{-1} \hat{\chi})_{i,j}\quad (4.26)$$

where the elements of the matrix \hat{M} are given by

$$M_{i,j} = \lim_{\omega \rightarrow 0} \frac{1}{\omega} \text{Im} [\langle \partial_t \mathbf{J}_i; \partial_t \mathbf{J}_j \rangle(\omega)],\quad (4.27)$$

4.3. RELAXATION-TIME FROM MEMORY MATRIX

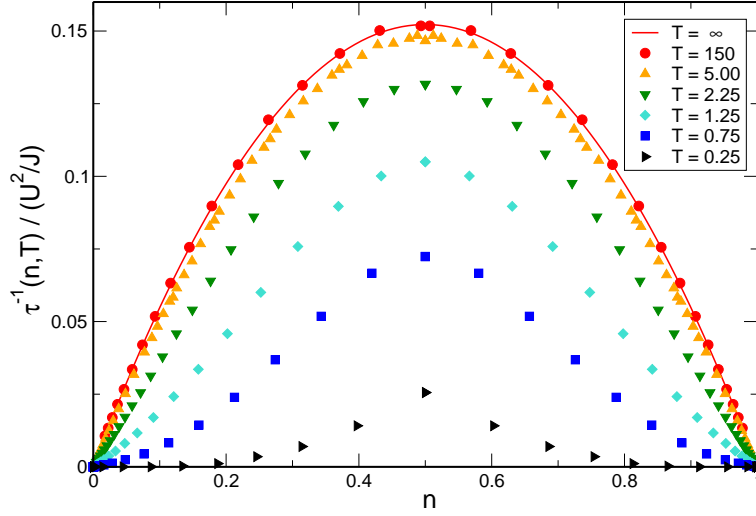


Figure 4.1: Inverse scattering rate as function of the density for several temperatures.

and the respective generalized susceptibilities χ_i by

$$\chi_i = \sum_{k, \sigma} g_i(k)^2 (1 - f_{k\sigma}) f_{k\sigma}, \quad (4.28)$$

see appendix C.4.3 for details of the calculation. Both, the matrix of correlation functions and the susceptibilities depend on the chemical potential μ and the temperature T through the Fermi distribution functions. They can be computed with moderate numerical effort by Monte Carlo integration for fixed μ and T . From this data set, a formula for the scattering rates as function of particle density and temperature can be obtained by fitting to a suitable function with few parameters. Here, the function

$$\tau^{-1}(\beta, n) = \frac{4A(1-n)n}{1 - 16\frac{A}{S}} \quad (4.29)$$

was used to produce a fit with parameters A and S for each temperature β . From the obtained set of fit parameters, a continuous fit as function of n and β was obtained by fitting the parameters A and S as function of β with the functions

$$\begin{aligned} A(\beta) &= a \arctan(b\beta + c\beta^2) \\ S(\beta) &= \tilde{a} \arctan(\tilde{b}\beta + \tilde{c}\beta^2). \end{aligned} \quad (4.30)$$

The resulting parameters for the actual data set were $a = 0.09691$, $b = 0.64611$, $c = 0.70832$, $\tilde{a} = 0.38767$, $\tilde{b} = 0.12932$, $\tilde{c} = 0.20087$.

The transport coefficients L_{EE}, L_{ET}, L_{TT} are identical to the components $\sigma_{1,1}, \sigma_{1,4}, \sigma_{4,4}$ of the matrix of conductivities. Using the expressions derived for the transport coefficients in relaxation time approximation, equations (1.21) and (1.23), one obtains one relaxation time per transport coefficient, namely

$$\frac{1}{\tau_1} = \frac{\chi_{J_p J_p}}{L_{EE}}, \quad \frac{1}{\tau_2} = \frac{\chi_{J_p J_\epsilon}}{L_{ET}}, \quad \frac{1}{\tau_3} = \frac{\chi_{J_\epsilon J_\epsilon}}{L_{TT}} \quad (4.31)$$

With each obtained relaxation time, the solution of the linearized Boltzmann equation, equation (4.6), matches the respective transport coefficient. Thus, one has to make a choice

which effect shall be governed in the best way and perform an average that suits this purpose. Here it turns out that the temperature of the described experiment is that high in the whole trap that heat transport plays only a minor role, and the best choice of τ is such that the particle current conductivity is matched.

Figure 4.1 shows the inverse scattering rate τ^{-1} fitted to match the transport coefficient L_{EE} as function of the filling for some temperatures.

4.4 Results

Since all parameters of the model are adjusted to match the experimental situation, the results can directly be compared. From the obtained distribution functions, the density profiles of each time-step are calculated easily.

In the two-dimensional expansion, the cloud is prepared three-dimensional and then separated by changing the depth of the lattice in z -direction. Therefore, the obtained images show an average over several expansions in different layers, with different starting conditions. To make a reasonable comparison, the simulation is also done for each two-dimensional slice separately, and the final density profile is obtained by summing over them.

Figure 4.2 shows the experimental and theoretical density profiles after 25ms expansion for different interaction strength U/J . Clearly, the cloud becomes rectangular for small interactions, while the circular shape of the starting cloud stays better conserved the higher the interaction strength is.

The experimentally imaged clouds have similar shapes for repulsive and attractive interactions of the same magnitude. This can be explained by a symmetry argument of the Hubbard model, pointed out by E. Demler, see [104]. Consider two Hubbard-type Hamiltonians,

$$\mathcal{H}_{\pm} = -J \sum_{\langle i,j \rangle, \sigma} c_{i\sigma}^{\dagger} c_{j\sigma} \pm U \sum_i n_{i\uparrow} n_{i\downarrow}, \quad (4.32)$$

which differ only in the sign of the interaction term. For an initial state and a measured quantity that are both invariant under the symmetry operations time-reversal and momentum shift by $Q = (\pi, \pi, \pi) \times 2/\lambda$, the time-evolution is equal for repulsive and attractive interaction.

The measured operator in the experiment, the density operator $n(\mathbf{r})$, fulfills the required symmetries, as well as the initial state, which consists of atoms that are completely localized within individual wells.

Since the experimental system is a good realization of the Hubbard model, the symmetry applies. Consequently, the density distributions, and hence the characteristic width, of the attractive and repulsive cases are equal.

In the zero interaction case, the scattering term vanishes and the dynamics is completely governed by the semiclassical motion. The Boltzmann equation, equation (4.6), for x and y direction decouples, and each momentum eigenstate expands with its group velocity. Effectively, for each momentum eigenstate a distribution in the shape of the starting cloud moves through the system. The superposition of all momenta has maxima at finite r , so the product of the x and y distributions has the characteristic square shape, which can be seen well also in the experimental data.

For finite interaction, in the high density region a part of the ballistically moving atoms is scattered into the equilibrium distribution function, which is isotropic. This leads to diffusive instead of ballistic transport, and the resulting density distribution becomes more circular with increasing interaction strength U .

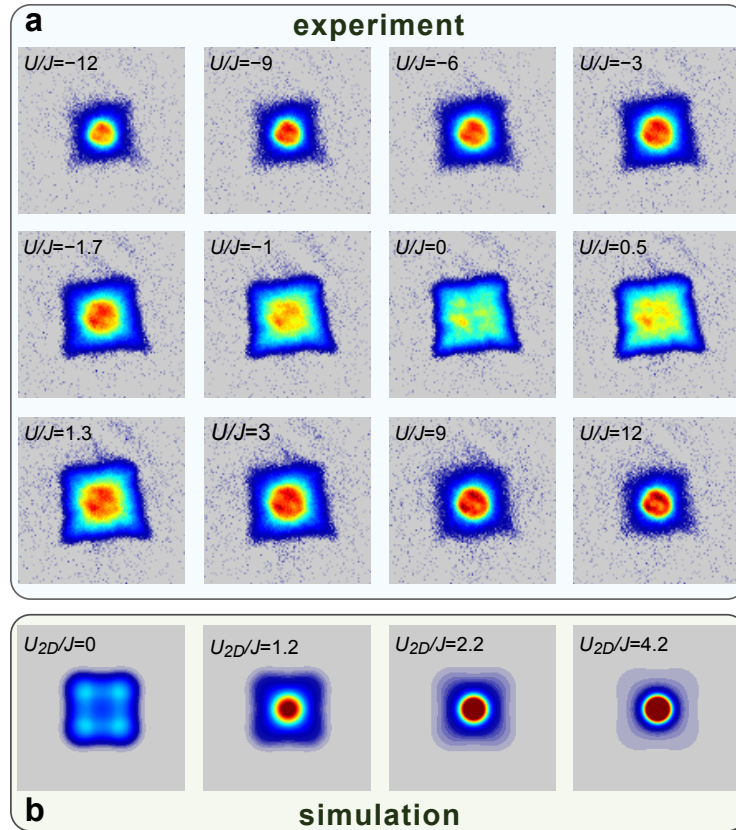


Figure 4.2: Density profiles after 25ms of expansion for different interaction strength U/J , averaged over all occupied two-dimensional layers. The experimental results look similar for positive and negative U , which can be explained by a symmetry argument (see text). At low interactions, the cloud takes a rectangular shape, while it stays ever more circular with increasing interaction. These features are reproduced well by the lattice-Boltzmann simulation (image by U. Schneider, with theoretical data by S. Mandt and the author).

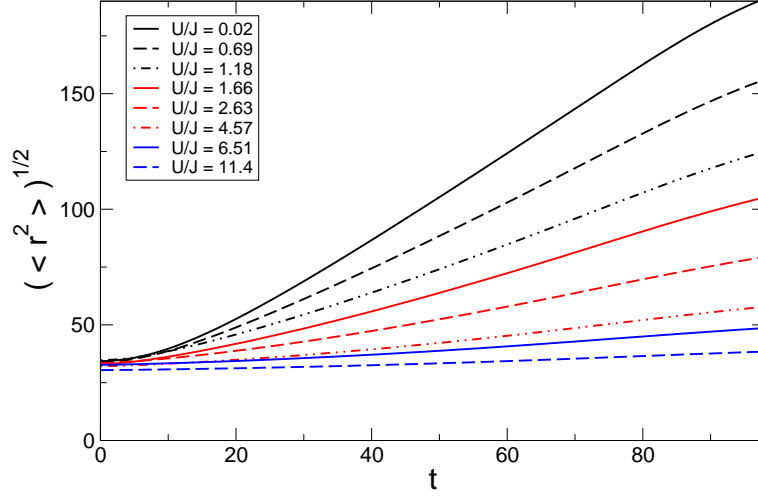


Figure 4.3: Cloud size $\sqrt{\langle r^2 \rangle}$ as a function of expansion time for various interaction strength. Initial conditions are chosen to match the experiment.

From the density profiles obtained from the numerical simulation, the second moment of the density distribution can be calculated easily. The result for various interaction strength as a function of expansion time is shown in figure 4.3. In this measure, the circular or rectangular shape of the cloud is averaged out. The expansion is fastest for vanishing interaction, and the expansion rate decreases monotonically with increasing interaction strength.

However, for a comparison with the experiment, the second moment is not suitable. It measures the characteristic width of a distribution optimally, but can not be obtained from the experimental data due to inaccuracies. In particular, it is impossible to extract the zero density bottom line from the background noise in the low density limit.

Instead of calculating the second moment, the full width at half maximum R_H is extracted from radially averaged density profiles as the characteristic width. This approach puts the focus on the core dynamics, in contrast to the second moment $\langle r^2 \rangle$, which is dominated by ballistic particles in the low density tails of the cloud.

We applied the same procedure to our numerical data to compare the widths of the experimental and theoretical profiles.

As an estimate of the expansion velocity, the *core expansion velocity* v_c is obtained by fitting the time-dependence of the characteristic width as

$$R_H(t) = \sqrt{R_H(0)^2 + v_c^2 t^2}. \quad (4.33)$$

In figure 4.4, the core expansion velocities v_c in units of $\lambda J/(2\hbar)$ as function of interaction strength U/J is shown. The experimental data comes from measurements in lattices with different depth between 7 and $12E_r$. As a function of interaction over bandwidth, which depends on the lattice depth, the velocities v_c for the different parameters lie on a single line. The maximum of the core expansion velocity lies at $U/J = 0$, the case of free expansion. At finite interactions, the expansion velocity is symmetric with respect to the sign of the interaction strength, which is due to the dynamical $U \rightarrow -U$ symmetry of the Hubbard model discussed before, and the small influence of the Hartree term. With increasing interaction strength, the core expansion velocity decays rapidly and reaches even negative values for interactions $|U/J| \gtrsim 3$. In this regime, the diffusive core dissolves by emitting ballistic particles and therefore shrinks in size.

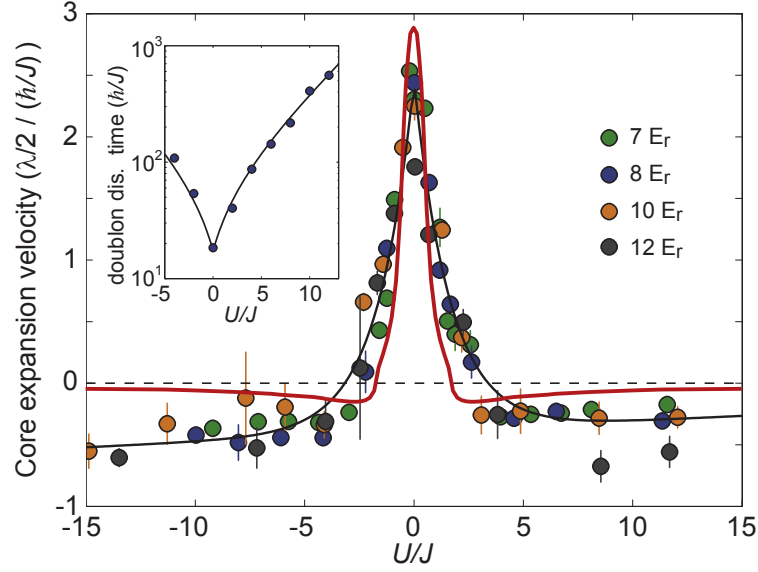


Figure 4.4: Core expansion velocities v_c of the cloud as function of the interaction strength U/J in units of lattice spacing times bandwidth $\lambda/2/(\hbar/J)$, experimental and theoretical values. The experimental results for optical lattices of different depths nicely fall onto a line (black line as guide to the eye) as function of U/J , with a pronounced peak at $U/J = 0$. In this regime the transport is ballistic and the velocities are matched well by the theoretical simulation (red line). With increasing interaction, the velocity decays rapidly, to become negative for interactions $|U| \gtrsim 3J$, the strongly diffusive regime. In the theoretical simulation the decay is faster than the experimental results, but at very high interactions, the measured velocities are stronger negative. The inset shows the measured dissolution time of double occupancies. (image by U. Schneider, with theoretical data by S. Mandt and the author).

The peak around zero interaction is matched well by the theoretical results, however, the decay of the core expansion velocity is slightly faster than in the experiment. In contrast to the experimental data, the theoretical velocities increase again for very big interactions.

Qualitatively, the numerical simulation captures all features of the experimental core expansion velocities. Quantitative discrepancies in the high interaction limit might be due to the breakdown of the relaxation rate approximation in the crossover region from diffusive to ballistic behavior, where the colliding atoms are far from equilibrium.

Uncertainties of the parameters U and J can not explain the quantitative deviations, since they are known to good accuracy. In the non-interacting case, the agreement between simulation and experiment is quiet good, apart from very long expansion times, or large clouds respectively, where inhomogeneities in the optical lattice start to play a role.

A problem could be the calculation of the scattering rate with the memory matrix formalism, which gives only a lower bound to the conductivity, and thus for the scattering rate $1/\tau$. Indeed, the experimentally observed cloud sizes are consistently bigger than the theoretically predicted ones, so an underestimation of the scattering time is probably not the main mistake. More seriously, the calculation of the conductivity is perturbative in U/J , so its validity theoretically is limited to small interactions $|U/J| \ll 4$.

The main problem of the simulation is probably the breakdown of the relaxation time description in the regime of intermediate density. In the low density regime, ballistic transport dominates, which is described well by the numerics, while the high density regime is diffusive

with a scattering rate $1/\tau$ constructed to match the diffusion constant. Despite the small size of the crossover regime, the characteristic width of the diffusive core, which mostly depends on the diffusive regime, is affected strongly by the mistakes made at intermediate densities.

Being aware of this problem, the relaxation time Boltzmann approach used in this project proves itself a useful method to model inhomogeneous time-dependent problems in ultracold atom settings.

A Calculation of Phonon Lifetime

Here the calculation of the Phonon self-energy to second order shall be carried out. The standard rules for finite temperature diagrammatic perturbation rules (see e. g. [2]) are applied. As pointed out in chapter 2, the relevant processes can be described by a single diagram with an effective vertex. In formulas, this diagram reads

$$\Pi^{\text{el-ph}}(\mathbf{q}, i\Omega) = - \sum_{\xi_n, \Delta\Omega_m} \sum_{\Delta\mathbf{q}, \mathbf{k}} (M_{\mathbf{q}, \mathbf{q}+\Delta\mathbf{q}}^{\text{eff}})^2 D^0(\mathbf{q} + \Delta\mathbf{q}, i\Omega + i\Delta\Omega_m) \times G^0(\mathbf{k} + \Delta\mathbf{q}, i\xi_n + i\Delta\Omega_m) G^0(\mathbf{k}, i\xi_n), \quad (\text{A.1})$$

where D^0 and G^0 are free Green's functions for phonons and fermions, respectively, and the minus sign in front is due to from the closed fermion loop. The sums run over all internal momenta and frequencies. For the latter, $\Delta\Omega_m$ are bosonic Matsubara frequencies and ξ_n fermionic ones.

A.1 Calculating the Imaginary Part with Branch Cuts

The Matsubara frequency sums can be transformed to real integrals by using the branch cuts of the Green's functions. For this purpose the fermionic bubble $G^0(i\xi_n + i\Delta\Omega_m)G^0(i\xi_n)$ shall be regarded as one bosonic propagator $F(i\Delta\Omega)$ (the momenta are not of concern for the moment and are dropped temporarily).

The remaining diagram contains a sum over the internal frequency $i\Delta\Omega$, in which the Green's functions D and F have branch cuts. When going from the Matsubara sum to a contour integration in the complex frequency plane, one can deform the standard Matsubara contour from vertical paths around the poles of the counting functions to horizontal paths along the branch cuts.

Since the paths run in opposite directions above and below the cut, the contribution to the real part of the integral from the two paths exactly cancels, while the imaginary part is accounted for twice, due to the opposite prefactor. For bosonic frequencies, the counting function contributes a Bose-function, for fermionic ones a Fermi-function.

In the case studied here, there is one branch cut in D^0 at $i\Delta\Omega_m = -i\Omega$ and one in F at $i\Delta\Omega_m = 0$. Thus, one can write

$$\sum_{i\Delta\Omega_m} D^0(i\Delta\Omega_m + i\Omega) F(i\Delta\Omega_m) = \int \frac{d\Delta\Omega}{\pi} (n_B(\Delta\Omega) \text{Im} [D^0(\Delta\Omega)] F(\Delta\Omega - i\Omega) + n_B(\Delta\Omega) D^0(\Delta\Omega + i\Omega) \text{Im} [F(\Delta\Omega)]), \quad (\text{A.2})$$

where in every term the respective branch cut has been shifted to $i\Delta\Omega = 0$. Now one applies the analytic continuation by replacing $i\Omega \rightarrow \Omega + i\delta$ and taking the limit $\delta \rightarrow 0^+$. To ensure

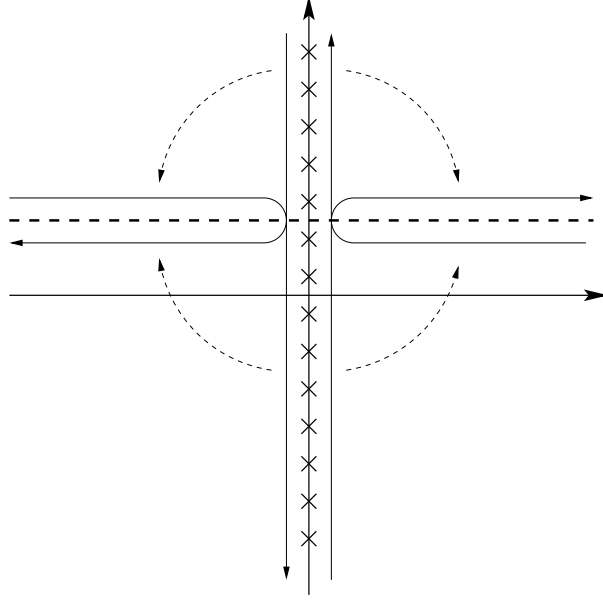


Figure A.1: Deformation of the Matsubara contour around a branch cut. The summation of the Matsubara frequencies translates into twice the integral of the imaginary part along the cut (dashed line).

to keep retarded Green's functions, in cases where the argument is $-i\Omega$ one has to take the complex conjugate at this point. Taking the imaginary part of the whole expression, one obtains

$$\text{Im} \left[\sum_{i\Delta\Omega_m} D^0(i\Delta\Omega_m + i\Omega) F(i\Delta\Omega_m) \right] = \int \frac{d\Delta\Omega}{\pi} (n_B(\Delta\Omega) - n_B(\Delta\Omega + \Omega)) \times \text{Im} [D^0(\Delta\Omega + \Omega)] \text{Im} [F(\Delta\Omega)]. \quad (\text{A.3})$$

For this expression, the frequency shift has been revoked. By the same technique the imaginary part of the auxiliary bosonic propagator $F(i\Delta\Omega) = \sum_{\xi_n} G_1^0(i\xi_n + i\Delta\Omega) G_2^0(i\xi_n)$ can be calculated. The subscripts 1, 2 are introduced to keep track of the momentum arguments. There are branch cuts at $i\xi_n = -i\Delta\Omega$ and $i\xi_n = 0$. One yields

$$\sum_{\xi_n} G_1^0(i\xi_n + i\Delta\Omega) G_2^0(i\xi_n) = \int \frac{d\xi}{\pi} (n_F(\xi) \text{Im} [G_1^0(\xi)] G_2^0(\xi - i\Delta\Omega) + n_F(\xi) G_1^0(\xi + i\Delta\Omega) \text{Im} [G_2^0(\xi)]), \quad (\text{A.4})$$

and after analytic continuation and shifting back the frequencies for the imaginary part

$$\text{Im} [F(\Delta\Omega)] = \int \frac{d\xi}{\pi} (n_F(\xi) - n_F(\xi + \Delta\Omega)) \text{Im} [G_1^0(\xi + \Delta\Omega)] \text{Im} [G_2^0(\xi)]. \quad (\text{A.5})$$

Inserting this back into (A.1), one obtains for the imaginary part of the phonon self-energy

$$\begin{aligned} \text{Im} [\Pi^{\text{el-ph}}(\mathbf{q}, \Omega)] &= \sum_{\Delta\mathbf{q}, \mathbf{k}} \int \frac{d\xi d\Delta\Omega}{\pi^2} (n_F(\xi + \Delta\Omega) - n_F(\xi)) (n_B(\Delta\Omega) - n_B(\Delta\Omega + \Omega)) \\ &\times (M_{\mathbf{q}, \mathbf{q}+\Delta\mathbf{q}}^{\text{eff}})^2 \text{Im} [D^0(\mathbf{q} + \Delta\mathbf{q}, \Delta\Omega + \Omega)] \text{Im} [G^0(\mathbf{k} + \Delta\mathbf{q}, \xi + \Delta\Omega)] \text{Im} [G^0(\mathbf{k}, \xi)]. \end{aligned} \quad (\text{A.6})$$

The frequency integrations can be done on general grounds by making use of the two latter imaginary parts of the free propagators, which are of course delta functions. This yields for $\xi = \varepsilon_k$ and for $\Delta\Omega = \varepsilon_{k+q} - \varepsilon_k$. For the whole expression one obtains

$$\begin{aligned} \text{Im} [\Pi^{\text{el-ph}}(\mathbf{q}, \Omega)] &= \sum_{\Delta\mathbf{q}, \mathbf{k}} \frac{1}{\pi^2} (n_F(\varepsilon_{k+q}) - n_F(\varepsilon_k)) (n_B(\varepsilon_{k+q} - \varepsilon_k) - n_B(\varepsilon_{k+q} - \varepsilon_k + \Omega)) \\ &\quad \times (M_{\mathbf{q}, \mathbf{q}+\Delta\mathbf{q}}^{\text{eff}})^2 \text{Im} [D^0(\mathbf{q} + \Delta\mathbf{q}, \varepsilon_{k+q} - \varepsilon_k + \Omega)]. \end{aligned} \quad (\text{A.7})$$

A.2 Low Energy Limit of Effective Vertex

In the calculation of the phonon lifetime, the effective vertex always appears squared, since the process is symmetric under time inversion. Thus, the limit of small external momentum \mathbf{q} of $(M_{\mathbf{q}, \mathbf{q}+\Delta\mathbf{q}}^{\text{eff}})^2$ is needed. The momentum enters the expression via $\Omega = v_P |\mathbf{q}|$. The square of the vertex thus reads

$$(M_{\mathbf{q}, \mathbf{q}+\Delta\mathbf{q}}^{\text{eff}})^2 = \frac{V_{\text{el-ph}}^4 \hbar^6}{4M^2 N^2 m^2 v_P^4} \frac{\mathbf{q}^2 (\mathbf{q} + \Delta\mathbf{q})^2 ((\mathbf{q} + \Delta\mathbf{q}) \cdot \mathbf{q})^2}{|\mathbf{q}| |\mathbf{q} + \Delta\mathbf{q}| |\mathbf{q} + \Delta\mathbf{q}|^4}. \quad (\text{A.8})$$

Here, the independence of $V_{\text{el-ph}}$ of the momentum has been assumed. One obtains the dominant contribution, namely the part with the lowest power of $|\Delta\mathbf{q}|$ which will later lead to the lowest power of T , as

$$(M_{\mathbf{q}, \mathbf{q}+\Delta\mathbf{q}}^{\text{eff}})^2 \approx \frac{V_{\text{el-ph}}^4 \hbar^6}{4M^2 N^2 m^2 v_P^4} \mathbf{q}^2. \quad (\text{A.9})$$

In the case of one-dimensional fermion, only the parallel component \mathbf{q}_{\parallel} of the external momentum enters the formula.

A.3 Momentum Summation for Three-Dimensional Fermions

The momentum sum is as usual evaluated as an integration. In the case of three-dimensional fermions, it can be carried out using spherical coordinates for both integration variables \mathbf{k} and $\Delta\mathbf{q}$, with the angles θ between \mathbf{k} and $\Delta\mathbf{q}$, and ϕ between $\Delta\mathbf{q}$ and \mathbf{q} . The integral reads

$$\begin{aligned} \frac{1}{\tau_q^{3D}} &= 2 \text{Im} [\Pi^{\text{el-ph}}(\mathbf{q}, \Omega)]^{3D} = \frac{2V_{\text{el-ph}}^4 \hbar^6}{M^2 m^2 v_P^4} \frac{a^6}{(2\pi)^6} \int_0^\infty d\Delta q \int_0^\infty dk \int_{-1}^1 d\eta \int_{-1}^1 d\eta' q^2 \Delta q^2 k^2 \\ &\quad \times (n_F(\varepsilon_{k+\Delta q}) - n_F(\varepsilon_k)) (n_B(\varepsilon_{k+\Delta q} - \varepsilon_k) - n_B(\varepsilon_{k+\Delta q} - \varepsilon_k + \omega_q)) \\ &\quad \times (\delta(\varepsilon_{k+\Delta q} - \varepsilon_k + \omega_q - \omega_{q+\Delta q}) - \delta(\varepsilon_{k+\Delta q} - \varepsilon_k + \omega_q + \omega_{q+\Delta q})), \end{aligned} \quad (\text{A.10})$$

with $\eta = \cos \phi$ and $\eta' = \cos \theta$. For simplification, the energies can be linearized for small values of q , Δq , and k , successively in this order. Together with the abbreviation C for the

A.4. MOMENTUM SUMMATION FOR ONE-DIMENSIONAL FERMIONS

prefactor, this yields

$$\begin{aligned} \frac{1}{\tau_q^{3D}} = C \int_0^\infty d\Delta q \int_0^\infty dk \int_{-1}^1 d\eta' \int_{-1}^1 d\eta q^2 \Delta q^2 k^2 & (n_F(\varepsilon_F + v_F k + v_F \Delta q \eta') - n_F(\varepsilon_F + v_F k)) \\ & \times (n_B(v_F \Delta q \eta') - n_B(v_F \Delta q \eta' + v_P \Delta q)) \frac{1}{v_F \Delta q} \left(\delta\left(\eta' - \frac{v_P}{v_F}\right) - \delta\left(\eta' + \frac{v_P}{v_F} \frac{q + \Delta q}{\Delta q}\right) \right). \end{aligned} \quad (A.11)$$

Again, the dominant term with the highest temperature power is the latter δ function, which produces a lower power of Δq in the integrand, leading to a higher power of temperature. Performing the integration over the angles, after some regrouping one obtains

$$\begin{aligned} \frac{1}{\tau_q^{3D}} = \frac{C q^2}{v_F} \int_0^\infty d\Delta q \Delta q & (n_B(v_P q) - n_B(v_P(2q + \Delta q))) \\ & \times \int_0^\infty dk k^2 (n_F(\varepsilon_F + v_F k + v_P(q + \Delta q)) - n_F(\varepsilon_F + v_F k)). \end{aligned} \quad (A.12)$$

The integration over k can be done now by substituting $\xi = v_F k/T$, yielding a factor of $v_P \pi^2 T^2 / (3v_F^3)(q + \Delta q)$. Thus, in the dominant contribution, the latter integral is independent of Δq . Therefore the integration over Δq , which again is done by substituting $\chi = v_P \Delta q/T$, results in a factor of $\pi^2 T / (3v_P)q$. In total the phonon lifetime in second order perturbation theory with electron-phonon interaction with three-dimensional electrons then is

$$\frac{1}{\tau_q^{3D}} = \frac{a^6}{2^6 9 \pi^2 m^2 M^2} \left(\frac{q V_{\text{el-ph}}}{v_F v_P} \right)^4 T^3. \quad (A.13)$$

A.4 Momentum Summation for One-Dimensional Fermions

In the case of scattering from one-dimensional fermions, the calculation is slightly different since the accessible phase space is smaller. In particular the result becomes dependent on the angle between the one-dimensional manifolds the fermions are confined to and the propagation direction of the phonon. The integral that must be calculated is

$$\begin{aligned} \frac{1}{\tau_q^{1D}} = 2 \text{Im} [\Pi^{\text{el-ph}}(\mathbf{q}, \Omega)]^{1D} = \frac{2 V_{\text{el-ph}}^4 \hbar^6}{M^2 m^2 v_P^4} \frac{a^4}{(2\pi)^4} \sum_{\pm} \int_0^\infty d\Delta q \int_{-\infty}^\infty dk \int_{-1}^1 d\eta' q_{\parallel}^2 \Delta q^2 \\ \times (n_F(\varepsilon_F \pm v_F k + v_F \Delta q \eta') - n_F(\varepsilon_F \pm v_F k)) (n_B(v_F \Delta q \eta') - n_B(v_F \Delta q \eta' + v_P q)) \\ \times (\delta(v_F \Delta q \eta' + v_P \Delta q - v_P |\mathbf{q} + \Delta \mathbf{q}|) - \delta(v_F \Delta q \eta' + v_P \Delta q + v_P |\mathbf{q} + \Delta \mathbf{q}|)). \end{aligned} \quad (A.14)$$

Linearization of the fermionic dispersion leads to a sum over contributions from the two Fermi-points with \pm in the arguments of the Fermi distribution. The δ -functions can be transformed to

$$\frac{1}{v_F \Delta q} \left(\left(\eta' + \frac{v_P}{v_F} - \frac{v_P}{v_F} \frac{|\mathbf{q} + \Delta \mathbf{q}|}{\Delta q} \right) - \delta \left(\eta' + \frac{v_P}{v_F} + \frac{v_P}{v_F} \frac{|\mathbf{q} + \Delta \mathbf{q}|}{\Delta q} \right) \right).$$

Clearly, for $v_F \ll v_P$, there can not be a contribution from the second term. So evaluating the η' integral yields

$$\begin{aligned} \frac{1}{\tau_q^{1D}} = & \frac{\tilde{C}}{v_F} \int_0^\infty d\Delta q \int_{-\infty}^\infty dk \Delta q q_{||}^2 (n_F(\varepsilon_F + v_F k + v_P \Delta q - v_P |\mathbf{q} + \Delta \mathbf{q}|) - n_F(\varepsilon_F + v_F k)) \\ & \times (n_B(v_P \Delta q - v_P |\mathbf{q} + \Delta \mathbf{q}|) - n_B(v_P q + v_P \Delta q - v_P |\mathbf{q} + \Delta \mathbf{q}|)). \end{aligned} \quad (\text{A.15})$$

The integration over k again can be done elementary and yields to leading order in the offset between the two Fermi functions $-v_P/(v_F)(\Delta q - |\mathbf{q} + \Delta \mathbf{q}|) \approx -v_P/(v_F)q_{||}$. By use of similar substitutions as in the case of three-dimensional fermions, the remaining Δq integral can be done, leading to the final result

$$\frac{1}{\tau_q^{1D}} = \frac{a^4 V_{\text{el-ph}}^4}{4\pi^2 m^2 M^2 v_F^2 v_P^4} q^4 T \cos^2(\phi). \quad (\text{A.16})$$

Apparently, the reduced accessible phase space of the fermions due to the lower dimensionality leads to a temperature power of one instead of three. On top of that, the lifetime becomes angle dependent, with no scattering in the direction perpendicular to the fermionic manifolds.

B Bosonization Calculations

B.1 Time-Derivatives of Currents for Spin Chain

Commutators are evaluated using the elementary relations

$$[\phi(x), \partial_{x'}\theta(x')] = i\pi\delta(x - x') \quad (\text{B.1})$$

$$[\hat{A}\hat{B}, \hat{C}] = \hat{A}[\hat{B}, \hat{C}] + [\hat{A}, \hat{C}]\hat{B} \quad (\text{B.2})$$

$$[\hat{A}, f(\hat{B})] = [\hat{A}, \hat{B}]f'(\hat{B}) \quad \text{if} \quad [[\hat{A}, \hat{B}], \hat{B}] = 0 \quad (\text{B.3})$$

$$\begin{aligned} \partial_t^U J_s &= i[J_s, H_U] = i \frac{vKg}{\pi(2\pi a)^2} \int dx \int dx' [\partial_x \theta(x), e^{i\Delta k x'} e^{i4\phi(x')} + h.c.] \\ &= i \frac{vKg}{\pi(2\pi a)^2} \int dx \int dx' (e^{i\Delta k x'} (-i\pi)\delta(x - x') 4ie^{i4\phi(x')} - h.c.) \\ &= i \frac{4vKg}{(2\pi a)^2} \int dx (e^{i\Delta k x} e^{i4\phi(x)} - h.c.) \end{aligned} \quad (\text{B.4})$$

The Umklapp time-derivative of the heat-current can be reduced to a function of that of the spin current by partial integration:

$$\begin{aligned} \partial_t^U J_H &= i[J_H, H_U] = i \frac{v^2 g}{(2\pi a)^2} \int dx \int dx' [\partial_x \theta(x), e^{i\Delta k x'} e^{i4\phi(x')} + h.c.] \partial_x \phi(x) \\ &= i \frac{v^2 g}{(2\pi a)^2} \int dx \int dx' (e^{i\Delta k x'} (-i\pi)\delta(x - x') 4ie^{i4\phi(x')} \partial_x \phi(x) + h.c.) \\ &= \frac{v^2 g}{(2\pi a)^2} \int dx (e^{i\Delta k x} (\partial_x e^{i4\phi(x)}) - h.c.) \stackrel{P.I.}{=} \frac{v^2 g}{(2\pi a)^2} \int dx ((\partial_x e^{i\Delta k x}) e^{i4\phi(x)} - h.c.) \\ &= \frac{v\Delta k}{4K} \partial_t^U J_s \end{aligned} \quad (\text{B.5})$$

$$\begin{aligned} \partial_t^{\text{dis}} J_s &= i[J_s, H_{\text{dis}}] = i \frac{vK}{2\pi^2 a} \int dx \int dx' \eta(x') [\partial_x \theta(x), ie^{i2\phi(x')} - ie^{-i\phi(x')}] \\ &= - \frac{vK}{2\pi^2 a} \int dx \int dx' \eta(x') (-i\pi)\delta(x - x') (2ie^{i2\phi(x')} - h.c.) \\ &= - \frac{vK}{\pi a} \int dx \eta(x) (e^{i2\phi(x)} + h.c.) \end{aligned} \quad (\text{B.6})$$

$$\begin{aligned} \partial_t^{\text{dis}} J_H &= i[J_H, H_{\text{dis}}] = i \frac{v^2}{2\pi a} \int dx \int dx' \eta(x') [\partial_x \theta(x), (ie^{i2\phi(x')} + h.c.)] \partial_x \phi(x) \\ &= \frac{v^2}{2a} \int dx (\partial_x e^{i2\phi(x)} - h.c.) \end{aligned} \quad (\text{B.7})$$

B.2 $4k_F$ Correlation Function

Symmetry of $4k_F$ correlation function $\Gamma(\Delta k, \omega) \sim \langle e^{i4\phi(x)} e^{-i4\phi(x')} \rangle (\Delta k, \omega)$: For small ω

$$\begin{aligned}
 \Gamma(\Delta k, \omega) &\approx -i\omega \int_{-\infty}^{\infty} dt \int_{-\infty}^{\infty} dx te^{-i\Delta kx} \Gamma(x, t) \\
 &= -i\omega \int_0^{\infty} dt \int_{-\infty}^{\infty} dx te^{-i\Delta kx} (\Gamma(x, t) - \Gamma(x, -t)) \\
 &= -i\omega \int_0^{\infty} dt \int_{-\infty}^{\infty} dx te^{-i\Delta kx} (\Gamma(x, t) - \Gamma(x, t)^*) \\
 &= -2\omega \int_0^{\infty} dt \int_{-\infty}^{\infty} dx te^{-i\Delta kx} \text{Im}(\Gamma(x, t))
 \end{aligned} \tag{B.8}$$

Since $\text{Im}\Gamma(x, t)$ is odd with respect to t , as can be seen by applying time-reversal, the integration interval can be chosen symmetric again. Inserting the correlation function

$$\langle e^{i4\phi(x)} e^{-i4\phi(x')} \rangle = e^{16\langle\phi(x)\phi(x')\rangle} = \left(\frac{(\frac{\pi T a}{v})^2}{\sinh(\frac{\pi T}{v}(x - x' + ivt)) \sinh(\frac{\pi T}{v}(x - x' - ivt))} \right)^{4K} \tag{B.9}$$

with $K = 1/2$ and substituting $s = \pi T t$ and $z = \pi T x/v$ gives the integral

$$\Gamma(\Delta k, \omega) = -\tilde{\omega} \frac{\varepsilon^2 a^2}{2v} \int_{-\infty}^{\infty} ds \int_{-\infty}^{\infty} dz se^{-i\tilde{k}z} \left(\frac{1}{\sinh^2(z + is) \sinh^2(z - is)} - h.c. \right), \tag{B.10}$$

where the abbreviations $\tilde{\omega} = \omega/(\pi T)$, $\tilde{k} = v\Delta k/(\pi T)$ and $\varepsilon = \pi T a/v$ have been introduced. To get retarded correlation functions, analytic continuation must be performed, which means in these variables sending is to $s + i\varepsilon$. This, together with another variable transformation $x_+ = z + s$ and $x_- = z - s$, yields

$$\begin{aligned}
 \Gamma &= -\tilde{\omega} \frac{\varepsilon^2 a^2}{4v} \int_{-\infty}^{\infty} dx_+ \int_{-\infty}^{\infty} dx_- (x_+ - x_-) e^{-i\tilde{k}(x_+ + x_-)/2} \left(\frac{1}{\sinh^2(x_+ + i\varepsilon) \sinh^2(x_- - i\varepsilon)} - h.c. \right) \\
 &= -\tilde{\omega} \frac{\varepsilon^2 a^2}{4v} \left(\int_{-\infty}^{\infty} dx_+ \frac{x_+ e^{-i\tilde{k}x_+/2}}{\sinh^2(x_+ + i\varepsilon)} \int_{-\infty}^{\infty} dx_- \frac{e^{-i\tilde{k}x_-/2}}{\sinh^2(x_- - i\varepsilon)} \right. \\
 &\quad \left. - \int_{-\infty}^{\infty} dx_+ \frac{e^{-i\tilde{k}x_+/2}}{\sinh^2(x_+ + i\varepsilon)} \int_{-\infty}^{\infty} dx_- \frac{x_- e^{-i\tilde{k}x_-/2}}{\sinh^2(x_- - i\varepsilon)} - h.c. \right) \\
 &= -i\tilde{\omega} \frac{\varepsilon^2 a^2}{v} ((\partial_{\tilde{k}} I_+(-\tilde{k}/2)) I_-(-\tilde{k}/2) - I_+(-\tilde{k}/2) (\partial_{\tilde{k}} I_-(-\tilde{k}/2))),
 \end{aligned} \tag{B.11}$$

with the definition of I as

$$I_{\pm}(\nu) = \int_{-\infty}^{\infty} dx \frac{e^{i\nu x}}{\sinh^2(x \pm i\varepsilon)}. \tag{B.12}$$

The latter integral can be done by contour integration. Its integrand has poles at $x = -i\varepsilon + n\pi$ with residues

$$\text{Res}_{-i\varepsilon + i n \pi} \left(\frac{e^{i\nu x}}{\sinh^2(x + i\varepsilon)} \right) = i\nu e^{\nu(\varepsilon - n\pi)}. \quad (\text{B.13})$$

For $\nu > 0$ closing the contour in the upper half plane encloses the poles at $n = 1, 2, \dots$, for $\nu < 0$ in the lower one with $n = \dots, -2, -1, 0$ yielding

$$\begin{aligned} I_+(\nu) &= \left\{ \begin{array}{l} 2\pi i \sum_{n=1}^{\infty} i\nu e^{\nu(\varepsilon - n\pi)} \\ -2\pi i \sum_{n=-\infty}^0 i\nu e^{\nu(\varepsilon - n\pi)} \end{array} \xrightarrow{\varepsilon \rightarrow 0} -2\pi|\nu| \left(\sum_{n=1}^{\infty} e^{-n\pi|\nu|} + \Theta(-\nu) \right) \right. \\ &= -2\pi|\nu| \left(\frac{1}{e^{\pi|\nu|} - 1} + \Theta(-\nu) \right) \end{aligned} \quad (\text{B.14})$$

Analogously, $I_-(\nu)$ evaluates to

$$I_-(\nu) = -2\pi|\nu| \left(\frac{1}{e^{\pi|\nu|} - 1} + \Theta(\nu) \right), \quad (\text{B.15})$$

since in this case the central pole lies in the lower plane. By introducing the symmetric function

$$f(\nu) = -2\pi|\nu| \left(\frac{1}{e^{\pi|\nu|} - 1} + \frac{1}{2} \right) \quad (\text{B.16})$$

this can be simplified to $I_{\pm}(\nu) = f(\nu) \mp \pi\nu$. Reentering the physical variables, one obtains as final result

$$\Gamma(\Delta k, \omega) = -i\omega \frac{\pi^2 a^4 \Delta k^2}{2\nu} n'_B \left(\frac{\nu \Delta k}{2} \right), \quad (\text{B.17})$$

where n'_B is the derivative of the Bose-function $n_B(\omega) = 1/(e^{\omega/T} - 1)$ with respect to the argument.

B.3 Local Correlation Functions for Disorder Memory Matrix

$$\begin{aligned} M_{ss}^{\text{dis}} &\sim i\omega D_{\text{dis}} \int dt \int dx t e^{4\langle \phi(x,t) \phi(x,0) \rangle} = i\omega D_{\text{dis}} \int dt \int dx t \left(\frac{(\frac{\pi T a}{\nu})^2}{\sinh(\pi T i t) \sinh(-\pi T i t)} \right)^K \\ &= -i\omega D_{\text{dis}} V \int dt \frac{\pi T a}{\nu} \frac{t}{\sinh(\pi T (t + ia))} = -i\omega D_{\text{dis}} V \int \frac{ds}{\pi T} \frac{\pi T a}{\nu} \frac{s}{\pi T} \frac{1}{\sinh(s + i\frac{a}{\pi T})} \\ &= -i\omega D_{\text{dis}} V \frac{\pi a}{\nu T} \end{aligned} \quad (\text{B.18})$$

In the second last step $s = \pi T t$ has been substituted. The resulting integral can be done elementary.

$$\begin{aligned} M_{HH}^{\text{dis}} &\sim i\omega D_{\text{dis}} \int dt \int dx t (-\partial_x^2) e^{4\langle \phi(x,t) \phi(x,0) \rangle} \\ &= -i\omega D_{\text{dis}} \int dt \int dx t 4 e^{4\langle \phi(x,t) \phi(x,0) \rangle} \left(4 (\partial_x \langle \phi(x,t) \phi(x,0) \rangle)^2 + \partial_x^2 \langle \phi(x,t) \phi(x,0) \rangle \right) \end{aligned} \quad (\text{B.19})$$

B.4. SUSCEPTIBILITY OF HEAT CURRENT

The first derivative of the ϕ – ϕ correlation function vanishes for $\Delta x = 0$, the second derivative for $K = 1/2$ is

$$\partial_x^2 \langle \phi(x, t) \phi(x, 0) \rangle = -\frac{1}{4} \frac{\left(\frac{\pi T}{v}\right)^2}{\sinh(\pi T i t)^2} \quad (\text{B.20})$$

This yields

$$\begin{aligned} M_{HH}^{\text{dis}} &\sim i\omega D_{\text{dis}} V \int dt a t \frac{\left(\frac{\pi T}{v}\right)^3}{\sinh(\pi T(t + ia))^3} = i\omega D_{\text{dis}} V \int \frac{ds}{\pi T} a \frac{s}{\pi T} \frac{\left(\frac{\pi T}{v}\right)^3}{\sinh(s + i\frac{a}{\pi T})^3} \\ &= i\omega D_{\text{dis}} V \frac{\pi T a \pi^2}{v^3} \frac{1}{2} \end{aligned} \quad (\text{B.21})$$

for the disorder heat current scattering rate.

B.4 Susceptibility of Heat Current

Since in the ongoing study more susceptibilities will be needed, the relatively simple heat current shall be treated as an example and be demonstrated in greater detail here. In particular, the susceptibilities of currents in the Luttinger liquid behave very similar.

$$\begin{aligned} \chi_{HH} &= \frac{1}{V} \int dx \int d\tau \langle j_H(0) j_H(\tau) \rangle \\ &= \frac{v^4}{V} \int dx \int d\tau \langle \partial_x \phi(x, 0) \partial_x \theta(x, 0) \partial_x \phi(x, \tau) \partial_x \theta(x, \tau) \rangle \\ &= \frac{v^4}{V} \int dx \int d\tau \langle \partial_x \phi(x, 0) \partial_x \phi(x, \tau) \rangle \langle \partial_x \theta(x, 0) \partial_x \theta(x, \tau) \rangle \\ &= \frac{v^4}{K^2 V} \int dx \int d\tau \langle \partial_x \phi(x, 0) \partial_x \phi(x, \tau) \rangle^2 \\ &= \frac{v^4}{K^2 V} \frac{K^2}{16} \left(\frac{\pi T}{v}\right)^4 \int dx \int d\tau \left(\frac{1}{\sinh\left(\pi T \left(\frac{x-x}{v} + i\tau\right)\right)^2} + \frac{1}{\sinh\left(\pi T \left(\frac{x-x}{v} - i\tau\right)\right)^2} \right)^2 \\ &= \frac{\pi^4 T^4}{16V} \int \frac{v d\tilde{x}}{\pi T} \int \frac{d\tilde{t}}{\pi T} \frac{2}{\sinh(\tilde{t} - i\delta)^2 \sinh(-\tilde{t} + i\delta)^2} = \frac{\pi v T^2}{3} \end{aligned} \quad (\text{B.22})$$

The entered j_H is the current density corresponding to the heat current J_H . In the last step, the volume factor $1/v$ cancels with the integration over x .

B.5 Elementary Correlation Functions for Luttinger Liquids

Here for completeness, the Luttinger liquid correlation functions and some relations are written down, which are used frequently in this thesis and can be found in any textbook about bosonization, e.g. [40]. They are typically the same for charge and spin fields, so they are just labeled by α , which can be both.

$$\langle \phi_\alpha(x, t) \phi_\alpha(0, 0) \rangle = -\frac{K_\alpha}{4} \ln \left(\frac{\sinh\left(\pi T \left(\frac{x}{v_\alpha} + t - i\delta\right)\right) \sinh\left(\pi T \left(\frac{x}{v_\alpha} - t + i\delta\right)\right)}{\left(\frac{\pi a T}{v_\alpha}\right)^2} \right) \quad (\text{B.23})$$

$$\langle \partial_x \phi_\alpha(x, t) \partial_x \phi_\alpha(0, 0) \rangle = \frac{K_\alpha}{4} \left(\frac{\pi T}{v_\alpha} \right)^2 \left(\frac{1}{\sinh(x_\alpha^+)^2} + \frac{1}{\sinh(x_\alpha^-)^2} \right) \quad (\text{B.24})$$

with the light cone variables $x_\alpha^\pm = \pi T(x/v_\alpha \pm t \mp i\delta)$. The mixed correlation function gives

$$\langle \partial_x \phi_\alpha(x, t) \partial_x \theta_\alpha(0, 0) \rangle = \frac{1}{4} \left(\frac{\pi T}{v_\alpha} \right)^2 \left(\frac{1}{\sinh(x_\alpha^+)^2} - \frac{1}{\sinh(x_\alpha^-)^2} \right). \quad (\text{B.25})$$

$$\langle \partial_x^2 \phi_\alpha(x, t) \partial_x^2 \phi_\alpha(0, 0) \rangle = \frac{K_\alpha}{2} \left(\frac{\pi T}{v_\alpha} \right)^4 \left(\frac{2 \cosh(x_\alpha^+)^2 + 1}{\sinh(x_\alpha^+)^4} + \frac{2 \cosh(x_\alpha^-)^2 + 1}{\sinh(x_\alpha^-)^4} \right), \quad (\text{B.26})$$

$$\langle \partial_x^2 \phi_\alpha(x, t) \partial_x^2 \theta_\alpha(0, 0) \rangle = \frac{1}{2} \left(\frac{\pi T}{v_\alpha} \right)^4 \left(\frac{2 \cosh(x_\alpha^+)^2 + 1}{\sinh(x_\alpha^+)^4} - \frac{2 \cosh(x_\alpha^-)^2 + 1}{\sinh(x_\alpha^-)^4} \right), \quad (\text{B.27})$$

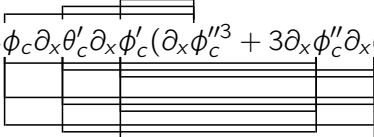
Correlation functions of θ are related to the ones above by

$$\langle \partial_x \theta_\alpha(x, t) \partial_x \theta_\alpha(0, 0) \rangle = \frac{1}{K_\alpha^2} \langle \partial_x \phi_\alpha(x, t) \partial_x \phi_\alpha(0, 0) \rangle. \quad (\text{B.28})$$

B.6 Band Curvature Corrections to Susceptibilities

$$\begin{aligned} \chi_{J_c, J_H} = & -v_c K_c \sqrt{2} \frac{1}{6\sqrt{2}m} \int dx d\tau \sum_{i=c, s} v_i^2 \left\langle \partial_x \theta_c(x, 0) \partial_x \theta_i(x, \tau) \partial_x \phi_i(x, \tau) \right. \\ & \times \int dx' d\tau' \left(\partial_{x'} \phi_c(x')^3 + 3 \partial_{x'} \phi_c(x') (\partial_{x'} \phi_s(x')^2 + \partial_{x'} \theta_s(x')^2 + \partial_{x'} \theta_c(x')^2) \right. \\ & \left. \left. + 6 \partial_{x'} \theta_c(x') \partial_{x'} \theta_s(x') \partial_{x'} \phi_s(x') \right) \right\rangle \end{aligned} \quad (\text{B.29})$$

The evaluation is done by using Wick's theorem, which requires all possible contractions of the respective expectation value. For the charge part of the heat conductivity, $i = c$, only terms containing no spin fields from the band curvature Hamiltonian have to be retained, namely

$$\langle \partial_x \phi_c \partial_x \theta_c' \partial_x \phi_c'' (\partial_x \phi_c''^3 + 3 \partial_x \phi_c'' \partial_x \theta_c''^2) \rangle \quad (\text{B.30})$$


The different dashed lines represents the respective coordinate sets of the fields. Only combinations with different coordinates within all contractions give a finite contribution. Contractions with the $\partial_x \phi_c^3$ term have multiplicity 6, those with $\partial_x \theta_c''^2$ multiplicity 2.

Due to the symmetry of the band curvature Hamiltonian, the expectation value with the spin part of the heat current has the same form, with all fields marked with one dash replaced by the corresponding spin fields. Thus the spinon contribution can be extracted from the charge part of the susceptibility, which is given by

$$\begin{aligned} \chi_{J_c, J_H}^c = & -v_c^3 K_c \sqrt{2} \frac{1}{6\sqrt{2}m} \int dx d\tau \int dx' d\tau' \\ & \times 6 \left(\langle \partial_x \phi_c \partial_x \phi_c'' \rangle \langle \partial_x \theta_c' \partial_x \phi_c'' \rangle \langle \partial_x \phi_c' \partial_x \phi_c'' \rangle + \langle \partial_x \phi_c \partial_x \phi_c'' \rangle \langle \partial_x \theta_c' \partial_x \phi_c'' \rangle \langle \partial_x \phi_c' \partial_x \theta_c'' \rangle \right. \\ & \left. + \langle \partial_x \phi_c \partial_x \theta_c'' \rangle \langle \partial_x \theta_c' \partial_x \theta_c'' \rangle \langle \partial_x \phi_c' \partial_x \phi_c'' \rangle + \langle \partial_x \phi_c \partial_x \phi_c'' \rangle \langle \partial_x \theta_c' \partial_x \phi_c'' \rangle \langle \partial_x \phi_c' \partial_x \theta_c'' \rangle \right) \end{aligned} \quad (\text{B.31})$$

B.7. CORRELATION FUNCTIONS OF UMKLAPP TIME-DERIVATIVES

Setting in the known correlation functions, the integrals can be done once more elementary, giving for the charge part $\chi_{J_c, J_H}^c = -\pi T^2 / (3m v_c)$. To get the spinon contribution, all correlation functions containing a charge field with coordinate set (x, τ) must be replaced by spin correlation functions, which in total leads to a relative factor v_c / v_s , the different prefactor already included.

Hence the total band curvature correction to χ_{J_c, J_H} is given by

$$\chi_{J_c, J_H} = \frac{\pi T^2}{3m} \left(\frac{1}{v_c} + \frac{1}{v_s} \right). \quad (\text{B.32})$$

The calculation of the other element with non-vanishing band curvature correction, $\chi_{J_c, P_{LL}}$, is very similar to the one above, since the two parts of the mode differ from their counterparts only by the missing v_α^2 . Thus the result can be easily generalized for the Luttinger liquid momentum, giving

$$\chi_{J_c, P_{LL}} = \frac{\pi T^2}{3m} \left(\frac{1}{v_c^3} + \frac{1}{v_s^3} \right) \quad (\text{B.33})$$

B.7 Correlation Functions of Umklapp Time-Derivatives

$$\begin{aligned} \langle \partial_t^U J_c \partial_t^U J_c \rangle(\omega) &= -\frac{(g_{mn_c n_s}^U)^2}{(2\pi a)^{2n_c}} 4v_c^2 K_c^2 n_c^2 \pi^2 \int_{-\infty}^{\infty} dt i\omega t \int_{-\infty}^{\infty} dx \langle (1 + \partial_x q(x))(1 + \partial_{x'} q(x')) \rangle \\ &\quad \times \left\langle \left(e^{i\Delta k x} e^{i\sqrt{2}(n_c \phi_c(x) + n_s \phi_s(x))} - h.c. \right) \left(e^{i\Delta k x'} e^{i\sqrt{2}(n_c \phi_c(x') + n_s \phi_s(x'))} - h.c. \right) \right\rangle \\ &\approx \frac{(g_{mn_c n_s}^U)^2}{(2\pi a)^{2n_c}} 8v_c^2 K_c^2 n_c^2 \pi^2 \int_{-\infty}^{\infty} dt i\omega t \int_{-\infty}^{\infty} dx e^{i\Delta k x} e^{2n_c^2 \langle \phi_c(x) \phi_c(0) \rangle} e^{2n_s^2 \langle \phi_s(x) \phi_s(0) \rangle} \end{aligned} \quad (\text{B.34})$$

For the second equality the identity (3.35) has been used. The terms containing phonon fields $q(x)$ are subleading and therefore neglected.

$$\begin{aligned} \langle \partial_t^U P_{LL} \partial_t^U P_{LL} \rangle(\omega) &= \frac{(\pi g_{mn_c n_s}^U)^2}{(2\pi a)} \int_{-\infty}^{\infty} dt i\omega t \int_{-\infty}^{\infty} dx \langle (1 + \partial_x q(x))(1 + \partial_{x'} q(x')) \rangle \\ &\quad \times \left\langle \left(e^{i\Delta k x} \left(\partial_x e^{i\sqrt{2}(n_c \phi_c(x) + n_s \phi_s(x))} \right) + h.c. \right) \left(e^{i\Delta k x'} \left(\partial_{x'} e^{i\sqrt{2}(n_c \phi_c(x') + n_s \phi_s(x'))} \right) + h.c. \right) \right\rangle \\ &\approx \frac{2(\pi g_{mn_c n_s}^U)^2}{(2\pi a)} \int_{-\infty}^{\infty} dt i\omega t \int_{-\infty}^{\infty} dx e^{i\Delta k(x-x')} \partial_x \partial_{x'} \left\langle e^{2n_c^2 \langle \phi_c(x) \phi_c(x') \rangle} e^{2n_s^2 \langle \phi_s(x) \phi_s(x') \rangle} \right\rangle \\ &\stackrel{PI}{=} \frac{2(\pi g_{mn_c n_s}^U)^2}{(2\pi a)} \int_{-\infty}^{\infty} dt i\omega t \int_{-\infty}^{\infty} dx (-\Delta k^2) e^{i\Delta k(x-x')} \left\langle e^{2n_c^2 \langle \phi_c(x) \phi_c(x') \rangle} e^{2n_s^2 \langle \phi_s(x) \phi_s(x') \rangle} \right\rangle \\ &= \frac{\Delta k^2}{4v_c^2 K_c^2 n_c^2} \langle \partial_t^U J_c \partial_t^U J_c \rangle(\omega) \end{aligned} \quad (\text{B.35})$$

Again the terms with phonon fields are neglected. By partial integration, the auto-correlation function of the time-derivative of the Luttinger liquid momentum turns out to be up to a

prefactor the same as the one of the charge current. The same holds, with only one partial integration, for the cross-correlation function of the two:

$$\langle \partial_t^U J_c \partial_t^U P_{LL} \rangle(\omega) = \frac{\Delta k}{2v_c K_c n_c} \langle \partial_t^U J_c \partial_t^U J_c \rangle(\omega) \quad (\text{B.36})$$

$$\begin{aligned} \langle \partial_t^U J_H \partial_t^U J_H \rangle(\omega) &= \frac{(\pi g_{mn_c n_s}^U)^2}{(2\pi a)^{2n_c}} \int_{-\infty}^{\infty} dt i\omega t \int_{-\infty}^{\infty} dx \langle (1 + \partial_x q(x))(1 + \partial_{x'} q(x')) \rangle \\ &\times \left\langle \left(e^{i\Delta k x} \left(v_c^2 \left(\partial_x e^{i\sqrt{2}n_c \phi_c(x)} \right) e^{i\sqrt{2}n_s \phi_s(x)} + v_s^2 \left(e^{i\sqrt{2}n_c \phi_c(x)} \left(\partial_x e^{i\sqrt{2}n_s \phi_s(x)} \right) \right) + h.c. \right) \right. \right. \\ &\times \left. \left(e^{i\Delta k x'} \left(v_c^2 \left(\partial_{x'} e^{i\sqrt{2}n_c \phi_c(x')} \right) e^{i\sqrt{2}n_s \phi_s(x')} + v_s^2 \left(e^{i\sqrt{2}n_c \phi_c(x')} \left(\partial_{x'} e^{i\sqrt{2}n_s \phi_s(x')} \right) \right) + h.c. \right) \right) \right\rangle \\ &\approx -\frac{2(\pi g_{mn_c n_s}^U)^2}{(2\pi a)^{2n_c}} \int_{-\infty}^{\infty} dt i\omega t \int_{-\infty}^{\infty} dx e^{i\Delta k(x-x')} \left(v_c^4 \left(\partial_x^2 e^{2n_c^2 \langle \phi_c(x) \phi_c(x') \rangle} \right) e^{i2n_s^2 \langle \phi_s(x) \phi_s(x') \rangle} \right. \\ &\quad + 2v_c^2 v_s^2 \left(\partial_x e^{2n_c^2 \langle \phi_c(x) \phi_c(x') \rangle} \right) \left(\partial_x e^{2n_s^2 \langle \phi_s(x) \phi_s(x') \rangle} \right) \\ &\quad \left. + v_s^4 e^{i2n_c^2 \langle \phi_c(x) \phi_c(x') \rangle} \left(\partial_x^2 e^{2n_s^2 \langle \phi_s(x) \phi_s(x') \rangle} \right) \right) \end{aligned} \quad (\text{B.37})$$

$$\begin{aligned} \langle \partial_t^U P_{LL} \partial_t^U J_H \rangle(\omega) &= \frac{(\pi g_{mn_c n_s}^U)^2}{(2\pi a)^{2n_c}} \int_{-\infty}^{\infty} dt i\omega t \int_{-\infty}^{\infty} dx \left\langle \left(e^{i\Delta k x} \left(\partial_x e^{i\sqrt{2}(n_c \phi_c(x) + n_s \phi_s(x))} \right) + h.c. \right) \right. \\ &\times \left. \left(e^{i\Delta k x'} \left(v_c^2 \left(\partial_{x'} e^{i\sqrt{2}n_c \phi_c(x')} \right) e^{i\sqrt{2}n_s \phi_s(x')} + v_s^2 \left(e^{i\sqrt{2}n_c \phi_c(x')} \left(\partial_{x'} e^{i\sqrt{2}n_s \phi_s(x')} \right) \right) + h.c. \right) \right) \right\rangle \\ &= \frac{2(\pi g_{mn_c n_s}^U)^2}{(2\pi a)^{2n_c}} \int_{-\infty}^{\infty} dt i\omega t \int_{-\infty}^{\infty} dx e^{i\Delta k(x-x')} \left(v_c^2 \left(\partial_x^2 e^{2n_c^2 \langle \phi_c(x) \phi_c(x') \rangle} \right) e^{2n_s^2 \langle \phi_s(x) \phi_s(x') \rangle} \right. \\ &\quad + (v_c^2 + v_s^2) \left(\partial_x e^{2n_c^2 \langle \phi_c(x) \phi_c(x') \rangle} \right) \left(\partial_x e^{2n_s^2 \langle \phi_s(x) \phi_s(x') \rangle} \right) \\ &\quad \left. + v_s^2 \left(e^{2n_c^2 \langle \phi_c(x) \phi_c(x') \rangle} \right) \left(\partial_x^2 e^{2n_s^2 \langle \phi_s(x) \phi_s(x') \rangle} \right) \right) \end{aligned} \quad (\text{B.38})$$

$$\begin{aligned} \langle \partial_t^U J_c \partial_t^U J_H \rangle(\omega) &= -i \frac{2(\pi g_{mn_c n_s}^U)^2 v_c K_c n_c}{(2\pi a)^{2n_c}} \int_{-\infty}^{\infty} dt i\omega t \int_{-\infty}^{\infty} dx \langle (1 + \partial_x q(x))(1 + \partial_{x'} q(x')) \rangle \\ &\times \left\langle \left(e^{i\Delta k x} e^{i\sqrt{2}(n_c \phi_c(x) + n_s \phi_s(x))} - h.c. \right) \left(e^{i\Delta k x'} \left(v_c^2 \left(\partial_{x'} e^{i\sqrt{2}n_c \phi_c(x')} \right) e^{i\sqrt{2}n_s \phi_s(x')} \right. \right. \right. \\ &\quad \left. \left. + v_s^2 \left(e^{i\sqrt{2}n_c \phi_c(x')} \left(\partial_{x'} e^{i\sqrt{2}n_s \phi_s(x')} \right) \right) + h.c. \right) \right) \right\rangle \\ &\approx \frac{4(\pi g_{mn_c n_s}^U)^2 v_c K_c n_c}{(2\pi a)^{2n_c}} \int_{-\infty}^{\infty} dt i\omega t \int_{-\infty}^{\infty} dx e^{i\Delta k(x-x')} \left(v_c^2 \left(\partial_x e^{2n_c^2 \langle \phi_c(x) \phi_c(x') \rangle} \right) e^{2n_s^2 \langle \phi_s(x) \phi_s(x') \rangle} \right. \\ &\quad \left. + v_s^2 e^{2n_c^2 \langle \phi_c(x) \phi_c(x') \rangle} \left(\partial_x e^{2n_s^2 \langle \phi_s(x) \phi_s(x') \rangle} \right) \right) \end{aligned} \quad (\text{B.39})$$

B.8 Calculation of Phonon Propagator

For taking into account the interaction between three-dimensional phonons in the one-dimensional system, the radial part of the phonon propagator is needed in its real space representation. Starting from the momentum space representation of the time-ordered correlation function, which reads for positive times

$$G_P^{3D}(\mathbf{k}, t) = \frac{1}{|\mathbf{k}|} \left(n_{\mathbf{k}} e^{i v_P |\mathbf{k}| t} + (1 + n_{\mathbf{k}}) e^{-i v_P |\mathbf{k}| t} \right), \quad (\text{B.40})$$

the Fourier transform can be done using spherical coordinates,

$$\begin{aligned} G_P(r, t) &= \int_0^\infty dk k^2 \left(\int_{-1}^1 e^{i k r \eta} d\eta \right) \frac{1}{k} \left(n_{\mathbf{k}} e^{i v_P k t} + (1 + n_{\mathbf{k}}) e^{-i v_P k t} \right) \\ &= \int_0^\infty dk \frac{1}{i r} (e^{i k r} - e^{-i k r}) \left(n_{\mathbf{k}} e^{i v_P k t} + (1 + n_{\mathbf{k}}) e^{-i v_P k t} \right) \end{aligned} \quad (\text{B.41})$$

The time argument of the correlation function is already in real time, but for simplicity the infinitesimal shift into the complex plane are suppressed during the calculation and entered at the end. Making use of an elementary identity for the Bose function,

$$1 + n_{\mathbf{k}} = n_{-\mathbf{k}}, \quad (\text{B.42})$$

and changing labels $\mathbf{k} \rightarrow -\mathbf{k}$ in the second part, the integral transforms to

$$G_P(r, t) = \frac{1}{i r} \int_{-\infty}^{\infty} dk \frac{1}{e^{v_P k / T} - 1} \left(e^{i k(r + v_P t)} - e^{-i k(r - v_P t)} \right) \quad (\text{B.43})$$

One obtains an Bose function without mod to Fourier transform with respect to $\xi_+ = r + v_P t$ and $\xi_- = -r + v_P t$, which is not zero for $\mathbf{k} \rightarrow -\infty$, but -1 . This can be done by splitting the integral into the Fourier transform of $-\theta(-\mathbf{k})$ and

$$\int_{-\infty}^{\infty} dk \left(\frac{1}{e^{v_P k / T} - 1} + \theta(-k) \right) e^{i k \xi_{\pm}}. \quad (\text{B.44})$$

The latter integral is the Fourier transform of an odd function of \mathbf{k} , thus only the imaginary part of the exponential must be retained, and the integral is twice the integral over the positive part of the integration interval. The remaining integral can be done elementary:

$$\int_0^\infty dk \frac{1}{e^{v_P k / T} - 1} \sin(k \xi_{\pm}) = \frac{1}{2} \left(-\frac{1}{\xi_{\pm}} + \frac{\pi T}{v_P} \coth \left(\frac{\pi T}{v_P} \xi_{\pm} \right) \right) \quad (\text{B.45})$$

The terms $1/\xi_{\pm}$ cancel exactly with the Fourier transform of the theta function which is still missing, giving in total for the phonon propagator along the chains

$$G_P(r, t) = \frac{1}{r} \frac{\pi T}{v_P} \left(\coth \left(\pi T \left(\frac{r}{v_P} + t \right) \right) - \coth \left(\pi T \left(-\frac{r}{v_P} + t \right) \right) \right). \quad (\text{B.46})$$

The time-argument t is related to the complex time by $it = \tau$, so the retarded correlation function is obtained by replacing t with $t - i\epsilon \text{sign}(t)$, where $\epsilon = 0^+$.

B.9 Calculation of Band-Curvature Memory Matrix

The correlation function for the single finite element of the BC memory matrix is given by

$$\begin{aligned} \langle \partial_t^{\text{BC}} J_H \partial_t^{\text{BC}} J_H \rangle(\omega) &= \frac{(v_c^2 - v_s^2)^2}{16m^2} \int dt i\omega t \int dx \\ &\times \left(\langle \partial_x^2 \phi_c(x) \partial_x^2 \phi_c(0) \rangle \langle ((\partial_x \phi_s(x))^2 + (\partial_x \theta_s(x))^2) ((\partial_x \phi_s(0))^2 + (\partial_x \theta_s(0))^2) \rangle \right. \\ &\quad + 4 \langle \partial_x^2 \theta_c(x) \partial_x^2 \theta_c(0) \rangle \langle \partial_x \phi_s(x) \partial_x \theta_s(x) \partial_x \phi_s(0) \partial_x \theta_s(0) \rangle \\ &\quad \left. + 4 \langle \partial_x^2 \phi_c(x) \partial_x^2 \theta_c(0) \rangle \langle ((\partial_x \phi_s(x))^2 + (\partial_x \theta_s(x))^2) \partial_x \phi_s(0) \partial_x \theta_s(0) \rangle \right). \quad (\text{B.47}) \end{aligned}$$

Here the arguments of the fields are combined variables of x and t . Also derivatives like $\partial_x \theta_s(0)$ are shorthand for first differentiating the field with respect to its spatial variable, and then setting it to zero.

The expectation values in the spin sector simplify by use of Wick's theorem to

$$\begin{aligned} &\langle ((\partial_x \phi_s(x))^2 + (\partial_x \theta_s(x))^2) ((\partial_x \phi_s(0))^2 + (\partial_x \theta_s(0))^2) \rangle \\ &= 2 \langle \partial_x \phi_s(x) \partial_x \phi_s(0) \rangle^2 \left(1 + \frac{1}{K_s^4} \right) + 4 \langle \partial_x \phi_s(x) \partial_x \theta_s(x) \rangle^2 \quad (\text{B.48}) \end{aligned}$$

$$\begin{aligned} &\langle \partial_x \phi_s(x) \partial_x \theta_s(x) \partial_x \phi_s(0) \partial_x \theta_s(0) \rangle \\ &= \frac{1}{K_s^2} \langle \partial_x \phi_s(x) \partial_x \phi_s(0) \rangle^2 + \langle \partial_x \phi_s(x) \partial_x \theta_s(0) \rangle^2 \quad (\text{B.49}) \end{aligned}$$

$$\begin{aligned} &\langle (\partial_x \phi_s(x)^2 + \partial_x \theta_s(x)^2) \partial_x \phi_s(0) \partial_x \theta_s(0) \rangle \\ &= \left(1 + \frac{1}{K_s^2} \right) \langle \partial_x \phi_s(x) \partial_x \phi_s(0) \rangle \langle \partial_x \phi_s(x) \partial_x \theta_s(0) \rangle \quad (\text{B.50}) \end{aligned}$$

From the definition of the correlation functions $\langle \partial_x \phi_s(x) \partial_x \phi_s(0) \rangle$ and $\langle \partial_x \phi_s(x) \partial_x \theta_s(0) \rangle$, see B.5, it can be seen easily that they can be written in left- and right-moving fields, usually referred to as *chiral fields*, as

$$\langle \partial_x \phi_s(x) \partial_x \phi_s(0) \rangle = K_s (\langle \partial_x \phi_L(x) \partial_x \phi_L(0) \rangle + \langle \partial_x \phi_R(x) \partial_x \phi_R(0) \rangle) \quad (\text{B.51})$$

$$\langle \partial_x \phi_s(x) \partial_x \theta_s(0) \rangle = (\langle \partial_x \phi_L(x) \partial_x \phi_L(0) \rangle - \langle \partial_x \phi_R(x) \partial_x \phi_R(0) \rangle). \quad (\text{B.52})$$

with

$$\langle \partial_x \phi_{L/R}(x) \partial_x \phi_{L/R}(0) \rangle = \frac{1}{4} \left(\frac{\pi T}{v_s} \right)^2 \frac{1}{\sinh(x_s^{+/-})^2}. \quad (\text{B.53})$$

The chiral fields are related to the usual ones by $\phi_R = K_c \theta_c - \phi_c$ and $\phi_L = K_c \theta_c$. They can also be obtained by rescaling the fields $\phi_c \rightarrow K_c^{1/2} \phi_c$ and $\theta_c \rightarrow K_c^{-1/2} \theta_c$, which is equivalent to a Bogoliubov transformation of the Hamiltonian. The rescaled Hamiltonian has $\tilde{K} = 1$, which is the analogon of free fields, implying the separation of left- and right-movers, see e.g. [40].

Thus, after using the identity $\langle \partial_x \theta_\alpha \partial_x \theta_\alpha \rangle = \langle \partial_x \phi_\alpha \partial_x \phi_\alpha \rangle / K_\alpha^2$, one obtains for the complete integrand of equation B.47

$$\begin{aligned} &\langle \partial_x^2 \phi_c \partial_x^2 \phi_c \rangle \left(2 \left(1 + \frac{1}{K_s^4} + \frac{2}{K_s^2 K_c^2} \right) \langle \partial_x \phi_s \partial_x \phi_s \rangle^2 + 4 \left(1 + \frac{1}{K_c^2} \right) \langle \partial_x \phi_s \partial_x \theta_s \rangle^2 \right) \\ &+ \langle \partial_x^2 \phi_c \partial_x^2 \theta_c \rangle 4 \left(1 + \frac{1}{K_c^2} \right) \langle \partial_x \phi_s \partial_x \phi_s \rangle \langle \partial_x \phi_s \partial_x \theta_s \rangle \quad (\text{B.54}) \end{aligned}$$

B.9. CALCULATION OF BAND-CURVATURE MEMORY MATRIX

For symmetry reasons, only terms proportional to a product of a left- and a right-mover correlation function in the spin sector give a finite contribution.

In the first term, the contribution from $\langle \partial_x \phi_s \partial_x \phi_s \rangle^2$ is $2K_s^2 \langle \partial_x \phi_L \partial_x \phi_L \rangle \langle \partial_x \phi_R \partial_x \phi_R \rangle$, the second term produces the same but with a minus sign and no K_s^2 in front, and the last term due to its mixed product gives no contribution. One obtains

$$\langle \partial_x^2 \phi_c \partial_x^2 \phi_c \rangle \left(\left(4 + \frac{4}{K_s^4} + \frac{8}{K_c^2 K_s^2} \right) K_s^2 - \left(8 + \frac{8}{K_c^2} \right) \right) \langle \partial_x \phi_L \partial_x \phi_L \rangle \langle \partial_x \phi_R \partial_x \phi_R \rangle \quad (\text{B.55})$$

As the two terms containing K_c^2 cancel, one finds as final result for the auto correlation function of the band curvature time derivative of the the heat current

$$\begin{aligned} \langle \partial_t^{\text{BC}} J_H \partial_t^{\text{BC}} J_H \rangle (\omega) &= i\omega \frac{(v_c^2 - v_s^2)^2}{16m^2} \left(K_s^2 + \frac{1}{K_s^2} - 2 \right) \int dt \int dx \\ &\quad \times \langle \partial_x^2 \phi_c \partial_x^2 \phi_c \rangle \langle \partial_x \phi_L \partial_x \phi_L \rangle \langle \partial_x \phi_R \partial_x \phi_R \rangle \end{aligned} \quad (\text{B.56})$$

Inserting the definitions of the correlation functions and scaling out the temperature dependence from the integral, one obtains for the memory matrix element

$$M_{J_h, J_H}^{\text{BC}} = \frac{(v_c^2 - v_s^2)^2}{v_c^4 v_s^4} v_c K_c \left(K_s^2 + \frac{1}{K_s^2} - 2 \right) \frac{\pi^8 T^8}{32m^2} B \left(\frac{v_s}{v_c} \right), \quad (\text{B.57})$$

with the dimensionless integral

$$B(\lambda) = \int_0^\infty dt \int_{-\infty}^\infty dx t \text{Im} \left(\frac{2 + \cosh(x + t - i\delta)^2}{\sinh(x + t - i\delta)^4} \frac{1}{\sinh(x\lambda + t - i\delta)^2 \sinh(x\lambda - t + i\delta)^2} \right), \quad (\text{B.58})$$

which can be computed numerically for several cutoffs δ , to obtain the limit δ to zero by extrapolation.

C Appendices for Expanding Cloud

C.1 Experimental Parameters

The following parameters have been used in the different runs in the experiment:

| U/D_0 | b_0/D_0 | β^0/D_0 |
|---------|-----------|---------------|
| 0.015 | 18.9088 | 0.148521 |
| 0.693 | 18.4573 | 0.152064 |
| 1.178 | 19.3808 | 0.144987 |
| 1.245 | 19.2025 | 0.146302 |
| 1.663 | 17.36 | 0.159007 |
| 2.214 | 19.2634 | 0.14585 |
| 2.632 | 17.9512 | 0.156238 |
| 4.152 | 18.5231 | 0.151537 |
| 4.570 | 16.4521 | 0.170045 |
| 6.091 | 20.0344 | 0.14036 |
| 6.508 | 17.0967 | 0.163825 |
| 8.029 | 21.2687 | 0.132379 |
| 9.967 | 20.6544 | 0.136232 |
| 11.354 | 14.6795 | 0.189815 |

C.2 Error Estimate for Low-Density Limit

The inverse temperatures in the experiment are close to zero, thus a high temperature expansion of the distribution functions may be used. The particle number with Maxwell-Boltzmann statistics is

$$n_{MB}(z, \beta) = \int d\mathbf{k} z e^{-\beta \epsilon(\mathbf{k})} \approx z \int d\mathbf{k} e^0 = z \quad (\text{C.1})$$

Using the Fermi-Dirac statistics, one obtains in the same limit

$$n_{FD}(z, \beta) = \int d\mathbf{k} \frac{1}{e^{\beta \epsilon(\mathbf{k})}/z + 1} \approx \int d\mathbf{k} \frac{z}{e^0 + z} = \frac{z}{1+z} \quad (\text{C.2})$$

Thus by using the Maxwell-Boltzmann distribution function instead of the Fermi-Dirac, one makes a relative error of

$$\Delta n = \frac{n_{FD}(z, \beta) - n_{MB}(z, \beta)}{n_{FD}(z, \beta)} \approx \frac{\frac{z}{1+z} - z}{\frac{z}{1+z}} = z \quad (\text{C.3})$$

For the relative error $\Delta \epsilon$ of the energy, the same calculation applies, with a remaining integral over the energy remaining in both expressions. Thus $\Delta \epsilon \approx z$ is valid analogously.

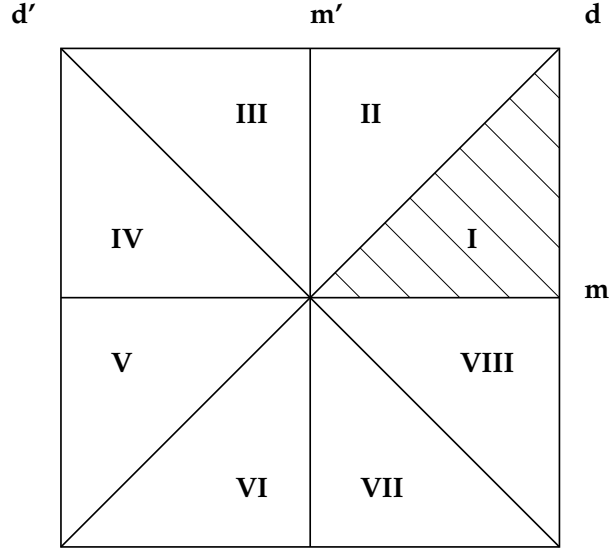


Figure C.1: Symmetry group of a plain square. There are eight equivalent sectors, connected by rotations by multiples of $\pi/2$ and reflections with respect to the four depicted axes

C.3 Symmetries of the System

The symmetry group of the two-dimensional simple cubic lattice combined with a rotational invariant trap is that of a square.

It contains the rotations C_n by multiples of $\pi/2$ and reflections M, M' and D, D' with respect to the four symmetry axes, i.e. the m and m' axes plus the diagonals d and d' , see figure C.1. Practically, the distribution function of the whole system can be constructed from the simulated wedge by applying only reflections. The table below shows how for each sector the distribution function is related to the one of sector I.

| sector | symmetry operation | p_x | p_y |
|--------|----------------------|--------|--------|
| II | D | p_y | p_x |
| III | $M' \circ D$ | $-p_y$ | p_x |
| IV | M' | $-p_x$ | p_y |
| V | $M \circ M'$ | $-p_x$ | $-p_y$ |
| VI | $D \circ M \circ M'$ | $-p_y$ | $-p_x$ |
| VII | $D' \circ M$ | p_y | $-p_x$ |
| VIII | M | p_x | $-p_y$ |

C.4 Scattering Rate

C.4.1 Time-Derivative of Currents

$$\partial_t J_i = i [J, H^{\text{int}}] = i \sum_{p, \sigma} f_i(p) U \sum_{k, k', q} \left[c_{p\sigma}^\dagger c_{p\sigma}, c_{k+q\uparrow}^\dagger c_{k\uparrow} c_{k'-q\downarrow}^\dagger c_{k'\downarrow} \right] \quad (\text{C.4})$$

The contained commutator is equal to

$$\left[c_{p\sigma}^\dagger c_{p\sigma}, c_{k+q\uparrow}^\dagger c_{k\uparrow} \right] c_{k'-q\downarrow}^\dagger c_{k'\downarrow} + c_{k+q\uparrow}^\dagger c_{k\uparrow} \left[c_{p\sigma}^\dagger c_{p\sigma}, c_{k'-q\downarrow}^\dagger c_{k'\downarrow} \right] \quad (\text{C.5})$$

With the elementary commutator

$$\left[c_{p\sigma}^\dagger c_{p\sigma}, c_{k+q\sigma'}^\dagger c_{k\sigma'} \right] = \delta_{\sigma,\sigma'} \delta_{p,k+q} c_{k+q\sigma}^\dagger c_{k\sigma} - \delta_{\sigma,\sigma'} \delta_{p,k} c_{k+q\sigma'}^\dagger c_{k\sigma} \quad (\text{C.6})$$

the time derivative of the current evaluates by performing two sums over Kronecker-deltas to

$$\partial_t J_i = iU \sum_{q,k,k'} (f_i(\mathbf{k} + \mathbf{q}) - f_i(\mathbf{k}) + f_i(\mathbf{k}' - \mathbf{q}) - f_i(\mathbf{k}')) c_{k+q\uparrow}^\dagger c_{k\uparrow} c_{k'-q\downarrow}^\dagger c_{k'\downarrow} \quad (\text{C.7})$$

C.4.2 Real Time Correlation Function

$$\begin{aligned} \langle \partial_t J_i; \partial_t J_j \rangle(\omega) &= \int dt e^{i\omega t} (-i\theta(t)) \langle [\partial_t J_i(t), \partial_t J_j(0)] \rangle \\ &= \int dt e^{i\omega t} (-i\theta(t)) \left\langle e^{-iH^{\text{kin}}t} (\partial_t J_i) e^{iH^{\text{kin}}t} (\partial_t J_j) - (\partial_t J_j) e^{-iH^{\text{kin}}t} (\partial_t J_i) e^{iH^{\text{kin}}t} \right\rangle \\ &= iU^2 \int dt e^{i\omega t} \theta(t) \sum_{q,k,k'} \sum_{\tilde{q},\tilde{k},\tilde{k}'} (g_i(\mathbf{k} + \mathbf{q}) - g_i(\mathbf{k}) + g_i(\mathbf{k}' - \mathbf{q}) - g_i(\mathbf{k}')) \\ &\quad \times (g_j(\tilde{\mathbf{k}} + \tilde{\mathbf{q}}) - g_j(\tilde{\mathbf{k}}) + g_j(\tilde{\mathbf{k}}' - \tilde{\mathbf{q}}) - g_j(\tilde{\mathbf{k}}')) \\ &\quad \times \left(e^{-i\varepsilon_0 t} \left\langle c_{k+q\uparrow}^\dagger c_{k\uparrow} c_{k'-q\downarrow}^\dagger c_{k'\downarrow} e^{iH^{\text{kin}}t} c_{\tilde{k}+\tilde{q}\uparrow}^\dagger c_{\tilde{k}\uparrow} c_{\tilde{k}'-\tilde{q}\downarrow}^\dagger c_{\tilde{k}'\downarrow} \right\rangle \right. \\ &\quad \left. - e^{i\varepsilon_0 t} \left\langle c_{\tilde{k}+\tilde{q}\uparrow}^\dagger c_{\tilde{k}\uparrow} c_{\tilde{k}'-\tilde{q}\downarrow}^\dagger c_{\tilde{k}'\downarrow} e^{-iH^{\text{kin}}t} c_{k+q\uparrow}^\dagger c_{k\uparrow} c_{k'-q\downarrow}^\dagger c_{k'\downarrow} \right\rangle \right) \end{aligned} \quad (\text{C.8})$$

Since H^{kin} is diagonal in the c_k^\dagger , the eigenvalues in the last two lines can be read of directly as

$$e^{i(\varepsilon_0 - \varepsilon_{\tilde{k}'} + \varepsilon_{\tilde{k}'-\tilde{q}} - \varepsilon_{\tilde{k}} + \varepsilon_{\tilde{k}+\tilde{q}})t} \left\langle c_{k+q\uparrow}^\dagger c_{k\uparrow} c_{k'-q\downarrow}^\dagger c_{k'\downarrow} c_{\tilde{k}+\tilde{q}\uparrow}^\dagger c_{\tilde{k}\uparrow} c_{\tilde{k}'-\tilde{q}\downarrow}^\dagger c_{\tilde{k}'\downarrow} \right\rangle \quad (\text{C.9})$$

and

$$e^{-i(\varepsilon_0 - \varepsilon_{k'} + \varepsilon_{k'-q} - \varepsilon_k + \varepsilon_{k+q})t} \left\langle c_{\tilde{k}+\tilde{q}\uparrow}^\dagger c_{\tilde{k}\uparrow} c_{\tilde{k}'-\tilde{q}\downarrow}^\dagger c_{\tilde{k}'\downarrow} c_{k+q\uparrow}^\dagger c_{k\uparrow} c_{k'-q\downarrow}^\dagger c_{k'\downarrow} \right\rangle \quad (\text{C.10})$$

The expectation values can be evaluated using Wick's theorem. The two are identical by exchanging all momenta with and without \sim .

$$\langle \dots \rangle = \delta_{k+q,\tilde{k}} \tilde{f}_{\tilde{k}\uparrow} \delta_{k,\tilde{k}+\tilde{q}} (1 - f_{k\uparrow}) \delta_{k'-q,\tilde{k}'} \tilde{f}_{\tilde{k}'\downarrow} \delta_{k',\tilde{k}'-\tilde{q}} (1 - f_{k'\downarrow}) \quad (\text{C.11})$$

For the other term emerging from the Wick decoupling, the prefactor in the sum vanishes and it can be dropped. Inserting this back into the correlation function, one obtains

$$\begin{aligned} \langle \partial_t J_i; \partial_t J_j \rangle(\omega) &= iU^2 \int dt e^{i\omega t} \theta(t) \sum_{q,k,k'} \sum_{\tilde{q},\tilde{k},\tilde{k}'} \left(e^{i(\varepsilon_0 - \varepsilon_{\tilde{k}'} + \varepsilon_{\tilde{k}'-\tilde{q}} - \varepsilon_{\tilde{k}} + \varepsilon_{\tilde{k}+\tilde{q}})t} - h.c. \right) \\ &\quad \times (g_i(\tilde{\mathbf{k}} + \tilde{\mathbf{q}}) - g_i(\tilde{\mathbf{k}}) + g_i(\tilde{\mathbf{k}}' - \tilde{\mathbf{q}}) - g_i(\tilde{\mathbf{k}}')) (g_j(\mathbf{k} + \mathbf{q}) - g_j(\mathbf{k}) + g_j(\mathbf{k}' - \mathbf{q}) - g_j(\mathbf{k}')) \\ &\quad \times \delta_{k+q,\tilde{k}} \tilde{f}_{\tilde{k}\uparrow} \delta_{k,\tilde{k}+\tilde{q}} \delta_{k'-q,\tilde{k}'} \delta_{k',\tilde{k}'-\tilde{q}} \tilde{f}_{\tilde{k}'\downarrow} (1 - f_{k\uparrow}) \tilde{f}_{\tilde{k}'\downarrow} (1 - f_{k'\downarrow}) \end{aligned} \quad (\text{C.12})$$

The time integration has the simple structure

$$i \int dt e^{i\omega t} \theta(t) (e^{i\Delta\varepsilon t} - e^{-i\Delta\varepsilon t}) \quad (\text{C.13})$$

C.4. SCATTERING RATE

of which only the imaginary part is needed.

$$\begin{aligned}
\text{Im} \langle \partial_t \mathbf{J}_i; \partial_t \mathbf{J}_j \rangle(\omega) &\sim \text{Im} \left[i \int_0^\infty dt \left(e^{i(\omega+\Delta\epsilon)t} - e^{i(\omega-\Delta\epsilon)t} \right) \right] \\
&= \text{Im} \left[\lim_{\delta \rightarrow 0} i \int_0^\infty dt \left(e^{i(\omega+\Delta\epsilon)t} - e^{i(\omega-\Delta\epsilon)t} \right) e^{-\delta t} \right] \\
&= \text{Im} \left[i \lim_{\delta \rightarrow 0} \left(\frac{1}{-i(\omega + \Delta\epsilon) + \delta} - \frac{1}{-i(\omega - \Delta\epsilon) + \delta} \right) \right] \\
&= \pi (\delta(\omega + \Delta\epsilon) - \delta(-\omega + \Delta\epsilon))
\end{aligned} \tag{C.14}$$

In total one gets after summing over the deltas and renaming the momenta

$$\begin{aligned}
\text{Im} \langle \partial_t \mathbf{J}_i; \partial_t \mathbf{J}_j \rangle(\omega) &= \pi U^2 \sum_{\mathbf{k}_1, \mathbf{k}_2, \mathbf{k}_3, \mathbf{k}_4, \mathbf{G}} \prod_{l=i,j} (g_l(\mathbf{k}_1) + g_l(\mathbf{k}_2) - g_l(\mathbf{k}_3) - g_l(\mathbf{k}_4)) \\
&\quad \times (\delta(\omega - (\epsilon_{\mathbf{k}_4} + \epsilon_{\mathbf{k}_3} - \epsilon_{\mathbf{k}_2} - \epsilon_{\mathbf{k}_1})) - \delta(-\omega - (\epsilon_{\mathbf{k}_4} + \epsilon_{\mathbf{k}_3} - \epsilon_{\mathbf{k}_2} - \epsilon_{\mathbf{k}_1}))) \\
&\quad \times \delta_{\mathbf{k}_1 + \mathbf{k}_2, \mathbf{k}_3 + \mathbf{k}_4 + \mathbf{G}} f_{\mathbf{k}_1} f_{\mathbf{k}_2} (1 - f_{\mathbf{k}_3}) (1 - f_{\mathbf{k}_4})
\end{aligned} \tag{C.15}$$

C.4.3 Susceptibilities

$$\begin{aligned}
\chi_i &= \frac{1}{V} \langle \mathbf{J}_i \mathbf{J}_i \rangle = \frac{1}{V} \sum_{\mathbf{k}, \mathbf{k}', \sigma, \sigma'} g_i(\mathbf{k}) g_i(\mathbf{k}') \langle c_{\mathbf{k}\sigma}^\dagger c_{\mathbf{k}\sigma} c_{\mathbf{k}'\sigma'}^\dagger c_{\mathbf{k}'\sigma'} \rangle \\
&= \frac{1}{V} \sum_{\mathbf{k}, \mathbf{k}', \sigma, \sigma'} g_i(\mathbf{k}) g_i(\mathbf{k}') \left(\langle c_{\mathbf{k}\sigma}^\dagger c_{\mathbf{k}\sigma} \rangle \langle c_{\mathbf{k}'\sigma'}^\dagger c_{\mathbf{k}'\sigma'} \rangle + (1 - \langle c_{\mathbf{k}'\sigma'}^\dagger c_{\mathbf{k}'\sigma'} \rangle) \langle c_{\mathbf{k}\sigma}^\dagger c_{\mathbf{k}\sigma} \rangle \right) \\
&= \frac{1}{V} \sum_{\mathbf{k}, \mathbf{k}', \sigma, \sigma'} g_i(\mathbf{k}) g_i(\mathbf{k}') (1 - \delta_{\sigma, \sigma'} \delta_{\mathbf{k}, \mathbf{k}'} f_{\mathbf{k}\sigma}) \delta_{\mathbf{k}, \mathbf{k}'} \delta_{\sigma, \sigma'} f_{\mathbf{k}\sigma} = \sum_{\mathbf{k}, \sigma} g_i(\mathbf{k})^2 (1 - f_{\mathbf{k}\sigma}) f_{\mathbf{k}\sigma} \tag{C.16}
\end{aligned}$$

The odd term in the second line does not give a contribution.

Bibliography

- [1] J. M. Ziman. *Electrons and Phonons: The Theory of Transport Phenomena in Solids*. Oxford University Press, London, 1960.
- [2] G. D. Mahan. *Many Particle Physics*. Plenum Press, New York, 1990.
- [3] S. R. de Groot. *Thermodynamics of Irreversible Processes*. North-Holland Publishing Co., Amsterdam, 1951.
- [4] L. Boltzmann. *Vorlesungen über Gastheorie*. Barth, Leipzig, 1896.
- [5] R. Kubo. Statistical-mechanical theory of irreversible processes. I general theory and simple applications to magnetic and conduction problems. *J. Phys. Soc. Japan*, 12:570, 1957.
- [6] M. S. Green. Markoff random processes and the statistical mechanics of time-dependent phenomena. *J. Phys. Chem.*, 20:1281, 1952.
- [7] H. Mori. Transport, collective motion, and brownian motion. *Prog. Theor. Phys.*, 33(3):423, 1965.
- [8] R. Zwanzig. *Lectures in Theoretical Physics*, volume 3. Interscience, New York, 1961.
- [9] W. Götze and P. Wölfle. Homogeneous dynamical conductivity of simple metals. *Phys. Rev. B*, 6:1226, 1972.
- [10] D. Forster. *Hydrodynamic Fluctuations, Broken Symmetry, and Correlation Functions*. Frontiers in Physics. W. A. Benjamin, Reading, 1975.
- [11] P. Jung and A. Rosch. Lower bounds for the conductivities of correlated quantum systems. *Phys. Rev. B*, 75:245104, 2007.
- [12] D. Belitz. Electronic transport in solids: the resolvent method revisited. *J. Phys. C: Solid State Phys.*, 17:2735, 1984.
- [13] T. Giamarchi. Umklapp process and resistivity in one-dimensional fermion systems. *Phys. Rev. B*, 44:2905, 1991.
- [14] A. Rosch and N. Andrei. Conductivity of a clean one-dimensional wire. *Phys. Rev. Lett.*, 85:1092, 2000.
- [15] M.-R. Li and E. Orignac. Heat conduction and Wiedemann-Franz law in disordered Luttinger liquids. *Europhys. Lett.*, 60(3):432, 2002.

- [16] E. Shimshoni, N. Andrei, and A. Rosch. Thermal conductivity of spin-1/2 chains. *Phys. Rev. B*, 68:104401, 2003.
- [17] E. Boulat, P. Mehta, N. Andrei, E. Shimshoni, and A. Rosch. Heat transport of clean spin-ladders coupled to phonons: Umklapp scattering and drag. *Phys. Rev. B*, 76:214411, 2007.
- [18] A. B. Migdal. Interaction between electrons and lattice vibrations in a normal metal. *Soviet Physics Journal of experimental and theoretical Physics*, 7:996, 1958.
- [19] F. Steglich, J. Aarts, C. D. Bredl, W. Lieke, D. Meschede, W. Franz, and H. Schäfer. Superconductivity in the presence of strong pauli paramagnetism: CeCu_2Si_2 . *Phys. Rev. Lett.*, 43:1892, 1979.
- [20] G. R. Stewart. Non-Fermi-liquid behavior in d - and f -electron metals. *Rev. Mod. Phys.*, 73:797, 2001.
- [21] P. Jordan and E. Wigner. Über das Paulische Äquivalenzverbot. *Zeitschrift für Physik*, 47(9):631, 1928.
- [22] M. Raczkowski, P. Zhang, F. F. Assaad, T. Pruschke, and M. Jarrell. Phonons and the coherence scale of models of heavy fermions. *Phys. Rev. B*, 81:54444, 2010.
- [23] G. Zhao, K. K. Singh, and D. E. Morris. Oxygen isotope effect on neel temperature in various antiferromagnetic cuprates. *Phys. Rev. B*, 50:4112, 1994.
- [24] R. Hlubina and G. K. Sadiek. Isotope effect on exchange in antiferromagnetic insulators. *Phys. Rev. B*, 55:2733, 1997.
- [25] L. Pietronero, S. Strässler, and C. Grimaldi. Nonadiabatic superconductivity. i. vertex corrections for the electron-phonon interactions. *Phys. Rev. B*, 52:10516, 1995.
- [26] C. Grimaldi, L. Pietronero, and S. Strässler. Nonadiabatic superconductivity. ii. generalized eliasberg equations beyond migdal's theorem. *Phys. Rev. B*, 52:10530, 1995.
- [27] C. Grimaldi, L. Pietronero, and S. Strässler. Nonadiabatic superconductivity: Electron-phonon interaction beyond migdal's theorem. *Phys. Rev. Lett.*, 75:1158, 1995.
- [28] N. W. Ashcroft and N. D. Mermin. *Solid State Physics*. Thomson Learning, New York, 1976.
- [29] L. D. Landau. On the vibrations of the electronic plasma. *J. Phys. Moscow*, 10:25, 1946.
- [30] L. D. Landau. Theory of fermi-liquids. *Soviet Physics Journal of experimental and theoretical Physics*, 3:920, 1956.
- [31] L. D. Landau. Oscillations in a fermi-liquid. *Soviet Physics Journal of experimental and theoretical Physics*, 5:101, 1957.
- [32] F. Bloch. Zum elektrischen Widerstandsgesetz bei tiefen Temperaturen. *Zeitschrift für Physik*, 59:208, 1930.
- [33] A. Matthiessen. *Rep. Brit. Ass.*, 32:144, 1862.

-
- [34] N. D. Mermin and H. Wagner. Absence of ferromagnetism or antiferromagnetism in one- or two-dimensional isotropic heisenberg models. *Phys. Rev. Lett.*, 17:1133, 1966.
 - [35] S. Coleman. There are no goldstone bosons in two dimensions. *Comm. Math. Phys.*, 31(4):259, 1973.
 - [36] J. M. Luttinger. An exactly soluble model of a many-fermion system. *J. Math. Phys.*, 15:609, 1963.
 - [37] D. C. Mattis. New wave-operator identity applied to the study of persistent currents in 1d. *J. Math. Phys.*, 15:609, 1974.
 - [38] A. Luther and I. Peschel. Single-particle states, Kohn anomaly, and pairing fluctuations in one dimension. *Phys. Rev. B*, 9:2911, 1974.
 - [39] F. D. M. Haldane. Coupling between charge and spin degrees of freedom in the one-dimensional Fermi gas with backscattering. *J. Phys. C*, 12:4791, 1979.
 - [40] T. Giamarchi. *Quantum Physics in One Dimension*, volume 121 of *International Series of Monographs on Physics*. Oxford University Press, New York, 2004.
 - [41] J. van Delft and H. Schoeller. Bosonization for beginners - refermionization for experts. *Annalen der Physik*, 4:225, 1998.
 - [42] A. V. Sologubenko, K. Giannó, H. R. Ott, U. Ammerahl, and A. Revcolevschi. Thermal conductivity of the hole-doped spin ladder system $\text{Sr}_{14-x}\text{Ca}_x\text{Cu}_{24}\text{O}_{41}$. *Phys. Rev. Lett.*, 84:2714, 2000.
 - [43] A. V. Sologubenko, E. Felder, K. Giannó, H. R. Ott, A. Vietkine, and A. Revcolevschi. Thermal conductivity and specific heat of the linear chain cuprate Sr_2CuO_3 : Evidence for thermal transport via spinons. *Phys. Rev. B*, 62:R6108, 2000.
 - [44] A. V. Sologubenko, K. Giannó, H. R. Ott, A. Vietkine, and A. Revcolevschi. Heat transport by lattice and spin excitations in the spin-chain compounds SrCuO_2 and Sr_2CuO_3 . *Phys. Rev. B*, 64:054412, 2001.
 - [45] A. V. Sologubenko, T. Lorenz, J. A. Mydosh, A. Rosch, K. C. Shortsleeves, and M. M. Turnbull. Field-dependent thermal transport in the Haldane chain compound NENP . *Phys. Rev. Lett.*, 100:137202, 2008.
 - [46] C. Hess, C. Baumann, U. Ammerahl, B. Büchner, F. Heidrich-Meisner, W. Brenig, and A. Revcolevschi. Magnon heat transport in $(\text{Sr}, \text{Ca}, \text{La})_{14}\text{Cu}_{24}\text{O}_{41}$. *Phys. Rev. B*, 64:184305, 2001.
 - [47] K. Kudo, S. Ishikawa, T. Noji, T. Adachi, Y. Koike, K. Maki, S. Tsuji, and K. Kumagai. Spin gap and hole pairing of $\text{Sr}_{14-x}\text{A}_x\text{Cu}_{24}\text{O}_{41}$ ($\text{A} = \text{Ca}$ and La) single crystals studied by the electrical resistivity and thermal conductivity. *J. Low Temp. Phys.*, 117:1689, 1999.
 - [48] C. Hess. Heat conduction in low-dimensional quantum magnets. *Eur. Phys. J. Special Topics*, 151:73, 2007.
 - [49] X. Zotos, F. Naef, and P. Prelovsek. Transport and conservation laws. *Phys. Rev. B*, 55:11029, 1997.

- [50] F. Naef and X. Zotos. Spin and energy correlations in the one dimensional spin-1/2 heisenberg model. *J. Phys. Condens. Matter*, 10:L183, 1998.
- [51] X. Zotos. Finite temperature drude weight of the one-dimensional spin- 1/2 heisenberg model. *Phys. Rev. Lett.*, 82:1764, 1999.
- [52] F. Heidrich-Meisner, A. Honecker, D. C. Cabra, and W. Brenig. Thermal conductivity of anisotropic and frustrated spin- $\frac{1}{2}$ chains. *Phys. Rev. B*, 66:140406, 2002.
- [53] F. Heidrich-Meisner, A. Honecker, D. C. Cabra, and W. Brenig. Zero-frequency transport properties of one-dimensional spin-1/2 systems. *Phys. Rev. B*, 68:134436, 2003.
- [54] F. Heidrich-Meisner, A. Honecker, D. C. Cabra, and W. Brenig. Thermal conductivity of one-dimensional spin-systems. *Physica B: Condensed Matter*, 359:1394, 2005.
- [55] F. Heidrich-Meisner, A. Honecker, and W. Brenig. Thermal transport of the xxz chain in a magnetic field. *Phys. Rev. B*, 71:184415, 2005.
- [56] A. Klümper and K. Sakai. The thermal conductivity of the spin-1/2 XXZ chain at arbitrary temperature. *J. Phys. A*, 35:2173, 2002.
- [57] K. Sakai and A. Klümper. Non-dissipative thermal transport in the massive regimes of the xxz chain. *J. Phys. A*, 36:11617, 2003.
- [58] J. Benz, T. Fukui, A. Klümper, and C. Scheeren. On the finite temperature drude weight of the anisotropic heisenberg chain. *Journal of the Physical Society of Japan*, 74S:181, 2005.
- [59] K. R. Thurber, A. W. Hunt, T. Imai, and F. C. Chou. O NMR study of $q = 0$ spin excitations in a nearly ideal $s = 1/2$ 1D heisenberg antiferromagnet, Sr_2CuO_3 , up to 800 K. *Phys. Rev. Lett.*, 87:247202, 2001.
- [60] J. Sirker, R. G. Pereira, and I. Affleck. Diffusion and ballistic transport in clean one-dimensional conductors. *Phys. Rev. Lett.*, 103:216602, 2009.
- [61] S. Langer, F. Heidrich-Meisner, J. Gemmer, I. P. McCulloch, and U. Schollwöck. Real-time study of diffusive and ballistic transport in spin- $\frac{1}{2}$ chains using the adaptive time-dependent density matrix renormalization group method. *Phys. Rev. B*, 79:214409, 2009.
- [62] P. Jung and A. Rosch. Lower bounds for the conductivities of correlated quantum systems. *Phys. Rev. B*, 75:245104, 2007.
- [63] P. Jung and A. Rosch. Spin conductivity in almost integrable spin chains. *Phys. Rev. B*, 76:245108, 2007.
- [64] A. L. Chernyshev and A. V. Rozhkov. Thermal transport in antiferromagnetic spin-chain materials. *Phys. Rev. B*, 72:104423, 2005.
- [65] K. Louis, P. Prelovšek, and X. Zotos. Thermal conductivity of one-dimensional spin-1/2 systems coupled to phonons. *Phys. Rev. B*, 74:235118, 2006.
- [66] F. D. M. Haldane. 'Luttinger liquid theory' of one-dimensional quantum fluids. i. properties of the Luttinger model and their extension to the general 1d interacting spinless Fermi gas. *J. Phys. C*, 14:2585, 1981.

- [67] H. Bethe. Zur Theorie der Metalle. *Z. Phys.*, 71:205, 1931.
- [68] C. A. Doty and D. S. Fisher. Effects of quenched disorder on spin-1/2 quantum XXZ chains. *Phys. Rev. B*, 45:2167, 1992.
- [69] A. V. Sologubenko, K. Berggold, T. Lorenz, A. Rosch, E. Shimshoni, M. D. Phillips, and M. M. Turnbull. Magnetothermal transport in the spin-1 / 2 chains of copper pyrazine dinitrate. *Phys. Rev. Lett.*, 98:107201, 2007.
- [70] E. Shimshoni, D. Rasch, P. Jung, A. Rosch, and A. V. Sologubenko. Large thermomagnetic effects in weakly disordered Heisenberg chains. *Phys. Rev. B*, 79:064406, 2009.
- [71] J. Hubbard. Electron correlations in narrow energy bands. *Proc. R. Soc. A*, 276:238, 1963.
- [72] B. J. Kim, H. Koh, E. Rotenberg, S.-J. Oh, H. Eisaki, N. Motoyama, S. Uchida, T. Tohyama, S. Maekawa, Z.-X. Shen, and C. Kim. Distinct spinon and holon dispersions in photoemission spectral functions from one dimensional SrCuO_2 . *Nature Physics*, 2:397, 2006.
- [73] G. Wiedemann and R. Franz. Ueber die Wärme-Leitungsfähigkeit der Metalle. *Ann. Phys.*, 89:497, 1853.
- [74] M. S. Dresselhaus, G. Chen, M. Y. Tang, R. Yang, H. Lee, D. Wang, Z. Ren, J.-P. Fleurial, and P. Gogna. New directions for low-dimensional thermoelectric materials. *Advanced Materials*, 19:1, 2007.
- [75] G. D. Mahan. Good thermoelectrics. In H. Ehrenreich and F. Spaepen, editors, *Solid State Physics: Advances in Research and Applications*, volume 51, page 82, San Diego, 1998. Academic Press.
- [76] N. F. Mott. The basis of the electron theory of metals, with special reference to the transition metals. *Proc. Phys. Soc. A*, 62:416, 1949.
- [77] A. Luther and V. J. Emery. Backward scattering in the one-dimensional electron gas. *Phys. Rev. Lett.*, 33:589, 1974.
- [78] A. Garg, D. Rasch, E. Shimshoni, and A. Rosch. Large violation of wiedemann franz law in luttinger liquids. *Phys. Rev. Lett.*, 103:096402, 2009.
- [79] J. W. Negele and H. Orland. *Quantum Many-Particle Systems*. Frontiers in Physics. Addison-Wesley, Reading, MA, 1988.
- [80] S. Lukyanov. Low energy effective Hamiltonian for the XXZ spin chain. *Nucl. Phys. B*, 522:533, 1998.
- [81] G. Mennenga, L. J. de Jongh, W. J. Huiskamp, and J. Reedijk. Specific heat and susceptibility of the 1-dimensional image Heisenberg antiferromagnet $\text{Cu}(\text{Pyrazine})(\text{NO}_3)_2$. evidence for random exchange effects at low temperatures. *J. Magn. Magn. Mater.*, 44:89, 1984.

- [82] P. R. Hammar, M. B. Stone, D. H. Reich, C. Broholm, P. J. Gibson, M. M. Turnbull, C. P. Landee, and M. Oshikawa. Characterization of a quasi-one-dimensional spin-1/2 magnet which is gapless and paramagnetic for $g\mu_B H \lesssim J$ and $k_B T \ll J$. *Phys. Rev. B*, 59:1008, 1999.
- [83] A. Santoro, A. D. Mighell, and C. W. Reimann. The crystal structure of a 1 : 1 cupric nitrate–pyrazine complex $\text{Cu}(\text{NO}_3)_2(\text{C}_4\text{N}_2\text{H}_4)$. *Acta Crystallogr. Sect. B*, 26:979, 1970.
- [84] M. B. Stone, D. H. Reich, C. Broholm, K. Lefmann, C. Rischel, C. P. Landee, and M. M. Turnbull. Extended quantum critical phase in a magnetized spin-1/2 antiferromagnetic chain. *Phys. Rev. Lett.*, 91:037205, 2003.
- [85] T. Lancaster, S. J. Blundell, M. L. Brooks, P. J. Baker, F. L. Pratt, J. L. Manson, and C. Baines. Muon-spin relaxation study of the spin-1/2 molecular chain compound $\text{Cu}(\text{HCO}_2)_2(\text{C}_4\text{H}_4\text{N}_2)$. *Phys. Rev. B*, 73:172403, 2006.
- [86] Peter Jung. *Transport and Approximate Conservation Laws in Low Dimensional Systems*. PhD thesis, Universität zu Köln, 2007.
- [87] T. Giamarchi and A. Millis. Conductivity of a luttinger liquid. *Phys. Rev. B*, 46:9325, 1992.
- [88] M. Greiner, O. Mandel, T. Esslinger, T. W. Hänsch, and I. Bloch. Quantum phase transition from a superfluid to a Mott insulator in a gas of ultracold atoms. *Nature*, 415:39, 2002.
- [89] M. Greiner, O. Mandel, T. W. Hänsch, and I. Bloch. Collapse and revival of the matter wave field of a Bose-Einstein condensate. *Nature*, 419:51, 2002.
- [90] U. Schneider, L. Hackermüller, S. Will, T. Best, I. Bloch, T. A. Costi, R. W. Helmes, D. Rasch, and A. Rosch. Metallic and insulating phases of repulsively interacting fermions in a 3d optical lattice. *Science*, 322:1520, 2008.
- [91] R. Jördens, N. Strohmaier, K. Günter, H. Moritz, and T. Esslinger. A Mott insulator of fermionic atoms in an optical lattice. *Nature*, 455:204, 2008.
- [92] R. W. Helmes, T. A. Costi, and A. Rosch. Mott transition of fermionic atoms in a three-dimensional optical trap. *Phys. Rev. Lett.*, 100:56403, 2008.
- [93] A. Hubener, M. Snoek, and W. Hofstetter. Magnetic phases of two-component ultracold bosons in an optical lattice. *Phys. Rev. B*, 80:245109, 2009.
- [94] R. Jördens, L. Tarruell, D. Greif, T. Uehlinger, N. Strohmaier, H. Moritz, T. Esslinger, L. De Leo, C. Kollath, A. Georges, V. Scarola, L. Pollet, E. Burovski, E. Kozik, and M. Troyer. Quantitative determination of temperature in the approach to magnetic order of ultracold fermions in an optical lattice. *arXiv*, 0912:3790, 2009.
- [95] I. Bloch, J. Dalibard, and W. Zwerger. Many-body physics with ultracold gases. *Rev. Mod. Phys.*, 80:885, 2008.
- [96] T. Kinoshita, T. Wenger, and D. S. Weiss. A quantum Newton’s cradle. *Nature*, 440:900, 2006.

- [97] S. Folling, S. Trotzky, P. Cheinet, M. Feld, R. Saers, A. Widera, T. Müller, and I. Bloch. Direct observation of second-order atom tunnelling. *Nature*, 448:1029, 2007.
- [98] A.S. Sørensen, E. Altman, M. Gullans, J. V. Porto, M. D. Lukin, and E. Demler. Adiabatic preparation of many-body states in optical lattices. *arXiv*, 0906:2567, 2009.
- [99] K. Winkler, G. Thalhammer, F. Lang, R. Grimm, J. H. Denschlag, A. J. Daley, A. Kantian, H. P. Büchler, and P. Zoller. Repulsively bound atom pairs in an optical lattice. *Nature*, 441:853, 2006.
- [100] A. Rosch, D. Rasch, B. Binz, and M. Vojta. Metastable superfluidity of repulsive fermionic atoms in optical lattices. *Phys. Rev. Lett.*, 101:265301, 2008.
- [101] F. Heidrich-Meisner, S. R. Manmana, M. Rigol, A. Muramatsu, A. E. Feiguin, and E. Dagotto. Quantum distillation: Dynamical generation of low-entropy states of strongly correlated fermions in an optical lattice. *Phys. Rev. A*, 80:041603, 2009.
- [102] N. Strohmaier, D. Greif, R. Jördens, L. Tarruell, H. Moritz, T. Esslinger, R. Sensarma, D. Pekker, E. Altman, and E. Demler. Observation of elastic doublon decay in the Fermi-Hubbard model. *arXiv*, 0905:2963, 2009.
- [103] L. Hackermüller, U. Schneider, M. Moreno-Cardoner, T. Kitagawa, S. Will, T. Best, E. Demler, E. Altman, I. Bloch, B. Paredes, et al. Anomalous expansion of attractively interacting fermionic atoms in an optical lattice. *arXiv*, 0910:3598, 2009.
- [104] U. Schneider, L. Hackermüller, J. P. Ronzheimer, T. Best, S. Will, S. Braun, K.-C. Fong, I. Bloch, E. Demler, S. Mandt, D. Rasch, and A. Rosch. Breakdown of diffusion: From collisional hydrodynamics to a continuous quantum walk in a homogeneous Hubbard model. *in preparation*, 2010.
- [105] F. Bloch. Über die quantenmechanik der elektronen in kristallgittern. *Z. Physik*, 52:555, 1929.
- [106] C. Waschke, H. G. Roskos, R. Schwedler, K. Leo, H. Kurz, and K. Köhler. Coherent submillimeter-wave emission from bloch oscillations in a semiconductor superlattice. *Phys. Rev. Lett.*, 70:3319, 1993.
- [107] M. Gustavsson, E. Haller, M. J. Mark, J. G. Danzl, G. Rojas-Kopeinig, and H.-C. Nägerl. Control of interaction-induced dephasing of bloch oscillations. *Phys. Rev. Lett.*, 100:080404, 2008.
- [108] J. Jäcke. *Einführung in die Transporttheorie*. Vieweg, Braunschweig, 1978.

Danksagung

An erster Stelle möchte ich meinem Doktorvater Prof. Achim Rosch für die Betreuung dieser Arbeit danken. Sein fachlicher Sachverstand, seine Begeisterungsfähigkeit und seine Fairness als Vorgesetzter haben die Zusammenarbeit mit ihm zu etwas Besonderem gemacht.

Prof. Matthias Vojta danke ich sehr für seine freundliche Bereitschaft, als Zweitguachter zu fungieren. Ich danke außerdem besonders Ricardo Doretto, Mario Zacharias und Stefan Mandt für das gewissenhafte Korrekturlesen meiner Arbeit, das sehr zum Gelingen beigetragen hat.

Die vielen wechselnden Mitgliedern der Arbeitsgruppe(n) Festkörpertheorie, Fabrizio Anfuso, Benedikt Binz, Heidrun Weber, Ricardo Doretto, Markus Garst, Lars Fritz, Mario Zacharias, Matthias Sitte, Tobias Meng, Tanja Rindler-Daller, Akos Rapp, Etienne Gärtner, Alexander Wollny, Lucas Holender, Eran Sela, Andrew Mitchell, Adel Benlagra, Michael Becker und Ralf Bulla, haben mit ihrer Gegenwart während meiner Promotion sehr zur Freude an der Arbeit beigetragen. Ihnen, und besonders meinen Bürokollegen Rolf Helmes, Peter Jung, Karin Everschor, Stefan Mandt und Christoph Schütte möchte ich für die kollegiale Arbeitsatmosphäre und ihre ständige Hilfsbereitschaft danken.

Nicht zuletzt danke ich Andreas Sindermann für seine immer kompetente und schnelle Hilfe bei Computerproblemen und Frau Hochscheidt für ihre freundliche Unterstützung bei der Literatursuche.

Erklärung

Ich versichere, dass ich die von mir vorgelegte Dissertation selbständig angefertigt, die benutzten Quellen und Hilfsmittel vollständig angegeben und die Stellen der Arbeit - einschließlich Tabellen, Karten und Abbildungen -, gemacht habe; dass diese Dissertation noch keiner anderen Fakultät oder Universität zur Prüfung vorgelegen hat; dass sie - abgesehen von unten angegebenen Teilpublikationen - noch nicht veröffentlicht worden ist sowie, dass ich eine solche Veröffentlichung vor Abschluss des Promotionsverfahrens nicht vornehmen werde. Die Bestimmungen der Promotionsordnung sind mir bekannt. Die von mir vorgelegte Dissertation ist von Prof. Dr. Achim Rosch betreut worden.

Teilpublikationen:

- U. Schneider, L. Hackermüller, S. Will, T. Best, I. Bloch, T. A. Costi, R. W. Helmes, D. Rasch, A. Rosch, *Metallic and Insulating Phases of Repulsively Interacting Fermions in a 3D Optical Lattice*, Science 322, 1520 (2008).
- A. Rosch, D. Rasch, B. Binz, M. Vojta, *Metastable superfluidity of repulsive fermionic atoms in optical lattices*, Phys. Rev. Lett. 101, 265301 (2008).
- E. Shimshoni, D. Rasch, P. Jung, A. V. Sologubenko, A. Rosch, *Large thermomagnetic effects in weakly disordered Heisenberg chains*, Phys. Rev. B 79, 064406 (2009).
- A. Garg, D. Rasch, E. Shimshoni, A. Rosch, *Large violation of Wiedemann Franz law in Luttinger liquids*, Phys. Rev. Lett. 103, 096402 (2009).
- U. Schneider, L. Hackermüller, J. P. Ronzheimer, T. Best, S. Will, S. Braun, K.-C. Fong, I. Bloch, E. Demler, S. Mandt, D. Rasch, and A. Rosch *Breakdown of diffusion: From collisional hydrodynamics to a continuous quantum walk in a homogeneous Hubbard model*, in Vorbereitung.

Lebenslauf

Persönliche Daten

| | |
|---------------------|-----------------------------------|
| Name | David Rasch |
| Geburtsdatum | 01.03.1982 |
| Geburtsort | Viernheim |
| Familienstand | verheiratet mit Silke Feuchtinger |
| Staatsangehörigkeit | deutsch |

Schulbildung

| | |
|-------------|------------------------------------|
| 1987 - 1992 | Bessunger Grundschule, Darmstadt |
| 1992 - 1997 | Schulzentrum Marienhöhe, Darmstadt |
| 1997 - 2000 | Viktoriaschule, Darmstadt |
| Juni 2000 | Abitur |

Hochschulstudium

| | |
|-----------------|--|
| 2002 - 2007 | Studium der Physik, Philipps-Universität Marburg |
| September 2003 | Vordiplom |
| Januar 2007 | Diplom |
| seit April 2007 | Promotionsstudium am Institut für Theoretische Physik der Universität zu Köln Anfertigung der vorliegenden Dissertation |

Arbeitsverhältnisse

| | |
|-------------|--|
| 2000 - 2001 | Zivildienst Niederramstädter Diakonie |
| seit 2007 | Wissenschaftlicher Mitarbeiter am Institut für Theoretische Physik der Universität zu Köln |